Novel strategies for transition metal catalysis in living cells

James, C.C.

Publication date
2022
Document Version
Final published version

Novel Strategies for Transition Metal Catalysis in Living Cells

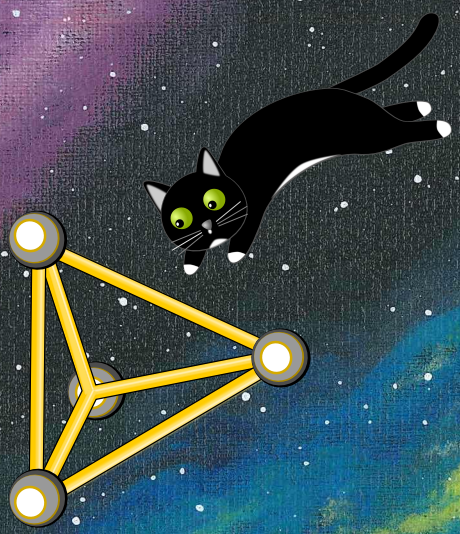

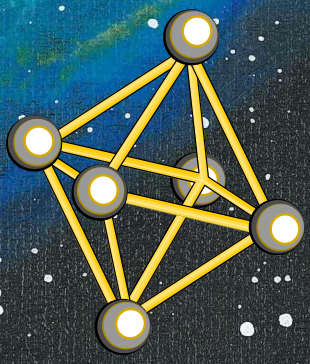

Catriona C. James

Novel Strategies for Transition Metal Catalysis in Living Cells

ACADEMISCH PROEFSCHRIFT

ter verkrijging van de graad van doctor
aan de Universiteit van Amsterdam
op gezag van de Rector Magnificus
prof. dr. ir. K.I.J. Maex
ten overstaan van een door het College voor Promoties ingestelde commissie,
in het openbaar te verdedigen in de Agnietenkapel
op dinsdag 11 oktober 2022, te 12.00 uur

door Catriona Charlotte James
geboren te Edinburgh

Promotiecommissie

Promotores:	prof. dr. J.N.H. Reek	Universiteit van Amsterdam
	prof. dr. B. de Bruin	Universiteit van Amsterdam
Overige leden:	prof. dr. J.H. van Maarseveen	Universiteit van Amsterdam
	dr. S. Pullen	Universiteit van Amsterdam
	dr. F. Mutti	Universiteit van Amsterdam
	dr. J.C. Slootweg	Universiteit van Amsterdam
	prof. dr. A. Kros	Universiteit Leiden
	prof. dr. S.A. Bonnet	Universiteit Leiden

Faculteit der Natuurwetenschappen, Wiskunde en Informatica

ISBN: 978-94-6421-846-6

Printed by Ipskamp Printing

Enschede, the Netherlands, 2022

“It is possible to commit no mistakes and still lose. That is not a weakness; that is life.”

– Captain Jean-Luc Picard

Table of Contents

Chapter 1

In Vivo Transition Metal Catalysis: Progress, Challenges, and Novel Supramolecular Solutions

ABSTRACT

The importance of transition metal catalysis is exemplified by its wide range of applications, for example in the synthesis of chemicals, natural products, and pharmaceuticals. However, one relatively new application is for carrying out new-to-nature reactions inside living cells. The complex environment of a living cell is not welcoming to transition metal catalysts, as a diverse range of biological components have the potential to inhibit or deactivate the catalyst. This chapter reviews the current progress in the field of transition metal catalysis, and analyses catalysis efficiency in living cells and under biological conditions. Catalyst poisoning is a ubiquitous problem in this field, and we propose that encapsulation of transition metal catalysts within the cavities of supramolecular cages may provide a route to prevent poisoning by spatially separating the catalyst from biomolecules, as well as improving the activity or selectivity of the catalyst.

LIST OF ABBREVIATIONS

ADC	antibody drug conjugate
ADP	adenosine diphosphate
ATP	adenosine triphosphate
ArM	artificial metalloenzyme
DMEM	Dulbecco's modified eagle medium
4-DMN	4-*N*,*N*-dimethylamino-1,8-naphthalimide
DNP	dinitrophenol
ETC	electron transport chain
FBS	foetal bovine serum
5FU	fluorouracil
GSH	L-glutathione
GSSG	L-glutathione dimer
HEPES	4-(2-hydroxyethyl)-1-piperazineethanesulfonic acid
MMAE	monomethyl auristatin E
NADH	nicotinamide adenine dinucleotide (reduced form)
NP	nanoparticle
PBS	phosphate buffered saline
ROS	reactive oxygen species
SAHA	suberoylanilide hydroxamic acid
SAV	streptavidin
SCNP	single-chain nanoparticle
TOF	turnover frequency
TON	turnover number

INTRODUCTION

Catalysis is an invaluable tool for many different areas of chemistry. Transition metal catalysts provide a facile route to achieve otherwise difficult transformations, such as carbon-carbon bond forming reactions, which means that transition metal catalysis plays a pivotal role in a vast range of applications, for example the synthesis of natural products and bioactive compounds, and the development of pharmaceuticals.[1, 2] Although chemists have harnessed the powerful reactivity of transition metals to gain access to these useful compounds, nature is able to selectively and efficiently synthesise complex molecules without the help of metals. In cells catalysis is naturally carried out by enzymes: simple amino acid building blocks are joined together to generate intricate 3D structures which are responsible for mediating the production of a huge range of compounds which are necessary for the functioning of the cell. While enzyme catalysis is celebrated for achieving levels of selectivity which chemists are often unable to match with synthetic metal catalysts, this selectivity comes with a price. The substrate scope for a particular enzyme can be very small, and if the desired target compound for a reaction is not naturally produced in the cell, there may not be a naturally occurring enzyme available which is able to catalyse the desired reaction.[3, 4] Therefore an exogenous catalyst is required to carry out reactions in cells which are new to nature.

The power of catalytically controlling reactions in living cells has important applications for biomolecular labelling and imaging, as well as for pharmaceuticals. Catalytic activation of prodrugs provides the opportunity for localised drug activation, which in the context of cancer treatment could help to decrease system-wide toxicity and reduce the fairly severe side effects which are typically associated with traditional chemotherapy. Therefore, achieving selective, efficient, bioorthogonal catalysis for new to nature reactions is an important goal. This need has brought about the birth of a relatively new field, where transition metal catalysts are applied in living cells. Using a synthetic transition metal catalyst, instead of endogenous or modified enzymes, provides the means to increase the reaction and substrate scopes to obtain non-natural reactivity. Another advantage of transition metals is that it is relatively easy to tune the metal centre to achieve the desired reactivity, by modifying the ligands surrounding the metal centre.

Over the last 20 years there have been many examples of transition metal catalysis either inside or in the presence of living cells. However, this field is still in its infancy. Poor catalytic activity is ubiquitous, and low yields, very high catalyst loadings, and low turnover numbers (TON), where they can be determined at all, are generally accepted; in contrast to the high yields and efficiencies which are strived for outside of the biological setting. Therefore, new strategies are required to improve the reactivity of transition metal catalysts in biological settings. This chapter highlights the progress already achieved in this field, and discusses the application of supramolecular cages to solve some of the problems currently faced.

TRANSITION METAL CATALYSIS IN LIVING SYSTEMS

The root of the challenges faced in the field of *in vivo* catalysis is that the conditions within a cell are very hostile towards transition metals and the reactions that they catalyse. The first hurdle to overcome is entry of the reaction components into the inside of the cell. Prokaryotic cells, such as bacteria, are enclosed by a cell wall, which is permeable to most compounds. Beyond the cell wall is the periplasm, which is separated from the interior of the cell (the cytoplasm) by a cell membrane. In contrast, eukaryotic cells, such as mammalian cells, are enclosed only by a cell membrane. The cell membrane is comprised of an amphiphilic phospholipid bilayer, the structure of which is shown in Figure 1. The head of the phospholipid is a hydrophilic phosphate group, which points outwards into the extracellular space, and inwards towards the cytosol; meanwhile hydrophobic lipid tails comprise the interior of the cell membrane. This means that while small neutral compounds can easily diffuse through the cell membrane, large hydrophilic or charged species are often impermeable and are unable to pass through the membrane.[5] However, once the reaction components have crossed the cell membrane to enter the cell, the next challenge is the compatibility of the reaction itself with the cell. Cells have an aqueous aerobic environment, and many reactions catalysed by metals are not tolerant to water and/or oxygen. Nevertheless, even after selecting a water/oxygen-tolerant reaction, the specific conditions required to sustain most biological systems still have to be adhered to: namely temperature of 37 °C, a pH of around 7, and high salt concentrations. In addition there are high quantities of nucleophiles and thiols, the most important of which is glutathione (GSH), which is found in 1–10 mM amounts, and commonly poisons transition metal catalysts.[6] Finally, whereas in a normal synthetic reaction there would only be substrate present, there is a huge variety of other biomolecules present in a cell, which in principle could compete with your desired substrate, or also inhibit the catalysis.

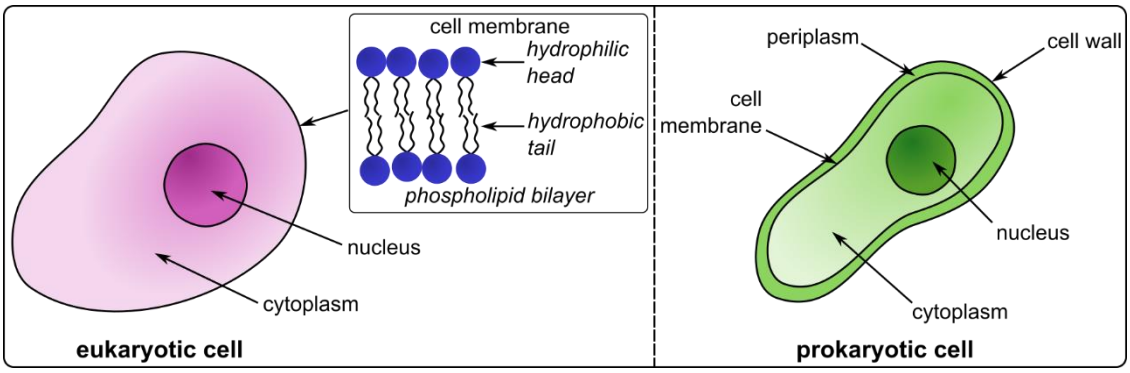

Figure 1. Basic structures of eukaryotic and prokaryotic cells, and the phospholipid bilayer cell membrane.

Despite these challenges, it is still possible to successfully carry out transition metal catalysis inside living cells. There are three general strategies used for transition metal catalysis in biological systems, namely homogenous, where a molecular catalyst is deployed, heterogeneous, where nanoparticles, nanozymes, or other supramolecular structures are used, and artificial metalloenzymes, where molecular catalysts are docked inside a protein scaffold. A diverse range of catalysts of all three of these types have been used under biological

conditions (where experiments are carried out in the lab in the presence of biological additives or in cell culture media), in living cells (where catalysis is carried out inside cells which have been cultured on a plate), and even in whole organisms (where the reaction components are injected into a living animal such as a mouse or zebrafish embryo and the catalysis). Additionally, a wide range of different types of reaction have been employed for *in vivo* catalysis. Many initial studies utilise relatively simple transformations, such as redox reactions, transfer hydrogenations, or deprotection reactions. However more complex, bond-making, systems have also been developed, involving both intra- and intermolecular cyclisation reactions, and even cross-coupling reactions. Here, the efficiency of different catalysts for each type of reaction will be discussed, where this information is available. The analysis and quantification of catalysis in cells is challenging, as many of the typical techniques used for monitoring a catalytic reaction (for example, NMR spectroscopy or GC analysis) are unable to be applied to the cellular setting. Therefore, one of the most straightforward ways to determine if a reaction is successful is to design a system where the product results in the "switch-on" of an easily monitored property, such as fluorescence or cytotoxicity. For this reason, almost all *in vivo* reactions involve the synthesis or activation of a fluorescent dye or cytotoxic drug. The structures of the most commonly used dyes and drugs are illustrated in Figure 2. However, although this provides a handle for a simple confirmation if the reaction worked at all, it is often challenging to quantify yields or TONs of reactions. This is in part because often the uptake efficiencies of all the components of the reaction are unknown, so the actual concentration of substrate and the real catalyst loading inside the cell is not clearly defined, so often it is only possible to obtain qualitative data about the reaction efficiency. The following section will discuss the efficiencies of reactions which have been carried out under biological conditions, in cells, or in whole organisms, and analyse what aspects of these reactions should be improved.

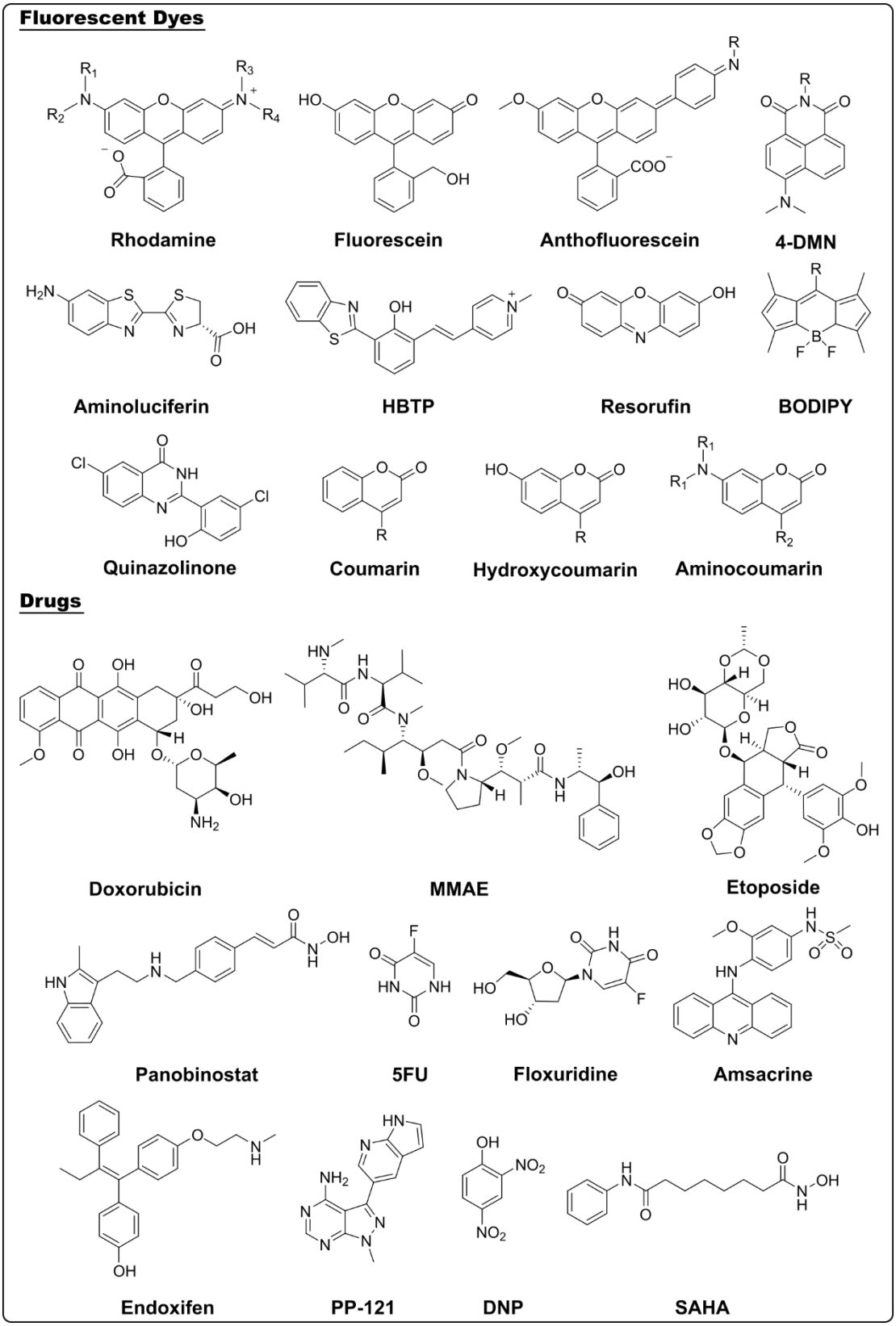

Figure 2. Structures of drugs and fluorescent dyes which are commonly used as the product of a transition metal catalysed reaction inside living cells.

OXIDATION AND REDUCTION REACTIONS

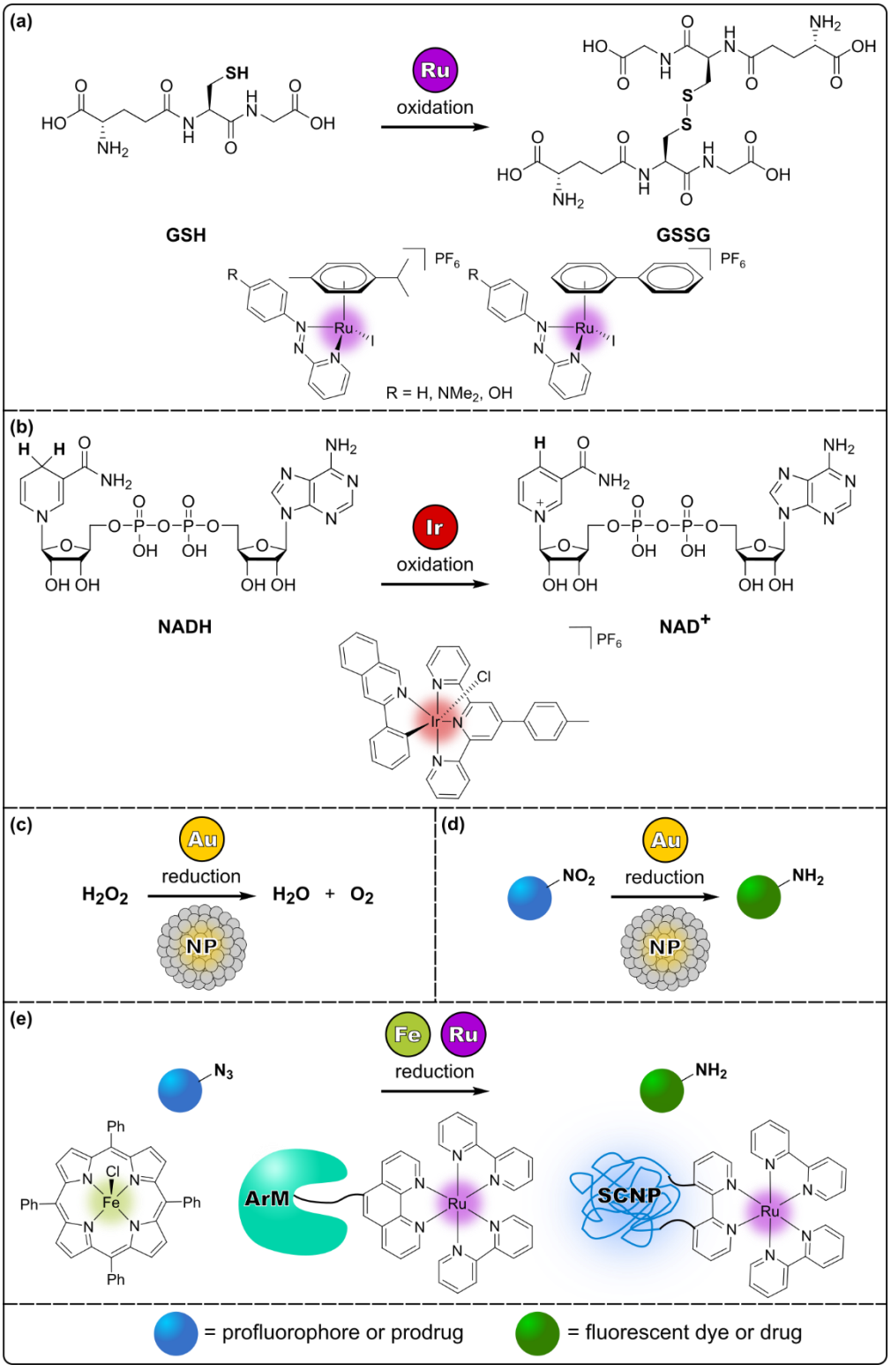

Figure 3. Overview of the oxidation and reduction reactions carried out in cells. (a) Ruthenium catalysed glutathione oxidation (ref 8). (b) Iridium catalysed NADH oxidation (ref 10). (c) Gold catalysed ROS reduction (ref 12). (d) Gold catalysed nitrate reduction (ref 13). (e) Iron and ruthenium catalysed azide reduction (refs 14–19).

Various types of redox reactions have been used to exploit different reactivities in cells; for example, influencing the cellular redox balance, and chemical and photoreductions to uncage fluorophores and prodrugs. The maintenance of the cellular redox balance is vital for a range of processes, including cellular metabolism, cell death, cell differentiation and development, immune responses, and circadian rhythm. Cellular redox homeostasis is the process by which oxidising and reducing reactions within the cell are kept in balance, and is maintained by several reducing agents, such as glutathione, thioredoxin, and reduced nicotinamide adenine dinucleotide (NADH).[7] Therefore, altering the intracellular concentrations of these compounds can have serious consequences for the viability of the cells. Sadler *et al.* used this alteration to their advantage, by using Ru(II) piano-stool complexes to catalyse the oxidation of glutathione to its dimer, GSSG (Figure 3a). The catalytic cycle proceeds via an azo-intermediate, the generation of which is dependent upon the concomitant hydrogenation of dissolved oxygen to generate hydrogenation peroxide. The iodide, after displacement from the ruthenium centre by glutathione, then catalyses its decomposition back into oxygen, and water (Figure 4a). This reactivity was monitored in A549 human lung cancer cells via an increase in reactive oxygen species (ROS) and the resultant decrease in cell survival.[8] Since glutathione is the primary antioxidant in cells, a decrease of the glutathione levels induces this build-up of ROS (Figure 4b), ultimately leading to cell death.[9]

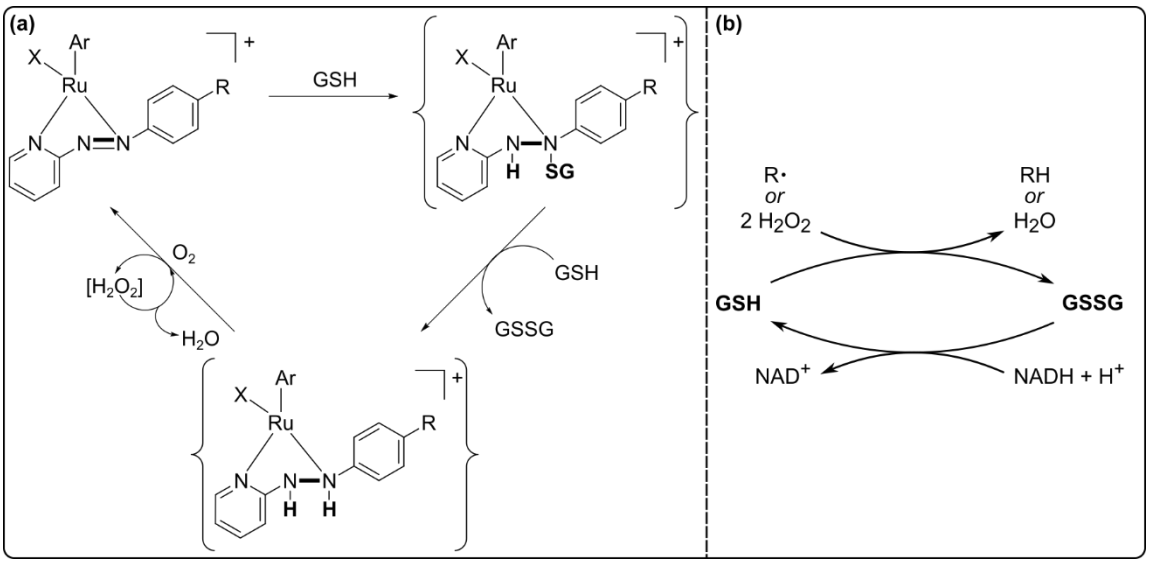

Figure 4. (a) Catalytic cycle for the ruthenium catalysed oxidation of GSH to GSSG. (b) GSH-mediated regulation of ROS levels in cells.

Recently, the same group developed a cyclometallated Ir(III) photoredox catalyst, which catalyses both the photooxidation of NADH to NAD^+ and the concurrent photoreduction of cytochrome *c* (cyt *c*) (Figure 3b). The catalytic cycle is depicted in Figure 5a. After excitation with blue light, the complex extracts an electron from NADH to generate the radical cation, which is readily deprotonated to form the neutral carbon-centred radical, $NAD^{\bullet}$. Under regular oxygen levels (20% O_2), molecular oxygen re-oxidises the iridium complex while generating superoxide radicals, which extracts an electron from $NAD^{\bullet}$ and consumes two protons from the surrounding medium, to generate NAD^+ and peroxide. However, in hypoxic cells (1% O_2),

such as A549 lung cancer cells, oxidised cytochrome c (cyt c_{ox}) can replace the role of the superoxide radicals, and is reduced by both the iridium(II) intermediate and the NAD$^{\bullet}$ radical. This cellular catalysis resulted in a significant decrease in NADH and disrupted the mitochondrial electron transport chain (ETC), as evidenced by a decrease in the mitochondrial membrane potential.[10] The mitochondrial ETC is responsible for generating energy in the form of adenosine triphosphate (ATP) during cellular respiration, and the first step of this chain is oxidation of NADH (Figure 5b). Therefore, decreasing the amount of NADH available inhibits the generation of ATP, which results in the cell death in the form of apoptosis and necrosis.[11] Lower toxicity towards normal cells in the dark compared to cancer cells in the light was observed.[10] This photo-targeted oxygen-dependent activity is a promising outlook for targeted chemotherapy.

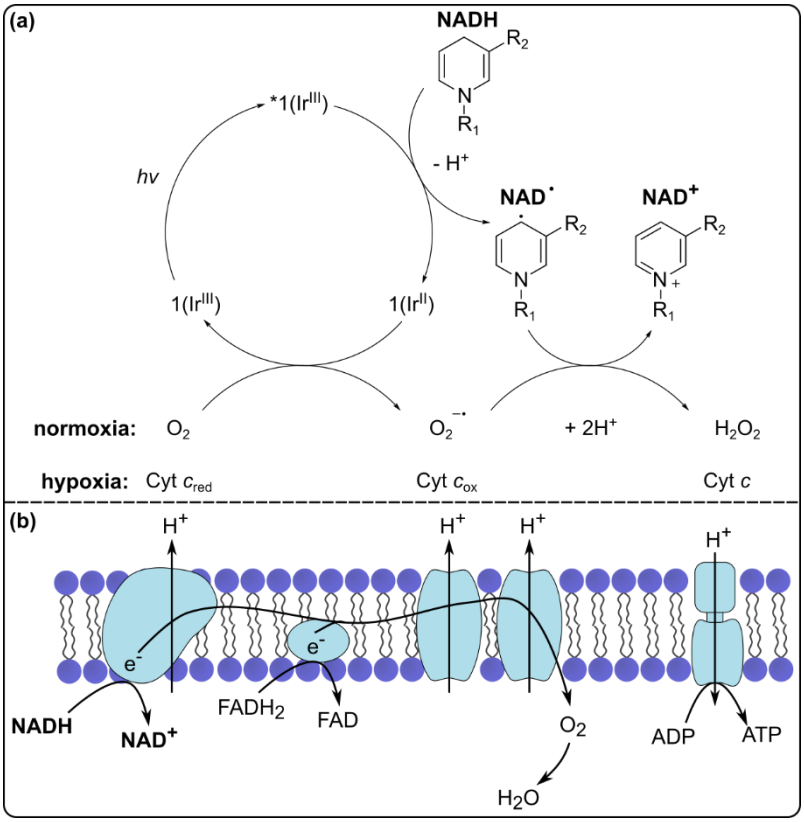

Figure 5. (a) Catalytic cycle for the iridium photocatalysed oxidation of NADH to NAD$^+$ via a neutral carbon radical NAD$^{\bullet}$ intermediate. Under normoxic conditions the iridium complex is re-oxidised by molecular oxygen; under hypoxic conditions the iridium complex is re-oxidised by cyt *c*. (b) The electron transport chain which takes place in the mitochondrial membrane, which relies upon NADH to generate energy in the form of ATP.

Instead of activating a photocatalyst, light has also been used *in vivo* to switch-on the catalytic activity of a ROS scavenger (Figure 3c). The reactivity of silica-supported gold nanoparticles decorated with *trans*-azobenzene is blocked by the encapsulation of the azobenzene moiety in cyclodextrin. However, UV light irradiation induces isomerisation to *cis*-azobenzene, resulting in the release of the cyclodextrin, thereby unblocking the catalytic sites of the nanoparticle. The active nanoparticle is able to catalyse the reduction of toxic ROS, such as hydrogen peroxide into water and oxygen (Figure 6). Using sodium ascorbate (NaAsc)

as a reducing agent, both endogenous ROS and exogenous H_2O_2 levels could be lowered in MCF-7 human breast cancer cells after incubation of the nanoparticle and irradiation with UV light. The ROS level could even be controlled by varying the length of irradiation time.[12] This control over catalyst activation is important for maintaining cell viability and metabolic balance.

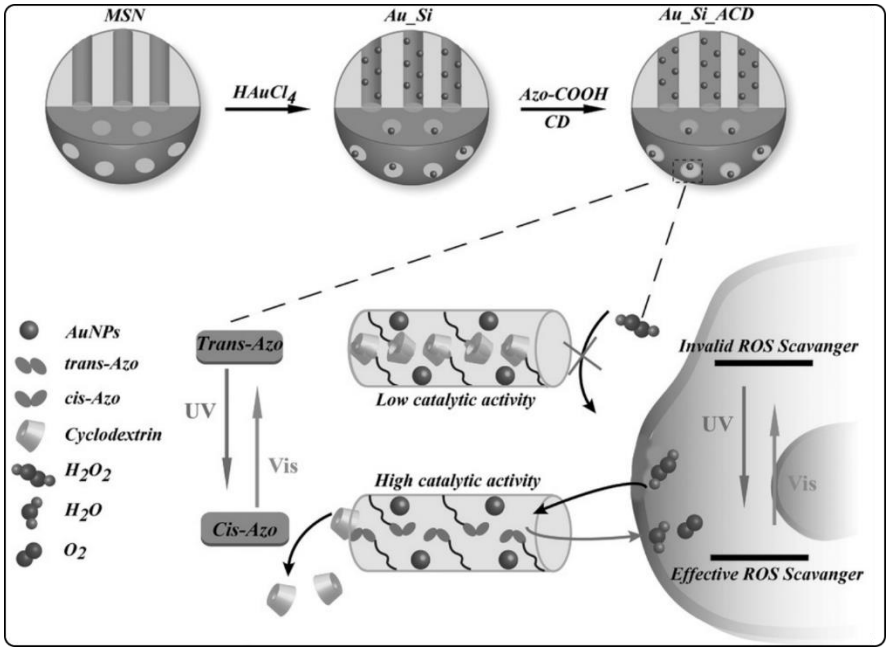

Figure 6. Preparation of the gold nanoparticles: 1. mesoporous silica (MSN) was used as the support for gold nanoparticles (Au_Si) 2. the surface of MSN was then decorated with *trans*-azobenzene, to which cyclodextrin was bound (Au_Si_ACD). When the cyclodextrin is bound, the gold displays low catalytic activity towards the reduction of H_2O_2. Irradiation of the particles with UV light induced isomerisation to *cis*-azobenzene which results in the expulsion of cyclodextrin, and the gold nanoparticles are then able to efficiently catalyse the reduction of H_2O_2. Figure adapted from ref 12.

A photoreduction reaction has been used to activate a prodrug in cells. Gold nanoclusters were synthesised which perform similar reduction chemistry to the endogenous enzyme, nitroreductase (Figure 3d). Here, instead of being a poison, glutathione is actually required for the reaction: using light and glutathione and the electron source, the nanoclusters were able to reduce nitrobenzene to aniline. As a proof of concept, the reducing ability of the nanoclusters was first tested in A549 cells and HeLa human cervical cancer cells using the switch-on of fluorescence following the reduction of a non-fluorescent Bodipy-labelled nitrobenzene. The reaction was then applied to the reduction of an arylnitrate prodrug, CB1954, whereby upon irradiation the cell survival rate was reduced to <40%.[13]

Catalytic azide reduction to form amines is another tactic to switch-on fluorescence (Figure 3e). Currently the only iron complex to have been used *in vivo*, an Fe(III) porphyrin complex, [Fe(TPP)Cl], was used by Meggers *et al*. to catalytically reduce aryl azides, using a cellular thiol, L-cysteine, as reducing agent. The uncaging of bisazide-protected rhodamine 110 appeared to be successful in HeLa cells, with 10 mol% of the catalyst resulting in a 28-fold increase in fluorescence in just 10 minutes. However, when the same reaction was applied in

nematodes and zebrafish, a fluorescence signal increase was observed in the absence of catalyst, with the addition of catalyst having no effect on the signal, demonstrating that the bisazide was able to be metabolically reduced without the need for a metal catalyst.[14] This illustrates the complexity of biological systems, as in-cell reactivity does not always translate to whole, multicellular organisms.

In an alternative strategy to achieve azide reduction, Winssigner *et al*. have developed ruthenium (II) artificial metalloenzymes (ArMs) to photocatalytically reduce azides under biological conditions. Both the catalyst, $[Ru(bpy)_2(phen)]$, and azide-protected rhodamine were attached to biotin via linkers, and both were docked inside an oligomeric receptor, in order to bring the catalyst and substrate in close proximity (Figure 7). The selected target protein, acetyl CoA carboxylase (ACC), is a biotin-binding multicomponent protein found in *P. aeruginosa*, a pathogenic bacteria which does not contain streptavidin. Although the reaction requires stoichiometric amounts of sodium ascorbate to act as a reducing agent, it appeared that the cellular environment is sufficiently reducing to allow the reaction to proceed in the absence of sodium ascorbate, presumably by making use of NADH, with an 8-fold increase in fluorescence observed after irradiation with blue light. Following the success in bacteria, the system was also applied in MCF-7 cancer cells.[15] The system was expanded to different proteins and docking moieties, to uncage a quinazolinone-based precipitating dye (QPD). Extracellular catalysis was achieved by linking the catalyst to a covalent inhibitor for a membrane-associated tyrosine kinase receptor (EGFR), which was transfected onto HEK293T human embryonic kidney cells. After incubation of the cells with the inhibitor-dye conjugate and the azide-protected dye, and blue light irradiation, increased levels of fluorescence were observed centred around the membrane, indicating localised activation of the dye. Intracellular catalysis was then achieved by linking the catalyst to raloxifene, an oestrogen receptor-agonist, which binds to the oestrogen receptor in MCF-7 cells. Activation of the dye was observed localised in the nucleus.[16]

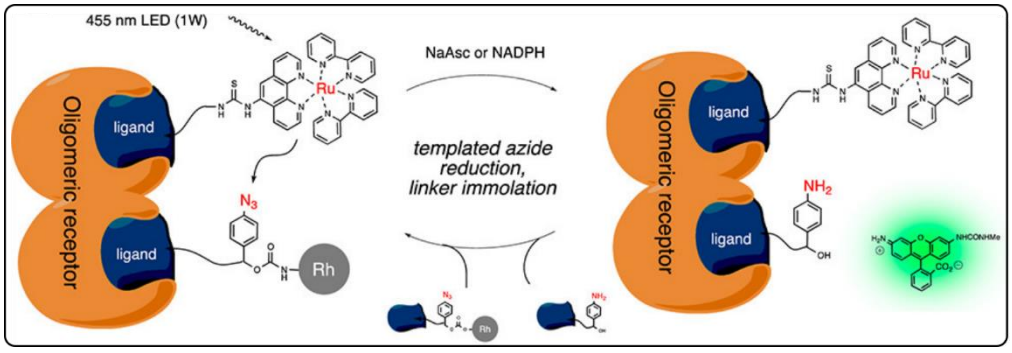

Figure 7. Schematic representation of both the artificial metalloenzyme with ruthenium photocatalyst and azide-protected rhodamine docked inside the protein. Following irradiation with blue light the ruthenium catalyst reduces the azide to an amine, which then cleaves and activates the rhodamine. Figure adapted from ref 15.

The photocatalytic ruthenium artificial metalloenzyme model was modified to make use of azide reduction for the application of labelling micro RNA (miRNA). Instead of docking the catalyst in a protein, the catalyst and the dye were bound to peptide nucleic acid (PNA)

strands, an artificial polymer which is similar DNA or RNA, where the backbone is comprised of *N*-(2-aminoethyl)-glycine units linked by peptide bonds. The PNA binds to base-matched miRNA, bringing the dye and the catalyst together, and reduction of an aryl azide within the dye linker releases a rhodamine-based dye (Figure 8). This reaction was carried out in BT474 human breast cancer cells which display a high expression of the corresponding miRNA. Either sodium ascorbate or NADH can be used as the reducing agent for this reaction, although fluorescence was observed in the cells without the addition of an external reducing agent, which indicates that endogenous levels of NADH are suitable for the reaction.[17] Finally, the reaction was also carried out in zebrafish embryos, in the first example of *in vivo* miRNA detection.[18]

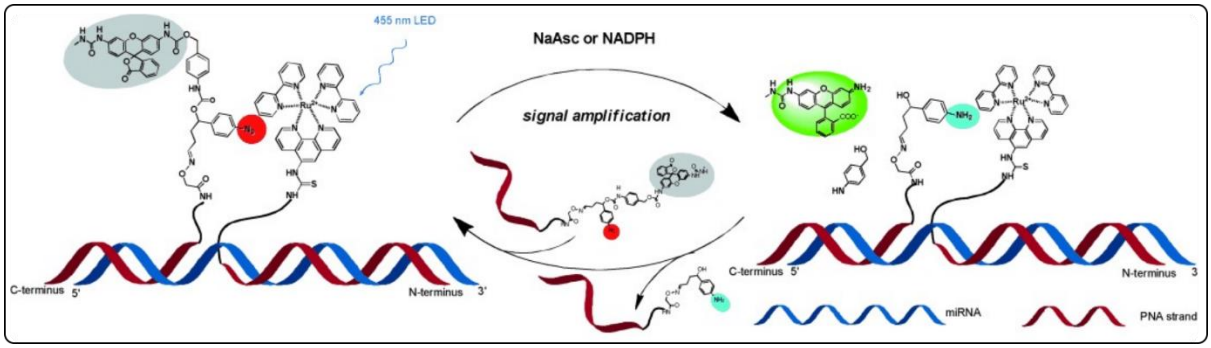

Figure 8. Schematic representation of the miRNA-templated azide reduction. The ruthenium photocatalyst and the azide-protected rhodamine are bound to PNA, which binds to the miRNA. The ruthenium photocatalyst reduces the azide to an amine following irradiation with blue light, which releases the activated rhodamine. Figure adapted from ref 17.

A recent example of *in vivo* photocatalytic azide reduction was used both concurrently and in tandem with an endogenous enzyme. A $Ru(bpy)_3$ catalyst incorporated within a single chain nanoparticle (SCNP) was able to photocatalytically activate azide-protected rhodamine 110 in the cytosol of HeLa cells (Figure 9). The compatibility of the Ru-SCNP with *β*-galactosidase (*β*-Gal), an enzyme which catalyses the hydrolysis of *β*-galactosides, was investigated in HeLa cell lysates. Both the Ru-SCNP and *β*-Gal were combined in the presence of two profluorophores and sodium ascorbate, then irradiated with blue light. The Ru-SCNP uncaged rhodamine 110 with an 84% yield, and the *β*-Gal produced a hydroxycoumarin derivative with 95%. Having established the orthogonality of both reactions, the Ru-SCNP was then bound to the *β*-Gal, and the complex was delivered into HeLa cells. Concurrent *in vivo* reactions were carried out for profluorophore activation, again with high yields of 83% and 90% for rhodamine 110 and hydroxycoumarin respectively; as well as for the deprotection of anticancer drugs doxorubicin and combretastatin, where increased cell death was observed when both drugs were uncaged at the same time compared to individually. Finally, the Ru-SCNP–*β*-Gal complex was used to carry out tandem reactions to synthesise hydroxycoumarin. Photocatalytic azide reduction to produce a galactose-protected intermediate could then be converted into hydroxycoumarin in cell lysates with around 20% conversion after only 10 min. Although the tandem reaction was unsuccessful in live HeLa cells, possibly due to substrate cell permeability, it was found to occur in *E. coli*.[19] This is a remarkable example of performing complex reactivity with artificial systems, even within an exceedingly complex biological setting.

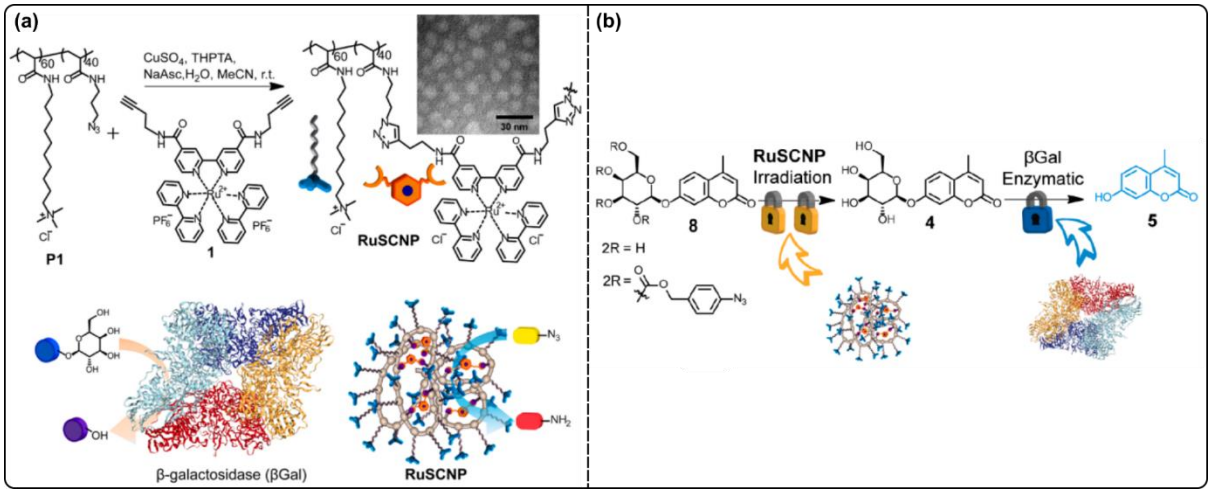

Figure 9. (a) Structure and synthesis of the Ru-SCNP. The water soluble polymer P1 is intramolecularly cross-linked to the ruthenium photocatalyst using a CuAAC reaction. (b) Ru-SCNP-*β*-Gal tandem reaction which generates hydroxycoumarin. Figure adapted from ref 19.

TRANSFER HYDROGENATION

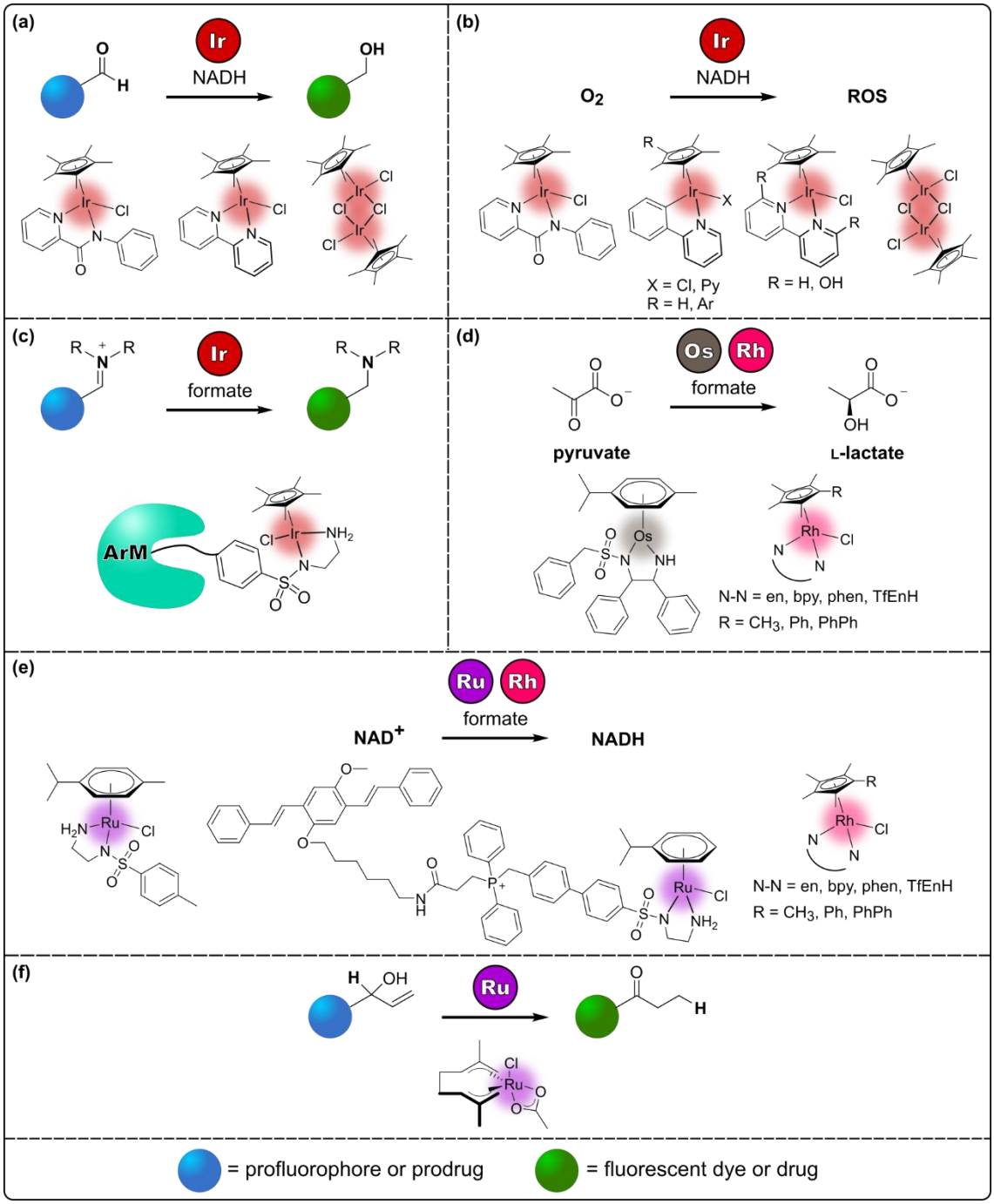

Figure 10. Overview of the transfer hydrogenation reactions carried out in cells. (a) Iridium catalysed hydride transfer from NADH to aldehydes to give alcohols (refs 20–21). (b) Iridium catalysed hydride transfer from NADH to oxygen to give ROS (refs 22–23). (c) Iridium catalysed hydride transfer from formate to imines to give amines (ref 24). (d) Osmium and rhodium catalysed hydride transfer from formate to pyruvate to give lactate (refs 29–31). (e) Ruthenium and rhodium catalysed hydride transfer from formate to NAD^+ to give NADH (refs 27–28). (f) Ruthenium catalysed intramolecular hydride transfer of allyl alcohols to give aldehydes (ref 32).

Transfer hydrogenation is a popular chemical transformation used inside living cells, and is commonly catalysed by iridium piano-stool complexes (Figure 10a). These type of Ir(III) complex have been used for the hydrogenation of aldehydes or ketones to alcohols, using NADH as the hydride source. Although this reaction is water and air tolerant, the efficacy of the reaction is very much dependent on the presence of various biomolecules. The conversion of benzaldehyde to benzyl alcohol using NADH as the hydride source is catalysed by a [Cp*Ir(N-phenyl-2-pyridinecarboxamidate)Cl] complex with high yields of up to 81–91%. Good yields of 61–77% are still obtained in the presence of glucose and ascorbic acid, and the presence of adenine lowers the yield to a modest 44%. However, thiols have a major inhibitory effect, due to coordination to the metal centre, with 1.0 mM of glutathione decreasing the yield to just 3%. Nevertheless, benzaldehyde is able to undergo reduction to benzyl alcohol in cell culture media (RPMI-1640 or M199) with modest yields of ~40–50%.[20] The catalytic activity of Ir(III) complexes for the reduction of aldehydes was then applied inside cells. Using a Bodipy-based probe, iridium complexes were used to reduce an aldehyde (Bodipy-CHO) to a fluorescent alcohol (Bodipy-OH), with NADH used as the hydride source. Although the reaction only gave a modest 20% yield in control reactions in the lab, it was carried out in the cytoplasm of NIH-3T3 mouse embryo fibroblast cells. Even though the probe was incubated with a huge catalyst loading of 66 mol%, only a 1.6-fold increase in fluorescence was observed, whereas when the Bodipy-OH probe was administered alone the fluorescence change was 2.2 fold, indicating that full conversion to the product was not achieved by the catalyst.[21]

Transfer hydrogenation from NADH to oxygen has also been demonstrated in cancer cells, in order to induce cell death (Figure 10b). This reactivity was first reported for cyclometallated iridium complexes. After incubation in A2780 human ovarian cancer cells, a decrease in cell proliferation was observed. This was attributed to catalytic hydrogen transfer from NADH to oxygen, as a large increase in ROS and peroxides (x 1230 and x 700 respectively) was observed. Not surprisingly, the presence of glutathione was found to deactivate the complexes.[22] A series of similar Ir(III) complexes were then used as a co-medicine in combination with cisplatin and carboplatin to enhance cancer cell death. When the metal complexes are incubated in cancer cells, the iridium catalyst converts NADH to NAD^+. The change in this ratio chemosensitises the cancer cells to the platinum drugs, which increases their efficacy. The iridium–hydride complex can then close the catalytic cycle by generating peroxides and other ROS from O_2, inducing oxygen oxidative stress in the cell. Co-administering the iridium catalyst with the platinum complex appears to exhibit cytotoxicity even in platinum-resistant cancer cell lines.[23]

Finally, iridium complexes have also been used for transfer hydrogenation reactions using an alternative hydride source (Figure 10c). Ward *et al.* exploited the low levels of glutathione in the periplasm of *E. coli* to achieve good catalytic activity for their artificial transfer hydrogenation metalloenzyme. Following overexpression of streptavidin in the periplasm, a biotinylated iridium complex was docked inside the protein.[24] Streptavidin is a protein which has an astonishingly high affinity for biotin, a small vitamin. Streptavidin has four binding sites which bind biotin with hydrogen bonding and van der Waals interactions. This binding is one of the strongest non-covalent interactions found in nature, and is much

stronger than typical protein-ligand interactions.[25] This therefore makes streptavidin a highly useful as a host for the generation of artificial metalloenzymes, as biotinylated metal complexes are able to be docked within the protein with great ease. As a convenient handle to monitor the reaction, transfer hydrogenation of a self-immolative substrate using formate as the hydride source was attempted.[24] Self-immolative groups provide a means for prodrug activation. A protective capping group is covalently linked to a spacer group, which is in turn covalently attached to the drug. Upon activation, the protective capping group is cleaved, which in turn leads to the spontaneous cleavage of the spacer group, leaving behind the active drug.[26] Here, transfer hydrogenation by the artificial metalloenzyme triggers self-immolation to release a coumarin dye (Figure 11). Initial results indicated that even the low levels of periplasmic glutathione was not enough to prevent catalysis inhibition, as less than 4% conversion was detected. In order to even further lower the levels of glutathione, [Cu(gly)$_2$], a Cu(II) complex known to catalyse the oxidation of glutathione, was added. Now, in the glutathione-free periplasm, the artificial metalloenzyme was able to catalyse the reaction with a respectable yield of 33%, and a TON of 137.[24]

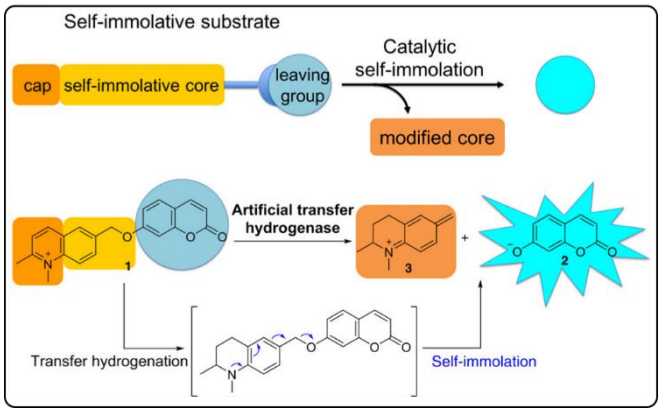

Figure 11. A protected coumarin substrate which undergoes a transfer hydrogenation reaction catalysed by the artificial transfer hydrogenase. The product of the transfer hydrogenation undergoes self-immolation to release activated coumarin. Figure adapted from ref 24.

Using ruthenium (II) Noyori-type catalysts, formate has also been used as a hydride source to catalyse the reduction of NAD^+ to NADH (Figure 10e). Sadler *et al.* investigated a wide range of ruthenium complexes, varying both the arene and bidentate substituents. With the goal of inducing cell death in cancer cells by altering the NAD^+/NADH ratio, the catalysts were incubated in A2748 cells along with formate. The best catalyst, [(*p*-cym)Ru(TsEn)Cl], exhibited a decrease in cell survival from 69% to just 1%. This decrease in cell viability was due to the catalytic reduction of NAD^+, with the NAD^+/NADH ratio decreasing from 4.78 to 0.74, giving an apparent turnover frequency of 0.19 ± 0.01 h^{-1}. Although the ruthenium–hydride complex was able to react with NAD^+, the authors also note that it is likely that it may also be reducing other biomolecules which are present, such as ketones and imines.[27] The intracellular NAD^+/NADH ratio was also altered by an oligo(*p*-phenylenevinylene) Ru(II) complex (OVP-Ru). In water, the complexes self-assemble into a nanoparticle through π–π stacking and hydrophobic interactions between the backbones (Figure 12). The linker contains a triphenylphosphine moiety to give the aggregate mitochondrial targeting properties. Indeed

initially the nanoparticles were localised in the mitochondria of A2780 cancer cells, but then after 24 h they had distributed in lysosomes. When formate was incubated in the cells along with the nanoparticles, the NAD^+/NADH ratio decreased by around 20% after 2 h, although by 24 h there was no difference between the blank cells and the OVP-Ru/formate cells, which the authors attribute to the fact that catalysis cannot proceed inside the lysosome. They also note that in the absence of formate, OVP-Ru still induces an 11% decrease in the NAD^+/NADH ratio, implying that endogenous reductants can also serve as a hydrogen source.[28]

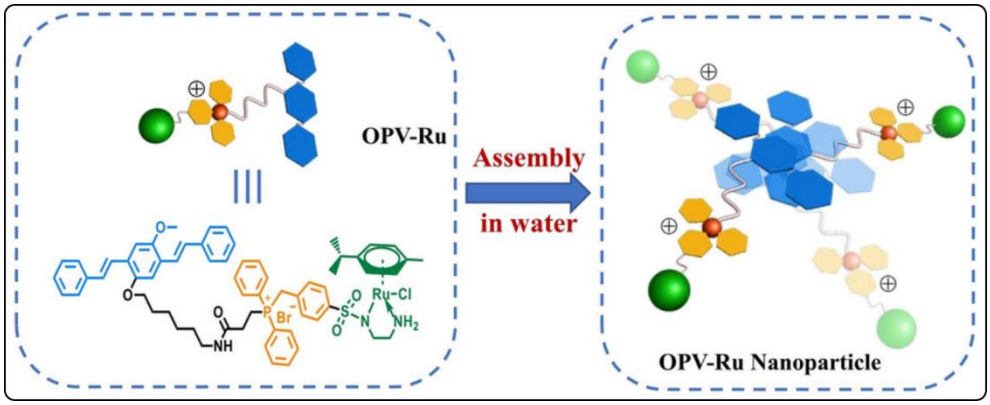

Figure 12. Schematic representation of the self-assembly of OPV-Ru complexes to generate a nanoparticle. Figure adapted from ref 28.

Other metals are also able to catalyse the transfer hydrogenation reaction in living cells. Sadler *et al*. have demonstrated the use of rhodium and osmium *in vivo*. Rh(III) half-sandwich complexes were found to be active for the reduction of NAD^+ to NADH, and the reduction of pyruvate to lactate, using formate as the hydride source. The activity of the complexes towards altering the NAD^+/NADH ratio was investigated in A2780 cancer cells. Although control experiments in the lab showed that the complexes can reduce pyruvate as well as NAD^+, both of which are endogenous to cells, competition experiments indicated that there was a preference for NAD^+, with pyruvate only being reduced after NAD^+ levels became very low. In spite of this, it is still very plausible that the transfer hydrogenation activity is not specific to NAD^+ in cells. Nevertheless, redox disruption in the cells led to decreases in cell survival of up to 50%. The catalytic activity of the rhodium complexes in control experiments was greater than for previously reported ruthenium catalysts; however, the antiproliferative activity (the ability of a compound to inhibit cell growth) in cells was less, with few turnover numbers achieved by the rhodium complexes. This was attributed to the fact that because rhodium is more reactive, it is also more susceptible to poisoning.[29]

Although rhodium complexes preferentially reduced NAD^+, a chiral osmium (II) complex was found to successfully carry out the asymmetric reduction of pyruvate to lactate using formate as a hydride source in living cells (Figure 10d). The *R*,*R* and *S*,*S* complexes produced L-lactate and D-lactate respectively with 83% e.e.. The reduction was carried out in A2780 cancer cells; the significant decrease in cell proliferation of around 85% was independent of the enantiomer of the complex used, although the enantioselectivity was maintained *in vivo*, and the activity of the catalyst was estimated to carry out around 13 TONs.

The precise reason for the cell death is not clear, as up to 2 mM concentrations of either enantiomer of lactate are non-toxic, implying that the lactate production is unlikely to be the source of cell death, although perturbing local concentrations may still have an knock-on effect for other cell pathways. Furthermore the specificity of the osmium complex was unknown, meaning that other unsaturated endogenous substrates may be targeted as well.[30] In order to gain more insight into the system, the authors went on to investigate the intracellular stability of the complex. A brominated analogue of the complex was synthesised, which was shown to have the same reactivity and properties as the original complex. It was then possible to follow the brominated complex in cells using a combination of inductively coupled plasma mass spectrometry (ICP-MS) and nanoscale synchrotron X-ray fluorescence (XRF) mapping in order to gain insight into the cellular uptake and mechanism of the complex. From these analyses it was deduced that the catalyst is in fact degraded within cancer cells, by transport into acidic lysosomes followed by reaction with cellular thiols. They then determined that the ligand was detached from the osmium centre, and transported into the nucleus, without the osmium.[31] While not usually done, such studies are vitally important to gain understanding of what are the causes of catalyst inhibition in cells, in order to be able to better develop more robust catalytic systems.

Finally, a redox neutral intramolecular hydride transfer reactions has been explored for a Ru(IV) complex *in vivo* (Figure 10f). A ruthenium bis-allyl complex has been used for the isomerisation of allyl alcohols to ketones. Analogous to the previous transfer hydrogenation reactions, a metal-hydride intermediate is required for intramolecular hydride transfer. This reaction displayed good bioorthogonality, with high yields of 79–91% observed for a range of aromatic and aliphatic substrates in the presence of cell lysates. This good reactivity was also observed in HeLa, A549, and Vero monkey kidney epithelial cells, as indicated by large increases in fluorescence intensity for the synthesis of a naphthalene-based dye. The reaction was even quantified by liquid chromatography mass spectrometry (LC-MS) analysis of methanolic extracts of the cells, revealing a calculated TON of 22.4 for 10 mol% of ruthenium complex. This isomerisation reaction was then used to generate GSH-depleting compounds. A decrease in the intracellular glutathione concentration was observed after the ruthenium catalysed formation of α,β-unsaturated ketones, by exploiting their Michael type reactivity towards thiols. Using 50 mol% of catalyst in HeLa cells along with the bis-allyl substrate saw a 40% decrease of glutathione levels.[32] The success of this example *in vivo* is extremely promising for this new reactivity to be further explored in biological settings.

Bond Cleavage Reactions

Cleavage of Terminal Groups

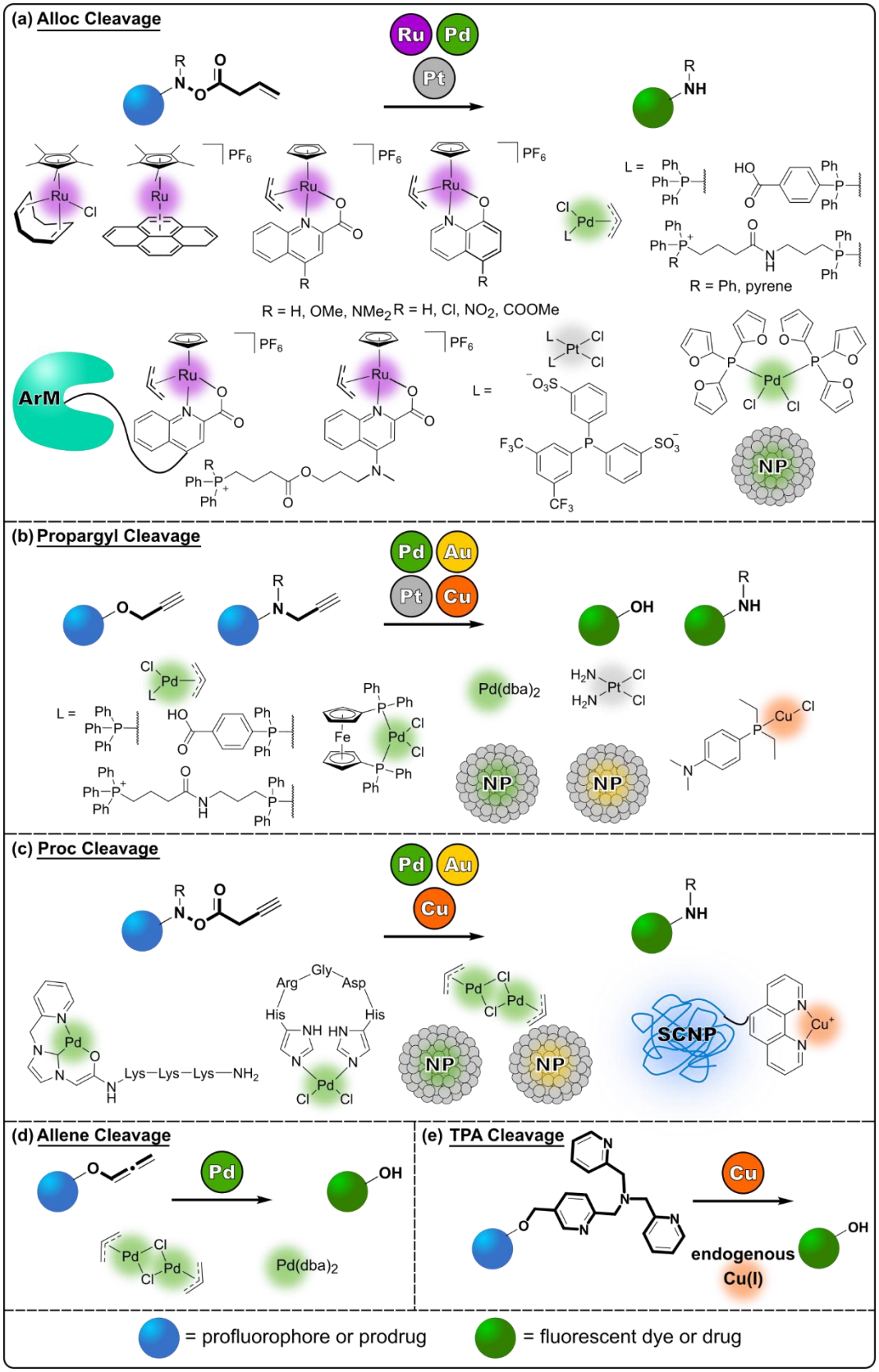

Figure 13. Overview of catalytic cleavage of terminal groups carried out in cells. (a) Ruthenium, palladium, and platinum catalysed alloc cleavage (refs 33–47). (b) Palladium, gold, platinum, and copper catalysed propargyl cleavage (refs 43, 48–56). (c) Palladium, gold, and copper catalysed proc cleavage (refs 57–61). (d) Palladium catalysed allene cleavage (ref 62). (e) Copper catalysed TPA cleavage (refs 63–64).

Many of the early examples of *in vivo* transition metal catalysed reactions are deprotection reactions, whereby a small, terminal, protecting group is cleaved from the substrate. The desired property of the compound is then switched-on upon cleaving of the protecting group. Such reactions are useful for catalysis proof of concept, where deprotecting a profluorophore provides an easy method of monitoring the catalysis, by simply looking for an increase in fluorescence intensity. In addition, developing a range of deprotection reactions provides new possibilities for prodrug activation. While such reactions are dominated by ruthenium and palladium catalysts, examples with gold, platinum, and copper are also known.

The [Cp*Ru(cod)Cl] complex has been used by several groups for *in vivo* allyloxycarbonyl (alloc) cleavage, whereby an allylcarbamate group is cleaved to produce either an amine or alcohol (Figure 13a). However, it was first utilised by Meggers *et al*. to produce amines. Not only is the reaction tolerant to air and water, but it was found to require the presence of thiols in water. The catalyst was found to deprotect rhodamine 110 inside HeLa cells with 80% yield, although 20 mol% of the complex was required, giving a very modest TON of 4.[33] Building on this work, Mascareñas *et al.* used the same catalytic system for the deprotection of DNA-binding agents in CEF chicken embryo fibroblast cells and Vero cells. The DNA-binders displayed protection-dependent spectroscopic properties, providing a handle to determine successful catalysis. Low amounts of fluorescence corresponding to the protected binders was observed, while high levels of fluorescence was observed following incubation with the catalyst, indicating that efficient catalysis took place, although quantification of the reaction was not provided.[34] The catalyst has also been deployed for controlled localised profluorophore activation, as well as localised prodrug activation. Rotello *et al*. deposited the catalyst in between decorative monolayers on a gold nanoparticle to create a nanozyme (Figure 14). Nanoparticles decorated with cationic ammonium groups were able to penetrate the cell membrane, while zwitterionic nanoparticles remained extracellular, resulting in the concurrent, spatially controlled alloc deprotection of two different profluorophores, rhodamine 110 and resorufin, inside and outside of HeLa cells respectively. In addition, the nanoparticles were used to deprotect an anticancer prodrug, alloc-doxorubicin, in and outside HeLa cells. Successful deprotection was indicated by a decrease in cell viability, although the observed cell viability was not as low as for doxorubicin alone, indicating that full deprotection was not obtained.[35]

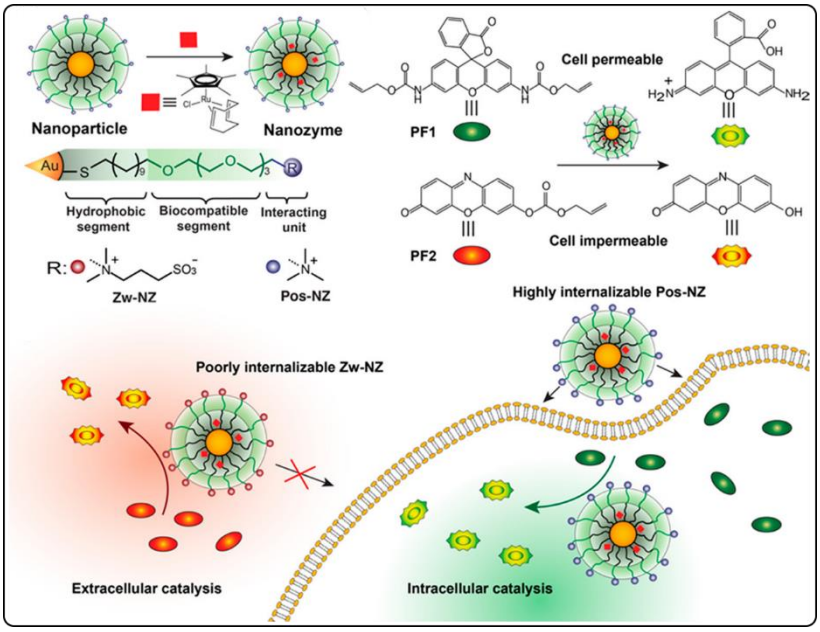

Figure 14. Schematic representation of the gold nanozyme containing the ruthenium catalyst. The zwitterionic nanozymes are cell impermeable and undergo catalysis in the extracellular space, while the positive nanozymes are cell permeable and are able to carry out catalysis inside the cell. Figure adapted from ref 35.

Also with a goal towards spatial control, Meggers *et al*. investigated a photoactivated version of the catalyst, [Cp*Ru(η^6-pyrene)](PF_6). Following irradiation with UV light, the pyrene moiety dissociates from the ruthenium, and the resultant complex can catalyse the deprotection of rhodamine 110. The reaction was carried out in HeLa cells, and resulted in a 70-fold increase in fluorescence intensity, indicating that catalysis was successful.[36] However the authors made no comment on the viability of the cells, as UV light is harmful to living cells, so although this example is a good proof of concept for light activation of a catalyst, for any potential application for drug activation, for example, the catalyst would need to be modified so that it would be activated by visible light instead.

Several Tsuji-Trost catalyst derivatives have been shown to successfully cleave alloc groups. Wender *et al*. showed that a methoxy derivative of the catalyst could deprotect alloc-caged aminoluciferen in biological media with moderate yields of 40–49%. However, when the reaction was attempted in 4T1 mouse mammary carcinoma cells, while catalytic deprotection was observed, it was shown that it had taken place extracellularly, as no fluorescence was observed when the cells were washed with phosphate buffered saline solution (PBS) after incubation with the catalyst.[37] While this indicated that this methoxy catalyst displayed poor cell penetrating properties, Meggers *et al*. used ester and amine derivatives of the complex in order to be able to use the catalyst intracellularly in HeLa cells. When 20 mol% of the amine derivative was used in cells, catalytic deprotection of rhodamine 110 was observed by a 130-fold increase in fluorescence intensity within the cytoplasm. Under the same conditions the anticancer drug doxorubicin was also activated, as seen by a decrease in cell viability, although only around 10% of the prodrug was activated.[38] In contrast, the ester derivative showed excellent activity under biological conditions, with high turnover numbers

of >300 and faster reaction rates of 580 $M^{-1}s^{-1}$, and its activity towards doxorubicin activation in HeLa cells was increased 10-fold.[39] The catalyst scaffold was further functionalised with a mitochondria-targeting moiety by Mascareñas *et al*. The presence of a cationic phosphonium group is required for accumulation within the mitochondria; however, this appears to make it a less active catalyst, as rhodamine 110 deprotection in water had a yield of only 14.2%, and in the presence of lysates it was barely active, with just 0.2% yield. Even so, the complex was used for the activation of 2,4-dinitrophenol (DNP), a compound known to decrease the mitochondrial membrane potential and switch off ATP production, in HeLa and Vero cells, and indeed activation of the compound appeared to take place, by an observed decrease in the mitochondrial membrane potential.[40]

Biotinylated derivatives of this catalyst have also been used by Ward *et al.* to generate an artificial metalloenzyme, by docking the catalyst inside streptavidin. The artificial allylic deallylase was anchored on the cell surface of *C. reinhardtii* and used to catalyse the activation of an aminocoumarin. Although in control experiments in the lab the isolated artificial metalloenzyme was able to efficiently carry out the reaction with an excellent yield of 81%, the on cell labelling yield was just 4%.[41] A cell-penetrating analogue of this artificial metalloenzyme was developed for intracellular catalysis in various mammalian cells, where a fluorescent cell-penetrating polymer was also docked inside streptavidin along with the catalyst. In this case, the artificial metalloenzyme was used to regulate a gene switch: catalytic alloc cleavage generated the thyroid hormone T_3, which upregulates a gene circuit that leads to the production of bioluminescent reporter (Figure 15), providing an elegant way by which the catalysis can be monitored; indeed, increased luminescence intensities were observed in the presence of ruthenium catalyst, with better activity seen for the artificial metalloenzyme than for the free catalyst alone.[42]

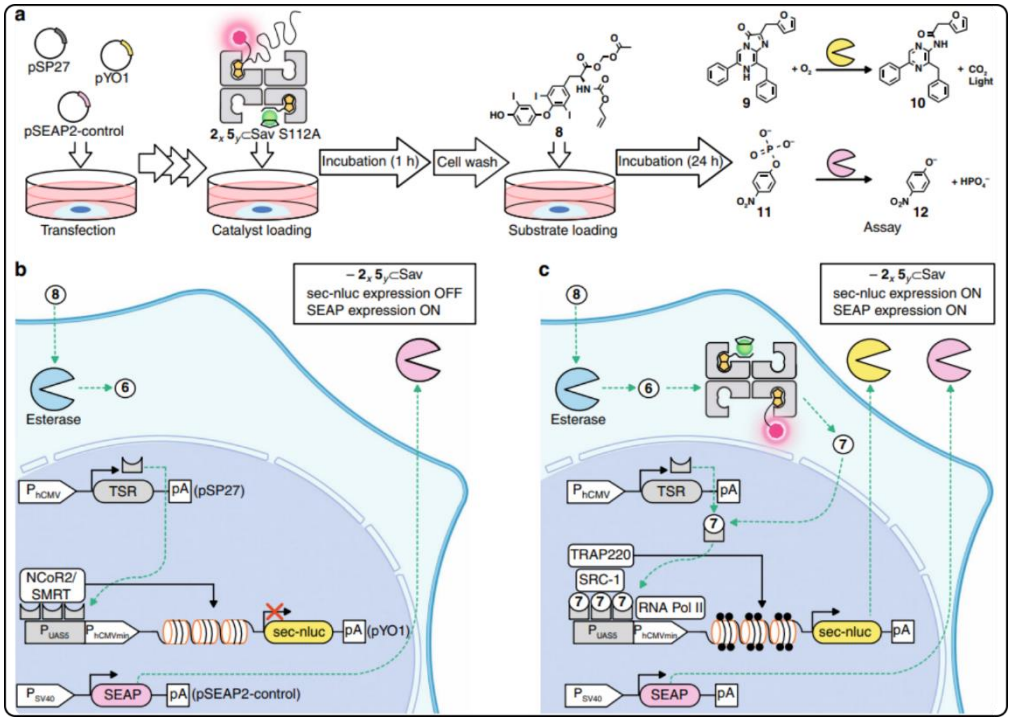

Figure 15. Schematic representation of the ArM catalysed deprotection reaction which regulates a gene switch. After transfection of the cells with the appropriate genes, the cells were incubated with the ArM followed by the alloc-protected substrate. The substrate is first hydrolysed by an esterase. In the absence of catalyst, T_3 remains protected by the alloc group, and cannot promote gene expression of sec-nluc. In the presence of the ArM the alloc group is cleaved to generate T_3, which triggers the gene expression of sec-nluc. Only when sec-nluc is expressed is the bioluminescent reporter produced. Therefore fluorescence is only observed in the presence of the ArM. In both cases the expression of SEAP was monitored as a control. Figure adapted from ref 42.

While molecular ruthenium catalysts are popular for this uncaging reaction, palladium catalysts are also widely used. Phosphine ligand-containing Pd(II) allyl complexes were used by Mascareñas *et al*. in combination with reducing agents, in order to generate the active Pd(0) species *in situ*. Both sodium ascorbate and glutathione were tested as additives: it was found that catalytic alloc deprotection in the presence of glutathione showed the best activity, with a yield of 94% in water, and a moderate yield of 33% in cell lysates. The catalytic system also proved to work in HeLa cells, with increased fluorescence observed after the deprotection of rhodamine 110.[43] Enhancement of catalytic activity in the presence of glutathione was also observed for Pd(0) microspheres, where palladium nanoparticles were entrapped within cross-linked resin beads. The microspheres' activity was investigated in HeLa cells by observing a fluorescence increase following rhodamine 110 deprotection, and by a cytotoxicity increase following the activation of an alloc-protected prodrug of amsacrine, an antineoplastic agent.[44, 45]

There are even some examples of this deprotection reaction catalysed by a palladium species taking place in live mice. A Pd(II) precatalyst, $PdCl_2(TFP)_2$ (TFP = tri-2-furylphosphine), encapsulated inside a poly(lactic-*co*-glycolic acid)-polyethyleneglycol (PLGA-PEG) nanoparticle (NP) was shown to display good catalytic activity, after *in situ*

reduction to the active Pd(0) species. The catalytic activity of the Pd-NP was demonstrated in cancer cells, with a >5000% fluorescence intensity increase after rhodamine deprotection; as well as a 340% intensity increase following an intramolecular Heck reaction to produce an aminocoumarin derivative. Encapsulating the catalyst within the nanoparticle has the double benefit of improving stability towards biological components, as well as improving intracellular uptake. In mice, safe, selective accumulation of the particle was observed within tumours compared to other organs. Within the live mice, the particles could be used to image the tumours, by catalytically deprotecting rhodamine 110. Finally, the catalyst was able to activate the anticancer drug doxorubicin, with more than 50% drug activation within the tumours. This had the effect of blocking tumour growth within the mice, although high doses were required.[46] This catalytic system was further extended to the deprotection of monomethyl auristatin E (MMAE), a potent anticancer drug which targets microtubules. The drug was successfully deprotected in cancer cells, with a yield of over 90%, as determined by decrease in cell viability. The drug was then successfully activated inside live mice, resulting in temporary blocking of tumour growth.[47] This targeted deprotection is extremely useful, as MMAE is too toxic for general systemic administration, so targeted catalytic activation is an attractive solution to overcome this problem.

Palladium complexes are also particularly well suited to the deprotection of propargyl groups, to form amines and alcohols. With the intention of developing a palladium-sensing system which could be applied in living systems, a propargyl-protected fluorescein was synthesised which could be used a switch-on fluorescence system to detect the presence of palladium. In control reactions in the lab, the propargyl group was shown to be labile to species of all oxidation states of palladium. Moving into biological systems, 5 day old zebrafish were incubated with 20 μM of the probe, and as little as 5 μM of $PdCl_2$ resulted in fluorescence, indicating that the cleavage was successful.[48] A series of Pd(0) and Pd(II) allyl complexes have also been used for the deprotection of a profluorophore, in Vero cells. Even though in cell lysates the yield for the reaction was very low, in the Vero cells estimated average TONs of 5–10 were observed.[43]

Prodrugs can also be protected with this propargyl group. A discrete palladium complex deposited in between monolayers on a gold nanoparticle also catalyses the deprotection reaction (Figure 16). Here, catalysis is controlled by supramolecular strategies. Cucurbit[7]uril (CB[7]) binds to the terminal monolayers, and the steric hindrance inhibits catalysis. However, after addition of 1-adamantylamine (ADA) as a competitive guest, the CB[7] dissociates from the nanoparticle to bind the adamantylamine, and frees up space for the catalysis to take place. This Pd-NP system exhibited this gated catalytic behaviour in HeLa cells with prodrug activation. After 48 h, most of the anticancer compound 5-fluorouracil (5FU) was activated.[49] Alternatively, a simple $Pd(dba)_2$ complex applied in stoichiometric amounts was shown to activate NO-releasing prodrugs. Upon cleavage of the propargyl group, the free diazeniumdiolates spontaneously release NO, which is known to induce cell death. The antiproliferative activity of 1 μM of prodrug was analysed with and without the palladium complex in a variety of cell lines. A significant enhancement in antiproliferative activity was observed in the presence of 1 μM of palladium, although the authors also observed a small

improvement in the presence of only 0.25 μM, indicating that this reaction can occur catalytically. Control reactions with an NO-sensitive fluorophore showed that NO was produced in the presence of palladium, indicating that the mechanism of antiproliferation indeed occurred through deprotection of the propargyl group and subsequent liberation of NO.[50]

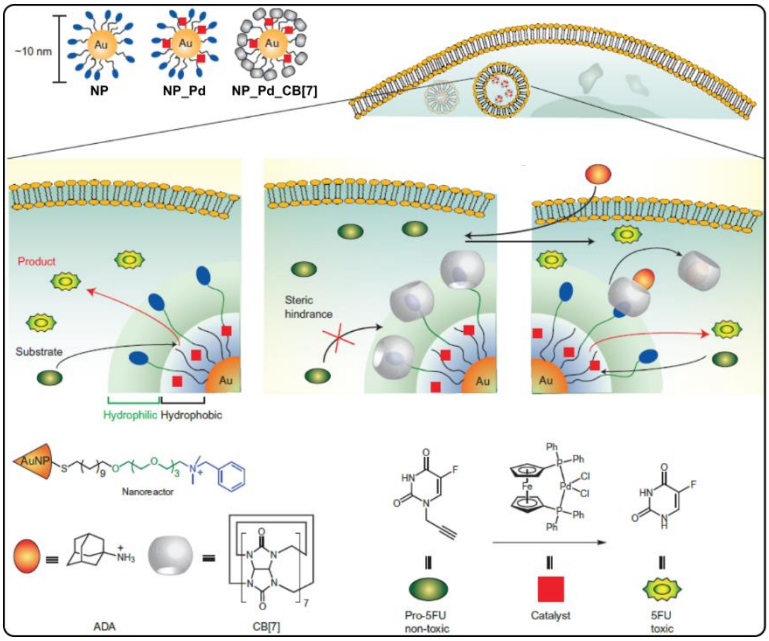

Figure 16. Schematic representation of the gold nanoparticle (NP) with the ruthenium catalyst deposited in between the monolayers (NP_Pd), and the monolayers capped with CB[7] (NP_Pd_CB[7]). NP_Pd is able to catalyst the activation of 5FU in cells. NP_Pd_CB[7] is unable to catalyse the transformation as steric hindrance prevents the substrate from reaching the catalyst. However, when ADA is added the CB[7] leaves the nanoparticle and instead binds the ADA, providing space for the catalysis to take place again. Figure adapted from ref 49.

Prodrugs have also been activated by nanoparticle systems. Pd^0-functionalised polyethylene glycol-polystyrene resins which are larger than human cells were designed for propargyl cleavage in extracellular space (Figure 17a). The propargyl-protected prodrug of 5FU was incubated with the Pd-resin in the presence of cancer cells. The antiproliferative activity and cytotoxicity observed were comparable to when the active drug 5FU was administered alone, indicating efficient deprotection by the Pd-resin. In addition, the bioorthogonality of the system was investigated in zebrafish embryos for the deprotection of rhodamine 110. Although fluorescence was observed in the area surrounding the Pd-resin in the yolk sac, fluorescence was also observed in the gastrointestinal system, which indicates that the profluorophore was activated by both the Pd-resin and by digestive enzymes, implying that *N*-Poc protected drugs would not be suitable for orally administered pharmaceuticals.[51] In a strategy to target cancer cells, palladium nanosheets were encapsulated inside exosomes derived from cancer cells (Pd-Exo) (Figure 17b). Exosomes, which are membrane-enclosed vesicles released by cells into extracellular space, are involved in the regulation of various physiological functions, and are involved in communication between cancer cells. Therefore by enclosing the palladium nanosheets in a cancer cell-derived exosome, the catalyst can be

delivered as a Trojan Horse to specific cancer cells. Catalytic activity of the Pd-Exo system was investigated for the activation of the propargyl-protected anticancer drug panobinostat, a pan-histone deacetylase inhibitor in cancer cells. Cells incubated with the prodrug and the Pd-Exo catalyst exhibited lower cell viability, confirming the catalytic activity of Pd-Exo in cells. This activity was found to be cell line-dependent, as exosomes derived from the same cell line as the cell in which the catalyst and prodrug are incubated showed good activity, but exosomes originating from different cell lines did not.[52]

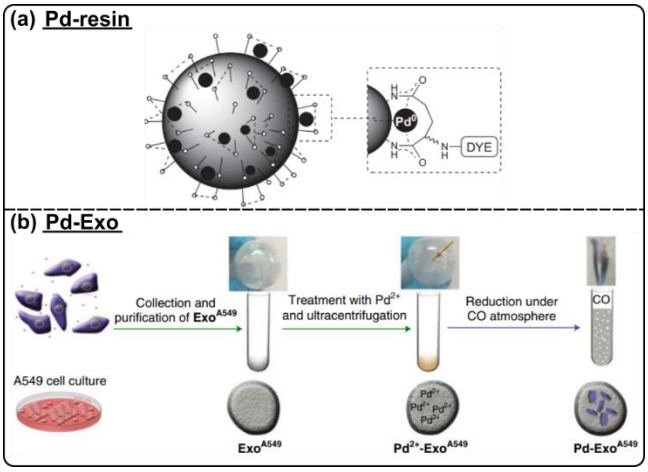

Figure 17. (a) Schematic representation of the Pd-resin. Adapted from ref 50. (b) Synthesis of the palladium nanosheets encapsulated within cancer cell derived exosomes (Pd-Exo). Exosomes were collected from A549 cancer cells, which were then treated with Pd^{2+}. The palladium nanosheets were then generated by reducing the Pd^{2+} under a CO atmosphere. Adapted from ref 52.

Gold nanoparticles have also shown profluorophore and prodrug propargyl deprotection. An Au-NP within a PEG-polystyrene resin ([Au]-resin) was investigated for its activity towards rhodamine 110 deprotection under biological conditions. It was found that small amounts of glutathione (≤50 μM) actually aided the reaction, by binding to the surface of the nanoparticle and activating the neighbouring alkyne, but at higher concentrations the glutathione inhibits reactivity by saturating the surface so that the alkyne cannot bind. The deprotection activity of the [Au]-resin was then investigated in A549 cells, for the activation of prodrugs of three anticancer compounds, floxuridine (FUdR), suberoylanilide hydroxamic acid (SAHA), and doxorubicin. For all three prodrugs, when administered in combination with the Au-resin, a decrease in cell viability was observed, confirming the catalytic activity *in vivo*. Finally, the biocompatibility of the Au-resin was investigated in the cranium of zebrafish embryos, with the deprotection of rhodamine 110. After implantation of one Au-resin bead and administration of the prodye, localised fluorescence surrounding the bead was observed, providing the first example of transition metal mediated catalysis in the brain of a living animal.[53] This Au-resin system was also shown to mediate propargyl cleavage from a novel prodrug of panobinostat. In PBS, 6 μM of the Au-resin was shown to cleanly convert a 200 μM solution of the prodrug into the active drug. Notably, palladium catalysts gave a mixture of products, which highlights the advantage of such a gold-based system. The authors then went on to demonstrate that not only does this deprotection reaction in A549 and U87 cells, but that the Au-resin can be recycled for multiple runs.[54]

Platinum has also been utilised as a deprotecting agent in cancer cells, with dual-action toxicity from both the released prodrug and from the active platinum complex itself (Figure 18). In this novel deprotection strategy, a propargyl-caged nitric-acid releasing prodrug is covalently linked to a "masked" Pt(IV) complex. This compound is stable and non-toxic in cancer cells; however, cancer cells reduce the platinum, resulting in the release cisplatin. The free cisplatin then induces cancer cell death through two mechanisms: it can enter the nucleus and platinate DNA; and it can catalyse the propargyl deprotection of the prodrug, which, upon activation, spontaneously releases two molecules of toxic NO. Since one molecule of cisplatin is released from every prodrug molecule, the platinum is present in stoichiometric amounts with respect to the prodrug activation. Although not catalytic, the platinum was successfully able to mediate prodrug activation in cancer A549 cells. Interestingly, the antiproliferative activity of the Pt-prodrug compound was much greater in cancer cells compared to human normal ovarian epithelial IOSE80 cells, with a selectivity factor of 518. This was attributed to the reducing environment of cancer cells being able to generate the cisplatin, whereas healthy cells the platinum is not reduced, and remains in its inactive Pt(IV) form. This selectivity was also observed in a xenograft zebrafish model, where the Pt-prodrug compound was shown to be stable *in vivo*, and only activated in the cancer cells.[55] Although conjugating 1 eq of metal complex to the prodrug results in only stoichiometric transformations rather than catalytic, the advantage of such a system is that the metal complex is always close by to the desired substrate, and administering the catalyst in its inactive form also prevents the complex from being inactivated by the cellular environment before reaching its target substrate or location. This is a good example of how *in situ* metal complex activation could be used to control the selective activation of anticancer prodrugs.

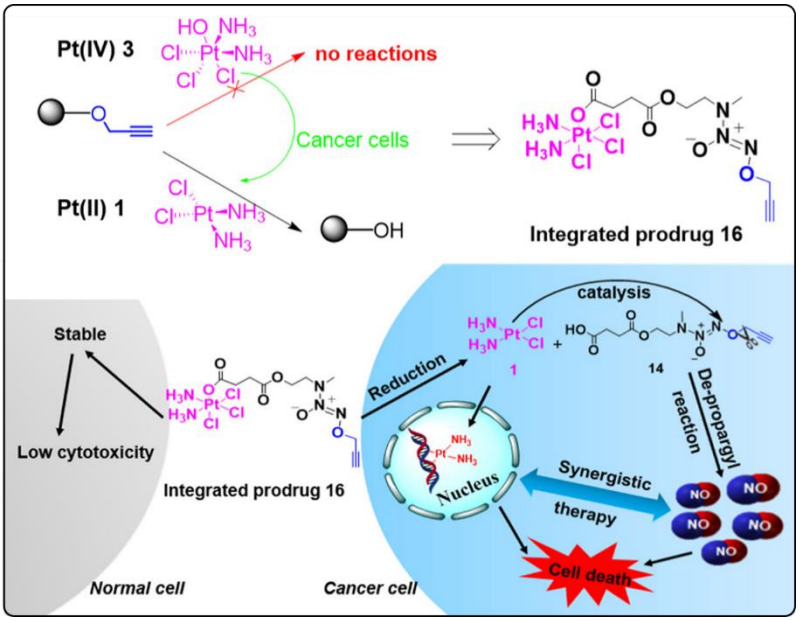

Figure 18. Dual-action toxicity of an NO-releasing prodrug bound to a platinum complex. In normal cells, the Pt(IV)-prodrug complex is stable and induces low levels of cytotoxicity. However the reductive environment of cancer cells is sufficient to reduce the Pt(IV) to Pt(II). This results in the release of cisplatin from the prodrug, which is then able to cleave the propargyl group. The activated drug then releases NO which induces cell death; in parallel, the cisplatin enters the nucleus and platinates DNA, which also induces cell death. Figure adapted from ref 55.

Although less widely used, copper also shows potential as a bond-cleavage mediator. In order to gain insight into the link between copper transporters and cisplatin resistance, platinum and copper were used to activate fluorophores so as to be able to carry out *in situ* imaging of platinum and copper distribution in cells. After a screening and optimisation of various ligands, it was found that a Pt-Danphos complex could efficiently deprotect allyl-protected Pittsburgh Green ether (APE), a fluorescein-based dye, under biological conditions, and a copper complex with 4-(diethylphosphanyl)-N,N-dimethylaniline ligand exhibited good activity towards a propargyl-protected analogue of the pro-fluorophore (PPE). Activation of APE by this platinum complex was then shown in cisplatin sensitive cells (HN30), and cisplatin resistant cells (HN30 R8). Following incubation of the probe with 40 eq of Danphos ligand and 0.4 eq of cisplatin, the observed fluorescence revealed that while the cisplatin-sensitive cells accumulate platinum throughout the entire cell, cisplatin-resistant cells accumulate overall less platinum, and is instead sequestered within lysosomes, which is why the cells do not experience toxicity. Incubation of the PPE probe with the 4-(diethylphosphanyl)-N,N-dimethylaniline ligand revealed that the endogenous levels of copper in cells was enough to turn on fluorescence; however there were no differences in copper distribution between the cisplatin sensitive and resistant cells, indicating that the platinum distribution in cisplatin-resistant cells is independent of copper distribution.[56] This research exemplifies the importance and applications of metal-mediated catalysis in the field of bio-imaging.

Another commonly used alkyne-containing terminal protecting group is the propargyloxycarbonyl (proc) group. Similar to the alloc protecting group, cleavage of the proc group generates an amine (Figure 13c) Pd(II) metallopeptides are known to catalyse the

cleavage. A carbene-based catalyst was connected to a cell-penetrating peptide, to make the complex able to enter PC-3 human prostate cancer cells. The catalyst was found to localise within the cytoplasm, which is expected for cationic peptides, but also within the nucleus. Once inside the cells the complex catalysed the deprotection of rhodamine 110, with flow cytometry analysis showing an increase in fluorescence intensity, indicating the formation of the fluorophore.[57] A bis(histidine) complex also made use of arginines to aid cell internalisation. Here, the palladium staples together two histidine residues on a small protein, inducing conformational strain on the peptide chain. The peptide complex catalyses the deprotection, while the free palladium source does not. The reaction is helped by the strained metal bridge, and the protein scaffold provides some protection against metal deactivation. The catalyst was able to catalyse the deprotection of fluorescent probes in a variety of cancer cells.[58]

Heterogeneous systems are also capable of proc cleavage to generate fluorophores. Chen *et al.* have reported the use of palladium nanoparticles and complexes for proc cleavage. A series of Pd(II), Pd(0), and Pd(IV) complexes were used for the catalytic deprotection of the amino acid lysine. Although the authors do not comment on the active catalytic species here, it has previously been reported that similar Pd(II) complexes readily form Pd nanoparticles under biological conditions, which leaves some ambiguity over whether or not the catalysis is truly carried out by the molecular complex. Nevertheless, the catalytic activity of the palladium was proven by deprotecting rhodamine 110 in HeLa cells. Furthermore, the catalyst was able to switch-on enzyme activity inside various cells. Lysine residues at the active sites of enzymes were protected with proc groups, inhibiting enzyme activity. However after treatment with palladium, the protecting groups were cleaved, with a yield of 28%, thus restoring activity to the enzyme.[59] The authors later went on to demonstrate the activity of Pd-NPs for the deprotection of neuramic acid (Neu) on cell surfaces. Proc-protected Neu (Neu5Proc) was metabolically incorporated onto cell surface glycans, and the deprotection reaction monitored by using click chemistry to follow the decrease in alkyne present on the cell surface, resulting in an average yield of 71% for deprotection efficiency.[60] Finally, a heterogeneous copper system has been shown to be active for profluorophore deprotection. Single-chain nanoparticles containing either a Cu(I)-phenantroline complex or Pd(II)-bipyridine complex were investigated for their activity towards deprotecting rhodamine (Figure 19). The activity of both catalysts was investigated in the presence of HeLa cells. While both the copper and the palladium catalysts were active for the deprotection in extracellular space, the Cu-SCNP exhibited faster reaction kinetics.[61]

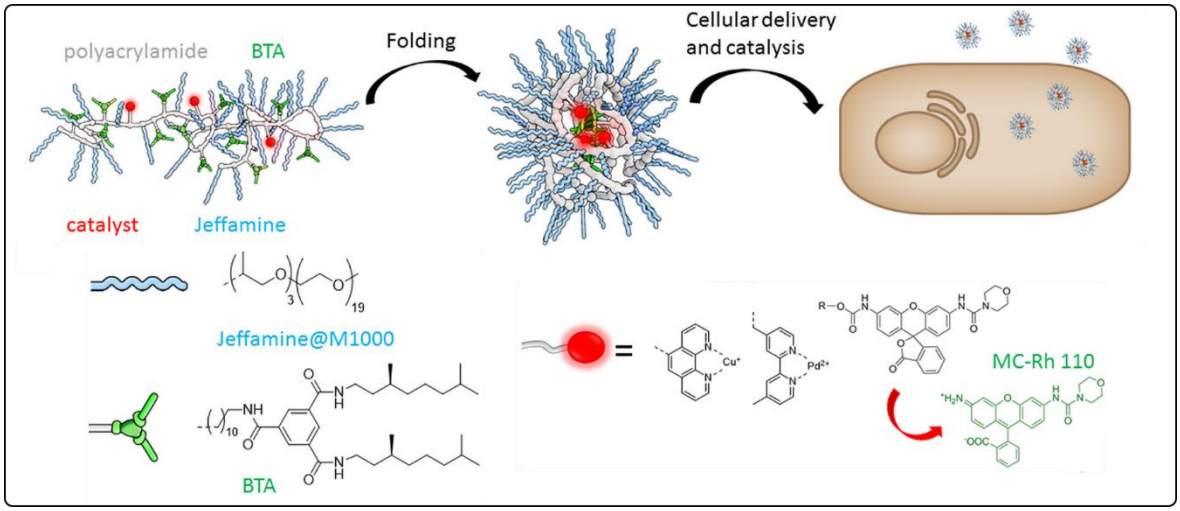

Figure 19. Schematic representation of the polymeric catalyst. Upon folding, it forms the SCNP which can be delivered into cells for catalysis. Figure adapted from ref 61.

Palladium complexes have also been shown to catalyse one other type of deprotection reaction, namely cleavage of an allenyl group from protected amino acids (Figure 13d). Pd(II) complexes were investigated for their uncaging activity towards allenyl-protected tyrosine residues on green fluorescent protein in HEK293T cells. The catalysts were able to successfully deprotect the tyrosine residues, and were found to catalyse the reaction with yields of up to 51%. The catalysts were then further applied to gain-of-function of an enzyme. When tyrosine residues in the active site of the anthrax lethal factor, the key toxin effector from *B. anthracis*, are protected with allenyl groups, the enzyme is inactive. However after incubation with the palladium complexes, the activity of the enzyme was restored.[62]

Finally, endogenous copper in cells have been shown to cleave a tris[(2-pyridyl)methyl]amine (TPA) group (Figure 13e). The TPA group was cleaved by Cu(I) to activate fluorescein in HEK 293T cells and in mouse embryonic fibroblasts,[63] and activation of luciferin by the same cleavage reaction was successfully applied both in PC3M-luc cells and in whole living mice.[64] However, control reactions in both instances used stoichiometric amounts of copper, so it is not clear if this reactivity occurs catalytically.

Cleavage of Internal Groups

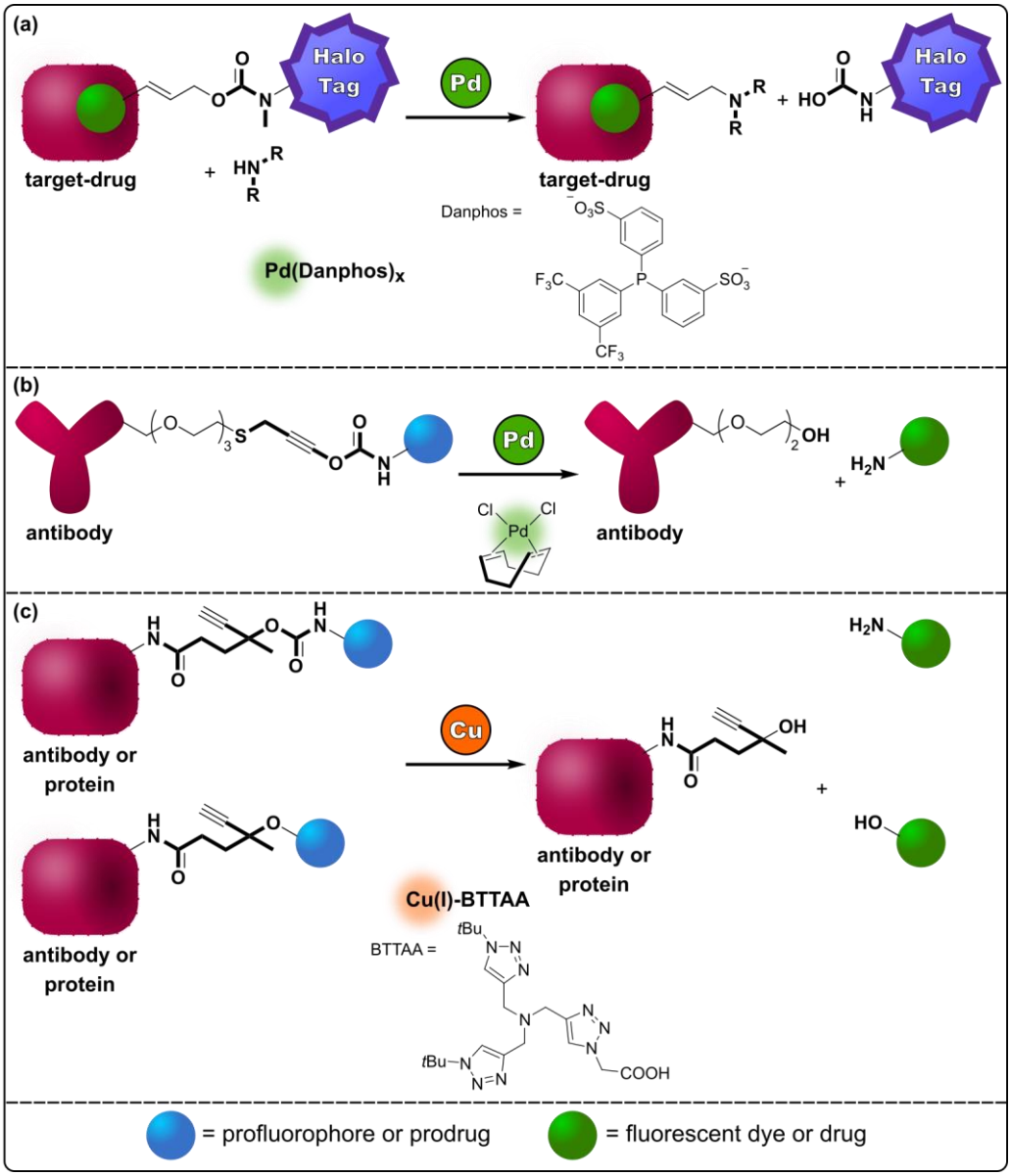

Figure 20. Overview of catalytic cleavage of internal groups carried out in cells. (a) Palladium catalysed cleavage of a HaloTag from a drug-target conjugate (ref 65). (b) Palladium catalysed cleavage of an antibody from a prodrug (ref 66). (c) Copper catalysed cleavage of antibodies or proteins from prodrugs or profluorophores (ref 67).

Although the most common example of metal-mediated bond cleavage reactions in cells is the deprotection of a small terminal groups, there are also a growing number of examples where internal linker groups are cleaved. These linkers find themselves joining together a drug or prodrug with a second targeting group. The first example of such a bifunctional linker was used to investigate drug-target interactions in cells (Figure 20a). A drug was linked to a capture tag (in this case a HaloTag) through a carbamate linker. The capture tag specifically binds to a desired protein: after allowing the drug to bind to its target in cells, the drug-target conjugate could be collected by lysing the cells and capturing the conjugate with an immobilised HaloTag protein which strongly binds the HaloTag. A $Pd(Danphos)_x$

complex could then cleave this carbamate linker between the HaloTag and the drug-target conjugate via the C-O bond, to release a carbamic acid which spontaneously decomposes to give an amine and CO_2. The liberated drug-target conjugate can then be analysed. This process is illustrated in Figure 21. Although this palladium cleavage worked with 100% efficiency in buffer solution, in the presence of HEK293T cell lysates only around 20% yield was obtained.[65] Another application bifunctional linkers is to attain spatial control over prodrug activation. Drugs can be linked to an antibody, to form a large structure known as an antibody drug conjugate (ADC) (Figure 20b). The antibody behaves as a targeting group, as the selected antibody will dock into the desired complementary antigen. However, if instead an inactive prodrug is used, cleavage of the linker group then liberates the activated drug, resulting in selected activation of the prodrug only at the desired location. Not surprisingly, due to the ubiquity of palladium in cleavage chemistry, the first examples shown *in vivo* again made use of simple palladium complexes. Doxorubicin was protected with a propargyl carbamate linker conjugated to the anti-HER2 nanobody 2Rb17c, which is an antibody against the HER2 antigen. In order to aid the cleavage, the linker contained a thioether adjacent to the alkyne moiety, which can interact with the palladium centre as a directing group. Upon addition of 10 eq of $Pd(cod)Cl_2$ in a sodium phosphate buffer solution full conversion to the cleaved product could be obtained. Although this ADC is non-toxic, when it was applied in a HER2-positive cell line (MCF-7) with 10 eq of palladium the toxicity reaches levels equal to that of free doxorubicin, indicating that even in cells the cleavage has high efficiency.[66]

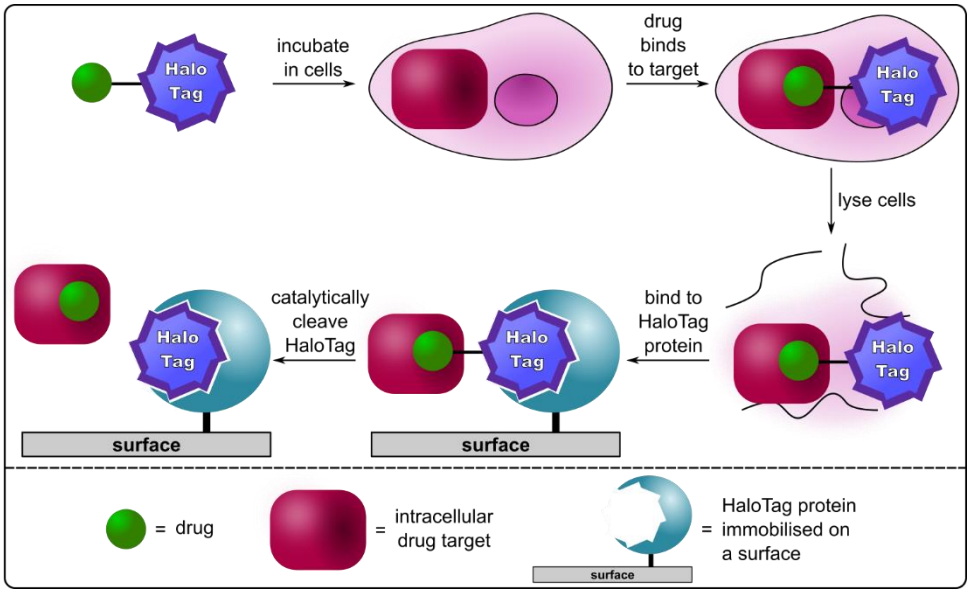

Figure 21. Isolation of a drug-target conjugate using a capture tag. The HaloTag is covalently linked to the drug, which is then incubated in cells. After the drug has bound to its target the cells are lysed and the drug-target conjugate is immobilised on a surface by binding the HaloTag to a HaloTag protein. The linker between the drug and HaloTag is then catalytically cleaved with a palladium complex, and the drug-target conjugate can be isolated.

The versatility of this ADC system was demonstrated by Chen *et al*. using a Cu(I) complex as catalyst (Figure 20c). Following a very large screening, the authors identified the complex Cu-BTTAA as being the most active towards propargyl cleavage from protected

amines and phenols. The Z_{HER2} affibody (a small peptide which targets the HER2 receptor) was selected as the bioconjugation partner. Drugs containing an amine (doxorubicin) and a phenol (Etoposide) were linked to this affibody through the propargyl linker. For both drugs, after incubation in SKBR-3 cells the addition of a stoichiometric amount of copper complex (20 eq and 1 eq respectively) resulted in toxicity levels comparable to the free drugs, indicating the successful cleavage of the linker (Figure 22a,b). This linker cleavage was then further used for reversible cell surface modifications. The propargyl linker was used to bind biotin to the surface of A549 cells. Incubation of the cells with fluorescently-labelled streptavidin resulted in strong fluorescence at the cells surface, due to the strong biotin-streptavidin binding. However, incubation with 20 eq of copper complex resulted in the almost complete disappearance of fluorescence at the cell surface after only 1 h, which again indicates successful cleavage of the linker from the cell surface (Figure 22c). Finally, the linker was also used for reversible protein mutagenesis, in order to provide a handle for modulating protein interactions. Site-selective protein modifications were achieved by incorporation of propargyl-caged lysine and tyrosine into a fluorescently-labelled Z_{HER2} affibody. While the native affibody binds to the HER2 receptors, resulting in strong fluorescence at the surface of SKBR-3 cells, when the modified Z_{HER2} containing the protected amino acid residues no fluorescence was observed, indicating a lack of binding. However, treatment with 10 μM of copper complex restored the fluorescence, showing that Z_{HER2}-HER2 binding can be controlled by the cleavage of propargyl protecting groups from protein residues (Figure 22d).[67] This work demonstrates the wider range of applications of metal-mediated bond-cleavage chemistry *in vivo* than simple deprotection reaction of fluorophores and prodrugs.

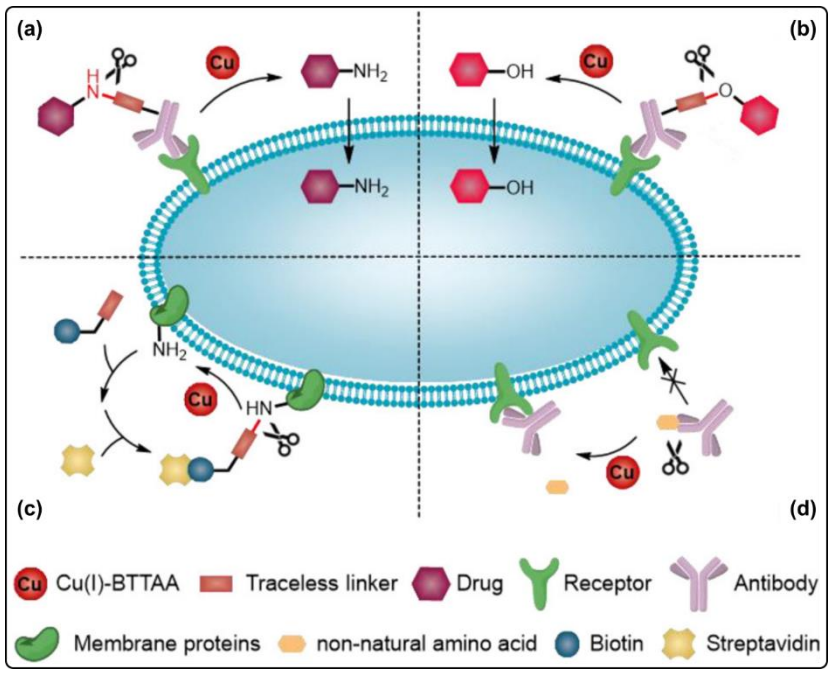

Figure 22. Copper catalysed cleavage of internal linkers. (a) Cleavage of an ADC to generate amine-containing drugs. (b) Cleavage of an ADC to generate hydroxyl-containing drugs. (c) Cleavage of a fluorescent biotin-streptavidin conjugate from cell membrane proteins. (d) Cleavage of a non-natural amino acid from an antibody to trigger binding of the antibody to a membrane receptor. Figure adapted from ref 67.

CYCLISATION REACTIONS

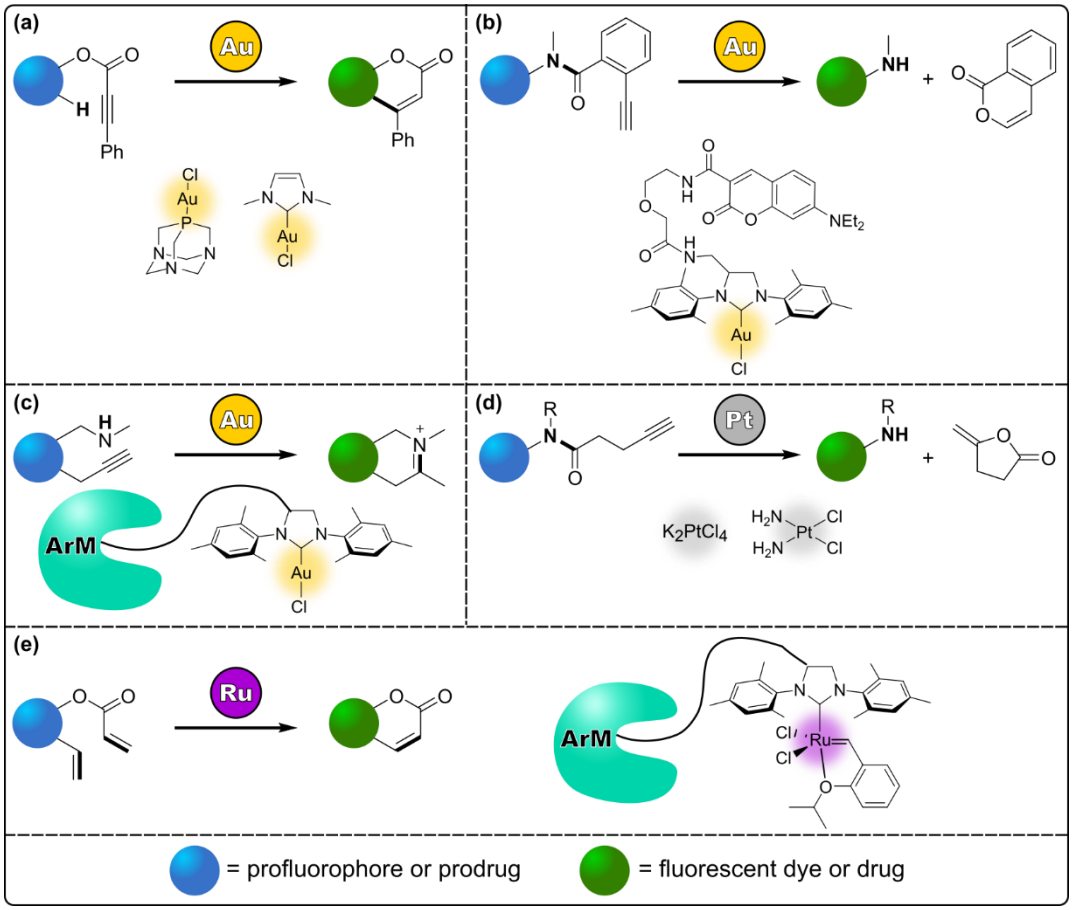

Figure 23. Overview of catalytic cyclisation reactions carried out in cells. (a) Gold catalysed intramolecular hydroarylation (ref 74–75). (b) Gold catalysed intramolecular hydroarylation to induce cleavage of a protecting group (ref 76). (c) Gold catalysed intramolecular hydroamination (ref 77). (d) Platinum catalysed intramolecular carbocyclisation to induce cleavage of a protecting group (refs 78–79). (e) Ruthenium catalysed ring closing olefin metathesis (refs 87–89).

Intramolecular Hydroarylations and Hydroalkylations

Gold is well known for its reactivity towards mediating cyclisation reactions. In fact this reactivity is the basis for several gold-sensing probes under biological conditions. These probes rely on an alkyne-containing profluorophore, which, after a Au(III)-mediated cyclisation, generates a dye. Although non-catalytic, these switch-on fluorescence systems are typically able to detect low levels of gold, and have been demonstrated to work in HeLa cells,[68, 69] HaCaT cells,[70, 71] and A549 cells.[72, 73] Building upon this concept, Mascareñas *et al*. used a Au(I) 1,3,5-triaza-7-phosphaadamantane (PTA) complex, [AuCl(PTA)], to carry out this hydroarylation cyclisation catalytically in cells (Figure 23a). The hydroarylation of procoumarin was investigated, in order to monitor catalysis by fluorescence. As gold is known to form strong bonds with thiols, the bioorthogonality of the reaction was first investigated. Although with 10 mol% of gold complex in the presence of 1 eq of some intracellular thiols (methionine, cytosine, histidine) high yields of 71–94% were still obtained, in the presence of other intracellular thiols (glutathione, cysteine or adenine) no yield was observed.

Nevertheless, the gold complex was still able to generate an aminocoumarin derivative in the presence of cell lysates and bacteria, with yields of 27% and 12% respectively. The reaction was further applied to HeLa cells, where a large increase in fluorescence intensity was seen after incubation of the profluorophore with the gold complex. Although the reaction was clearly able to take place inside cells, the reaction appears to be sub-stoichiometric, with the authors estimating a TON of just 1.12. Interestingly, it was also shown that this hydroarylation reaction could also occur concurrently in HeLa cells alongside a ruthenium catalysed deallylation reaction.[74] Although such gold catalysed cyclisations clearly have the potential to be successful bioorthogonal reactions, it is also clear that thiol-related poisoning is a very real problem for gold *in vivo*.

Conversely, Zou *et al*. used this strong thiol-gold interaction to their advantage by showing targeted anti-cancer activity of organogold(I) complexes in cancer cells and zebrafish. In order to achieve controlled activation of the catalyst, the authors designed a system in which an inactive gold complex undergoes a transmetallation reaction with palladium in order to generate a metal-chloride species which is both active towards intramolecular alkyne hydroarylation (Figure 23a), and cytotoxic towards cancer cells. The stable, non-toxic gold complex is able to transfer phenylacetylene to a Pd(II) complex, which then undergoes reductive elimination to produce 1,4-diphenylbuta-1,3-diyne and a Pd(0) species. The resultant gold species was then able to catalyse the cyclisation of a procoumarin derivative to generate the fluorescent product. Although this process occurred very efficiently in organic solvent with up to 96% yield, a large decrease in yield was observed when the reaction was moved to PB or PBS. Nevertheless, the authors demonstrated that their palladium-activated system showed much greater reactivity towards 1 eq of glutathione compared to the reaction with the analogous "pre-activated" complex. In addition, when the substrate, gold complex, and palladium complex were incubated in A549 cells notable fluorescence was observed in the cytoplasm, which was not seen for the other components alone. The catalysis was then further successfully applied inside zebrafish with similar results, although in neither case was the fluorescence quantified. As well as being catalytically active, the resultant gold complex was also shown to induce cytotoxicity in a range of cancer cells, by binding to thiol-containing enzymes, thioredoxin reductase, and inhibiting their function. This cytotoxicity was targeted towards cancer cells over healthy cells, by using a palladium source which was bound to a small stapled peptide, which targets integrin-overexpressing cancer cells. When the gold-palladium system was applied to HeLa cells considerable cell death was observed, while healthy cells with low integrin-expression remained viable. Zebrafish have been shown to be a good model to study tumour angiogenesis, so therefore the gold-palladium system was again applied in zebrafish. It was observed that blood vessel formation was impaired by the activated gold complex while the gold complex or palladium complex alone did not, demonstrating that this form of gold activation may be useful for improving spatiotemporal specificity of *in vivo* catalysis.[75]

Instead of directly using this type of cyclisation reaction as a tool for the synthesis of fluorophores or prodrugs, intramolecular hydroarylations have also been used as a method of bond cleavage for application in deprotection reactions (Figure 23b). To this end, a gold catalyst has been used to deprotect prodrugs through the cyclisation of a 2-alkynylbenzamide (ayba) protecting group. Following the cyclisation, a drug is released via the formation of a

secondary amide, as well as the ring closed by-product. Control reactions demonstrated that a gold-NHC complex was most active for this reaction, as 1 eq IPrAuCl successfully mediated the activation of ayba-protected endoxifen. Interestingly, this deprotection was also able to take place in parallel to the deprotection of alloc-protected and propargyl-protected doxorubicin by ruthenium and palladium respectively, showing that this gold-mediated deprotection has the potential to be used orthogonally to other deprotection reactions. Due to solubility reasons, a coumarin-modified analogue of the catalyst was used for reactions *in vivo*, which was used for the deprotection of ayba-protected doxorubicin. In multiple cancer cell lines (HeLa, A549, and PC3) a significant decrease in EC_{50} values was observed when the prodrug was incubated in the presence of the gold complex.[76] Although these results clearly indicate the successful uncaging of the prodrug inside cells, stoichiometric quantities of gold were used, indicating that, again, it is likely that the gold complex would be readily poisoned in biological environments.

In order to protect a gold catalyst from thiol poisoning a gold artificial metalloenzyme was developed, whereby a coumarin-modified NHC-Au(I) complex was docked inside an albumin scaffold in order to catalyse hydroamination reactions of 5-methyl phenanthridinium derivatives (Figure 23c). A bioorthogonality screening revealed the protective role of the protein scaffold: while the free complex exhibited almost no activity in the presence of glutathione or cell lysates, only a slight decrease in activity for the artificial metalloenzyme was observed, with high TON still obtained. The artificial metalloenzyme was then shown to be active in the cyclisation of a prodrug, in order to synthesise a cytotoxic anticancer compound. While low catalyst loadings gave moderate yields, at 20 mol% of artificial metalloenzyme full conversion could be achieved. When the reaction was then applied inside A549 cancer cells, the protective nature of the protein host was further demonstrated. The metalloenzyme was more efficient at prodrug activation than the free gold complex, as it was observed that only 0.63 μM of metalloenzyme was required to achieve a decrease in cell growth by 50%, whereas 2.5 μM of free complex was needed to reach the same level. Interestingly, it was also observed that docking the gold complex inside the protein scaffold reduced its cytotoxicity compared to the free complex. This research clearly demonstrates the dual protective role of shielding a gold complex from exposure to the cell: the gold complex can be protected from deactivation by biomolecules, and the cell can be protected from the cytotoxicity of the gold.[77]

Gold is not the only player in mediating cyclisations *in vivo*. Platinum has also been shown to be active for intramolecular carbocyclisations (Figure 23d). Cisplatin was first shown to catalyse 4-pentynoic acid cyclisations, at very low catalyst loadings. Just 1 mol% of platinum complex could give full conversion to the desired enol-lactone in water. However, the reaction was shown to be much less efficient under biological conditions, with a decreased rate observed when the reaction was carried out in blood plasma, which the authors attributed to interactions between blood proteins and the complex.[78] Simple platinum salts have also been used in cells to combine a carbocyclisation with the release of a secondary amine-containing drug. Following a carbocyclisation of an alkyne-amide or alkyne-carbamate, a lactone is released, while simultaneously generating a free amine. Although control reactions showed that cisplatin and K_2PtCl_4 could successfully deprotect alkyne amides or carbamates from secondary amines

at catalytic quantities in water, a large stoichiometric excess of platinum complex was required for reactions under biological conditions. The deprotection of an antineoplastic drug, MMAE, and anticancer drug, 5FU, was shown to proceed in HeLa cells. After incubation with the non-toxic prodrugs of MMAE (1 nM) and 5FU (100 μM), a 2-fold increase in toxicity was observed following the application of 20 μM of K_2PtCl_4 twice a day for three days. Despite this large amount of platinum added to the cells, the authors noted that in both cases the toxicity of the unmodified drugs was not reached, which indicates that even after 3 days full conversion to the deprotected drugs was not obtained. It is likely that glutathione was the root of this poor activity, as control reactions in the lab with 50 eq of platinum complex in the presence of 1.5 mM glutathione resulted in reduced conversions, although the reaction rates were still good. Nevertheless, MMAE was also shown to be successfully deprotected from an ADC, whereby an alkyne amide linker was used to conjugate the MMAE to the F16 antibody, which is known to specifically bind to the tenascin-C receptor, which is overexpressed in cancer cells. Again, large excesses of K_2PtCl_4 resulted in the liberation of MMAE from the ACD in HeLa cells. Finally, cisplatin was successfully applied in the uncaging of 5FU in zebrafish. Colorectal cancer (CRC) HCT116 zebrafish xenografts were generated for incubation with protected 5FU (1.65 mM) and cisplatin (34 μM). After 6 days, a significant decrease in tumour size was observed.[79] Although this work highlights the vulnerability of platinum complexes to biological environments, the fact that it could be effectively applied in whole zebrafish demonstrates the promise of platinum complexes as cyclisation and deprotecting agents *in vivo*.

Olefin Metathesis

Olefin metathesis is an extremely versatile reaction, with ring-closing metathesis, cross-metathesis and ring-opening polymerisation catalysis providing a means to access a wide range of useful products, notably for pharmaceutical production.[80, 81] Therefore it is not surprising that the pursuit of applying this reaction in living cells is of great interest. Indeed metathesis has been effectively used for protein modification.[82-86] However, to date there have only been a handful of examples of the reaction being applied in living cells, and they have all made use of the ArM strategy (Figure 23e).

Ward *et al*. were the first to develop an artificial metathesis metalloenzyme for *in vivo* reactivity, based on the biotin–streptavidin scaffold, whereby a biotinylated analogue of the Hoveyda-Grubbs second-generation catalyst was docked inside streptavidin (SAV). In order to avoid the thiol-rich environment of the cytosol, the thiol-poor environment of the periplasm of *E. coli* was selected for the catalysis to take place in. With this end in mind, customised *E. coli* expressing periplasmic SAV (SAV^{peri}) was selected, and indeed after incubation with the cofactor, the ruthenium complex accumulated inside the periplasm after binding to the SAV^{peri}. The ring-closing activity of the artificial metalloenzyme was investigated for the synthesis of the fluorophore umbelliferone, from the corresponding non-fluorescent diolefin, where an increase in fluorescence intensity could be observed. After directed evolution, an artificial metathesis metalloenzyme was found which was able to catalyse the ring-closing of a cationic diallyl-sulfonamide in cells with an average TON of around 500 x 10^3 per cell, with a background reactivity of approximately 30 x 10^3 per cell.[87] The ring-closing metathesis activity of the Hoveyda-Grubbs was extended to release protected cargo, via a 1,4-elimination

reaction from the ring-closed product. This reactivity was investigated with naphthalene precursors to release water, acids, alcohols, and amines and CO_2. While this reaction proceeded stoichiometrically in biological media with less than 5 mol% of catalyst, when 20 mol% of the ruthenium complex was used extracellularly in the presence of HeLa cells, a yield of 50% was achieved, corresponding to a TON of 10. However this reaction efficiency was decreased to a 27% yield and TON of 17 when the catalyst was docked inside the SAV scaffold and carried out in the periplasm of *E. coli*.[88]

An alternative artificial metalloenzyme developed for metathesis reactions used a coumarin-modified Hoveyda-Grubbs second generation catalyst docked inside of albumin. The length of the linker between the coumarin and the NHC ligand was optimised as such so that the complex resided within the hydrophobic pocket of the protein, and was therefore protected from thiol poisoning, as the hydrophilic intracellular thiols would be repulsed by the apolar nature of the cavity. Having optimised the structure of the ligand, it was shown that the complex could undergo ring closing metathesis with no reduction in activity in the presence of up to 20 mM glutathione. After decorating the exterior of the albumin with α(2,3)-linked sialic acid targeting groups, the artificial metalloenzyme was shown to accumulate in SW620 colon adenocarcinoma cells, by binding to overexpressed galectin-8 receptors. In the presence of these cells, the cyclisation of a prodrug to generate a cytotoxic compound was carried out, whereby cell growth could be decreased to <5%, while the artificial metalloenzyme without the targeting groups was much less active at inducing cytotoxic effects. While this observation made it clear that the targeting is important for the prodrug activation, it was not clear if this activation was taking place on the cell surface, or intracellularly.[89] The activity of these artificial metathesis metalloenzyme is an exciting development on the road to *in vivo* metathesis, where future work should focus on conducting the reaction in the cytoplasm and with molecular catalysts.

CLICK REACTIONS

Copper Catalysed Cycloadditions

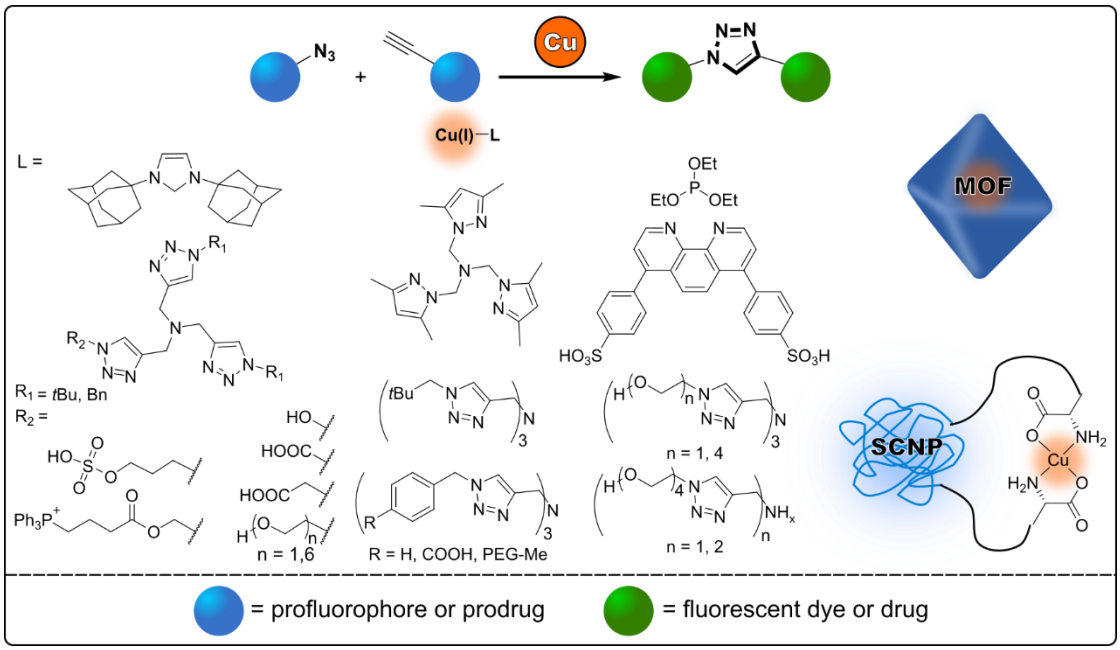

Figure 24. Overview of copper catalysed alkyne-azide cycloadditions carried out in cells (refs 91–107).

Alkyne-azide cycloadditions, known as click reactions, have long been known for their excellent bioorthogonality, as neither alkynes nor azides are endogenous to living systems, and typically both substrates, as well as the stable triazole product, exhibit low levels of cytotoxicity. In addition, fast reaction kinetics and high yields make such reactions very applicable to cellular conditions. Indeed, the metal-free strain-promoted alkyne-azide cycloaddition (SPAAC) has been successfully applied within Gram-negative bacteria in order to carry out *in situ* compartment-specific labelling in *E. coli*.[90] However, this reactivity is limited to only highly strained alkynes. The copper catalysed variant of this cycloaddition (CuAAC) provides a means to access an extraordinarily broad substrate scope. The reaction requires a Cu(I) catalyst, which is usually generated *in situ* from a Cu(II) source and reductant, most commonly $CuSO_4$ and sodium ascorbate, with a wide variety of ligands which have been used (Figure 24). Cai *et al*. have demonstrated the applicability reaction for protein labelling, using tris(triazole) based ligands. Reactions work under conditions similar to *in vivo*, in a buffer at 37 °C, but reactions which proceed in air exhibit lower yields than under anaerobic conditions.[91] In addition, Cu(I) is often not good for cells. It is responsible for some toxicity, plus they can generate ROS, and cause peptide and protein oxidation, although ligand binding can decrease this effect.[92]

Although this reaction works catalytically, some early examples in the field apply the copper stoichiometrically. Tirrel *et al*. labelled cell surface proteins on *E. coli*. Initial attempts involved incorporating azide-containing unnatural amino acids into the protein, then incubating the cells with a biotin-containing alkyne (in order to monitor the reaction with a biotin-streptavidin assay), sodium ascorbate, and 2 eq of $CuSO_4$ with respect to the alkyne. Despite

the large excess of copper, only 10–15% of the surface azides were labelled.[93] Optimisation of the copper complex increased the labelling yield 10-fold, although still 2 eq of copper was required.[94] Labelling was further extended to the surface of mammalian cells, with inversion of the reaction, to have alkyne amino acids incorporated in the protein and a hydroxycoumarin-azide, but an even larger excess of copper was used, with 8 eq of $CuSO_4$ with respect to azide.[95] In attempts to improve reaction kinetics, chelating azides have also been deployed as substrates, which are able to bind to the copper centre in a multidentate fashion. Taran *et al.* made use of a tetradentate chelating azide in order to label the microtubule skeleton inside cells with a fluorescent coumarin-based click product. Here 1 eq of copper was needed with respect to azide, as the preformed copper-azide complex was reacted with the alkyne-labelled proteins. Although reaction kinetics indeed proved to be extremely fast for this system, with rate constants observed of up to 1300 $M^{-1} s^{-1}$, the maximum yield obtained for control reactions in buffer or cell lysates was only 60%.[96]

Catalytic cell surface labelling is useful for understanding cellular recognition, receptor signalling and intracellular interactions. In this context, chelating azides have also been used for intracellular click reactions. The azide forms a bidentate complex with the copper, of which only 5 mol% is used, and alkyne modified proteins on the cell surface are labelled by forming a fluorescent coumarin-based click product. This chelating system reportedly allows for lower copper concentrations, which reduces toxicity, fast reaction kinetics, and results in up to 25-fold increase in protein labelling signal compared to a non-chelating azide.[97] Fast cell surface labelling of glycans has also been demonstrated using a copper-containing single chain nanoparticle (Cu-SCNP). Chen *et al.* developed a SCNP where a hydrophobic backbone aggregated in water can be cross-linked together, while excluding cationic and copper-binding side chains. These nanoparticles efficiently labelling alkyne-modified proteins in buffer solutions with fast rates and up to quantitative conversion, as well as labelling cell-surface glycans with enzyme-like saturation kinetics, and with low copper concentrations.[98] Cell-surface glycan labelling has even been shown to be compatible with zebrafish embryos, with 90% of the labelled embryos developing normally, further indicating the compatibility of this reaction extracellularly.[99]

Protein labelling has also been successfully carried out inside *E. coli*. Site specific labelling in such bacterial cells has the added challenge compared to mammalian cells of having to differentiate between the cytoplasm and the periplasm. However, one beneficial difference between these locations, is the much lower amounts of thiols inside the periplasm, where instead there is the oxidised form of glutathione (GSSG). Chen *et al.* have achieved protein labelling inside *E. coli* periplasm by expressing periplasm-specific alkyne-labelled proteins.[100] With periplasmic labelling yields as high as 80%, the pH dependent fluorescence of the resultant 4-DMN (4-*N*,*N*-dimethylamino-1,8-naphthalimide) based click product could be used as an *in situ* pH sensor.[101] Further developing their pH-sensing system, using azide labelled proteins and tridentate triazole ligands, cytoplasmic proteins were also able to be selectivity labelled, with yields of around 70%. When used in combination with the labelled periplasmic proteins, it was possible to measure the pH gradient across the cytoplasmic membrane.[102]

Moving away from the bacterial periplasm and into intracellular conditions means having to carry out catalysis in the presence of much higher concentrations of thiols, which tend to be accompanied by decreased yields. Cai *et al*. showed protein labelling with a coumarin dye, both on the cell surface and intracellularly, with a cell-penetrating peptide attached to the tridentate triazole ligand to ensure entrance of the catalyst into the cell. While the surface labelling took place with a very modest yield of 18%, inside the cell a yield of only 0.8% was achieved. This low yield was attributed to the presence of catalyst-poisoning thiols, and indeed after taking measures to reduce thiol content the yield could be increased up to 14%, indicating the extremely detrimental effects of intracellular thiols.[103]

Intracellular chemistry has been extended to broader reaction scopes than only protein labelling, with several examples of small molecule synthesis *in vivo*. Mascareñas *et al*. achieved the synthesis of a fluorescent anthracene derivative inside of mammalian cells. Although the obtained yields were not high, with a maximum yield of 18%, the reaction was able to proceed without the addition of any external reducing agent.[104] There are also several heterogeneous examples of intracellular small molecule synthesis. Cu-SCNPs (Figure 25) were used to synthesise an antimicrobial agent inside *E. coli*. While the yield of the reaction was not quantified, proof of concept was confirmed by a strong inhibition of bacterial cell growth, which was not observed in the absence of catalyst.[105] *In situ* drug formation in mammalian cells has been demonstrated with entrapped copper nanoparticle catalysts (E-Cu-NPs), where copper nanoparticles were distributed inside resin beads. These catalytic beads were used to synthesise combretastatin A4, a tubulin polymerisation inhibitor which is highly cytotoxic. The inhibitor was synthesised inside HeLa cells, where an increase in cell apoptosis from 13% to 48% was seen, comparing untreated cells to cells containing the catalyst and alkyne and azide precursors. Synthesis of a coumarin dye inside zebrafish embryos further demonstrated the potential applicability of this catalyst to living systems.[106]

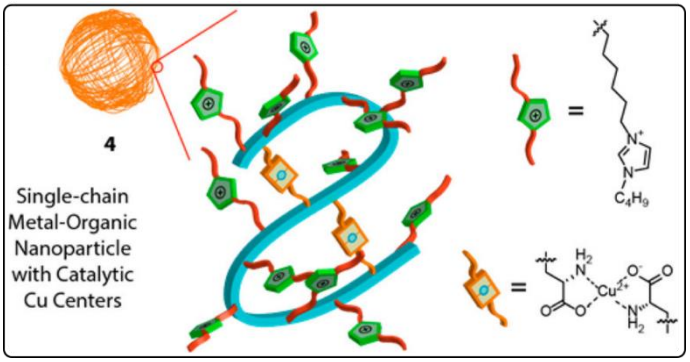

Figure 25. Schematic representation of the copper-containing single chain nanoparticle. Figure adapted from ref 105.

Finally, Qu *et al*. have applied their heterogeneous click catalyst to whole living systems. Here, ultrafine copper nanoparticles were distributed throughout a zirconium metal-organic framework (MOF), which was subsequently decorated with a triphenyl phosphine (TPP) moiety, which is known to target mitochondria (Figure 26). Indeed the MOF-Cu-TPP was observed to accumulate inside the mitochondria of MCF-7 cells. Initial catalytic activity within these cells was confirmed by the synthesis of resveratrol, an anticancer agent. The *in*

situ formation of this drug was confirmed by an increase in apoptotic cells and a decrease in cell viability. Furthermore, biocompatibility of the catalyst was confirmed by catalytic hydroxycoumarin-based fluorophore formation inside living worms, *C. elegans*. After illustrating that the catalyst had no detrimental effects to the worms, the catalyst and resveratrol precursors were administered to live mice, where *in situ* formation of the drug led to better antitumour activity than administering the pre-synthesised drug.[107] This is a strong argument for the benefit of targeted, catalytic drug formation *in situ*, demonstrating the minimisation of the side effects which are typically associated with non-specific drug delivery and distribution.

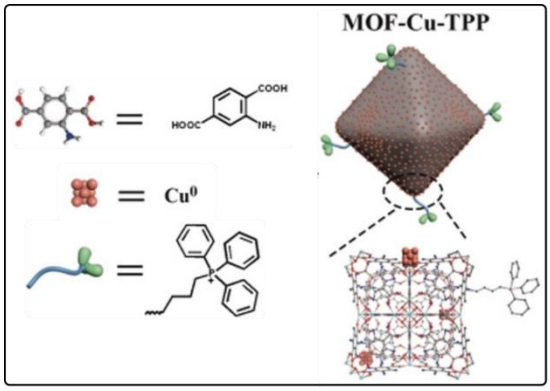

Figure 26. Structure of the copper containing MOF decorated with TPP (MOF-Cu-TPP). Figure adapted from ref 107.

Non-Copper Catalysed Cycloadditions

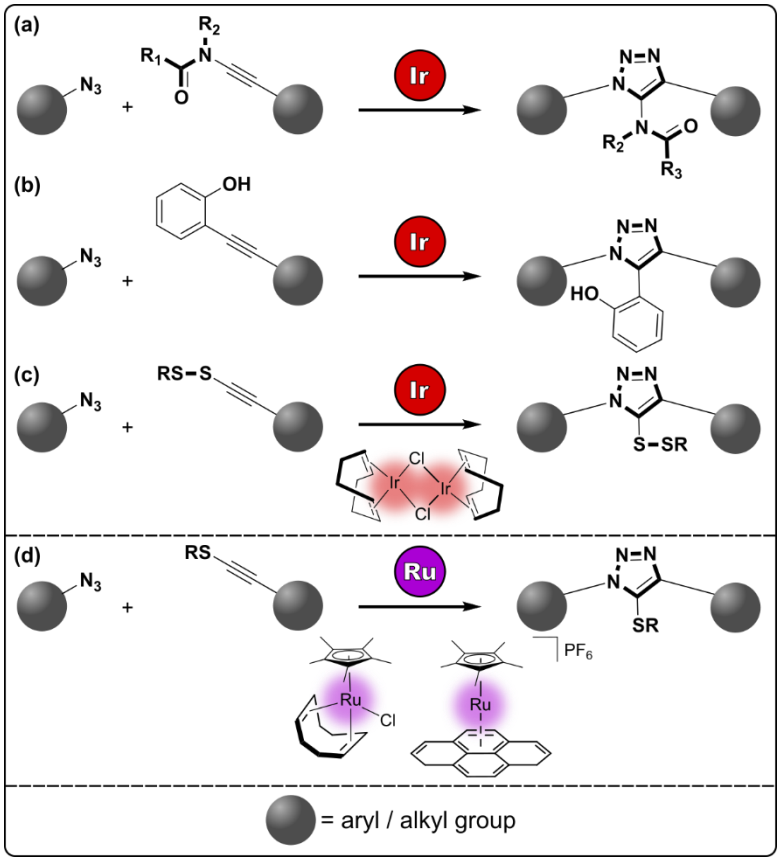

Figure 27. Overview of non-copper catalysed alkyne-azide cycloadditions carried out under biological conditions. (a) Iridium catalysed ynamide-azide cycloaddition (ref 108). (b) Iridium catalysed hydroxylalkyne-azide cycloaddition (ref 109). (c) Iridium catalysed disulfidealkyne-azide cycloaddition (ref 110). (d) Ruthenium catalysed internal thioetheralkyne-azide cycloaddition (refs 111–112).

Despite the ubiquity of copper for this reaction, other metals are also capable of mediating azide-alkyne cycloadditions. Iridium has recently proven itself to be a viable candidate for catalysing cycloadditions under biological conditions which are difficult for copper. Alkyl substituted ynamides cannot be reacted with azides using copper under bioorthogonal conditions, as high temperatures are required due to the electron rich nature of the alkyne. Although ruthenium catalysts are able to afford 5-amido fully substituted 1,2,3-triazoles, they do so in a non-selective manner. However, $[Ir(cod)Cl]_2$ was able to catalyse the reaction with high yields and excellent selectivity in water, with only one regio-isomer formed (Figure 27a). This reactivity was even preserved under biological conditions, where high yields were maintained when using just 2.5 mol% of iridium complex in biological media, such as PBS and DMEM, in UM-1 cell lysates, and in mouse and lung cancer patient serum.[108] Phenolic alkynes have also been shown to be challenging for copper catalysts, with no yield observed; however for $[Ir(cod)Cl]_2$ the hydroxyl moiety acts as a directing group, allowing for excellent yields and selectivity (Figure 27b). Again, good bioorthogonality was observed, with a 90% yield obtained with 2 mol% catalyst in cell culture media (PBS, DMEM, FBS). Interestingly, a 54% yield could still be obtained even in the presence of 20 eq glutathione,

indicating that thiol poisoning is not such a problem for iridium.[109] Finally, the $[Ir(cod)Cl]_2$ complex could also selectively catalyse cycloadditions with disulfide-containing alkynes (Figure 27c), with better yields than for copper, cobalt, rhodium, or ruthenium catalysts. While moderate to high yields were maintained when 5 mol% catalyst was applied in cell culture media (PBS, DMEM and FBS), in this case 2 eq glutathione resulted in no yield at all, with the authors hypothesising this was due to glutathione-induced reduction of the disulfide on the substrate. However, still a very respectable 54% yield was observed in HeLa cell lysates.[110] These results indicate that this iridium complex could work very efficiently in a cellular environment. However, despite the fact that these examples demonstrated extremely good bioorthogonality, to date no iridium complex has been applied inside living cells to catalyse a cycloaddition.

Ruthenium catalysts are also good alternatives to copper for cycloadditions requiring internal thioalkynes (Figure 27d). Mascareñas *et al.* showed that quantitative formation of the triazole product can be achieved using Cp*Ru(cod)Cl as catalyst, in comparison to copper complexes which cannot catalyse this transformation. Similarly to the iridium complexes described previously, 5 mol% of ruthenium complex shows excellent tolerance to glutathione (60% yield can be obtained in the presence of 20 eq glutathione), and gives excellent yield in cell culture media (PBS, DMEM, and FBS) as well as in HeLa cell lysates. However, while CuAAC reactions are known to work well at the dilute concentrations needed for *in vivo* catalysis, for this catalyst dilution results in a drastic decline in yield. Nevertheless, when 10 mol% of catalyst was applied at 100 μM concentration in PBS in the presence of *E. coli* in order to synthesise an anthracene-based fluorescent product, an 8-fold increase in fluorescence compared to controls was observed.[111] Having established the applicability of this system in the presence of bacteria, the authors went on to carry out a light-controlled variation of the system in the presence of mammalian cells. Upon irradiation, the inactive photo-protected catalyst, $[Cp^*Ru(pyrene)]PF_6$, expulses its arene ligand to generate the catalytically active solvated complex, $[Cp^*Ru(solvent)_3]PF_6$. This cationic catalyst had improved reactivity under dilute conditions compared its neutral counterpart, and 50 mol% of ruthenium in the presence of 500 μM substrate resulted in high yield upon irradiation, both in water/acetonitrile mixtures and under biological conditions (PBS, cell culture media, and HeLa cell lysates). The reaction was also shown to be applicable to biological substrates, and 72–84% yields after irradiation could be obtained for the bioconjugation of thioalkynes to peptide and oligonucleotide azide partners. Finally, the reaction was carried out in a DMEM/HEPES mixture in the presence of HeLa cells. While LC-MS analysis indeed proved that product was found in the cells, the authors speculate that product accumulated there after being formed.[112] Although this photoactivatable ruthenium complex is a robust catalyst to biological settings, these results indicate that a lack of cell penetration may be problem for applying this reaction inside living cells.

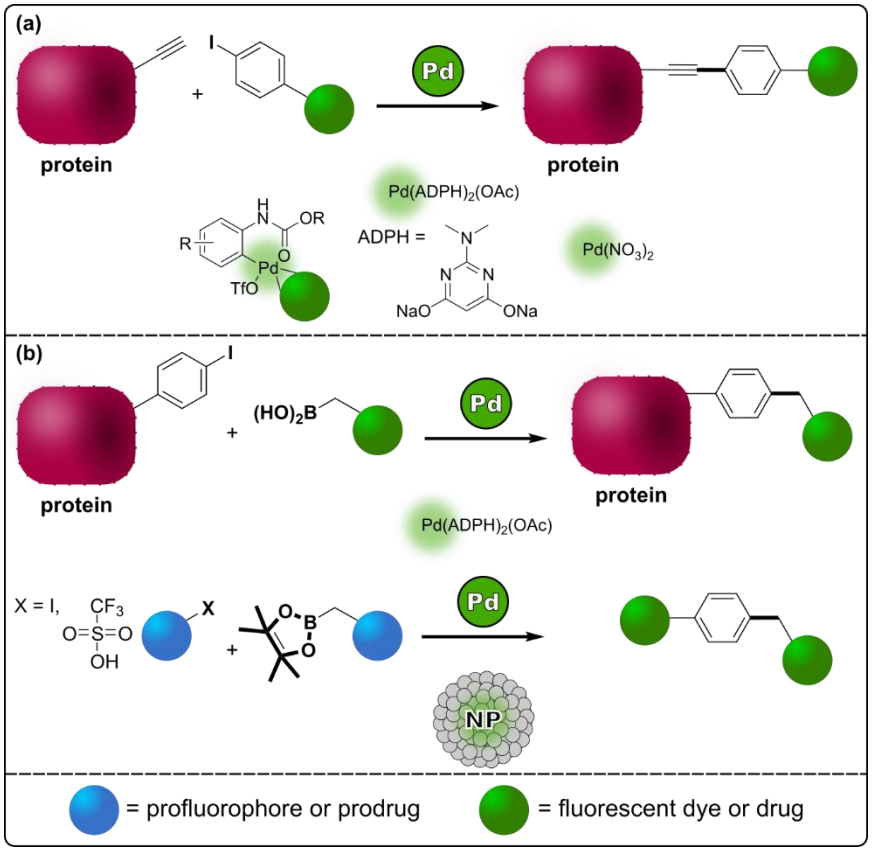

Figure 28. Overview of cross-coupling reactions carried out in cells. (a) Palladium catalysed Sonogashira couplings (refs 114–118). (b) Palladium catalysed Suzuki-Miyaura couplings (refs 44, 119–122).

Sonogashira Coupling

Palladium catalysed cross-coupling reactions are extremely useful tools for achieving carbon-carbon bond formations in organic synthesis. Therefore, it is no surprise that achieving this reactivity inside living cells is of great interest, as it would provide access to the synthesis of a wide range of drugs *in situ*. The Sonogashira cross-coupling reaction couples together terminal alkynes with aryl halides to generate acetylene derivatives (Figure 28a). The palladium catalysed reaction typically uses a Cu(I) co-catalyst and the presence of amines, although there are many examples of copper-free reactions.[113] Indeed, palladium *N*-phenylcarbamate metallocycles have been shown to promote the labelling of alkyne-encoded proteins via a Sonogashira-type reaction. The potential applicability of the reaction *in vivo* was exemplified by the extremely fast reaction kinetics, with the rate constant rivalling that of the CuAAC reaction, although the coupling partner for the alkyne was used as a ligand for the palladium, resulting in 4 eq of palladium complex being used with respect to one equivalent of alkyne-modified protein.[114]

All examples of the Sonogashira reaction applied in the presence of cells have used a copper-free system. However, the reaction is yet to be carried out catalytically, as these first

examples of the transformation *in vivo* required not just stoichiometric amounts of palladium, but even large excesses with respect to the alkyne. A 2-amino-4,6-dihydroxypyrimidine (ADHP) Pd(II) complex was investigated for its reactivity towards labelling alkyne-encoded proteins with aryl iodides. Although this copper-free $Pd(ADHP)_2(OAc)_2$ system was able to catalyse the reaction between aryl iodide an alkyne-modified unnatural amino acid with 30 mol% of palladium with excellent yields of 70–95%, when the reaction was applied to a protein containing an alkyne-modified residue, 50 eq of the palladium and aryl iodide were required to obtain good yields. Furthermore, when the protein was labelled with a fluorescent resorufin-based aryl iodide in *E. coli* cells, an extraordinary 100 eq of palladium complex with respect to aryl iodide was used.[115] This procedure was updated to instead use a pre-formed aryl iodide–Pd complex. Although the reaction is still stoichiometric, the relative amount of palladium was reduced to 8 eq of pre-activated complex with respect to protein, and was also applied to labelling proteins on the surface of mammalian HEK293T cells.[116] Further expanding the reactivity to intracellular labelling, 500 μM of this stoichiometric palladium complex resulted in 67% yield for fluorescently labelling the alkyne-encoded protein inside *E. coli* cells. However, despite using the pre-formed complex, when the system was applied inside HEK293T cells, only a very modest yield of around 12% was achieved.[117]

Stoichiometric quantities of palladium nanoparticles were able to promote the Sonogashira coupling inside of bacterial cells. $Pd(NO_3)_2$ was used to generate palladium nanoparticles *in situ* for the coupling of alkyne- or iodide-encoded proteins with fluorescent or biotin-based labels. Equimolar quantities of palladium and probe were successfully used to label proteins in two types of Gram-negative bacteria (*E. coli* and *Shigella*).[118] Although these reports demonstrate the bioorthogonality of the Sonogashira reaction *in vivo* as a labelling alternative to the CuAAC reaction, this is clearly a very challenging reaction to achieve in cells, and further research is required in this field. For the reaction to ever be used for more than just protein labelling, such as pharmacological applications like *in situ* drug formation, reactions which are able to rely on catalytic amounts of palladium need to be developed.

Suzuki-Miyaura Coupling

The Suzuki-Miyaura reaction is a different kind of palladium catalysed cross-coupling reaction, which instead couples together mainly aryl halides with aryl boronic acids or esters (Figure 28b). Although homogeneous catalysts for this reaction typically require phosphine ligands bound to the palladium centre, a water soluble phosphine-free Pd(II) system has been developed by Davis *et al*. for Suzuki-Miyaura mediated labelling on the *E. coli* cell surface. Incorporating the unnatural amino acid *p*-iodophenylalanine (*p*IPhe) into a pore-forming receptor-binding protein on *E. coli* allowed these pores to be labelled with a fluorescein-based boronic acid, after incubation with the catalyst, resulting in a 55% increase in fluorescence intensity. Additionally, the palladium complex did not exhibit any toxicity at the levels required for catalysis, although this may be due to the complete lack of cell permeability of the complex.[119] This *p*IPhe-tagged protein on *E. coli* cell surface was also be coupled with carbohydrate-based boronic acids, providing a handle for lectin binding to the surface.[120] Although in both cases, the catalytic system is described as a molecular complex, the authors

describe palladium concentration-dependent "switch-on" catalysis, whereby a critical threshold of 330–450 μM was observed, below which no catalysis occurred, and above which labelling efficiency was not improved. In addition, Pd(II) complexes are known to generate Pd(0) nanoparticles in biological settings. Together this indicates that the reaction could be catalysed by palladium nanoparticles, instead of discrete metal–ligand based complexes.

Palladium nanoparticle-containing microspheres have also been shown to catalyse Suzuki-Miyaura reactions in mammalian cells. As well as being active for alloc cleavage from profluorophores (see section *Cleavage of Terminal Groups*), Pd(0) nanoparticles distributed within polystyrene microspheres (Pd-resin, Figure 29a) are also able to catalyse the carbon-carbon bond forming reaction for the *in situ* synthesis of a fluorophore. A mono-triflate containing profluorophore was coupled to a TTP-containing boronic ester in the cytoplasm of HeLa cells to generate anthofluorescein. The mitochondrial targeting moiety (TPP) incorporated into the dye resulted in selective fluorescence of mitochondria.[44] This ground breaking reaction is the first ever non-enzymatic aryl-aryl bond formation to have taken place inside a living cell. The light-dependent synthesis of this fluorophore has also been demonstrated by silica-supported Pd(0) nanoparticles modified with an azobenzene photoswitch (Figure 29b). Similar to the gold-based ROS scavenger (see section *Oxidation and Reduction Reactions*) after photo-isomerisation from *trans*- to *cis*-azobenzene, cyclodextrin is lost from the nanoparticle, and the catalyst is activated. Following this light-gated activation, the nanoparticle was able to catalyse the *in situ* formation of anthofluorescein in HeLa cells, again localised to the mitochondria. Furthermore, the nanoparticle was able to catalyse the propargyl cleavage from an anticancer prodrug, generating 5FU in HeLa cells.[121] This light-dependent drug synthesis would be especially beneficial for localised cancer chemotherapy.

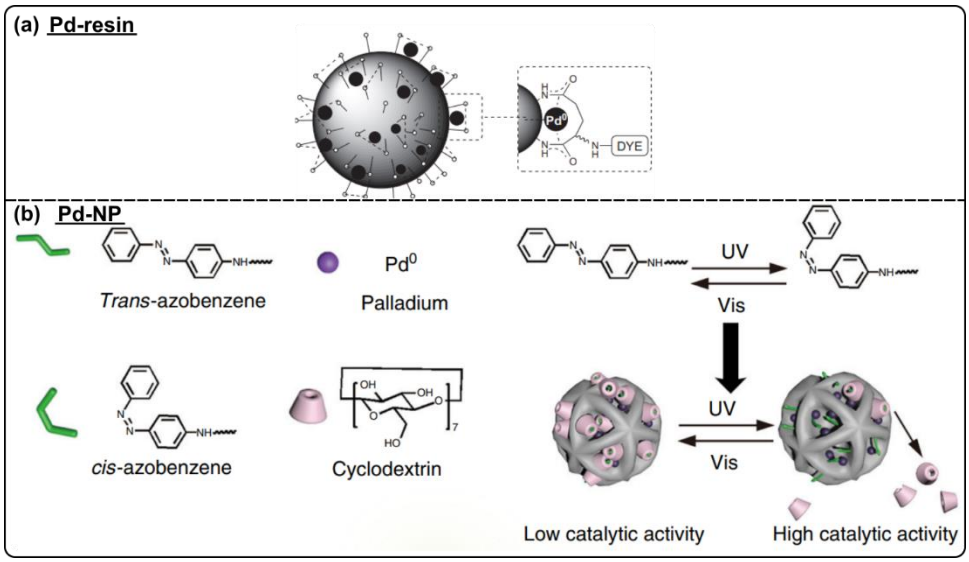

Figure 29. (a) Schematic representation of Pd nanoparticles distributed within a polystyrene microsphere (Pd-resin). Adapted from ref 44. (b) Silica-supported Pd nanoparticles (Pd-NP) with an azobenzene switch. CD binds to the *trans*-azobenzene moieties which decorate the nanoparticle, and inhibit catalysis. However irradiation with UV light induces isomerisation to *cis*-azobenzene which triggers the release of the CD and switches on the catalytic activity of the Pd-NP. Adapted from ref 121.

The PdNP-microsphere was then adapted to target cancer cells, by decorating the surface with the cyclic peptide cRGDfE, which is known to be a potent antagonist of the $\alpha_v\beta_3$ receptor, which is overexpressed in many tumours. The structure of this nanoparticle is shown in Figure 30. This palladium catalyst was shown to simultaneously catalyse propargyl deprotection to generate 5FU, and to catalyse a Suzuki coupling to generate another anticancer drug, PP-121, from non-toxic precursors. When both reactions were carried out simultaneously in U87-MG cancer cells, cell viability was decreased to just 22%, whereas the decrease from 5FU and PP-121 alone was only 66% and 44% respectively.[122] This combination of dual drug synthesis and cancer cell specificity shows potential for future chemotherapy applications.

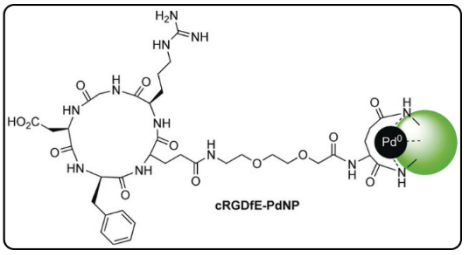

Figure 30. Structure of the Pd nanoparticle decorated with the cyclic peptide cRGDfE. Adapted from ref 122.

OTHER REACTIONS

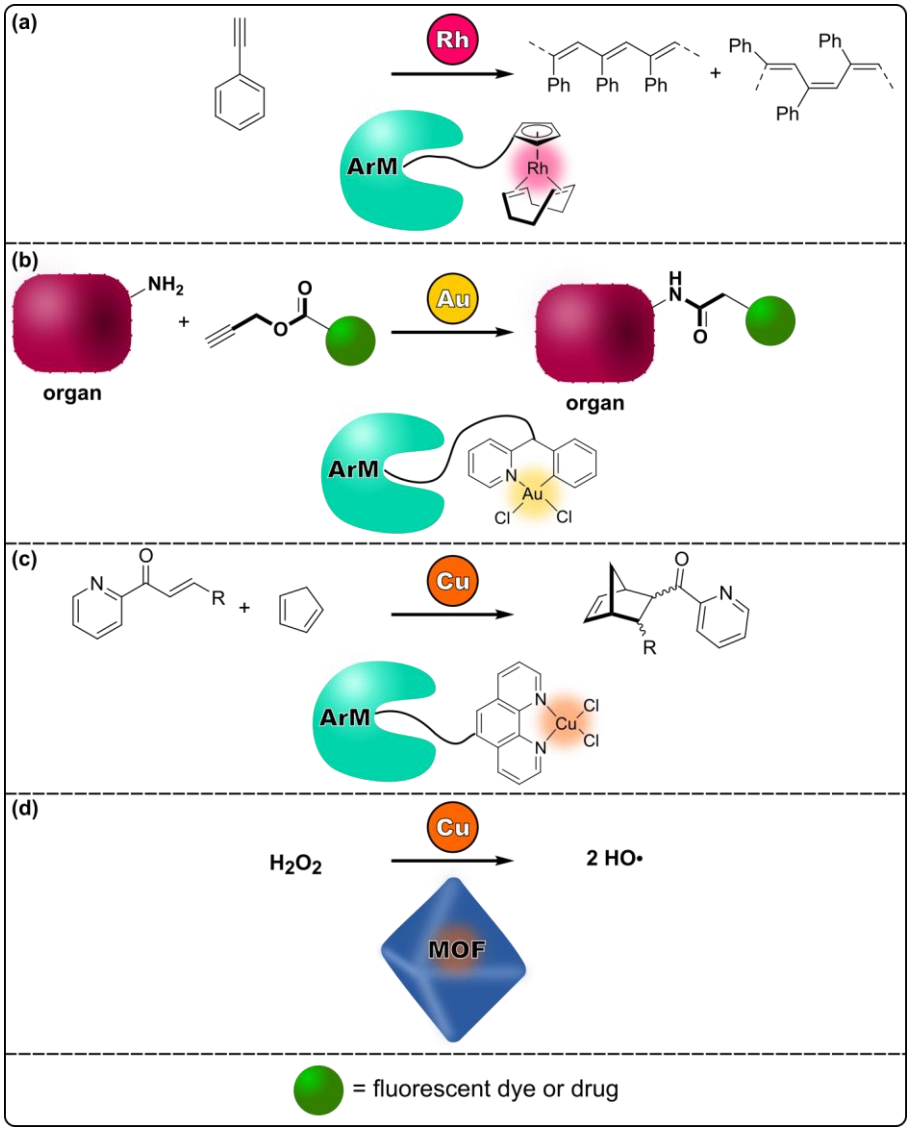

Figure 31. (a) Rhodium catalysed phenylacetylene polymerisation carried out on cell membranes (ref 123). (b) Gold catalyst propargyl ester amidation carried out on organs in live mice (ref 124). (c) Copper catalysed Diels-Alder cycloaddition carried out on cell surfaces (ref 125). (d) Copper catalysed hydroxyl radical formation carried out on live mice (ref 126).

Rhodium-based artificial metalloenzymes have been developed for catalysis on the surface of *E. coli* cells. Schwaneberg *et al*. anchored a Rh(cp)(cod) catalyst inside nitrobindin via a maleimide linker. This protein is located extracellularly, bound to the outer membrane. The free catalyst is active for the polymerisation of phenylacetylene (Figure 31a), with a TON of 5 x 10^3 and a 95% cis selectivity. When the catalyst is bound in the protein scaffold on the *E. coli* cells, the TON is as high as 39 x 10^6 per cell, and, interestingly, the selectivity is switched, with a cis:trans ratio of 20:80.[123] The authors comment that the TON achieved for this reaction was greater than the TON for Ward *et al.*'s artificial metathesis metalloenzyme (see section *Olefin Metathesis*), although these TON are not strictly comparable as they are for

different reactions with different catalysts. However, it indicates that conducting the reaction extracellularly does have the benefit of no inhibition from glutathione.

In the only example of a gold catalysed reaction which does not involve a cyclisation, Tanaka *et al*. made use of an artificial gold metalloenzyme to conduct propargyl ester amidation in live mice (Figure 31b). The artificial metalloenzyme was comprised of a coumarin-modified cyclometallated Au(III) complex coumarin docked inside of glycoalbumin (Glyco). Depending on the specific N-glycan structure used, the Glyco-Au adduct is able to target specific organs, specifically α(2-6)-disialoglycoalbumin (Sia) for targeting the liver, and galactosylglycoalbumin (Gal) for the intestine. After injection of the Glyco-Au complex into the mice, it selectively accumulates in an organ. Subsequent injection of a fluorescent propargyl ester results in gold-catalysed organ labelling, by forming amide bonds with surface amino groups on the tissue (Figure 32). Control reactions in the lab with 10 mol% of Glyco-Au complex with a lysine residue on the albumin in a H_2O/DMSO mixture resulted in the conjugation of about six fluorescent molecules to the protein after 20 h; oddly enough, no further control reactions are given, neither in biological media, nor in cells. Despite this, an increase in fluorescence intensity is observed in the mice, which is localised around the target organs which indicates that the reaction took place.[124]

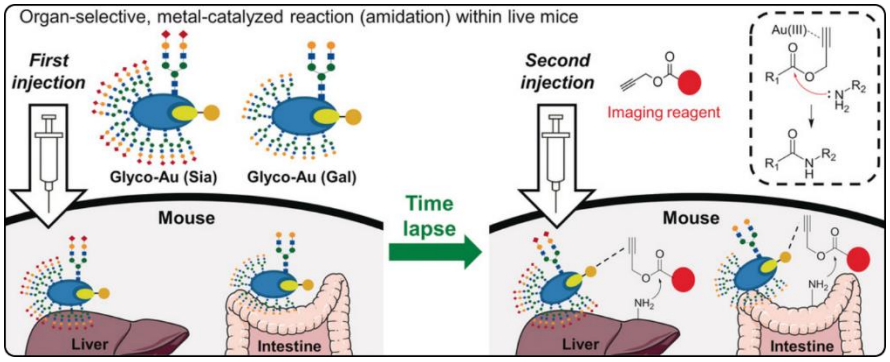

Figure 32. A gold catalyst docked inside glycoalbumin (Glyco-Au) is able to target either the liver or the intestines in mice depending on the nature of N-glycan structure used. The Glyco-Au adduct was first injected in live mice. A fluorescent propargyl ester is then also injected into the mice, and amino acid residues on the surface of the organs are labelled by the Glyco-Au adduct. Figure adapted from ref 124.

Copper catalysis in cells has not only been limited to the CuAAC reaction. Cu(II) phenathroline complexes were used to generate artificial metalloenzymes capable of catalysing a Diels-Alder cycloaddition (Figure 31c). The complexes were linked to an adenosine-like core which binds to the A_{2A} adenosine receptor (AR) and which is found in several A_{2A} AR antagonists. This scaffold is incorporated onto mammalian cells, in an attempt to avoid poisoning from intracellular components, by carrying out the catalysis on the surface of HEK cells. The catalytic activity of the adducts were monitored with the cycloaddition of cyclopentadiene and 2-azachalcones to generate chiral products. Although the on cell catalysis gave yields of 22–50% (with a max TON of 20) with endo selectivity, it should be noted that the free catalysts displayed similar yields, and the cells in the absence of copper complex also displayed some activity (4–8% yield), presumably from leached metals from dead cells.

Although the yields may not have been greatly improved for the ArM compared to free catalyst, the A_{2A} AR binding resulted in some enantioselectivity, with an e.e. of 14–28%. Curiously, the purified ArM produced lower yields than those attached to the cell surface, although the e.e. was higher.[125] This work exemplifies the first use of membrane receptors to generate artificial metalloenzymes.

Finally, a Cu(II)-containing MOF has been used in combination with an endogenous enzyme to encourage wound healing in mice by inducing bacterial cell death. Qu *et al.* used a 2D Cu-TCPP(Fe) nanosheet to which the enzyme glucose oxidase (GOx) was physically adsorbed. The 2D MOF nanosheet exhibits peroxidase-like activity and catalyses the conversion of hydrogen peroxide into hydroxyl radical, •OH (Figure 31d), which is extremely toxic to bacteria, and has been applied as a potent antimicrobial agent. However, using the 2D MOF alone would require the addition of high concentrations of external H_2O_2, which is also damaging to normal tissues. In addition, the nanosheets typically require acidic conditions of pH 3–4. Therefore, this issue was circumvented by using the GOx enzyme to use oxygen and glucose to generate H_2O_2 and gluconic acid *in situ*, thus lowering the local pH (Figure 33). This combined system exhibited good antibacterial properties in the presence of *E. coli* and *S. aureus*, with a bacterial inactivation of 88% and 90% respectively. A 2D MOF/GOx–plaster was then applied to wounded mice. The wounded mice treated with this plaster exhibited better healing than the control mice, with the bacteria decreased to just 9.1%.[126] This is an elegant example of the benefits of combining an artificial catalyst with an endogenous system.

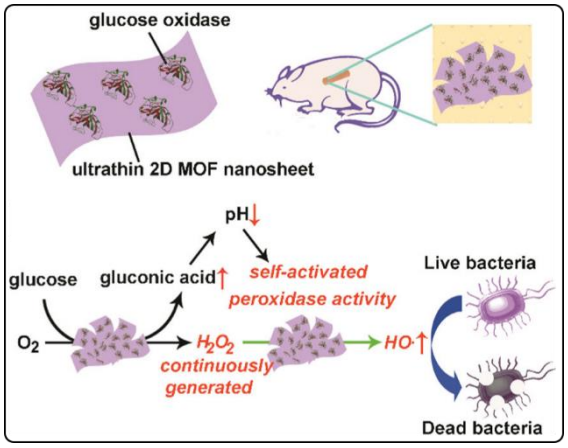

Figure 33. The enzyme glucose oxidase (GOx) was physisorbed onto a MOF based 2D Cu-TCPP(Fe) nanosheet (2D MOF). This was then applied as a plaster on wounded mice. The GOx uses glucose to convert oxygen into hydrogen peroxide while also producing gluconic acid. The gluconic acid decreases the local pH, which activates the activity of the 2D MOF. The 2D MOF then catalytically generates hydroxyl radical from the hydrogen peroxide. The hydroxyl radical kills bacteria, which promotes the healing of the wounded mice. Figure adapted from ref 126.

CONCLUSION

A diverse range of transition metal catalysts and reactions have been shown to exhibit some degree of compatibility with living cells. These reactions range from simple redox transformations, to intramolecular bond breaking and bond making reactions, and to

challenging intermolecular coupling reactions. These reactions provide routes to generate various drugs and fluorescent dyes *in situ* in living cells: from deprotection reactions, dominated by ruthenium and palladium catalysts; from gold or ruthenium catalysed cyclisation reactions; and from copper catalysed click reactions and palladium catalysed cross coupling reactions. The catalysts used are either large heterogeneous nanoparticles and other 3D nanostructures; discrete molecular catalysts, which are either applied as a small homogeneous catalyst; or are inserted into a protein to form an artificial metalloenzyme. All of these different strategies have their own advantages and limitations. While large heterogeneous structures may afford good reactivity, catalyst synthesis may require several steps, and very large structures may have difficulty crossing the cell membrane. Artificial metalloenzymes provide a route to targeted catalysis, for example by overexpressing the protein host in a particular location of the cell, such as the periplasm. However, large amounts of screening and protein evolution may be required to find the optimum host-guest structures to generate the most active metalloenzyme. Finally, while precise control over the reactivity of small metal complexes as catalysts is possible, for example by simple modifications to the ligand structure, the metal centre is often highly exposed to the cell environment and can be readily deactivated. While the reactivity of transition metal catalysts which has been achieved up until now is impressive, significant improvements upon the biocompatibility of the metals with the cell environment need to be achieved in order to make future progress in the field of *in vivo* transition metal catalysis.

SUPRAMOLECULAR METALLOCAGES

It is clear that one of the main road blocks in the way of achieving efficient catalysis is the inhibition and poisoning of the metals by endogenous biomolecules. This is largely due to the large quantities of glutathione present inside cells. While some reactions have used the presence of glutathione to its advantage, by using it either as a substrate or reducing agent for the reaction, this is not always a viable strategy, for example where the goal of the reaction does not include or does not tolerate perturbing the redox balance of the cell. In some instances, catalyst poisoning has been avoided by simply performing the reaction in a location where there is no or low levels of glutathione, for example extracellularly or in bacterial periplasm, or by intentionally adding oxidising agents to remove the glutathione. However, this is severely restricts both the types of reactions which can be done, and the applications of the catalysis. Mammalian cells do not have a periplasm, and for reasons of drug efficacy perhaps the catalysis needs to be localised within an intracellular organelle. In order to expand the toolbox of new-to-nature reactions, methods to efficiently protect the catalyst without hindering the reactivity need to be developed.

One answer to this problem could be encapsulating the catalyst inside supramolecular cages, in order to physically separate the catalyst from poisonous biomolecules. Many different types of 3D architectures are known, including bio-derived assembled structures comprised of DNA or peptides,[127-130] or synthetic structures, which can either be covalently linked,[131] or use supramolecular interactions to hold together building blocks.[132] However, here, the applicability of metallocages for encapsulating catalysts will be explored. Metallocages are superior to covalent cages in terms of ease of synthesis; where a covalent cage may require many difficult or cumbersome steps to obtain the final 3D structure, metallocages are formed from the self-assembly of simple metal salts with building blocks containing metal-binding moieties. The shape and size of the desired cage can usually be controlled by the size and bond angles of the building blocks, allowing for flexibility in design for the desired application.

ENCAPSULATED TRANSITION METAL CATALYSIS

Supramolecular metallocages are known to encapsulate both organic and metallic catalytically active species which can participate in a range of transformations.[133] Encapsulated transition metal catalysts often display different and interesting reactivity compared to free species. For example, Reek *et al*. showed that the selectivity and enantioselectivity for an asymmetric hydroformylation reaction could be improved by use of a supramolecular box. Confining the catalyst in a large, self-assembled bidentate ligand comprised of two Zn(salphen) moieties bound to two chiral phosphine ligands had the remarkable effect of reversing the selectivity for the hydroformylation of cis and trans 2-olefins: while the free ligand preferred hydroformylation to take place at the outside position to give the 2-aldehyde, the box ligand resulted in the preferred formation of the 3-aldehyde. The box ligand also displayed greatly improved enantioselectivities, with the trans olefin giving 80% of the major isomer, and the cis olefin giving 90%, outperforming the free catalyst as well as other commercially available chiral ligands.[134] It is clear that catalyst confinement can have

a large effect upon the outcome of a reaction. While there are many examples of cages influencing reactivity, such as for organic transformations and organic catalysts which are encapsulated, or where the cage itself behaves as the catalyst, here a selection of examples where the activity of a transition metal complex is altered by encapsulation in a supramolecular environment will be highlighted. Although improvements in reactivity often come down to a combination of reasons, a main factor which is influencing reactivity can often be identified. Therefore, in the following section catalytic reactions which experience cage effects will be broadly divided into several categories.

Increased Local Concentration and Pre-Organisation

One pronounced effect of carrying out a catalytic reaction inside of a microenvironment is the increase in local concentration of substrate around the catalyst. This strategy has been particularly effective for gold catalysed reactions. Several $(PPh_3)AuCl$ complexes were covalently bound to the inside of a $Pd_{12}L_{24}$ cage, and their catalytic reactivity was investigated by Reek *et al*. Heteroleptic spheres were prepared using varying stoichiometries of ditopic ligands which were functionalised with either an acetate group, or with a gold complex attached by a small alkyl spacer (Figure 34a). At the same time as keeping the global gold concentration the same, the local concentration of gold within the spheres was varied from between 0.05–1.1 M, by varying the ratio of unfunctionalised and gold-functionalised building blocks during sphere formation. The spheres containing a higher local gold concentration resulted in higher yields for the selective formation of the five membered ring for both allenol hydroalkoxylation (Figure 34b) and the intramolecular cycloisomerisation of 1,6-enyne. Interestingly, in contrast with the free molecular catalyst, PPh_3AuCl, chloride abstraction is not required to initiate the catalytic reactivity, likely due to the d10-d10 aurophilic interactions generated as a result of the high local concentrations of gold.[135] In an effort to expand the substrate and reaction scope for this system, a more robust Pt analogue of the mixed cage was also synthesised. For [4+2] cycloadditions catalysed by the neutral gold complex, the Pt cage was able to give very low conversions, whereas the Pd cage was inactive due to cage disassembly during the reaction. However, for reactions involving cationic gold the Pt cage provided excellent conversions (Figure 34c). The platinum spheres were sufficiently stable to allow chloride abstraction by silver, opening the door to a wider range of reaction possibilities. For most of the attempted cyclisation reactions, the high local concentration of cationic gold within the Pt sphere resulted in either higher conversions or different selectivities compared to the molecular gold reaction, as a result of the higher local gold concentration.[136]

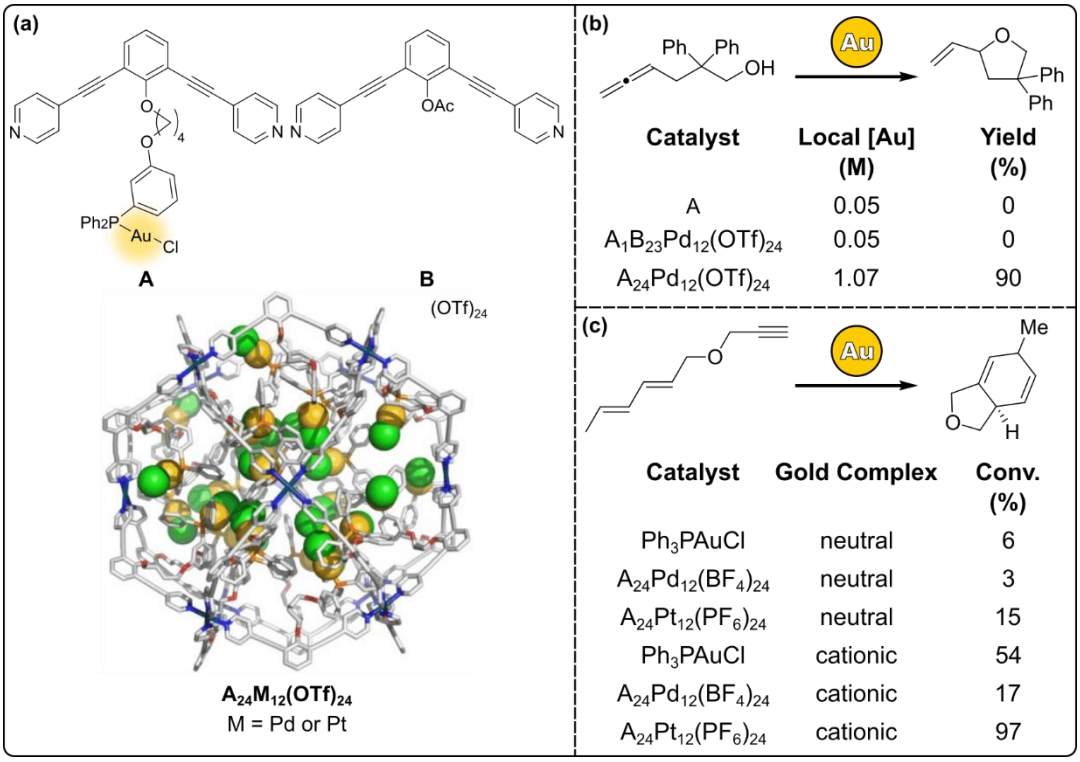

Figure 34. (a) Structure of the $M_{12}L_{24}$ cage containing covalently attached gold complexes, where M is either palladium or platinum. Figure adapted from ref 136. (b) Intramolecular allenol hydroalkoxylation catalysed by the encapsulated gold complex. While keeping the overall gold concentration the same, increasing the local gold concentration within the sphere drastically increases the yield of the cyclised product (ref 135). (c) Intramolecular [4+2] cycloaddition catalysed by the encapsulated gold catalyst. The neutral gold complexes give low conversions. However, when a cationic gold catalyst is generated upon addition of silver the stable Pt cage gives almost full conversion, while the unstable Pd cage decomposes and gives much lower conversion (ref 136).

Using a similar strategy of endohedrally functionalising a sphere with gold complexes, a $Pt_{12}L_{24}$ sphere was developed which can non-covalently bind negatively charged moieties (Figure 35a). Here the cage provides a scaffold upon which the catalyst and substrate are pre-organised. Spheres were prepared from building blocks which were functionalised with guanadinium groups, which are able to bind both carboxylated and sulfonated guests. Following the binding of a sulfonated gold catalyst, the reactivity towards the cyclisation of acetylenic acid to the corresponding enol lactone by cationic gold was investigated (Figure 35b). Following deprotonation, the substrate is able to bind to the guanidinium groups inside the cage. As the cyclic product is neutral it has no affinity for the cage, and therefore leaves the cavity of the cage and is separated from the catalyst, preventing product inhibition. This catalytic system resulted in a dramatic increase in substrate conversion, and a 40-fold increase in turnover frequency (TOF). Control experiments confirmed that this reactivity was a result of a pre-organisation effect of the substrate in proximity with the catalyst, rather than a local proton concentration effect.[137] This is an elegant example of how nature's strategies for efficient enzyme catalysis can also be applied in a synthetic setting.

The guanadinium sphere has been used to promote the copper catalysed cyclisation of alkynoic acids (Figure 35b). Previous reports had indicated the need for high catalyst loadings in order to achieve substantial conversions, and after conducting mechanistic studies to confirm that this is due to a dinuclear mechanism occurring, it was again predicted that this reaction could be promoted by the use of high local catalyst concentrations inside the sphere. Encapsulation of a sulfonated Xantophos-Cu(I) catalyst inside the $Pd_{12}L_{24}$ guanadinium cage indeed resulted in a dramatic increase in yield compared with the molecular catalyst, with this increase being only due to increased local concentrations, rather than pre-organisation effects.[138] Clearly, concentrating and organising catalysts and substrates inside a supramolecular cage can have large positive effects upon catalytic reactions, which could prove particularly useful for *in vivo* applications, where the overall catalyst concentration must be kept relatively low.

The advantages of this guanidinium $Pt_{12}L_{24}$ sphere have also been exploited to promote water oxidation catalysis (Figure 35c). Ruthenium catalysts are known to participate in water oxidation via a dinuclear mechanism, where two metal-oxo centres are required to interact. At dilute concentrations the rate of this reaction is slowed due to diffusion limitations, so it was hypothesised that organising the ruthenium catalysts inside the sphere could promote the reaction by increasing the local concentration. Indeed, it was observed that pre-organising the catalyst resulted in a 4-fold increase in catalytic current compared to the free molecular catalyst. In addition the local catalyst concentration was varied from 0.04–0.54 M by incorporating different equivalents of catalyst within the cage, and it was observed that increasing the local concentration could increase the reaction rate by 130-fold compared to the molecular catalyst, providing evidence that the dinuclear mechanism is promoted by pre-organising the catalyst.[139] This exemplifies that taking advantage of both local catalyst concentrations and pre-organisation effects can dramatically improve a catalyst system.

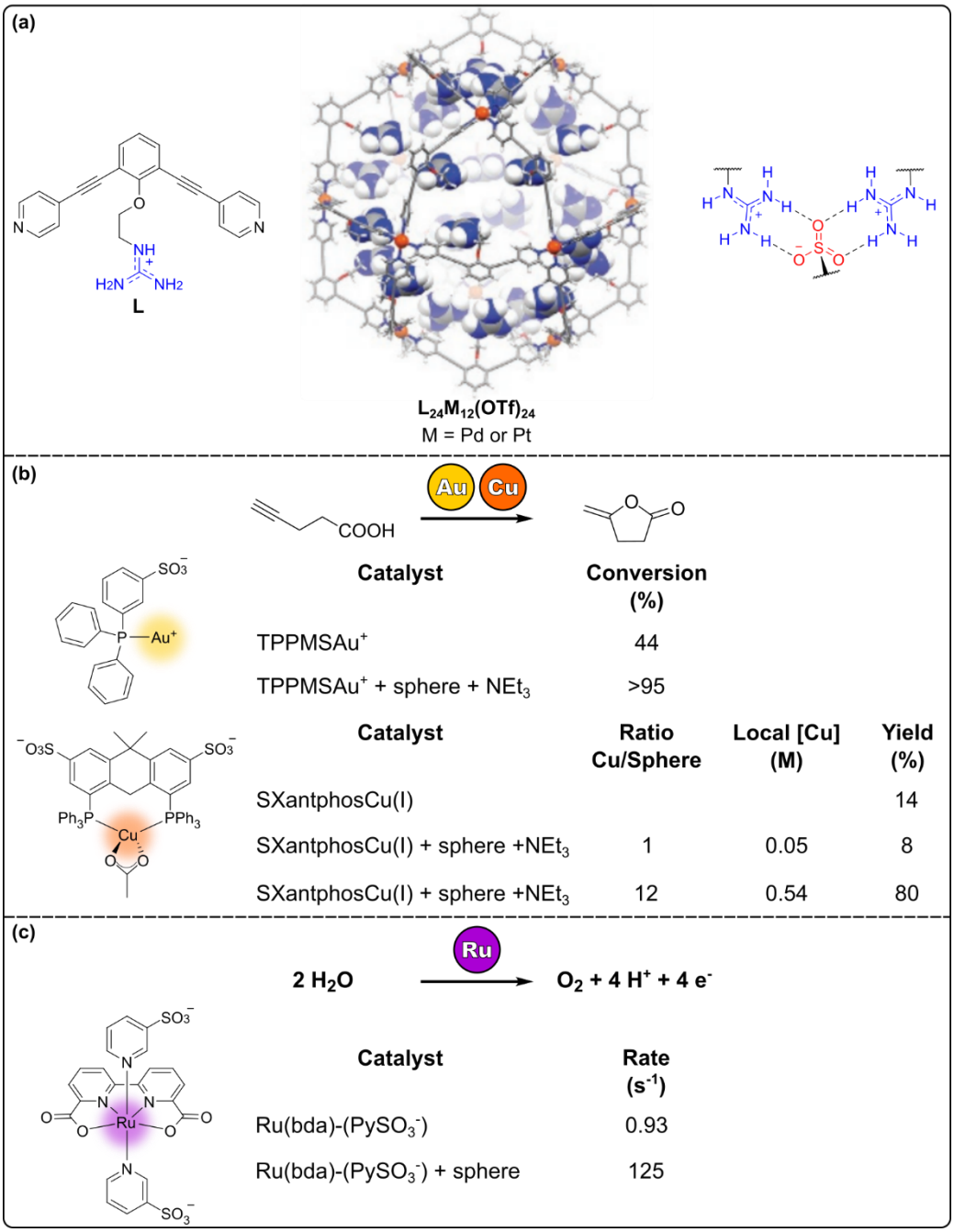

Figure 35. (a) Structure of the $M_{12}L_{24}$ guanadinium sphere. One sulfonated guest binds to two adjacent guanadinium moieties within the cage. Figure adapted from ref 137. (b) Cyclisation of acetylenic acid (ref 137). For the gold catalysed reaction, pre-organised gold catalysts within the cage gave higher conversions than for the free gold complex. For the copper catalysed reaction (ref 138), the dinuclear mechanism is aided by the increased local concentration of copper catalysts within the cage compared to the free catalyst. (c) Water oxidation catalysis (ref 139). The increased local concentration and pre-organisation of the ruthenium catalysts aids the dinuclear mechanism and gives higher rates compared to the free catalyst.

Size Selectivity

The group of Raymond *et al.* have exploited the small window size of a tetrahedral Ga_4L_6 cage (Figure 36a) in order to achieve size-selective catalysis. At the centre of this water

soluble cage is a small hydrophobic cavity, which is able to encapsulate small hydrophobic and monocationic guests, such as ammonium cations and, more interestingly, small metal complexes. Although initially demonstrated to take part in stoichiometric reactions, the cage was shown to discriminate between substrates for the C–H bond activation of aldehydes using a $[Cp^*(PMe_3)Ir(Me)(Et)]^+$ complex, where only small, non-bulky substrates could fit inside the cage and react with the metal centre (Figure 36b).[140] By use of a more reactive iridium complex, the scope of this reaction could also be expanded to include ethers, dihydrogen, and strained alkanes, with the same size and shape selectivity observed as for the aldehyde substrates.[141] Having established the size discrimination ability of this cage, Raymond and co-workers went on to further demonstrate this concept for catalytic reactions. One such example is the rhodium catalysed isomerisation of allyl alcohols and ethers (Figure 36c). After encapsulation of $(PMe_3)_2Rh(COD)^+$, the active species, $(PMe_3)_2Rh(OD_2)^{2+}$, was generated by hydrogenation with dihydrogen. While large and branched substrates are able to react with the free catalyst, they proved to be unreactive to the encapsulated catalyst, due to the fact that they are unable to fit through the window of the cage. This was further evidenced by inhibition experiments, which proved that the catalyst remains bound inside of the cage throughout the catalytic cycle.[142]

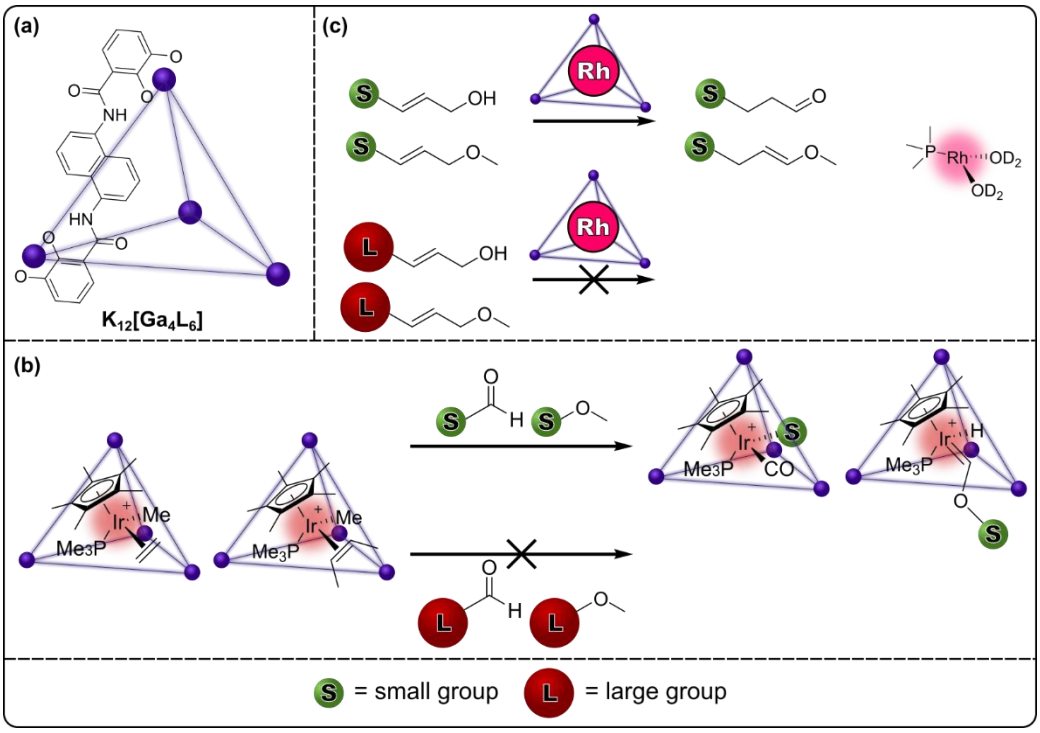

Figure 36. (a) Structure of the Ga_4L_6 tetrahedral cage. (b) Size-selective C–H activation of aldehydes and ethers by encapsulated iridium complexes (ref 140–141). (c) Size-selective rhodium catalysed isomerisation of allyl alcohols and ethers (ref 142).

Size selectivity has also been demonstrated for the hydroformylation reaction by Reek *et al*. A pre-activated rhodium bis-(Py_3P) catalyst was encapsulated in the apolar cavity of a tetrahedral Fe_4L_L cage by binding to the zinc porphyrins moieties which were incorporated into the ligand. While the free catalyst displays no size selective catalytic activity, the cage provides an opportunity to discriminate between aliphatic alkenes and aromatic substrates, due to the

limiting window size (Figure 37). This was demonstrated by the 78% conversion observed for 1-octene with the encapsulated catalyst compared to the almost no conversion observed for aromatic substrates. Indeed for a mixture of 1-octene and styrene, the encapsulated catalyst showed a 4-fold increase in selectivity for the smaller aliphatic substrate compared to the free catalyst. Interestingly, size selectivity was also observed amongst the aliphatic substrates. A distinct odd-even effect was observed, with even chain number substrates giving higher conversions than odd number chains; unsurprisingly, this effect is not observed for the free catalyst. It was postulated that the origin of this odd-even chain length difference is due to odd chain lengths resulting in more enthalpically favourable substrate-catalyst complexes inside the cage, leading to their lower reactivity.[143]

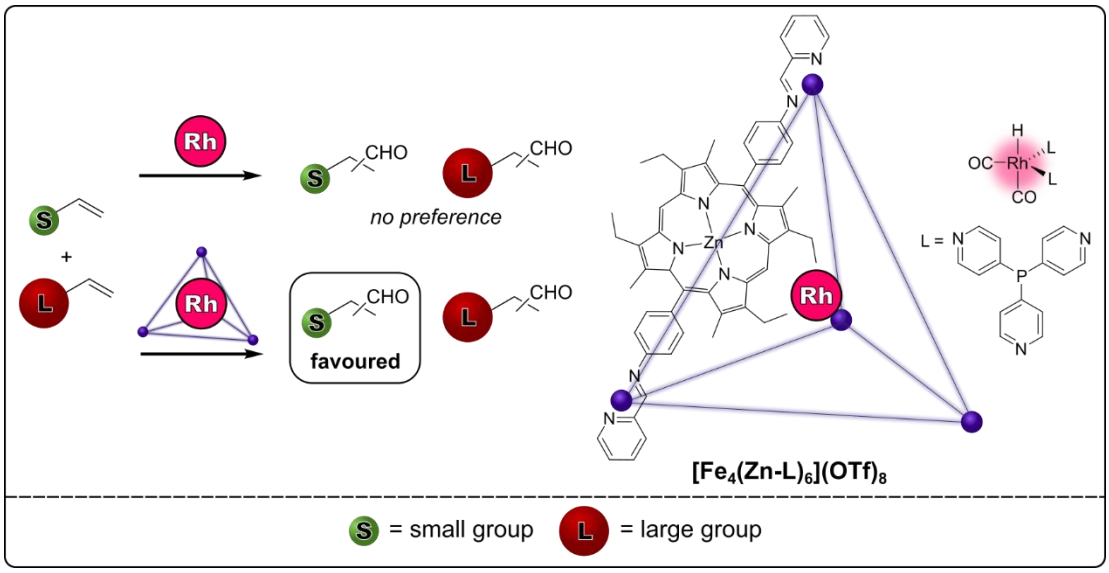

Figure 37. Encapsulation of a rhodium complex inside the tetrahedral $Fe_4(Zn\text{-}L)_6$ cage imparts size selectivity upon the hydroformylation of terminal alkenes (ref 143).

Finally, a cubic Fe_8L_6 cage has been demonstrated to be able to impart size selectivity on two different transformations. The large cubic cage comprised of zinc porphyrin faces encapsulates metal tetra(4-pyridyl)metalloporphyrins inside its cavity (Figure 38a). The cobalt complex was able to preferentially catalyse the cyclopropanation of smaller styrene and diazo substrates over larger substrates (Figure 38b). A mixture of a small and a large substrate were reacted with the cobalt catalyst. While the free catalyst exhibited no selectivity, the encapsulated catalyst resulted in a preference for the cyclopropanation of the smaller substrate.[144] The manganese complex inside the same cage similarly favoured smaller substrates for the epoxidation of styrenes (Figure 38c).[145] Although only a small number of cages have demonstrated the ability to distinguish between substrates based on size, this is a very promising concept for the protection of transition metal catalysts inside cells – while biomolecules which are the same size or smaller than the desired substrate would not be excluded based upon size, it is reasonable to hypothesise that a cage would provide a means by which large or bulky catalyst poisons could be spatially separated from the catalyst.

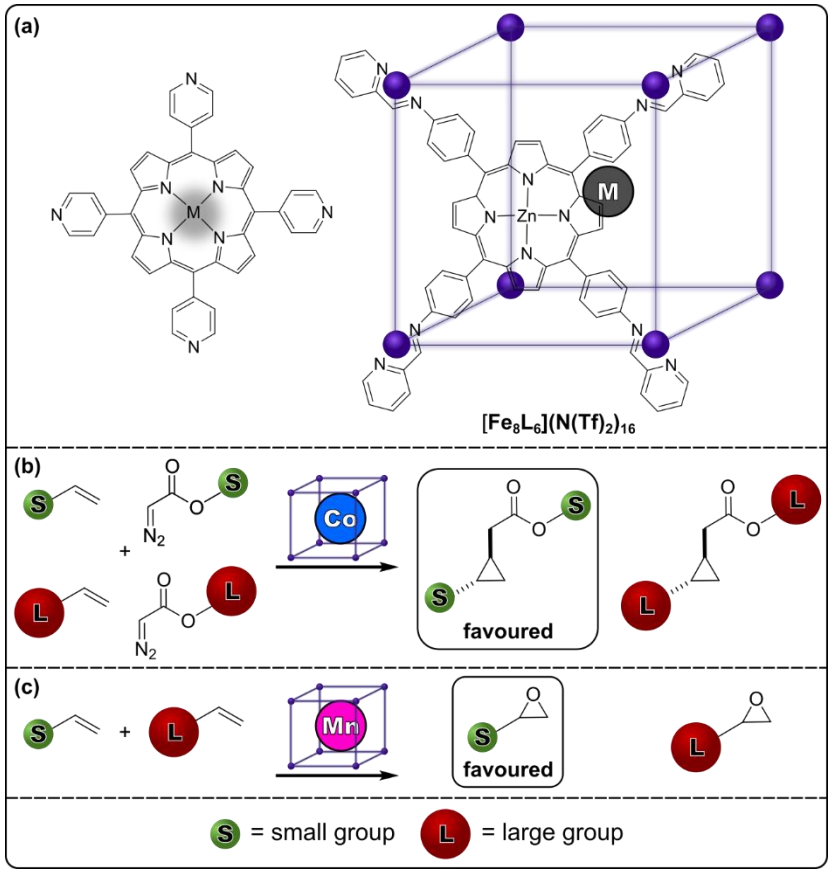

Figure 38. (a) Structures of the cubic $[Fe_8L_6](N(Tf_2)_{16}$ cage and the encapsulated metal tetra(4-pyridyl)metalloporphyrin. (b) Size selective cobalt catalysed cyclopropanation of styrene and diazo substrates (ref 144). (c) Size selective manganese catalysed epoxidation of styrene substrates (ref 145).

Stabilisation

In many examples of confined catalysis, the role of the cage is to stabilise the catalyst in some way, which leads to different, and often improved, catalytic activity. Raymond *et al.* have shown that their water soluble tetrahedral Ga_4L_6 is particularly useful for stabilising catalysts. In the presence of a small gold complex, PMe_3AuX, the cage shifts the equilibrium to give complete dissociation of the gold-halide bond, resulting the encapsulation of the cationic species $[PMe_3Au]^+$. Although typically in water such gold catalysts have a short lifetime due to decomposition, encapsulation of the catalyst allows the gold catalysed reaction to take place in water with an 8-fold increase in rate for the hydroalkoxylation of allenes, where the encapsulated catalyst gave a 48% yield of the cyclic product, compared to just 11% by the free catalyst.[146] Similarly, the cage protects cationic half sandwich ruthenium complexes from decomposition and improves their solubility. The encapsulated $[RuCp(PMe_3)(MeCN)_2]^+$ species was shown to be stable for days in up to 10 mM aqueous solutions, while the free PF_6 salt of the complex could only be solubilised in <1 mM solutions, and rapidly decomposed due to exchange of the MeCN ligands for D_2O, leading to further decomposition to give catalytically inactive species. The cage also provides protection from decomposition during the catalytic cycle for the isomerisation of 3-butan-2-ol. When encapsulated in the cage, the formation of an inactive complex is disfavoured, resulting in a TON of 1070, which is higher

than the free catalyst in organic solvent.[147] These two reactions were then combined alongside enzymes to generate tandem catalytic reactions (Figure 39). First, the encapsulated gold catalyst was shown to be compatible with hog liver esterase. The enzyme converted allenic acetate to the corresponding alcohol, which was then subsequently cyclised by the gold catalyst, giving full conversion to the final cyclised product over 20 h. While the free gold catalyst inhibits the enzyme due to interaction with the amino acid residues, the cage prevents this interaction and does not impact the enzymatic activity. The ruthenium catalysed isomerisation reaction was also shown to be compatible with enzymes. First, the encapsulated ruthenium complex generated the corresponding aldehyde from allyl alcohol. Secondly, alcohol dehydrogenase reduced the aldehyde to give the saturated alcohol. In order to regenerate the NADPH necessary for the enzyme to function, the reduction was coupled to formate hydrogenation by formate dehydrogenase. While less efficient than the enzyme-gold system, a 61% yield of propanol was achieved after 6 h.[148] These tandem reactions exemplify the compatibility of cages with biological components, and illustrate the importance of the cage in protecting both components from deactivation.

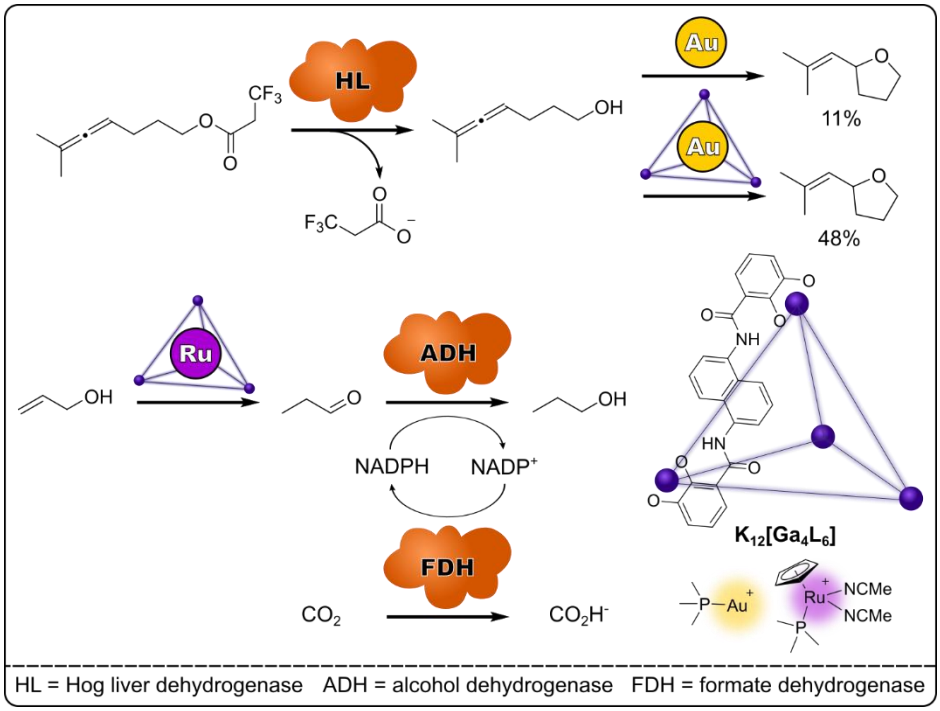

Figure 39. Tandem encapsulated catalyst-enzyme reaction with the Ga_4L_6 tetrahedral cage. Hog liver dehydrogenase (HL) hydrolyses the allene-ester to give the corresponding alcohol, which then undergoes a gold catalysed intramolecular hydroalkoxylation. The encapsulated gold catalyst exhibits better reactivity than the free gold catalyst. Encapsulated ruthenium catalyst isomerises allyl alcohol to the corresponding aldehyde, which is then reduced to give the saturated alcohol by alcohol dehydrogenase (ADH). The NADPH which is required by the ADH is replenished by formate dehydrogenase (FDH) (refs 146–148).

This same cage was also shown to protect a platinum catalyst from decomposition, with the role of supramolecular co-catalyst in a C–C bond forming reaction. Raymond *et al.* hypothesised that the cage would stabilise the transition state for C–C formation and catalyse

the reductive elimination of an alkane from a high-valent dialkyl metal complex. With proof of concept established stoichiometrically, first with a gold complex, it was found that 10 mol% of cage increased the rate of ethane elimination from $(Me_3P)(Me)_2AuI$ by 4000-fold compared to the free complex. This rate increase was further improved to 80,000-fold with the use of a slightly bulkier triethyl phosphine ligand, as this species was too large to form the inactive dimer within the cage. A rate increase of 2300-fold was also achieved for a platinum complex, $(Me_3P)(Me)_3PtI$. Interestingly, this platinum complex was also able to behave catalytically, where 10 mol% of platinum complex in combination with 5 mol% of cage could generate ethane from methyl iodide and a tetramethyl tin, albeit with no comment on the efficiency of the reaction (Figure 40).[149] Clearly a stabilising effect from a supramolecular cage can have a dramatic effect upon the rate and efficiency of a reaction.

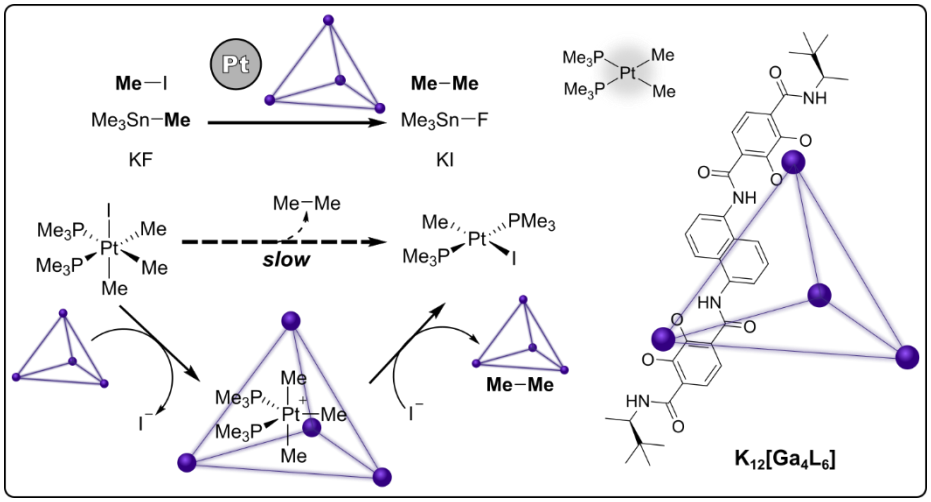

Figure 40. The tetrahedral Ga_4L_6 cage acts a co-catalyst to promote the platinum-mediated ethane formation from methyl iodide and tetramethyl tin (ref 149).

The first examples of a radical-type transformation involving diazo compounds inside of a supramolecular cage were achieved by using a cobalt catalyst inside of a Fe_8L_6 cube. Metalloporphyrins are ubiquitous catalysts used for a variety of transformations. However, they are easily deactivated through dimer formation, which are accessed by radical pathways. Therefore, de Bruin *et al*. proposed that encapsulation could provide a route by which to prevent this deactivation. The large cubic cage (see section *Size Selectivity*) encapsulated cobalt tetra(4-pyridyl)metalloporphyrin inside the cavity, and indeed from EPR studies it was shown that confinement in the cage prevented against self-aggregation. The benefit of preventing this dimerization was illustrated with the 50% yield and 60 TON of the radical cyclopropanation of styrene with ethyl diazoacetate achieved by the encapsulated catalyst; an improvement upon the 15% yield and TON of 18 with the free catalyst (Figure 41).[150] For this radical reaction, encapsulation had the effect of improving the lifetime and reactivity of the catalyst.

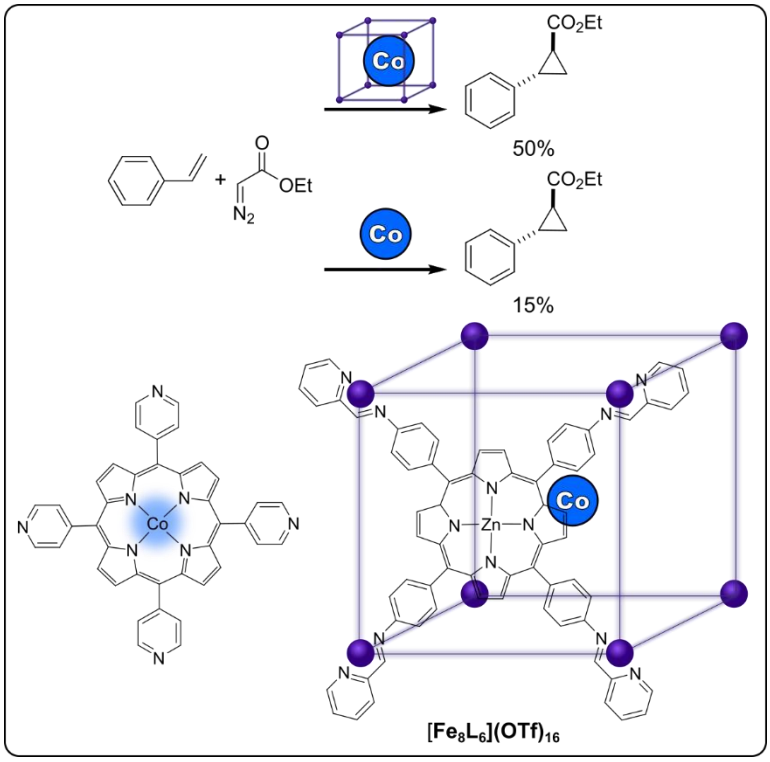

Figure 41. Structure of the Fe_8L_6 cubic cage which encapsulates a cobalt catalyst. The encapsulated cobalt complex catalyses the radical cyclopropanation of styrene and ethyl diazoacetate in better yields than the free cobalt complex (ref 150).

Cui *et al*. demonstrated that catalysts based upon M(salen) active sites which are prone to deactivation by dimerisation and oxidation could also be improved by confinement, this time by incorporating the catalyst into the ligand backbone of both an octahedral and tetrahedral cage. A homochiral, enantiopure Zn_4L_{12} octahedron containing 12 Mn(salen) sites in the ligand backbone was prepared, and its reactivity towards the oxidative kinetic resolution of racemic alcohol was tested (Figure 42a). The handedness of the cage determined the handedness of the product, with 54-59% yield and an e.e. of 91-99%. The free catalyst gave similar conversions, but a slightly lower e.e.. However, this difference in reactivity and selectivity was magnified at low catalyst loadings, due to the higher rate of deactivation of the free catalyst under those conditions. This greater difference in behaviour between the cage and the free catalyst was also observed for alkene epoxidation.[151] Tetrahedral analogues of this cage containing different metal centres at the salen active sites were able to carry out sequential catalytic reactions inside the same cage. Homoleptic cages containing either manganese or chromium could catalyse the asymmetric epoxidation of 2,2-dimethyl-2H-chromene (DMCH) and the asymmetric epoxide ring opening of 2,2-dimethyl benzopyran oxide respectively, both with good yields. A heteroleptic cage containing three manganese active sites and three chromium active sites was able to carry out both reactions sequentially, to give the final azido alcohol product in a 79% yield and 93% e.e. (Figure 42b). Interestingly, the catalytic activities and enantioselectivities, as well as the initial TOF, of the heteroleptic cage was higher than both a mixture of free catalysts, and a mixture of both homoleptic cages. The authors propose that this is due to the fact that both reactions can take place in the same cavity, so there is no loss of rate due to mass transfer between cages or metal centres. As for the homoleptic manganese cage reported

previously, these differences were amplified at lower catalyst loadings. Notably, the cages displayed catalytic activity even at very low loadings of 0.005–0.001 mol%, while the free catalysts were inactive.[152] Being able to prevent catalyst decomposition at low catalyst loadings by encapsulation would of course be a greatly useful tool to help lower catalyst loadings of catalysts applied in living cells.

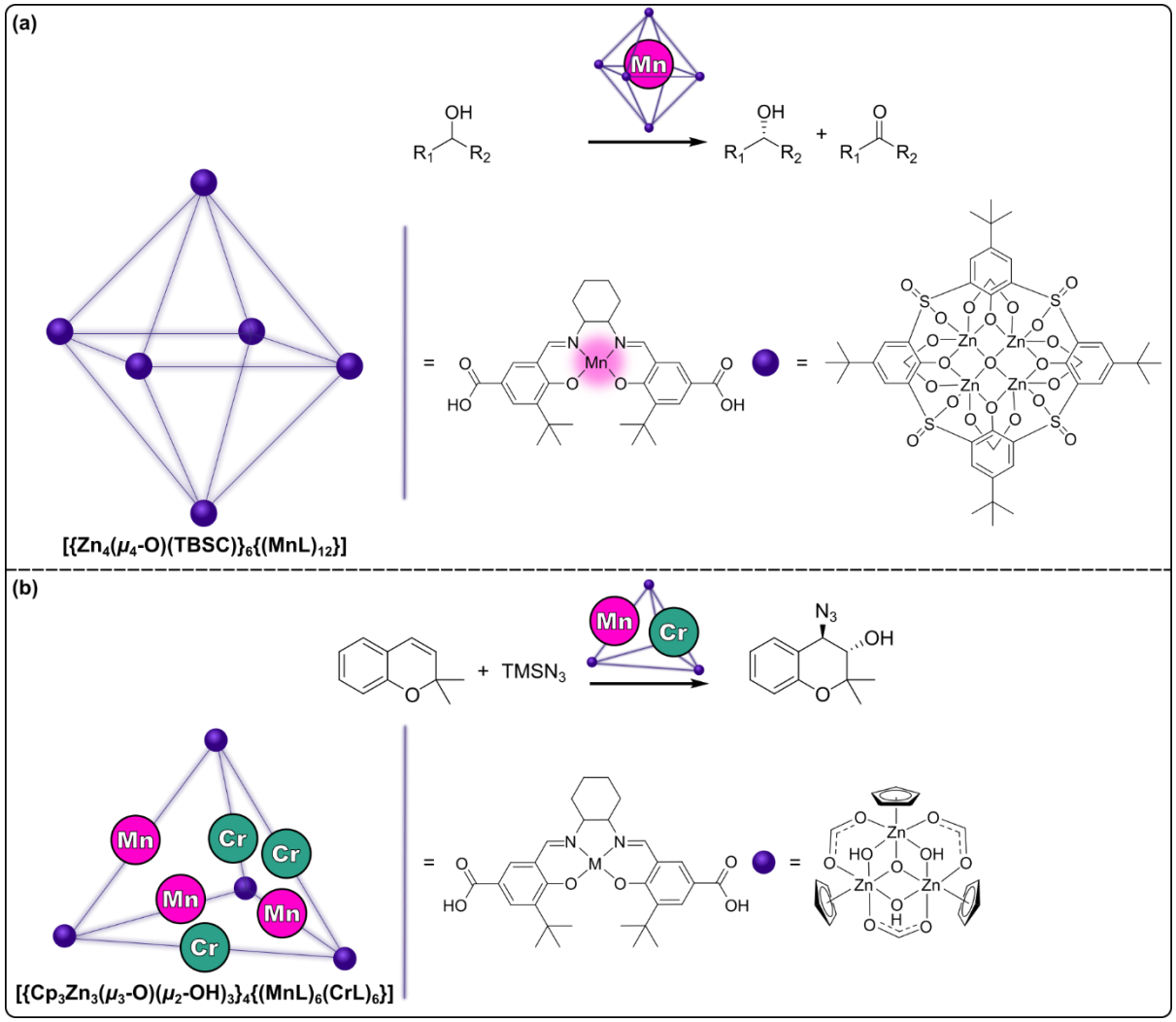

Figure 42. (a) Structure of the octahedral M_6L_{12} cage where manganese catalysts are incorporated into the ligand of the cage. The manganese centres catalyse the oxidative kinetic resolution of racemic alcohols (ref 151). (b) Structure of the tetrahedral M_4L_6 cage where chromium and manganese catalysts are incorporated into the ligands of the cage, generating a heteroleptic cage. The manganese centres catalyse the asymmetric epoxidation of DMCH and the chromium centres catalyse the asymmetric epoxide ring opening of 2,2-dimethyl benzopyran oxide (ref 152).

While photocatalysts do not suffer as greatly towards decomposition in cells compared to normal catalysts, as they often do not require a vacant site to which biomolecules could easily bind, it is also worth noting that the activity of photocatalysts can also be improved by encapsulation in a cage. A simple photocatalyst, $[Ru(bpy)_3]^{2+}$, was encapsulated inside an octahedral Co_6L_4 cage, PCC-2. The activity of the ruthenium complex was investigated by the photocatalytic degradation of the dicationic organic dye, methylene blue, into CO_2 and water

(Figure 43). Despite both the metal complex and the substrate have a positive charge of two, they are able to be co-encapsulated inside the anionic cage. This increased the degradation of the dye from 20% for the free catalyst, to 95% for the confined system, as free in solution charge repulsion can keep both species apart.[153] Even though the lifetime of photocatalysts in cells may not need improving, using a cage to bring the substrate together with the active site would of course be a great advantage in the complex environment of a cell.

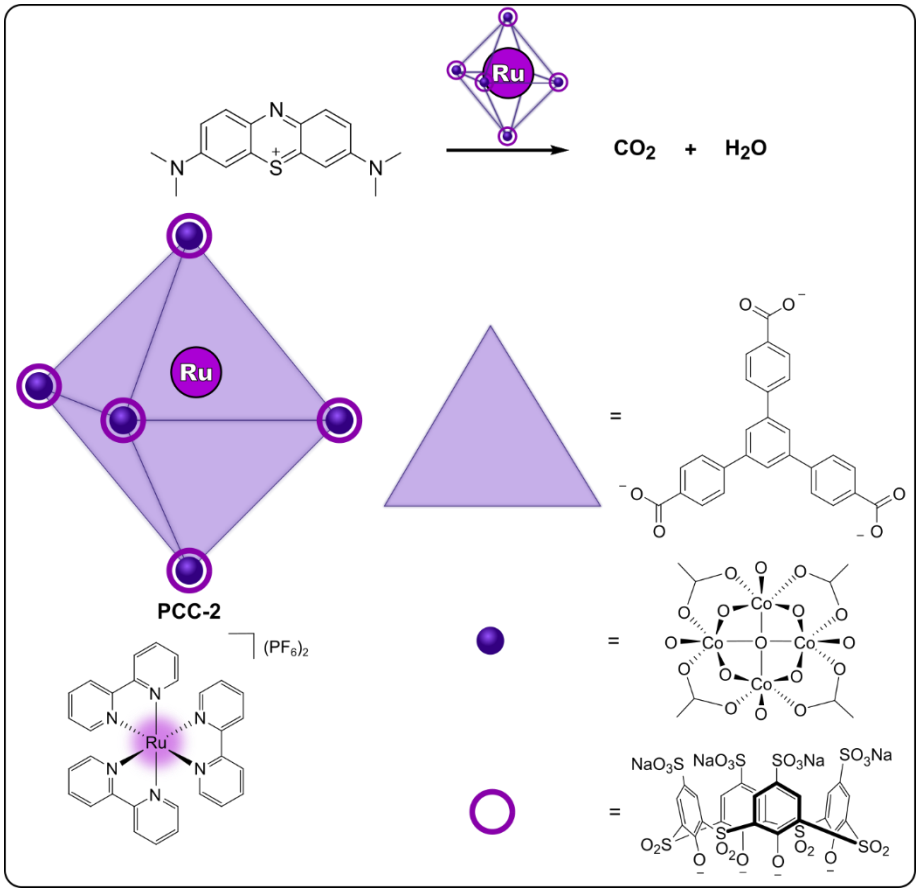

Figure 43. Structures of the octahedral M_6L_4 cage and encapsulated ruthenium complex. The complex photocatalytically decomposes methylene blue into CO_2 and water (ref 153).

METALLOCAGE BIOCOMPATIBILITY

Clearly the confinement of a transition metal catalyst inside of a supramolecular cage has the potential to improve the field of *in vivo* catalysis. The applicability of this concept to cells has already been somewhat illustrated. A copper catalyst coordinated to a covalent cage-like ligand exhibited better CuAAC reactivity in water in the presence of glutathione compared to a typical click system of Cu-TBTA.[154] However, the CuAAC reaction is already known to be a very efficient reaction in living cells, so it is still unknown if this strategy will also aid other catalysts for other reactions.

A second pertinent question is of course the compatibility of both the metallocages and the cellular components together. As the inside of a cell is an aqueous environment, ideally the cage should be soluble and stable in aqueous solution. Many water soluble architectures do

exist, and, as previously discussed, are able to house catalytically active species. However, it is important to consider how water solubility is achieved. Typically, it can either due to the inclusion of water soluble building blocks, or from the presence of water solubilising counterions. If the building blocks are themselves organic soluble, while polar counterions (such as sulfate) can render the structure hydrophilic, exchanging the counterions to a less polar species can result in the cage being apolar and only organic soluble.[155] This could present a problem inside cells, where a large number of charged species would have the potential to exchange with the desired cage counterion, rendering it insoluble and resulting in precipitation.

As well as exchanging with the intended counterion of the cage, small anions such as chlorides can have a considerable effect upon cage integrity. Palladium metal centres bound to pyridyl-derived ligands are very commonly used to create a diverse range of 3D structures.[156] However, the flexibility and lability of the of the palladium centre, while useful for synthesising cages, means that it is unstable to chlorides. The presence of chlorides triggers decomposition of the desired cage structure due to the formation of palladium-chloride bonds. Indeed Crowley *et al*. make use of this chloride-induced structural change to trigger cage decomposition and release cargo from the cavity.[157] However, platinum analogues of palladium cages could be a chloride-stable alternative. Platinum architectures are often more stable than their palladium counterparts: while a palladium cage decomposes in the presence of acid, base, or strong nucleophile, a platinum analogue of the same cage is kinetically more inert and remains intact.[158]

In addition, the same biomolecules which poison metal catalysts in cells, also have the potential to interact with the metal centres of the cages. Therefore, care should be taken to select an appropriate cornerstone for the cage. Hooley *et al.* have demonstrated that a tetrahedral cage containing octahedrally coordinated iron centres are stable to a small range of thiols – the cage acts as a catalyst for the thioetherification of activated alcohols and nucleophilic substitution reactions. In both cases, thiols are used as the substrate, and the cage is found to be in tact at the end of the reaction.[159, 160] However, these reactions take place at 80 °C: at elevated temperatures such cages are more dynamic, so if a thiol were to bind to the iron centre of the cage it would be easily substituted again. At the lower temperatures found in cells, it is possible that with less dynamicity, the binding of unwanted biomolecules could be less reversible.

Clearly the choice of metal centre is vitally important for designing a cage which would be stable to a biological environment. In addition, ideally the cage should be inert towards the cells themselves: in order for the catalysis to actually be able to take place inside the cell, the cage itself should not be toxic, and should not influence the cellular environment or participate in its own reactions. While there are in fact a small number of examples of metal organic cages being applied in living cells, most of which are platinum based, often they are used as cytotoxic agents themselves in cancer cells.[161, 162] A small palladium cage has been used in cells as a drug delivery system. Here, the cage itself is intended only as a vessel in which to carry cisplatin as cargo. However, no data on the stability of the cage itself under physiological conditions, or of its drug delivery mechanism, is provided.[163] The fact that palladium cages

are typically not stable to chlorides calls into question the integrity of the cage once it has reached the inside of the cell, or, if it can even penetrate the cell at all.

CONCLUSION AND OUTLOOK

Although still in its infancy, the field of *in vivo* transition metal catalysis shows a lot of promise. This new method of in cell reactivity grants access to non-natural transformations and paves the way to achieving targeted and selective drug therapies. Many systems with different mechanisms of action, such as molecular catalysts, heterogeneous nanoparticles, and photocatalysts, have been developed which are able to kill cancer cells with high levels of efficiency, or activate anticancer prodrugs. However, there is clearly a long way to go before any such system could have a practical, real-world biomedical application. The major downfall of metal catalysts is their poor stability to the cellular environment. Facile poisoning of the catalysts results in sluggish, almost stoichiometric, reactivity; meaning high catalyst loadings are required to achieve acceptable yields. To overcome this hurdle, progress needs to be made towards preventing catalyst deactivation and improving catalytic efficiency.

Poor efficiency and low yielding catalysis is of course not a problem which only plagues the field of cellular catalysis. As an answer to this problem in synthetic chemistry, encapsulation of metal complexes in supramolecular metallocages has been well studied. By confining the catalyst in a microenvironment, new and improved reactivity and selectivity can be achieved. These observed cage effects could also prove to be beneficial for metal complexes in living systems. Cages with small cavities or window sizes allows for discrimination between large and small substrates, which cannot be achieved by a free catalyst. In this way a cage could behave as a physical barrier against large, poisoning biomolecules, and improve catalyst specificity towards specific-sized substrates. Combining multiple metal centres inside one supramolecular structure increases the local concentration of catalyst, whilst keeping the global concentration the same. This could boost reactivity for the catalysts while still being able to maintain the low dosages required for cellular applications. Additionally, this could increase the spatial specificity of the catalysis inside the cell. Instead of relying upon every metal complex reaching the desired cell or subcellular component, only one cage molecule would need to reach the target location in order to deliver multiple metal centres at the same time. Finally, supramolecular cages can play a large role in the stabilisation of either the catalyst itself or in stabilising an intermediate or transition state within the catalytic cycle. As well as deactivation due to cellular conditions, other catalyst decomposition or deactivation pathways may also be at play. Encapsulation is effective for negating such pathways, particularly for cases which involve dimerization. Any strategy to keep the catalyst active for as long as possible will be beneficial for such a complex and challenging environment.

As these supramolecular cages also contain multiple metal centres, it is also important to choose the type of cage to use carefully, in order to prevent the same issues which effect the catalysts from affecting the cage itself. For example, a sphere comprised of palladium centres will be readily decomposed by the high concentrations of chlorides present inside the cell; however the same sphere containing platinum centres instead will likely be tolerable to them. Judicious choice of metal centre is also important for preventing damage to the cell as a result of metal toxicity. Several cages have been already applied in living cells, showing that it is indeed possible to design cages which are stable to the cell environment. However these have

been mostly used as cytotoxic agents against cancer cells. If the desired role of the cage would be as a catalyst microenvironment, instead of as a toxic agent or cargo delivery system, then less toxic metals, such as iron, should perhaps be considered.

Combining the areas of supramolecular and in cell catalysis has the potential to bring about great headway to both fields. Future progress of transition metal catalysis in living cells is dependent upon research into improving the reactivity and stability of the complexes used. We propose that intelligent design of supramolecular hosts could be one avenue towards this goal. There is a large scope of options of such hosts which could be considered, but the synthesis of metal organic cages is often made simple by the self-assembly process and provides leeway for flexibility of design and application.

THESIS OUTLINE

The ability to carry out efficient transition metal catalysis inside living cells has the potential to unlock a diverse range of new-to-nature transformations, allowing for precise control over biochemical pathways within cells. This provides the opportunity to gain insight into the working of biological systems by providing new routes towards biomolecular labelling and imaging. In addition, being able to carry out efficient unnatural transformations provides new routes to specific and controlled prodrug activation – access to such reactivity could have huge implications for areas of medicine such as cancer chemotherapy where non-specific activity leads to very severe side-effects. However, the road to achieving such reactivity is riddled with pitfalls, the root of which is the poor biocompatibility of metal catalyst with the cellular environment. The irreversible poisoning of metal catalysts by biomolecules, in particular intracellular thiols, results in deactivated complexes which are no longer catalytically active. Another hurdle is that very low catalyst concentrations and loadings are required to circumvent cytotoxicity induced by the metal complex. Together, this has the result that the majority of transition metal catalysed reactions carried out in living cells exhibit very poor catalytic activity, with low turnover numbers and low yields. Therefore, it is apparent that new strategies need to be developed in order to make progress towards achieving efficient *in vivo* transition metal catalysis. One such strategy which shows a lot of promise is the use supramolecular metallocages. Such cages are already known to improve the reactivity of metal catalysts, for example by pre-organisation effects or by increasing local catalyst concentrations and may also be able to act as a physical barrier between the catalyst and the inhibitory biomolecules.

In *Chapter 2* we explore the use of a small anionic $K_{12}[Ga_4L_6]$ metallocage as a protective host to improve the reactivity of a gold catalyst under biological conditions. Many useful organic transformations can be achieved by gold catalysts; however, they are known to be readily deactivated by the cellular environment. The $K_{12}[Ga_4L_6]$ cage is known to encapsulate and improve the reactivity of a gold catalyst in water; we therefore hypothesised that with its small windows it could also impart protection upon the catalyst under biological conditions. We therefore looked if catalyst encapsulation within a supramolecular host is a viable strategy to improve the *in vivo* reactivity of a gold catalyst. After determining the cytotoxicity of the reaction components and the uptake of the $K_{12}[Ga_4L_6]$ cage in HeLa cells, the catalytic activity of the encapsulated gold complex towards the formation of a fluorescent dye via an intramolecular hydroarylation was evaluated in the presence of cell culture media and biomolecules.

In *Chapter 3* a cationic $[Pt_6L_4](NO_3)_{12}$ metallocage was investigated as a supramolecular host for a palladium catalyst. Palladium catalysis is an extremely powerful tool to achieve intermolecular reactions – a diverse range of C–C bond coupling reactions are made possible through palladium catalysts. However, its application in cells for such coupling reactions has so far been limited; we hypothesised that the efficiency of such reactions could be improved by carrying them out within the cavity of a supramolecular cage. Although a palladium complex is known to undergo stoichiometric reactions within the $[Pt_6L_4](NO_3)_{12}$

cage, catalytic transformations are not yet known. After determining the stability of the cage to biological conditions, the encapsulation of a palladium complex within the cage was then investigated. Subsequently, the reactivity of the palladium complex within the cage towards several transformations was evaluated.

In *Chapter 4* we explore the use of the cationic $[Pt_6L_4](NO_3)_{12}$ metallocage as a host for a ruthenium complex. Ruthenium catalysed olefin metathesis is also a useful tool to achieve C–C bond forming reactions and can be used for both intra- and intermolecular transformations; yet its application in living cells is not well explored. We therefore hypothesised that carrying out olefin metathesis within the cavity of the $[Pt_6L_4](NO_3)_{12}$ cage could improve the reaction efficiency under biological conditions. First, the encapsulation of several apolar metathesis catalysts within the hydrophobic cavity of the cage was investigated. Next, the ring-closing metathesis activity of a water soluble metathesis catalyst was determined in the presence of the cage. While the presence of the cage was found to improve the yield of the desired ring-closed product, detailed NMR and kinetic studies determined that the origin of this improvement was in fact due to a rapid increase in reaction rate induced by the presence of the nitrate counterions from the cage, rather than due to the cage itself.

In *Chapter 5* we further investigated the improvement of the olefin metathesis reaction by the presence of nitrate salts. We proposed that the very fast reaction kinetics imparted upon the ring-closing metathesis reaction by the nitrate could mean that productive catalysis could occur faster than poisoning of the catalyst by biomolecules. Therefore, we investigated whether or not the presence of nitrate could impart kinetic protection from biomolecule poisoning. After determining the role of the nitrate within the catalytic system, detailed kinetic studies were carried out to gain understanding of how nitrate influences the rate of reaction. The performance of the nitrate system in the presence of biological additives was then evaluated.

In conclusion, we developed two novel strategies for improving the reactivity of transition metal catalysts under biological conditions. Physical protection can be achieved by encapsulating a catalyst within the cavity of a supramolecular cage: the cage behaves as a barrier to separate the vulnerable catalyst from poisoning by blocking the biomolecules from reaching the metal centre. Kinetic protection provides means that if the rate of catalysis is more rapid than the rate of catalyst poisoning by biomolecules, then high yields can still be achieved before the catalyst is deactivated. We believe that these strategies show great potential and could be expanded to other catalytic systems.

REFERENCES

[1] C. J. Borths, S. D. Walker, *Isr. J. Chem.* **2020**, 60, 340-350.
[2] J. E. Zweig, D. E. Kim, T. R. Newhouse, *Chem. Rev.* **2017**, 117, 11680-11752.
[3] L. Hedstrom, *eLS*, **2010**.
[4] M. T. Reetz, J. D. Carballeira, J. Peyralans, H. Höbenreich, A. Maichele, A. Vogel, *Chem.–Eur. J.* **2006**, 12, 6031-6038.
[5] V. S. Dave, D. Gupta, M. Yu, P. Nguyen, S. Varghese Gupta, *Drug Dev. Ind. Pharm.* **2017**, 43, 177-189.
[6] H. J. Forman, H. Zhang, A. Rinna, *Mol. Aspects Med.* **2009**, 30, 1-12.
[7] K. Le Gal, E. E. Schmidt, V. I. Sayin, *Antioxidants* **2021**, 10, 1377.
[8] S. J. Dougan, A. Habtemariam, S. E. McHale, S. Parsons, P. J. Sadler, *Proc. Nat. Acad. Sci.* **2008**, 105, 11628.
[9] A. Meister, M. E. Anderson, *Annu. Rev. Biochem.* **1983**, 52, 711-760.
[10] H. Y. Huang, S. Banerjee, K. Qiu, P. Zhang, O. Blacque, T. Malcomson, M. J. Paterson, G. J. Clarkson, M. Staniforth, V. G. Stavros, G. Gasser, H. Chao, P. J. Sadler, *Nat. Chem.* **2019**, 11, 1041-+.
[11] D. Nolfi-Donegan, A. Braganza, S. Shiva, *Redox Biol.* **2020**, 37, 101674.
[12] F. M. Wang, E. G. Ju, Y. J. Guan, J. S. Ren, X. G. Qu, *Small* **2017**, 13, 6.
[13] R. Liu, D. Cheng, Q. Zhou, F. Niu, K. Hu, *ACS Appl. Nano Mater.* **2021**, 4, 990-994.
[14] P. K. Sasmal, S. Carregal-Romero, A. A. Han, C. N. Streu, Z. Lin, K. Namikawa, S. L. Elliott, R. W. Köster, W. J. Parak, E. Meggers, *ChemBioChem* **2012**, 13, 1116-1120.
[15] K. K. Sadhu, T. Eierhoff, W. Römer, N. Winssinger, *J. Am. Chem. Soc.* **2012**, 134, 20013-20016.
[16] K. K. Sadhu, E. Lindberg, N. Winssinger, *Chem. Commun.* **2015**, 51, 16664-16666.
[17] K. K. Sadhu, N. Winssinger, *Chem.–Eur. J.* **2013**, 19, 8182-8189.
[18] L. Holtzer, I. Oleinich, M. Anzola, E. Lindberg, K. K. Sadhu, M. Gonzalez-Gaitan, N. Winssinger, *ACS Cent. Sci.* **2016**, 2, 394-400.
[19] J. Chen, K. Li, J. S. L. Shon, S. C. Zimmerman, *J. Am. Chem. Soc.* **2020**, 142, 4565-4569.
[20] A. H. Ngo, M. Ibañez, L. H. Do, *ACS Catal.* **2016**, 6, 2637-2641.
[21] S. Bose, A. H. Ngo, L. H. Do, *J. Am. Chem. Soc.* **2017**, 139, 8792-8795.
[22] Z. Liu., I. Romero-Canelón, B. Qamar, J. M. Hearn, A. Habtemariam, N. P. E. Barry, A. M. Pizarro, G. J. Clarkson, P. J. Sadler, *Angew. Chem. Int. Ed.* **2014**, 53, 3941-3946.
[23] L. Yang, S. Bose, A. H. Ngo, L. H. Do, *Chemmedchem* **2017**, 12, 292-299.
[24] J. Zhao, J. G. Rebelein, H. Mallin, C. Trindler, M. M. Pellizzoni, T. R. Ward, *J. Am. Chem. Soc.* **2018**, 140, 13171-13175.
[25] F. Liu, J. Z. H. Zhang, Y. Mei, *Sci. Rep.* **2016**, 6, 27190.
[26] A. Alouane, R. Labruère, T. Le Saux, F. Schmidt, L. Jullien, *Angew. Chem. Int. Ed.* **2015**, 54, 7492-7509.
[27] J. J. Soldevila-Barreda, I. Romero-Canelón, A. Habtemariam, P. J. Sadler, *Nat. Commun.* **2015**, 6, 6582.
[28] N. Dai, H. Zhao, R. Qi, Y. Chen, F. Lv, L. Liu, S. Wang, *Chem.–Eur. J.* **2020**, 26, 4489-4495.
[29] J. J. Soldevila-Barreda, A. Habtemariam, I. Romero-Canelón, P. J. Sadler, *J. Inorg. Biochem.* **2015**, 153, 322-333.
[30] J. P. C. Coverdale, I. Romero-Canelón, C. Sanchez-Cano, G. J. Clarkson, A. Habtemariam, M. Wills, P. J. Sadler, *Nat. Chem.* **2018**, 10, 347-354.
[31] E. M. Bolitho, J. P. C. Coverdale, H. E. Bridgewater, G. J. Clarkson, P. D. Quinn, C. Sanchez-Cano, P. J. Sadler, *Angew. Chem. Int. Ed.* **2021**, 60, 6462-6472.
[32] C. Vidal, M. Tomas-Gamasa, A. Gutierrez-Gonzalez, J. L. Mascarenas, *J. Am. Chem. Soc.* **2019**, 141, 5125-5129.
[33] C. Streu, E. Meggers, *Angew. Chem. Int. Ed.* **2006**, 45, 5645-5648.
[34] M. I. Sanchez, C. Penas, M. E. Vazquez, J. L. Mascarenas, *Chem. Sci.* **2014**, 5, 1901-1907.
[35] R. Das, R. F. Landis, G. Y. Tonga, R. Cao-Milán, D. C. Luther, V. M. Rotello, *ACS Nano* **2019**, 13, 229-235.

[36] P. K. Sasmal, S. Carregal-Romero, W. J. Parak, E. Meggers, *Organometallics* **2012**, 31, 5968-5970.
[37] H.-T. Hsu, B. M. Trantow, R. M. Waymouth, P. A. Wender, *Bioconjugate Chem.* **2016**, 27, 376-382.
[38] T. Völker, F. Dempwolff, P. L. Graumann, E. Meggers, *Angew. Chem. Int. Ed.* **2014**, 53, 10536-10540.
[39] T. Volker, E. Meggers, *ChemBiochem* **2017**, 18, 1083-1086.
[40] M. Tomás-Gamasa, M. Martínez-Calvo, J. R. Couceiro, J. L. Mascareñas, *Nat. Commun.* **2016,** 7, 12538.
[41] M. Szponarski, F. Schwizer, T. R. Ward, K. Gademann, *Commun. Chem.* **2018**, 1, 10.
[42] Y. Okamoto, R. Kojima, F. Schwizer, E. Bartolami, T. Heinisch, S. Matile, M. Fussenegger, T. R. Ward, *Nat. Commun.* **2018**, 9, 7.
[43] M. Martínez-Calvo, J. R. Couceiro, P. Destito, J. Rodríguez, J. Mosquera, J. L. Mascareñas, *ACS Catal.* **2018**, 8, 6055-6061.
[44] R. M. Yusop, A. Unciti-Broceta, E. M. V. Johansson, R. M. Sánchez-Martín, M. Bradley, *Nat. Chem.* **2011**, 3, 239-243.
[45] A. Unciti-Broceta, E. M. V. Johansson, R. M. Yusop, R. M. Sánchez-Martín, M. Bradley, *Nat. Protoc.* **2012**, 7, 1207-1218.
[46] M. A. Miller, B. Askevold, H. Mikula, R. H. Kohler, D. Pirovich, R. Weissleder, *Nat. Commun.* **2017**, 8, 15906.
[47] M. A. Miller, H. Mikula, G. Luthria, R. Li, S. Kronister, M. Prytyskach, R. H. Kohler, T. Mitchison, R. Weissleder, *ACS Nano* **2018**, 12, 12814-12826.
[48] M. Santra, S.-K. Ko, I. Shin, K. H. Ahn, *Chem. Commun.* **2010**, 46, 3964-3966.
[49] G. Y. Tonga, Y. Jeong, B. Duncan, T. Mizuhara, R. Mout, R. Das, S. T. Kim, Y.-C. Yeh, B. Yan, S. Hou, V. M. Rotello, *Nat. Chem.* **2015**, 7, 597-603.
[50] T. Lv, J. Wu, F. Kang, T. Wang, B. Wan, J.-J. Lu, Y. Zhang, Z. Huang, *Org. Lett.* **2018**, 20, 2164-2167.
[51] J. T. Weiss, J. C. Dawson, K. G. Macleod, W. Rybski, C. Fraser, C. Torres-Sánchez, E. E. Patton, M. Bradley, N. O. Carragher, A. Unciti-Broceta, *Nat. Commun.* **2014**, 5, 3277.
[52] M. Sancho-Albero, B. Rubio-Ruiz, A. M. Pérez-López, V. Sebastián, P. Martín-Duque, M. Arruebo, J. Santamaría, A. Unciti-Broceta, *Nat. Catal.* **2019**, 2, 864-872.
[53] A. M. Pérez-López, B. Rubio-Ruiz, V. Sebastián, L. Hamilton, C. Adam, T. L. Bray, S. Irusta, P. M. Brennan, G. C. Lloyd-Jones, D. Sieger, J. Santamaría, A. Unciti-Broceta, *Angew. Chem. Int. Ed.* **2017**, 56, 12548-12552.
[54] B. Rubio-Ruiz, A. M. Pérez-López, V. Sebastián, A. Unciti-Broceta, *Bioorg. Med. Chem.* **2021**, 41, 116217.
[55] T. Sun, T.Lv, J. Wu, M. Zhu, Y. Fei, J. Zhu, Y. Zhang, Z. Huang, *J. Med. Chem.* **2020**, 63, 13899-13912.
[56] D. Pham, C. J. Deter, M. C. Reinard, G. A. Gibson, K. Kiselyov, W. Yu, V. C. Sandulache, C. M. St. Croix, K. Koide, *ACS Cent. Sci.* **2020**, 6, 1772-1788.
[57] E. Indrigo, J. Clavadetscher, S. V. Chankeshwara, A. Megia-Fernandez, A. Lilienkampfa, M. Bradley, *Chem. Commun.* **2017**, 53, 6712-6715.
[58] S. Learte-Aymamí, C. Vidal, A. Gutiérrez-González, J. L. Mascareñas, *Angew. Chem. Int. Ed.* **2020**, 59, 9149-9154.
[59] J. Li, J. Yu, J. Zhao, J. Wang, S. Zheng, S. Lin, L. Chen, M. Yang, S. Jia, X. Zhang, P. R. Chen, *Nat. Chem.* **2014**, 6, 352.
[60] J. Wang, B. Cheng, J. Li, Z. Zhang, W. Hong, X. Chen, P. R. Chen, *Angew. Chem. Int. Ed.* **2015**, 54, 5364-5368.
[61] Y. Liu, S. Pujals, P. J. M. Stals, T. Paulöhrl, S. I. Presolski, E. W. Meijer, L. Albertazzi, A. R. A. Palmans, *J. Am. Chem. Soc.* **2018**, 140, 3423-3433.
[62] J. Wang, S. Zheng, Y. Liu, Z. Zhang, Z. Lin, J. Li, G. Zhang, X.Wang, J. Li, P. R. Chen, *J. Am. Chem. Soc.* **2016**, 138, 15118-15121.
[63] C. Y.-S. Chung, J. M. Posimo, S. Lee, T. Tsang, J. M. Davis, D. C. Brady, C. J. Chang, *Proc. Nat. Acad. Sci.* **2019**, 116, 18285.

[64] M. C. Heffern, H. M. Park, H. Y. Au-Yeung, G. C. Van de Bittner, C. M. Ackerman, A. Stahl, C. J. Chang, *Proc. Nat. Acad. Sci.* **2016**, 113, 14219.
[65] R. F. Ohana, S. Levin, M. G. Wood, K. Zimmerman, M. L. Dart, M. K. Schwinn, T. A. Kirkland, R. Hurst, H. T. Uyeda, L. P. Encell, K. V. Wood, *ACS Chem. Biol.* **2016**, 11, 2608-2617.
[66] B. J. Stenton, B. L. Oliveira, M. J. Matos, L. Sinatra, G. J. L. Bernardes, *Chem. Sci.* **2018**, 9, 4185-4189.
[67] X. Wan, Y. Liu, X. Fan, J. Wang, W. S. C. Ngai, H. Zhang, J. Li, G. Zhang, J. Lin, P. R. Chen, *J. Am. Chem. Soc.* **2019**, 141, 17133-17141.
[68] Y.-K. Yang, S. Lee, J. Tae, *Org. Lett.* **2009**, 11, 5610-5613.
[69] J.-B. Wang, Q.-Q. Wu, Y.-Z. Min, Y.-Z. Liu, Q.-H. Song, *Chem. Commun.* **2012**, 48, 744-746.
[70] M. J. Jou, X. Chen, K. M. K. Swamy, H. N. Kim, H.-J. Kim, S.-G. Lee, J. Yoon, *Chem. Commun.* **2009**, 7218-7220.
[71] J. H. Do, H. N. Kim, J. Yoon, J. S. Kim, H.-J. Kim, *Org. Lett.* **2010**, 12, 932-934.
[72] N. T. Patil, V. S. Shinde, M. S. Thakare, P. H.Kumar, P. R. Bangal, A. K. Baruic, C. R. Patra, *Chem. Commun.* **2012**, 48, 11229-11231.
[73] M. Üçüncü, E. Karakuş, M. Emrullahoğlu, *Chem.–Eur. J.* **2015**, 21, 13201-13205.
[74] C. Vidal, M. Tomás-Gamasa, P. Destito, F. López, J. L. Mascareñas, *Nat. Commun.* **2018**, 9, 1913.
[75] Y. Long, B. Cao, X. Xiong, A. S. C. Chan, R. W.-Y. Sun, T. Zou, *Angew. Chem. Int. Ed.* **2021**, 60, 4133-4141.
[76] K. Vong, T. Yamamoto, T.-C. Chang, K. Tanaka, *Chem. Sci.* **2020**, 11, 10928-10933.
[77] T.-C. Chang, K. Vong, T. Yamamoto, K. Tanaka, *Angew. Chem.* **2021**, 133, 12554-12562.
[78] J. Alemán, V. del Solar, C. Navarro-Ranninger, *Chem. Commun.* **2010**, 46, 454-456.
[79] B. L. Oliveira, B. J. Stenton, V. B. Unnikrishnan, C. R. de Almeida, J. Conde, M. Negrão, F. S. S. Schneider, C. Cordeiro, M. G. Ferreira, G. F. Caramori, J. B. Domingos, R. Fior, G. J. L. Bernardes, *J. Am. Chem. Soc.* **2020**, 142, 10869-10880.
[80] M. Yu, S. Lou, F. Gonzalez-Bobes, *Org. Process Res. Dev.* **2018**, 22, 918-946.
[81] C. S. Higman, J. A. M. Lummiss, D. E. Fogg, *Angew. Chem. Int. Ed.* **2016**, 55, 3552-3565.
[82] M. S. Messina, H. D. Maynard, *Mater. Chem. Front.* **2020**, 4, 1040-1051.
[83] Y. A. Lin, J. M. Chalker, B. G. Davis, *ChemBioChem* **2009**, 10, 959-969.
[84] Y. A. Lin, O. Boutureira, L. Lercher, B. Bhushan, R. S. Paton, B. G. Davis, *J. Am. Chem. Soc.* **2013**, 135, 12156-12159.
[85] J. M. Chalker, Y. A. Lin, O. Boutureira, B. G. Davis, *Chem. Commun.* **2009**, 3714-3716.
[86] A. Brik, *Adv. Synth. Catal.* **2008**, 350, 1661-1675.
[87] M. Jeschek, R. Reuter, T. Heinisch, C. Trindler, J. Klehr, S. Panke, T. R. Ward, *Nature* **2016**, 537, 661-+.
[88] V. Sabatino, J. G. Rebelein, T. R. Ward, *J. Am. Chem. Soc.* **2019**, 141, 17048-17052.
[89] S.Eda, I. Nasibullin, K. Vong, N. Kudo, M. Yoshida, A. Kurbangalieva, K. Tanaka, *Nat. Catal.* **2019**, 2, 780-792.
[90] B. Spangler, D. Dovala, W. S. Sawyer, K. V. Thompson, D. A. Six, F. Reck, B. Y. Feng, *ACS Infect. Dis.* **2018**, 4, 1355-1367.
[91] A. Kumar, K. Li, C. Cai, *Chem. Commun.* **2011**, 47, 3186-3188.
[92] S. Li, H. Cai, J. He, H. Chen, S. Lam, T. Cai, Z. Zhu, S. J. Bark, C. Cai, *Bioconjugate Chem.* **2016**, 27, 2315-2322.
[93] A. J. Link, D. A. Tirrell, *J. Am. Chem. Soc.* **2003**, 125, 11164-11165.
[94] A. J. Link, M. K. S. Vink, D. A. Tirrell, *J. Am. Chem. Soc.* **2004**, 126, 10598-10602.
[95] K. E. Beatty, J. C. Liu, F. Xie, D. C. Dieterich, E. M. Schuman, Q. Wang, D. A. Tirrell, *Angew. Chem. Int. Ed.* **2006**, 45, 7364-7367.
[96] V. Bevilacqua, M. King, M. Chaumontet, M. Nothisen, S. Gabillet, D. Buisson, C. Puente, A. Wagner, F. Taran, *Angew. Chem. Int. Ed.* **2014**, 53, 5872-5876.
[97] C. Uttamapinant, A. Tangpeerachaikul, S. Grecian, S. Clarke, U. Singh, P. Slade, K. R. Gee, A. Y. Ting, *Angew. Chem. Int. Ed.* **2012**, 51, 5852-5856.
[98] J. Chen, J. Wang, K. Li, Y. Wang, M. Gruebele, A. L. Ferguson, S. C. Zimmerman, *J. Am. Chem. Soc.* **2019**, 141, 9693-9700.

[99] D. Soriano del Amo, W. Wang, H. Jiang, C. Besanceney, A. C. Yan, M. Levy, Y. Liu, F. L. Marlow, P. Wu, *J. Am. Chem. Soc.* **2010**, 132, 16893-16899.
[100] Z. Hao, Y. Song, S. Lin, M. Yang, Y. Liang, J. Wang, P. R. Chen, *Chem. Commun.* **2011**, 47, 4502-4504.
[101] M. Yang, Y. Song, M. Zhang, S. Lin, Z. Hao, Y. Liang, D. Zhang, P. R. Chen, *Angew. Chem. Int. Ed.* **2012**, 51, 7674-7679.
[102] M. Yang, A. S. Jalloh, W. Wei, J. Zhao, P. Wu, P. R. Chen, *Nat. Commun.* **2014**, 5, 4981.
[103] S. Li, L. Wang, F. Yu, Z. Zhu, D. Shobaki, H. Chen, M. Wang, J. Wang, G. Qin, U. J. Erasquin, L. Ren, Y. Wang, C. Cai, *Chem. Sci.* **2017**, 8, 2107-2114.
[104] J. Miguel-Avila, M. Tomas-Gamasa, A. Olmos, P. J. Perez, J. L. Mascarenas, *Chem. Sci.* **2018**, 9, 1947-1952.
[105] Y. Bai, X. Feng, H. Xing, Y. Xu, B. K. Kim, N. Baig, T. Zhou, A. A. Gewirth, Y. Lu, E. Oldfield, S. C. Zimmerman, *J. Am. Chem. Soc.* **2016**, 138, 11077-11080.
[106] J. Clavadetscher, S. Hoffmann, A. Lilienkampf, L. Mackay, R. M. Yusop, S. A. Rider, J. J. Mullins, M. Bradley, *Angew. Chem. Int. Ed.* **2016**, 55, 15662-15666.
[107] F. Wang, Y. Zhang, Z. Liu, Z. Du, L. Zhang, J. Ren, X. Qu, *Angew. Chem. Int. Ed.* **2019**, 58, 6987-6992.
[108] W. Song, N. Zheng, *Org. Lett.* **2017**, 19, 6200-6203.
[109] R. Chen, L. Zeng, Z. Lai, S. Cui, *Adv. Synth. Catal.* **2019**, 361, 989-994.
[110] M. Li, N. Zheng, J. Li, Y. Zheng, W. Song, *Green Chem.* **2020**, 22, 2394-2398.
[111] P. Destito, J. R. Couceiro, H. Faustino, F. López, J. L. Mascareñas, *Angew. Chem. Int. Ed.* **2017**, 56, 10766-10770.
[112] A. Gutiérrez-González, P. Destito, J. R. Couceiro, C. Pérez-González, F. López, J. L. Mascareñas, *Angew. Chem. Int. Ed.* **2021**, 60, 16059-16066.
[113] R. Chinchilla, C. Nájera, *Chem. Soc. Rev.* **2011**, 40, 5084-5121.
[114] G. Cheng, R. K. V. Lim, C. P. Ramil, Q. Lin, *Chem. Commun.* **2014**, 50, 11679-11682.
[115] N. Li, R. K. V. Lim, S. Edwardraja, Q. Lin, *J. Am. Chem. Soc.* **2011**, 133, 15316-15319.
[116] R. K. V. Lim, N. Li, C. P. Ramil, Q. Lin, *ACS Chem. Biol.* **2014**, 9, 2139-2148.
[117] N. Li, C. P. Ramil, R. K. V. Lim, Q. Lin, *ACS Chem. Biol.* **2015**, 10, 379-384.
[118] J. Li, S. Lin, J. Wang, S. Jia, M. Yang, Z. Hao, X. Zhang, P. R. Chen, *J. Am. Chem. Soc.* **2013**, 135, 7330-7338.
[119] C. D. Spicer, T. Triemer, B. G. Davis, *J. Am. Chem. Soc.* **2012**, 134, 800-803.
[120] C. D. Spicer, B. G. Davis, *Chem. Commun.* **2013**, 49, 2747-2749.
[121] F. Wang, Y. Zhang, Z. Du, J. Ren, X. Qu, *Nat. Commun.* **2018**, 9, 1209.
[122] J. Clavadetscher, E. Indrigo, S. V. Chankeshwara, A. Lilienkampf, M. Bradley, *Angew. Chem. Int. Ed.* **2017**, 56, 6864-6868.
[123] A. R. Grimm, D. F. Sauer, T. Polen, L. Zhu, T. Hayashi, J. Okuda, U. Schwaneberg, *ACS Catal.* **2018**, 8, 2611-2614.
[124] K. Tsubokura, K. K. H. Vong, A. R. Pradipta, A. Ogura, S. Urano, T. Tahara, S. Nozaki, H. Onoe, Y. Nakao, R. Sibgatullina, A. Kurbangalieva, Y. Watanabe, K. Tanaka, *Angew. Chem. Int. Ed.* **2017**, 56, 3579-3584.
[125] W. Ghattas, V. Dubosclard, A. Wick, A. Bendelac, R. Guillot, R. Ricoux, J.-P. Mahy, *J. Am. Chem. Soc.* **2018**, 140, 8756-8762.
[126] X. Liu, Z. Yan, Y. Zhang, Z. Liu, Y. Sun, J. Ren, X. Qu, *ACS Nano* **2019**, 13, 5222-5230.
[127] R. P. Goodman, M. Heilemann, S. Doose, C. M. Erben, A. N. Kapanidis, A. J. Turberfield, *Nat. Nanotechnol.* **2008**, 3, 93-96.
[128] T. G. W. Edwardson, K. M. M. Carneiro, C. K. McLaughlin, C. J. Serpell, H. F. Sleiman, *Nat. Chem.* **2013**, 5, 868-875.
[129] J. Chen, N. C. Seeman, *Nature* **1991**, 350, 631-633.
[130] A. Korpi, E. Anaya-Plaza, S. Välimäki, M. Kostiainen, *Wiley Interdiscip. Rev. Nanomed. Nanobiotechnol.* **2020**, 12, e1578.
[131] M. Mastalerz, *Angew. Chem. Int. Ed.* **2010**, 49, 5042-5053.
[132] M. Frank, M. D. Johnstone, G. H. Clever, *Chem.–Eur. J.* **2016**, 22, 14104-14125.
[133] Y. Fang, J. A. Powell, E. Li, Q. Wang, Z. Perry, A. Kirchon, X. Yang, Z. Xiao, C. Zhu, L. Zhang, F. Huang, H.-C. Zhou, *Chem. Soc. Rev.* **2019**, 48, 4707-4730.

[134] T. Gadzikwa, R. Bellini, H. L. Dekker, J. N. H. Reek, *J. Am. Chem. Soc.* **2012**, 134, 2860-2863.
[135] R. Gramage-Doria, J. Hessels, S. H. A. M. Leenders, O. Tröppner, M. Dürr, I. Ivanović-Burmazović, J. N. H. Reek, *Angew. Chem. Int. Ed.* **2014**, 53, 13380-13384.
[136] S. H. A. M. Leenders, M. Dürr, I. Ivanović-Burmazović, J. N. H. Reek, *Adv. Synth. Catal.* **2016**, 358, 1509-1518.
[137] Q.-Q. Wang, S. Gonell, S. H. A. M. Leenders, M. Dürr, I. Ivanović-Burmazović, J. N. H. Reek, *Nat. Chem.* **2016**, 8, 225-230.
[138] S. Gonell, X. Caumes, N. Orth, I. Ivanović-Burmazović, J. N. H. Reek, *Chem. Sci.* **2019**, 10, 1316-1321.
[139] F. Yu, D. Poole III, S. Mathew, N. Yan, J. Hessels, N. Orth, I. Ivanović-Burmazović, J. N. H. Reek, *Angew. Chem. Int. Ed.* **2018**, 57, 11247-11251.
[140] D. H. Leung, D. Fiedler, R. G. Bergman, K. N. Raymond, *Angew. Chem. Int. Ed.* **2004**, 43, 963-966.
[141] D. H. Leung, R. G. Bergman, K. N. Raymond, *J. Am. Chem. Soc.* **2006**, 128, 9781-9797.
[142] D. H. Leung, R. G. Bergman, K. N. Raymond, *J. Am. Chem. Soc.* **2007**, 129, 2746-2747.
[143] S. S. Nurttila, W. Brenner, J. Mosquera, K. M. van Vliet, J. R. Nitschke, J. N. H. Reek, *Chem.–Eur. J.* **2019**, 25, 609-620.
[144] M. Otte, P. F. Kuijpers, O. Troeppner, I. Ivanović-Burmazović, J. N. H. Reek, B. de Bruin, *Chem.–Eur. J.* **2014**, 20, 4880-4884.
[145] P.F. Kuijpers, M. Otte, M. Dürr, I. Ivanović-Burmazović, J. N. H. Reek, B. de Bruin, *ACS Catal.* **2016**, 6, 3106-3112.
[146] Z. J. Wang, C. J. Brown, R. G. Bergman, K. N. Raymond, F. D. Toste, *J. Am. Chem. Soc.* **2011**, 133, 7358-7360.
[147] C. J. Brown, G. M. Miller, M. W. Johnson, R. G. Bergman, K. N. Raymond, *J. Am. Chem. Soc.* **2011**, 133, 11964-11966.
[148] Z. J. Wang, K. N. Clary, R. G. Bergman, K. N. Raymond, F. D. Toste, *Nat. Chem.* **2013**, 5, 100-103.
[149] D. M. Kaphan, M. D. Levin, R. G. Bergman, K. N. Raymond, F. D. Toste, *Science* **2015**, 350, 1235.
[150] M. Otte, P. F. Kuijpers, O. Troeppner, I. Ivanović-Burmazović, J. N. H. Reek, B. de Bruin, *Chem.–Eur. J.* **2013**, 19, 10170-10178.
[151] C. Tan, J. Jiao, Z. Li, Y. Liu, X. Han, Y. Cui, *Angew. Chem. Int. Ed.* **2018**, 57, 2085-2090.
[152] J. Jiao, C. Tan, Z. Li, Y. Liu, X. Han, Y. Cui, *J. Am. Chem. Soc.* **2018**, 140, 2251-2259.
[153] Y. Fang, Z. Xiao, A. Kirchon, J. Li, F. Jin, T. Togo, L. Zhang, C. Zhud, H.-C. Zhou, *Chem. Sci.* **2019**, 10, 3529-3534.
[154] T. V. Tran, G. Couture, L. H. Do, *Dalton Trans.* **2019**, 48, 9751-9758.
[155] E. G. Percástegui, J. Mosquera, T. K. Ronson, A. J. Plajer, M. Kieffer, J. R. Nitschke, *Chem. Sci.* **2019**, 10, 2006-2018.
[156] D. Bardhan, D. K. Chand, *Chem.–Eur. J.* **2019**, 25, 12241-12269.
[157] D. Preston, A. Fox-Charles, W. K. C. Lo, J. D. Crowley, *Chem. Commun.* **2015**, 51, 9042-9045.
[158] F. Ibukuro, T. Kusukawa, M. Fujita, *J. Am. Chem. Soc.* **1998**, 120, 8561-8562.
[159] C. Ngai, P. M. Bogie, L. R. Holloway, P. C. Dietz, L. J. Mueller, R. J. Hooley, *J. Org. Chem.* **2019**, 84, 12000-12008.
[160] P. M. Bogie, L. R. Holloway, C. Ngai, T. F. Miller, D. K. Grewal, R. J. Hooley, *Chem.–Eur. J.* **2019**, 25, 10232-10238.
[161] A. Ahmedova, *Front. Chem.* **2018**, 6, 20.
[162] H. Sepehrpour, W. X. Fu, Y. Sun, P. J. Stang, *J. Am. Chem. Soc.* **2019**, 141, 14005-14020.
[163] J. Han, A. F. B. Räder, F. Reichart, B. Aikman, M. N. Wenzel, B. Woods, M. Weinmüller, B. S. Ludwig, S. Stürup, G. M. M. Groothuis, H. P. Permentier, R. Bischoff, H. Kessler, P. Horvatovich, A. Casini, *Bioconjugate Chem.* **2018**, 29, 3856-3865.

Chapter 2

Protection of a Gold Catalyst by a Supramolecular Cage for Application in Living Cells

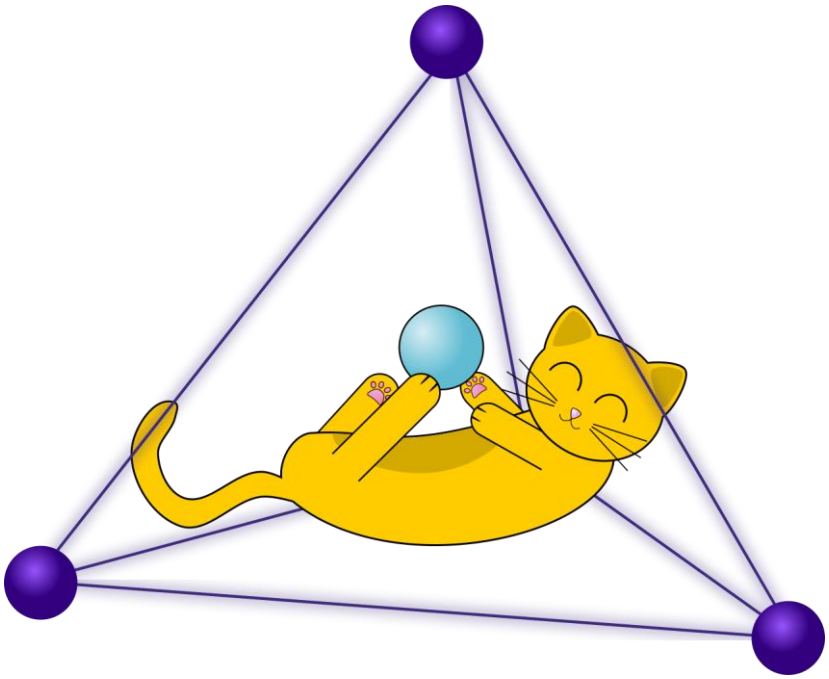

ABSTRACT

One of the major setbacks in the field of in vivo gold catalysis is the poor compatibility of the catalyst with the cellular components. In this chapter we show that encapsulation of the gold centre within the cavity of a supramolecular cage improves the reactivity of the gold catalyst under biological conditions. The gold complex catalyses an intramolecular hydroarylation to produce a fluorescent dye. The encapsulated gold complex was able to produce this dye in higher yields than the free gold complex under aqueous aerobic conditions and in the presence of biological additives. The substrate was found to be exhibit a high level of cytotoxicity, which means that a very low substrate concentration of 1 μM would be required to carry out the reaction inside living cells; however, catalysis in cell culture media carried out within this micromolar range was found to be completely inhibited. Confocal microscopy also revealed that the cage itself is unable to cross the cell membrane. Although this reaction was therefore unable to be applied inside living cells, we believe that this is a viable strategy to improve the reactivity of gold catalysts in vivo, provided that the catalytic system is optimised to include a non-toxic substrate, and a vehicle to transport the cage across the cell membrane.

INTRODUCTION

The selective activation of prodrugs and medicines is highly desirable, as it provides the ability to obtain precise spatial and temporal control over their activity which may minimise off-target reactivity.[1] This is particularly relevant for cancer treatment, where system-wide toxicity often goes hand in hand with cancer cell toxicity, often resulting in severe side effects.[2] In order to achieve such selectivity, a bioorthogonal trigger is needed to activate the drug, which should selectivity occur at the desired location and nowhere else. In addition, this trigger should be inert in the off-target cells and should not influence other endogenous processes within the cell. One strategy to accomplish this would be to design prodrugs which are activated by new-to-nature transformations. Transition metal catalysis is a potentially powerful tool to achieve this as it provides access to a wide scope reactivity which cannot be achieved by native enzymes.[3-7] Gold catalysed transformations are an attractive means for this purpose, as it provides a route to synthesise cyclic compounds, a motif commonly found in medicines and natural products, from alkynes.[8-11] Alkynes are known to have good bioorthogonality as they are generally not found naturally in the cell environment, which decreases the chances of reactivity with non-desired substrates.[12]

Gold catalysed cyclisations have already been performed *in vivo*; however, the activity of the gold catalyst itself is typically very low. The first example of a gold catalysed intramolecular hydroarylation was shown by Mascareñas *et al*. Although they showed that only 10 mol% of a small gold catalyst, (PTA)AuCl, could successfully convert substrate to generate a fluorescent coumarin derivative in water with almost quantitative conversion, when the reaction was applied inside HeLa cells the authors estimated a turnover number (TON) of just 1.12. As accurate quantification of catalytic reactions *in vivo* is challenging, the authors emphasised that this TON should only be taken as an approximation. Yet, it is clear that the cellular environment has a considerable detrimental effect on the activity of the gold complex. The root of this problem is the presence of high concentrations of strongly gold-binding thiol-containing biomolecules, such as glutathione (GSH).[13] A need to protect the gold catalyst from the cellular environment prompted Tanaka *et al.* to dock a NHC-Au(I) complex inside an albumin scaffold, to generate an artificial metalloenzyme. Indeed good conversions to generate an anticancer compound were achieved when the gold complex was docked inside the hydrophobic cavity of the protein, whereas the free complex was readily poisoned by thiols and therefore exhibited almost no reactivity. As such, the hydrophilic GSH molecules apparently cannot reach the complex when it is inside the hydrophobic cavity of the protein. In A549 cells it was shown that while high concentrations of gold complex were needed to synthesise the cytotoxic compound and induce cell death, much lower concentrations of metalloenzyme were needed to achieve the same levels of cytotoxicity, indicating that protection of the gold catalyst with the protein scaffold can prevent catalyst poisoning and improve reactivity.[14] This incompatibility of gold complexes with the cellular environment runs both ways. Cellular biomolecules have a detrimental effect on the catalytic activity, but gold complexes can also harm the cells by inducing toxicity themselves. Zou *et al.* therefore developed a system where an inactive and non-toxic gold complex was first applied in cells, which upon activation by a palladium species became both catalytically active for an

intramolecular hydroarylation reaction to synthesise a fluorescent coumarin derivative, and also became highly cytotoxic. This dual activity of the gold complex was demonstrated in both A549 cells and in zebrafish.[15]

Considering the poor compatibility of gold catalysts with the components in living cells, we aimed to design a simple system whereby protection could be provided for both the gold catalyst from the cell environment and the cell from the gold complex. To this end we looked for ways to encapsulate the gold complex in a supramolecular cage, eventually carrying out gold catalysis within the cavity of a cage. The molecular capsule should provide a physical barrier between the gold centre and the surrounding environment, leading to improved compatibility. In previous work, gold complexes have been encapsulated with the aim to improve their catalytic properties in terms of activity and selectivity. Reported benefits of confinement on catalysis have been due to: 1) pre-organisation of substrate and catalyst;[16, 17] 2) positive effects of increased local concentration of catalysts;[18-20] 3) cage effects that control the selectivity;[21-24] and 4) stabilisation of the catalyst by the cage.[25-29] Although there are several examples of gold catalysts being encapsulated in a range of different supramolecular cages,[30] we selected the small tetrahedral $K_{12}[Ga_4L_6]$ cage developed by Raymond *et al.* for the current goal (Figure 1).[31] Once encapsulated inside this cage, catalysts are known to participate in size-selective catalysis, where only substrates small enough to fit through the window are able to react.[23] With this in mind, we hypothesised that large biomolecules may be stopped from reaching the gold centre, while small substrate molecules may still access the active site. In addition, a gold catalyst, Me_3PAuCl, has been shown to bind inside the cavity of the cage. The encapsulated gold complex exhibited improved activity compared to the free complex,[32] and has also been shown to participate in a tandem reaction with enzymes, indicating its biocompatibility.[33] In this chapter we explore the use of encapsulated gold complexes for catalysis applications under biological conditions in living cells.

RESULTS AND DISCUSSION

APPROACH

The tetrahedral $K_{12}[Ga_4L_6]$ cage (see Figure 1) was prepared according to a literature procedure, and spectroscopic data were identical to those reported by Raymond *et al*.[32] Preparation of the encapsulated gold complex, $[Me_3PAu]^+$@cage, was achieved by mixing 1.2 eq of the cage with 1 eq of the commercially available gold catalyst, Me_3PAuCl. The catalytically active cationic gold species $[Me_3PAu]^+$ resides within the cavity, as the highly negative charged capsule is able to encapsulate cationic guests due to electrostatic interactions. For reactions with free Me_3PAuCl, no chloride-abstracting reagents were required as it is known that the chloride is able to dissociate from the gold centre in water.[13] Catalyst encapsulation in the aqueous phase was established by ^{1}H NMR spectroscopy and 2D ^{1}H diffusion ordered NMR spectroscopy (DOSY). Two new overlapping doublets appeared in the ^{1}H NMR spectrum (Figure E5) at -1.85 and -1.89 ppm which correspond to the phosphine alkyl protons of Me_3PAuCl, and these peaks are shifted upfield with respect to those of free Me_3PAuCl, which would appear at 1.64 ppm. Besides this, all the aromatic peaks belonging to the empty cage appear between 7.80 and 6.52 ppm, but in the presence of Me_3PAuCl they are all shifted downfield to between 7.84 and 6.57 ppm. In addition the DOSY spectrum (Figure E7) had only one band with a $\log_D$ value of -9.62, indicating that only one species is diffusing in solution. Together these data are characteristic of encapsulation of the gold complex within the cavity of the cage (Figure 1). In order to monitor catalytic conversions in the highly complex environment of the cell, typically substrates are used that become fluorescent upon product formation.[34-37] However, many fluorophores contain large aromatic groups in their structure, which may be too large to fit through the small windows of the cage (see section *Experimental*). We therefore designed a small alkyne-containing substrate, **1**, which upon a gold catalysed hydroarylation reaction generates a coumarin dye, **2a**. As a by-product, a non-fluorescent regio-isomer **2b** can also be formed (Figure 1). Substrate **1** was prepared using standard synthetic steps from commercially available building blocks (see section *Experimental*). To successfully demonstrate that catalysis can be performed in living cells, we need to: 1) explore the cytotoxicity of the substrate, catalyst, and product, which will set the boundary conditions for catalysis; 2) demonstrate that the caged catalyst enters the living cell in order to perform the catalytic transformation; and 3) explore the compatibility of the catalyst system with commonly abundant components in living cells. In the following sections these will be discussed.

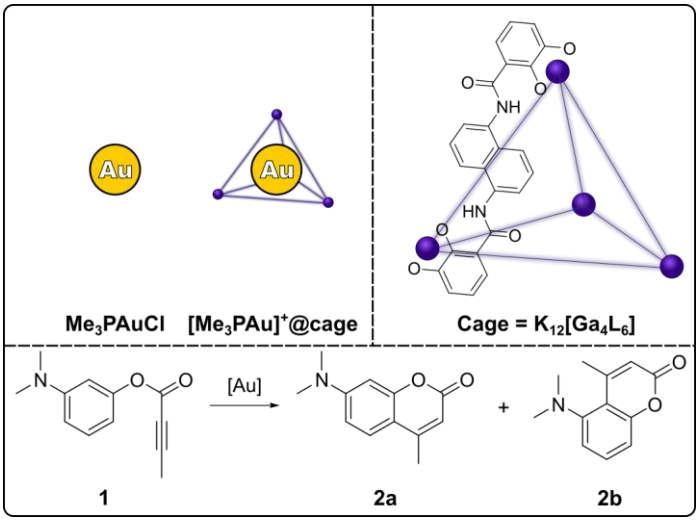

Figure 1. Above: Structures of Me_3PAuCl and the cage. Below: Gold catalysed intramolecular hydroarylation of substrate **1** to form fluorescent dye **2a** and the non-fluorescent regio-isomer **2b**.

TOXICITY AND CATALYST CONDITIONS

Before catalysis can be carried out, appropriate reaction conditions need to be found. The reaction conditions for transition metal catalysis inside cells is often vastly different to that of catalytic reactions in the lab. While typical catalysis reactions in the lab are often carried out with millimolar to molar concentrations of substrate, much lower concentrations within the 10–200 μM range are typically required for catalysis in cells, as high concentrations can result in cytotoxicity. Ideally, the reaction components for catalysis should induce as little cytotoxicity as possible, in order to ensure that the reaction mainly takes place inside of living cells, rather than extracellularly in the presence of dead cells. Therefore, the biocompatibility of the reaction components with living cells was first investigated in order to determine the appropriate reaction conditions for intracellular catalysis. To this end, the viability of human cervical cancer cells (HeLa cells) was determined in the presence of substrate **1**, product **2a**, the free Me_3PAuCl, the empty cage, and the encapsulated $[Me_3PAu]^+$@cage, using an MTT (3-(4,5-dimethylthiazol-2-yl)-2,5-diphenyltetrazolium bromide) assay (Figure 2). After HeLa cells were incubated with increasing concentrations of the compounds, the percentage of cells which remained alive compared to before incubation with the compounds, was determined. This gives the percentage cell viability for the different compounds at each concentration. For compounds with very low or no cytotoxicity the cell viability will remain high even at high concentrations, while very cytotoxic compounds will result in low levels of cell viability at low concentrations. The relative cytotoxicity of the different compounds can therefore be determined by comparing the cell viability in the presence of each of the compounds at a given concentration. Substrate **1** was found to induce very high levels of cytotoxicity: at only 10 μM, the cell viability was just 23%. In order to minimise cytotoxicity induced by substrate **1**, it should be applied in very low concentrations for catalysis, ideally at just 1 μM, as at this concentration a cell viability of 74% was observed. The cell viability of product **2a** at concentrations above 10 μM was higher than that for substrate **1**, and below this concentrations the cell viabilities of substrate **1** and product **2** are similar (67–74% and 57–53% respectively). This means that any product which would be formed during catalysis would not induce any

significant cytotoxicity at this concentration. Both of the gold complexes were also found to induce less cytotoxicity than the substrate. Gratifyingly, the encapsulated $[Me_3PAu]^+$@cage complex exhibited reduced cytotoxicity compared to the free Me_3PAuCl: 79% cell viability was observed for $[Me_3PAu]^+$@cage at 50 μM, while at the same concentration for free Me_3PAuCl the cell viability was only 59%. The cage itself was essentially non-cytotoxic, as around 100% cell viability was observed even at cage concentrations up to 500 μM. This means that it is possible that the cytotoxicity observed for $[Me_3PAu]^+$@cage could be due to leaching of the gold complex from the cage cavity into the cell. Although the cytotoxicity of the gold complex was reduced by encapsulation within the cage, the lack of cytotoxicity across all concentrations of cage brought into question the cell membrane permeability of the cage. The $[Me_3PAu]^+$@cage complex has a total negative charge of -11, and it is often challenging to transport large hydrophilic or charged cargo across the cell membrane.[38]

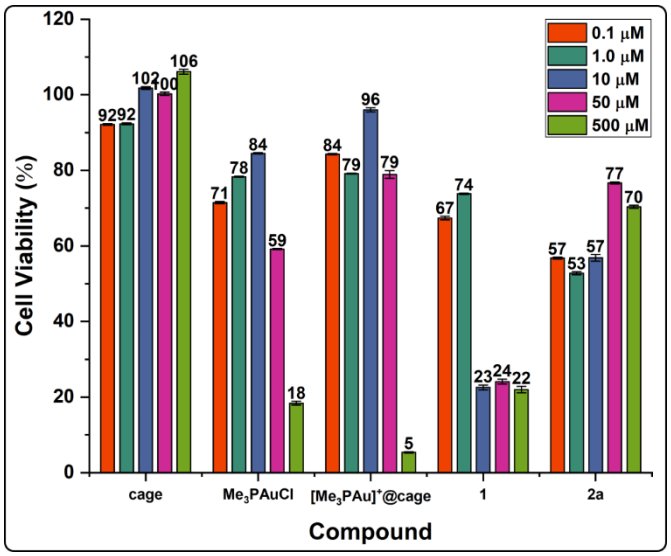

Figure 2. MTT assay of reaction components in HeLa cells at different concentrations.

UPTAKE OF CAGES IN LIVING CELLS

Confocal microscopy was used in order to visualise uptake of the cage using fluorescence. As the $[Me_3PAu]^+$@cage complex itself is not fluorescent, the cage was labelled with the fluorescent dye RhodamineB (RhoB), generating a fluorescent RhoB-cage complex. Although RhoB is very large, we hypothesised that electrostatic interactions could bind the dye to the cage, either by partial encapsulation of the alkyl groups within the cavity, or by binding to the exterior of the cage. A solution of 1 eq RhoB and 1.2 eq cage in water was stirred for 30 min at room temperature, and analysed with ^{1}H NMR spectroscopy, DOSY, UV/Vis spectroscopy, fluorescence spectroscopy, and cryospray ionisation high resolution mass spectrometry (CSI-HRMS). In the ^{1}H NMR spectrum of the RhoB and cage mixture (Figure E8), the quartet at 3.49 ppm and the triplet at 1.16 ppm of the free RhoB were shifted upfield and appeared as two broad singlets at 3.06 ppm and 0.94 ppm respectively. In addition, the aromatic signals of the free RhoB between 8.17–6.57 ppm and the aromatic signals of the empty cage between 7.80–6.47 ppm were all shifted to give a set of overlapping peaks between 7.53–6.44 ppm. All of these signals in the RhoB and cage mixture gave one band in the DOSY spectrum with a $\log_D$ value of -9.63 (Figure E9), indicating that there is one species in solution.

In addition, the CSI-HRMS spectrum had signals which correspond to 3-, 4-, and 5- species containing one cage and one RhoB. Finally, the UV/Vis spectrum of RhoB in the presence of cage also indicated binding (Figure E10). The absorption at 554 nm decreased from 1.09 for free RhoB to 0.86 for RhoB in the presence of cage, which is typical of a binding event. Having established that RhoB indeed binds to the cage, the fluorescence properties of the resultant complex was evaluated. Although the RhoB-cage complex indeed displays fluorescence, the intensity of the emission spectrum is lower than that of the free RhoB, indicating that fluorescence of the RhoB is partially quenched upon binding (Figure 3b). Therefore, if there would be fluorescence after incubation with cells with the RhoB-cage complex, comparing the fluorescence intensity with that of the free RhoB would give an indication of whether or not the RhoB is still bound to the cage and therefore show whether or not the cage had entered the cell. To this end, HeLa cells were incubated with a 1 μM solution of either RhoB or RhoB-cage for 30 min, followed by washing twice with PBS buffer. While fluorescence was observed in the cytoplasm of the cells incubated with free RhoB, only background fluorescence was seen for the RhoB-cage complex (Figure 3c). Therefore, the cage together with its cargo is not cell permeable, and the reason for the cage being non-toxic is due to the fact that it does not in fact enter the cell. This means that in order to carry out the reaction inside cells, the $[Me_3PAu]^+$@cage complex would need to be first brought into the cell using a cell-penetrating vehicle, such as a cell-penetrating peptide or lipid nanoparticle (LNP).

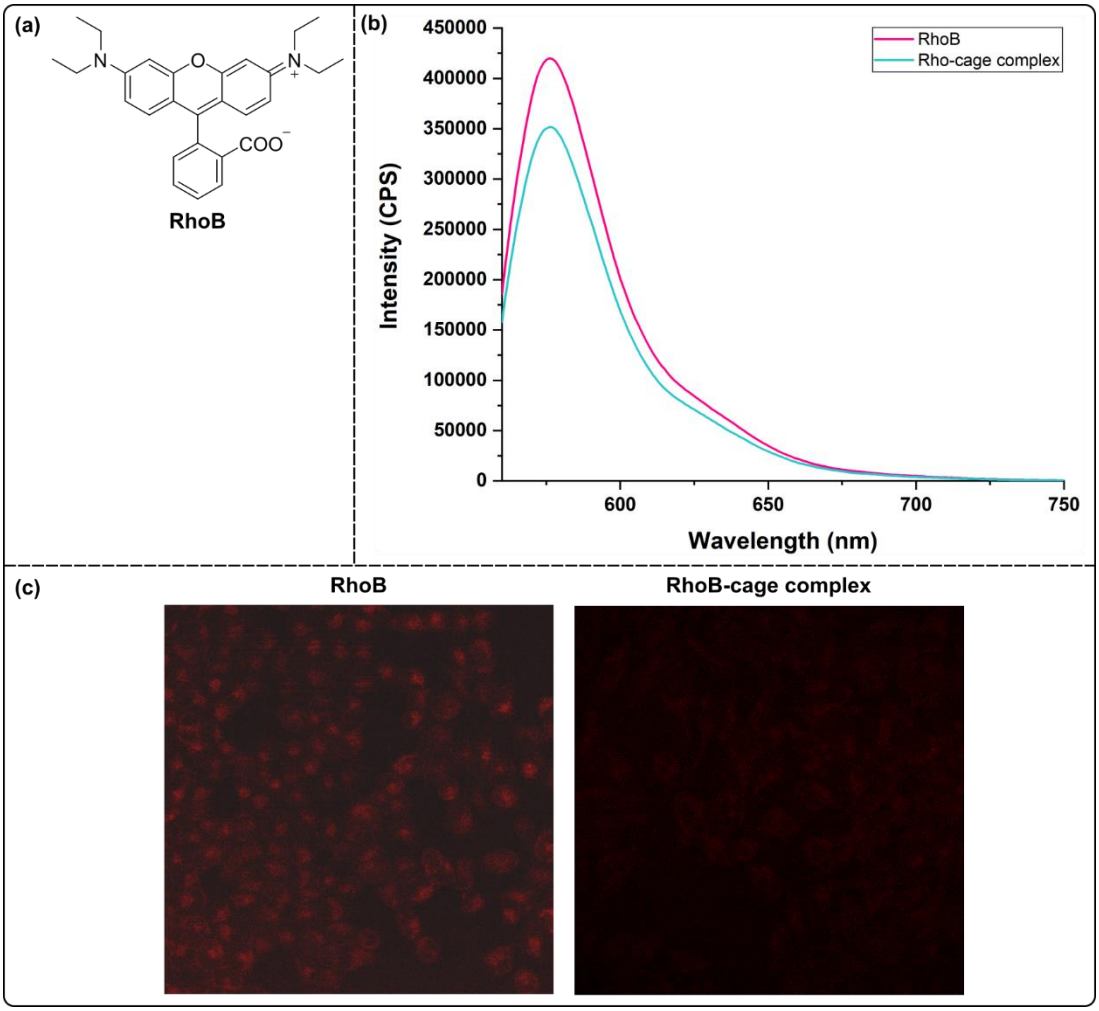

Figure 3. (a) Structure of RhoB. (b) Emission spectra of a 1 μM solution of RhoB and a 1 μM solution of RhoB-cage complex in water. (c) Confocal microscopy images of HeLa cells incubated with a 500 nM solution of RhoB or RhoB-cage complex.

EFFECT OF CATALYST ENCAPSULATION ON BIOCOMPATIBILITY

Having established the cytotoxicity of substrate **1** and the required concentration of the substrate for the reaction to be able to take place in cells, next the biocompatibility of the reaction itself was investigated. The reaction was carried out under biological conditions in the lab, rather than in cells, in order to gain insight into how the reaction behaves in the presence of biological components, as both the set-up and analysis is more facile in the lab compared to in cells. Catalysis was therefore carried out under dilute conditions in various cell culture media in order to determine if the reaction would be feasible *in vivo* (Table 1), as such media contains a complex mixture of proteins and biomolecules, similar to what is found inside of cells. Solutions of the catalysts were first prepared in water or DMSO before addition of the substrate. A solution of 50 mol% of either encapsulated $[Me_3PAu]^+$@cage in water or free Me_3PAuCl in DMSO was therefore added to cell culture media (either DMEM + 10% FBS, FBS, or FBS/PBS mixtures), followed by the addition of 1 eq of substrate **1** to give a final concentration of 10 μM of substrate. This concentration of substrate was selected so that even at low yields, product **2a** would still be able to be detected. The reaction mixtures were stirred at 37 °C for 16 h, after which they were directly analysed by fluorescence spectroscopy. However, in all cases, for

both encapsulated $[Me_3PAu]^+$@cage and free Me_3PAuCl, no fluorescence was detected, meaning that no product was formed. Therefore, catalysis with either free or encapsulated gold is not possible under the conditions which would be required for in cells.

Table 1. Catalysis of substrate **1** in cell culture media.[a]

Entry	Catalyst	Cell Culture Medium	Yield 2a (%)
1	Me_3PAuCl	DMEM + 10% FBS	0
2	Me_3PAuCl	FBS	0
3	Me_3PAuCl	FBS/PBS 1:1	0
4	Me_3PAuCl	PBS + 10% FBS	0
5	$[Me_3PAu]^+$@cage	DMEM + 10% FBS	0
6	$[Me_3PAu]^+$@cage	FBS	0
7	$[Me_3PAu]^+$@cage	FBS/PBS 1:1	0
8	$[Me_3PAu]^+$@cage	PBS + 10% FBS	0

[a]Conditions: 10 μM substrate **1**, 50 mol% Me_3PAuCl or $[Me_3PAu]^+$@cage, 2% DMSO in cell culture medium, 37 °C, 16 h. Yield determined by fluorescence spectroscopy.

In order to gain understanding into the reasons for catalysis inhibition, the reaction was carried out at higher substrate concentrations, under the typical catalysis conditions used in the literature for $[Me_3PAu]^+$@cage.[32, 33] Therefore 0.2 M of substrate **1** was stirred at 37 °C for 16 h in the presence of 2.5 mol% catalyst. Almost identical yields of the fluorescent product **2a** were obtained for both free Me_3PAuCl and encapsulated $[Me_3PAu]^+$@cage in water, with 69% and 70% yields respectively (Figure 4a). Due to solubility reasons, the reaction mixtures could not be analysed with ^1H NMR spectroscopy, and the yield of **2a** was instead determined by fluorescence intensity. When the catalysis was carried out in CH_3CN using PPh_3AuCl as catalyst, full conversion was achieved, resulting in a 7:3 ratio of fluorescent product **2a** and the non-fluorescent regio-isomer **2b**. Therefore it is likely that **2b** is also being formed during the catalysis water, and that the overall conversion is higher than the yield of **2a**. Having established the successful formation of **2a** by $[Me_3PAu]^+$@cage, we then looked to investigate the effect of the in the presence of biological additives; namely GSH, and L-histidine (His), an amino acid which contains a metal-binding imidazole moiety, and PBS buffer. 2.5 mol% of either free Me_3PAuCl or encapsulated $[Me_3PAu]^+$@cage was first mixed with 1.25 mol% His or GSH in water before addition of substrate **1**, and the resulting mixture was stirred at 37 °C for 16 h. In all cases, the encapsulated $[Me_3PAu]^+$@cage complex outperformed free Me_3PAuCl. His had the least effect upon the catalytic activity of the gold, with a 50% yield of **2a** for free Me_3PAuCl and 65% yield for encapsulated $[Me_3PAu]^+$@cage. The presence of PBS buffer had an inhibiting effect upon catalysis. When the reaction was carried out in a 8:2 mixture of PBS/water, the yield dropped to just 22% for free Me_3PAuCl, while it remained high for encapsulated $[Me_3PAu]^+$@cage, at 63%. While the high concentration of chlorides in

the PBS buffer (140 mM) disfavours dissociation of the chloride from the free Me_3PAuCl complex and therefore reduces the amount of active species in solution, it appears that this is not the case in the presence of the cage: once encapsulated inside the cage, recombination of the gold centre with the chloride is prevented, likely due to charge repulsion between the anionic cage and anionic chloride centre preventing them from coming in close proximity with each other. As expected, GSH behaved as a strong poison for the catalysis. Even in the presence of only 0.5 eq of GSH compared to the gold, free Me_3PAuCl only generated **2a** in a 2% yield. However, upon encapsulation a 6-fold increase in yield was observed, with a 13% yield for $[Me_3PAu]^+$@cage. When the reaction mixture was measured with high resolution electrospray ionisation mass spectrometry (Figure 4c), a peak at 852.0034 was observed, which corresponds to a species containing one GSH molecule and two $[Me_3PAu]^+$ cations. As no species corresponding to one GSH molecule and one $[Me_3PAu]^+$ cation was observed, it appears that one GSH molecule poisons the catalysis by irreversibly binding two gold centres. As GSH is found in concentrations of 2–5 mM in cells,[39] we looked to see the extent to which the cage could protect against this thiol poisoning. Catalysis was carried out in the presence of increasing equivalents of GSH with respect to the gold, and, unsurprisingly, no yield at all of **2a** was observed above 0.5 eq for free Me_3PAuCl (Figure 4b). However, for the $[Me_3PAu]^+$@cage complex **2a** was still observed with up to 2 eq of GSH, albeit in very low yields (<5%). Finally, catalysis was also carried out in the presence of all three biological additives combined. When both GSH and His are combined together in PBS buffer no yield at all is observed for free Me_3PAuCl, however **2a** was still produced in a 4% yield for encapsulated $[Me_3PAu]^+$@cage. Although the catalytic activity of encapsulated $[Me_3PAu]^+$@cage is quite drastically reduced in the presence of these biological additives, **2a** is still generated in consistently higher yields compared to free Me_3PAuCl. Therefore while poisoning still takes place, the cage indeed is able to provide partial protection against these biological additives. While it is clear that GSH is one source of catalysis inhibition under biological conditions, it should be noted that while these data give an indication of what may happen *in vivo*, they may not necessarily translate to the cell environment; the cell is a highly complex, heterogeneous environment,[40] and such simple test reactions in the lab may not paint an accurate picture of how the system will behave inside a cell.

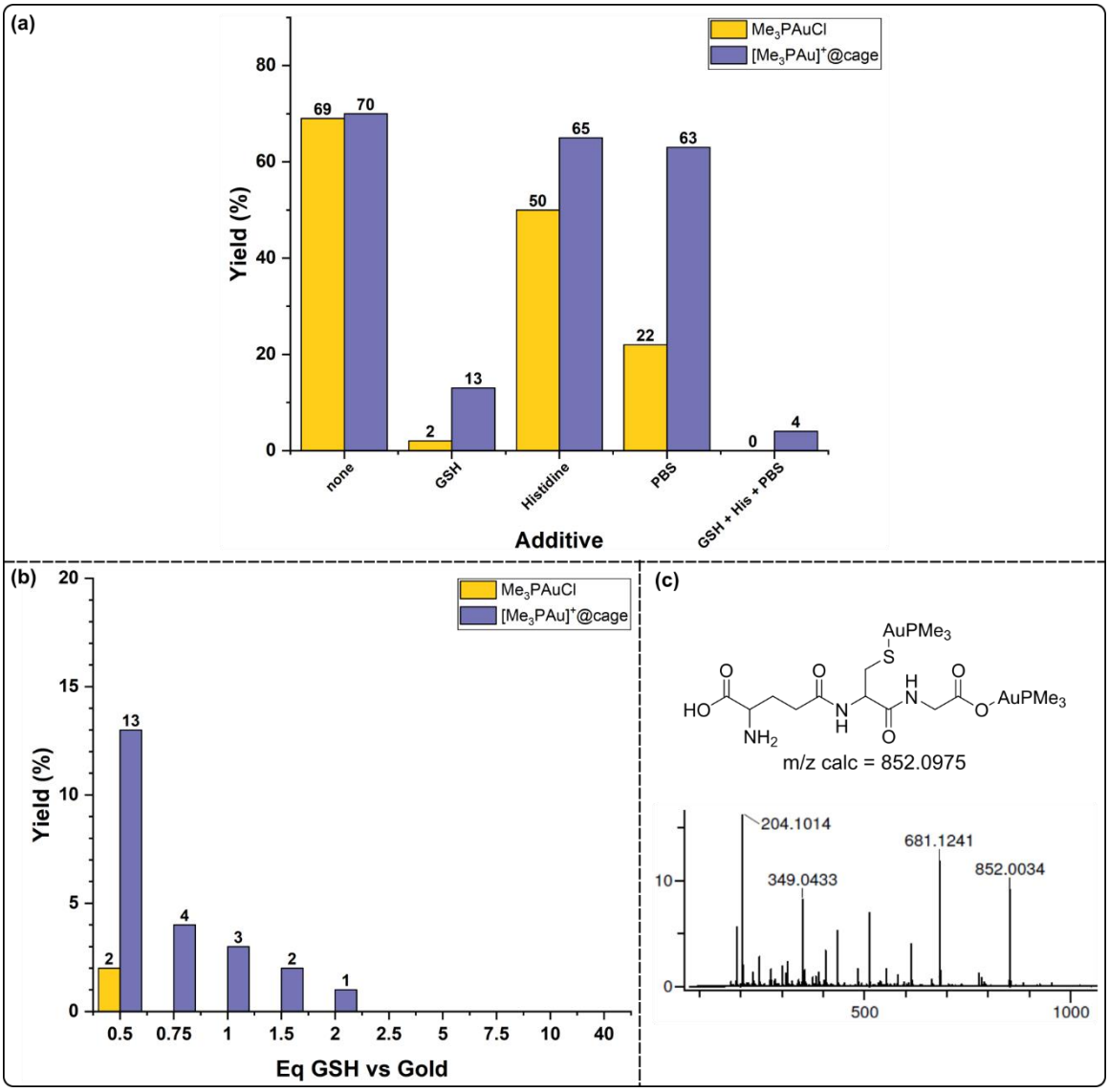

Figure 4. (a) Catalysis of substrate **1** with free Me_3PAuCl and encapsulated $[Me_3PAu]^+$@cage in the presence of biological additives. (b) Catalysis of substrate **1** with free and encapsulated catalyst in the presence of increasing equivalents of GSH. (c) ESI-HRMS spectrum (positive mode) of the reaction mixture of catalysis in the presence of 0.5 equivalents of GSH with respect to gold.

CONCLUSION AND OUTLOOK

An encapsulated gold catalyst was able to catalyse an intramolecular hydroarylation reaction to produce a fluorescent coumarin dye. Under catalytic conditions in the lab the encapsulated $[Me_3PAu]^+$@cage complex was able to generate the product with higher yields in both water and in the presence of biological additives than for free Me_3PAuCl. The cage was therefore able to provide partial protection for the gold catalyst by reducing poisoning by thiols and chlorides. The encapsulated $[Me_3PAu]^+$@cage complex afforded product **2a** in the presence of GSH, His, and PBS buffer, whereas free Me_3PAuCl was completely inactive under the same conditions. However, very low substrate concentrations would be required for the reaction to be carried out in cells, due to the high level of cytotoxicity induced by substrate **1**, and at 10 μM concentrations neither free Me_3PAuCl nor encapsulated $[Me_3PAu]^+$@cage was able to generate product **2a** in cell culture media. Moreover, the cage itself was found to be not cell permeable. However, there are several vehicles known to transport non-permeable cargo into cells,[41] and encapsulation of the encapsulated $[Me_3PAu]^+$@cage complex inside lipid nanoparticles (LNPs) may provide a viable route to deliver the protected catalyst into the cell.[42-44] Therefore, the intramolecular hydroarylation of substrate **1** is not an appropriate reaction to investigate the influence of the cage upon the reactivity of a gold catalyst inside living cells. In order to determine this, the substrate should be redesigned as such so that it is less toxic and can be used at higher substrate concentrations. In addition, an even smaller substrate may further improve the protection provided by the cage, and further enhance the activity of the encapsulated gold under biological conditions.

EXPERIMENTAL

MATERIALS AND METHODS

All commercially available compounds were used as received. Dulbecco's modified Eagle medium (DMEM) was obtained from Gibco, Life Technologies. Cage was synthesised according to a literature procedure.[45] Water was degassed by bubbling N_2 for 4 h. Organic solvents were distilled and degassed prior to use. Column chromatography was performed using silica gel (SiliCycle, SiliaFlash P_{60}, 40–63 μm, 230–400 mesh) while fractions were analysed using TLC (TLC silica gel 60 F_{254} from Merck KGaA) which was visualised with 254/350 nm light. Milli-Q Ultrapure grade water was used for catalysis, UV/Vis, and fluorescence measurements. All stock solutions for cell experiments were freshly prepared under an atmosphere of N_2 before each experiment and were only exposed to air immediately before incubation with the cells. NMR spectra were performed on a Bruker AV300, AV400, or AV500 spectrometer, with chemical shifts reported in ppm and referenced to solvent residual signal (7.26 ppm for $CDCl_3$, 4.79 ppm for D_2O). 2D ^1H DOSY NMR spectra were recorded with a calibrated gradient at 298 K. High resolution mass data were recorded on a HR ToF Bruker Daltonik Gmbh Impact II, an ESI-ToF MS capable of resolution of at least 40000 FWHM, which was coupled to a Bruker cryo-spray unit. Detection was in positive-ion or negative-ion mode and the source voltage was between 4 and 6 kV. The sample was introduced with syringe pump at a flow rate of 18 μL/hr. For electrospray ionisation (ESI), the drying gas (N_2) was held at 180 °C. For cryospray ionisation (CSI), the drying gas (N_2) was held at -35 °C and the spray gas was held at -40 °C. The machine was calibrated prior to every experiment via direct infusion of a TFA-Na solution, which provided a m/z range of singly charged peaks up to 3500 Da in both ion modes. Software acquisition Compass 2.0 for Otof series. Software processing Compass DataAnalysis 4.0 sri. UV/Vis spectra were recorded on a Hewlett Packard 8453 single beam spectrophotometer in a 1.0 cm path length quartz cuvette with H_2O or DMSO as background. Fluorescence spectra were recorded on a Fluorolog Jobin Yvon-SPEX together with their corresponding UV/Vis spectra (Shimadzu UV-2700 Spectrophotometer).

SYNTHESIS

Synthesis of compounds

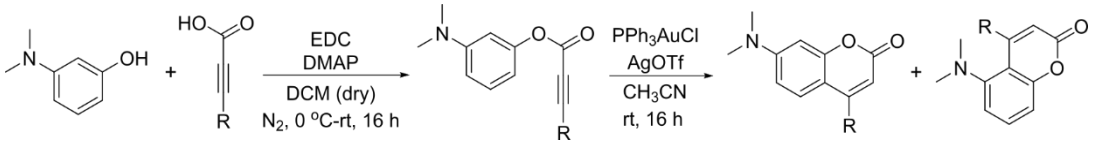

3-(Dimethylamino)phenyl but-2-ynoate, 1

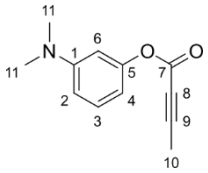

Under an atmosphere of N_2, 3-(Dimethylamino)phenol (1.65 g, 12.00 mmol, 1.2 eq) and but-2-ynoic acid (1.76 g, 10.00 mmol, 1 eq) were dissolved in dry degassed DCM (5 mL) and

cooled to 0 °C. A solution of EDC (1.55 g, 10 mmol, 1 eq) and DMAP (0.3 g, 2.5 mmol, 0.25 eq) in dry degassed DCM (20 mL) was added dropwise. The solution was stirred for 1 h at 0 °C, then at room temperature overnight. Under aerobic conditions, DCM (200 mL) was added, and the organic layer was washed with brine (100 mL), sat. aq. $NaHCO_3$ (100 mL) and water (2 × 100 mL). The organic phase was dried over Na_2SO_4, filtered, then dried *in vacuo*. The crude product was purified by column chromatography in PE / EtOAc 8:2 (R_f = 0.5). The product was collected as a pale yellow oil (1.14 g, 5.63 mmol, 56%). **^{1}H NMR** (300 MHz, $CDCl_3$): δ 7.22 (t, J = 8.2 Hz, 1H, *H3*), 6.59 (dd, J = 8.4, 2.3 Hz, 1H, *H2*), 6.51 – 6.44 (m, 1H, *H6*), 6.43 (t, J = 2.2 Hz, 1H, *H4*), 2.94 (s, 6H. *H11*), 2.05 (s, 3H, *H10*). **^{13}C NMR** (101 MHz, $CDCl_3$): δ 152.19 (C, *C7*), 151.66 (C, *C1*), 151.17 (CH, *C5*), 129.75 (CH, *C3*), 110.31 (CH, *C2*), 108.96 (CH, *C4*), 105.15 (CH, *C6*), 87.64 (C, *C9*), 72.31 (C, *C8*), 40.43 (CH_3, *C11*), 3.96 (CH_3, *C10*). **ESI-HRMS** (positive): m/z (calc) = 204.1013 (204.1025) $[M+H]^+$.

7-(Dimethylamino)-4-methyl-2H-chromen-2-one, 2a

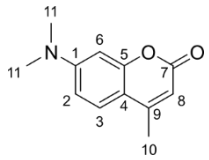

PPh_3AuCl (12 mg, 0.025 mmol, 0.1 eq) was dissolved in MeCN (5 mL). 3-(Dimethylamino)phenyl but-2-ynoate (50 mg, 49.1 µL, 0.25 mmol, 1 eq) then AgOTf (6 mg, 0.025 mmol, 0.1 eq) were added, and the solution was stirred at room temperature overnight. The solvent was removed *in vacuo*, and the product was isolated by column chromatography in PE / EtOAc 75:25 (R_f = 0.24). The product was collected as a yellow solid (32 mg, 0.16 mmol, 63%). **^{1}H NMR** (300 MHz, $CDCl_3$): δ 7.37 (d, J = 8.9 Hz, 1H, *H3*), 6.59 (dd, J = 8.9, 2.5 Hz, 1H, *H2*), 6.47 (d, J = 2.5 Hz, 1H, *H6*), 5.94 (s, 1H, *H8*), 3.03 (s, 6H, *H11*), 2.32 (s, 3H, *H10*). **^{13}C NMR** (101 MHz, $CDCl_3$): δ 162.09 (C, *C7*), 155.66 (C, *C5*), 152.90 (C, *C4*), 152.80 (C, *C1*), 125.29 (CH, *C3*), 109.68 (C, *C9*), 109.32 (CH, *C8*), 108.82 (CH, *C2*), 98.28 (CH, *C6*), 40.17 (CH_3, *C11*), 18.49 (CH_3, *C10*). **ESI-HRMS** (positive): m/z (calc) = 204.1018 (204.1025) $[M+H]^+$. **UV/Vis** (DMSO, 25 µM): λ_{max} = 368 nm, A = 0.5057. **Fluorescence** (DMSO, 10 µM, $\lambda_{excitation}$ = 369 nm): λ_{max} = 434 nm, I = 456110.

5-(dimethylamino)-4-methyl-2H-chromen-2-one, 2b

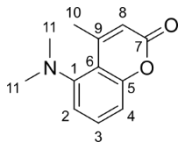

Same procedure as for 7-(dimethylamino)-4-methyl-2H-chromen-2-one. The product was isolated by column chromatography in PE / EtOAc 75:25 (R_f = 0.47). The product was collected as a yellow solid (7 mg, 0.03 mmol, 14%).**^{1}H NMR** (300 MHz, $CDCl_3$): δ 7.39 (d, J = 8.1 Hz, 1H, *H3*), 7.03 (dd, J = 8.1, 2.4 Hz, 2H, *H2* + *H4*), 6.15 (s, 1H, *H8*), 2.70 (s, 6H, *H11*), 2.69 (d, J = 1.0 Hz, 3H, *H10*). **^{13}C NMR** (101 MHz, $CDCl_3$): δ 160.66 (C, *C7*), 155.41 (C, *C6*), 154.00 (C, *C5*), 153.75 (C, *C1*), 131.24 (CH, *C3*), 115.87 (CH, *C2*), 115.52 (CH, *C8*), 115.37 (C, *C9*), 112.46 (CH, *C4*), 45.89 (CH_3, *C11*), 22.19 (CH_3, *C10*). **ESI-HRMS** (positive): m/z (calc) = 204.1023 (204.1025) $[M+H]^+$.

3-(Dimethylamino)phenyl 3-phenylpropiolate, 3

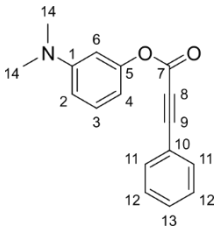

Under an atmosphere of N_2, 3-(Dimethylamino)phenol (1.65 g, 12.00 mmol, 1.2 eq) and 3-phenylpropiolic acid (1.46 g, 10.00 mmol, 1 eq) were dissolved in dry degassed DCM (11.2 mL) and cooled to 0 °C. EDC (2.33 g, 15 mmol, 1.5 eq) and DMAP (0.3 g, 2.5 mmol, 0.25 eq) were added. The solution was stirred for 1 h at 0 °C, then at room temperature overnight. Under aerobic conditions, DCM (200 mL) was added, and the organic layer was washed with 0.5 M aq. HCl (100 mL), sat. aq. $NaHCO_3$ (100 mL), brine (100 mL) and water (100 mL). The organic phase was dried over Na_2SO_4, filtered, then dried *in vacuo*. The crude product was purified by column chromatography in PE / EtOAc 8:2 (R_f = 0.4). The product was collected as a pale yellow oil (0.83 g, 3.13 mmol, 31%). **^{1}H NMR** (400 MHz, $CDCl_3$): δ 7.55 – 7.47 (m, 2H, *H11*), 7.40 – 7.32 (m, 1H, *H13*), 7.32 – 7.25 (m, 2H, *H12*), 7.13 (t, J = 8.2 Hz, 1H, *H3*), 6.50 (dd, J = 8.4, 2.2 Hz, 1H, *H2*), 6.42 (dd, J = 7.9, 1.6 Hz, 1H, *H4*), 6.38 (t, J = 2.1 Hz, 1H, *H6*), 2.84 (s, 6H, *H14*). **^{13}C NMR** (101 MHz, $CDCl_3$): δ 152.62 (C, *C7*), 151.71 (C, *C1*), 151.27 (C, *C5*), 133.19 (CH, *C11*), 130.97 (CH, *C13*), 129.82 (CH, *C3*), 128.69 (CH, *C12*), 119.43 (C, *C10*), 110.42 (CH, *C2*), 109.01 (CH, *C4*), 105.20 (CH, *C6*), 88.32 (C, *C9*), 80.51 (C, *C8*), 40.46 (CH_3, *C14*). **ESI-HRMS** (positive): m/z (calc) = 266.1176 (266.1161) $[M+H]^+$.

7-(Dimethylamino)-4-phenyl-2H-chromen-2-one, 4a

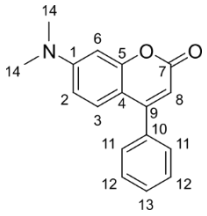

PPh_3AuCl (49 mg, 0.10 mmol, 0.1 eq) was dissolved in MeCN (20 mL). 3-(Dimethylamino)phenyl 3-phenylpropiolate (265 mg, 1.0 mmol, 1 eq) then AgOTf (25 mg, 0.10 mmol, 0.1 eq) were added, and the solution was stirred at room temperature overnight. The solvent was removed *in vacuo*, and the product was isolated by column chromatography in PE / EtOAc 8:2 (R_f = 0.29). The product was collected as a yellow solid (187 mg, 0.92 mmol, 70%). **^{1}H NMR** (400 MHz, $CDCl_3$): δ 7.50 – 7.45 (m, 3H, *H11* + *H13*), 7.44 – 7.38 (m, 2H, *H12*), 7.26 (d, J = 8.9 Hz, 1H, *H3*), 6.56 (d, J = 2.5 Hz, 1H, *H6*), 6.53 (dd, J = 8.9, 2.6 Hz, 1H, *H2*), 6.02 (s, 1H, *H8*), 3.04 (s, 6H, *H14*). **^{13}C NMR** (101 MHz, $CDCl_3$): δ 162.04 (C, *C7*), 156.42 (C, *C4*), 156.14 (C, *C5*), 152.88 (C, *C1*), 136.17 (C, *C10*), 129.31 (CH, *C11*), 128.68 (CH, *C13*), 128.40 (CH, *C12*), 127.70 (CH, *C3*), 108.88 (CH, *C2*), 108.85 (CH, *C8*), 108.43 (C, *C9*), 98.40 (CH, *C6*), 40.13 (CH_3, *C14*). **ESI-HRMS** (positive): m/z (calc) = 266.1186 (266.1181) $[M+H]^+$.

5-(dimethylamino)-4-phenyl-2H-chromen-2-one, 4b

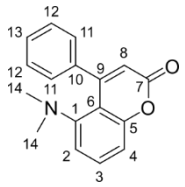

Same procedure as for 7-(dimethylamino)-4-phenyl-2H-chromen-2-one. The product was isolated by column chromatography in PE / EtOAc 75:25 (R_f = 0.52). The product was collected as a yellow solid (76 mg, 0.29 mmol, 29%). **^{1}H NMR** (400 MHz, $CDCl_3$) δ 7.45 – 7.29 (m, 6H, *H3* + *H11* + *H12* + *H13*), 6.99 (dd, J = 8.3, 1.1 Hz, 1H, *H4*), 6.83 (dd, J = 8.1, 1.1 Hz, 1H, *H2*), 6.23 (s, 1H, *H8*), 2.25 (s, 6H, *H14*). **^{13}C NMR** (101 MHz, $CDCl_3$) δ 160.88 (C, *C7*), 156.13 (C, *C5*), 155.73 (C, *C6*), 152.23 (C, *C1*), 138.20 (C, *C10*), 131.65 (CH, *C3*), 128.57 (CH, *C11*), 127.83 (CH, *C12*), 127.02 (CH, *C13*), 115.46 (CH, *C8*), 114.30 (CH, *C2*), 110.53 (C, *C9*), 110.20 (CH, *C4*), 43.52 (CH_3, *C14*). **ESI-HRMS** (positive): m/z (calc) = 266.1178 (266.1181) $[M+H]^+$.

ENCAPSULATIONS

[$Me_3PAu]^+$@cage

Under an atmosphere of N_2, a 2 mL vial was charged with solid Me_3PAuCl (0.77 mg, 2.50 µmol, 1 eq). To this vial, a solution of cage in degassed D_2O (5 mM, 0.6 mL, 3.00 µmol, 1.2 eq) was added, and the resulting mixture was stirred for 30 min at room temperature. The solution was then transferred by syringe to an NMR tube. ^{1}H and ^{31}P NMR data in accordance to the literature.[32] **^{1}H NMR** (300 MHz, D_2O): δ 7.80 – 7.64 (m, 24H), 7.10 (d, J = 8.1 Hz, 16H), 6.85 (t, J = 8.2 Hz, 10H), 6.66 (d, J = 5.7 Hz, 8H), 6.48 (t, J = 7.9 Hz, 12H), -1.89 – -2.04 (m, 9H). **^{31}P NMR** (122 MHz, D_2O): δ -17.17, -18.64. **2D ^{1}H DOSY NMR** (D_2O, 298 K): $\log_D$ = -9.623.

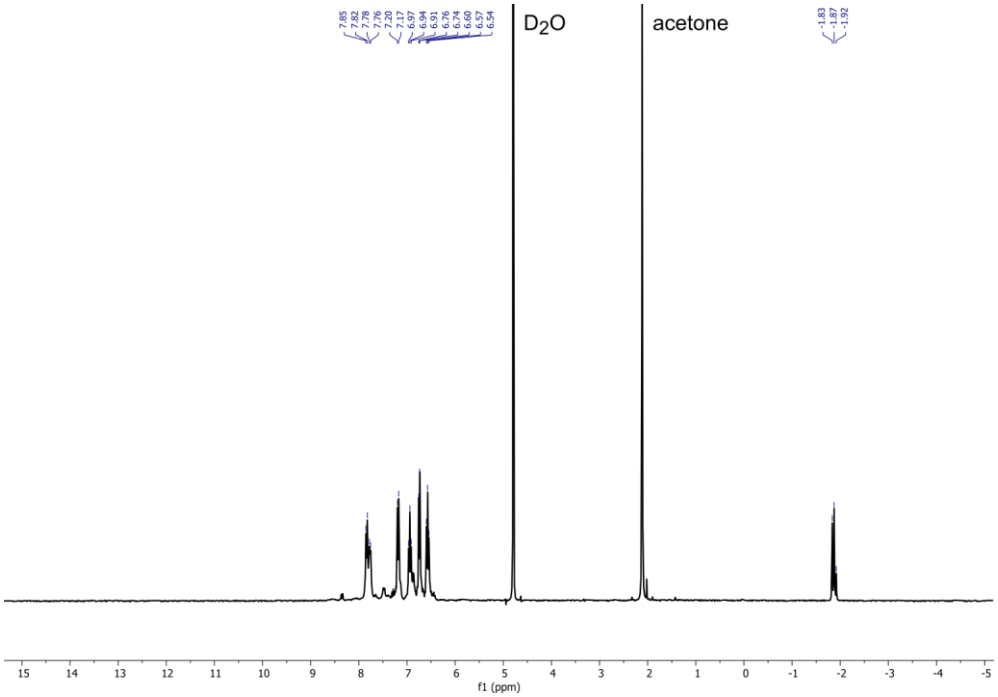

Figure E5. ^{1}H NMR spectrum of $[Me_3PAu]^+$@cage in D_2O. Acetone signal is from precipitation of the cage with acetone during synthesis.

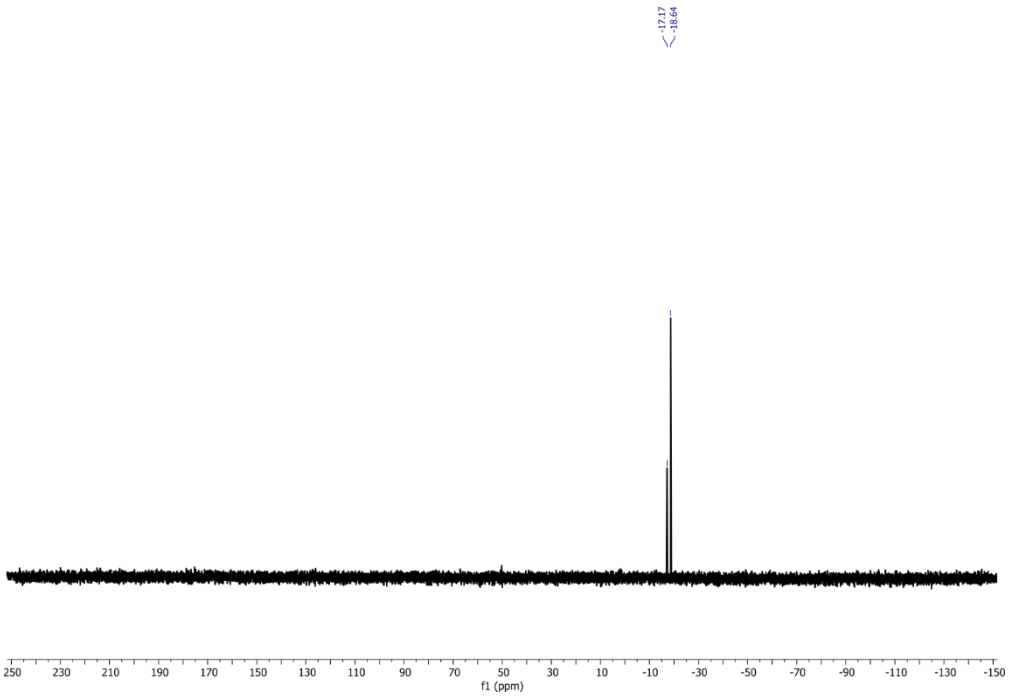

Figure E6. ^{31}P NMR spectrum of $[Me_3PAu]^+$@cage in D_2O.

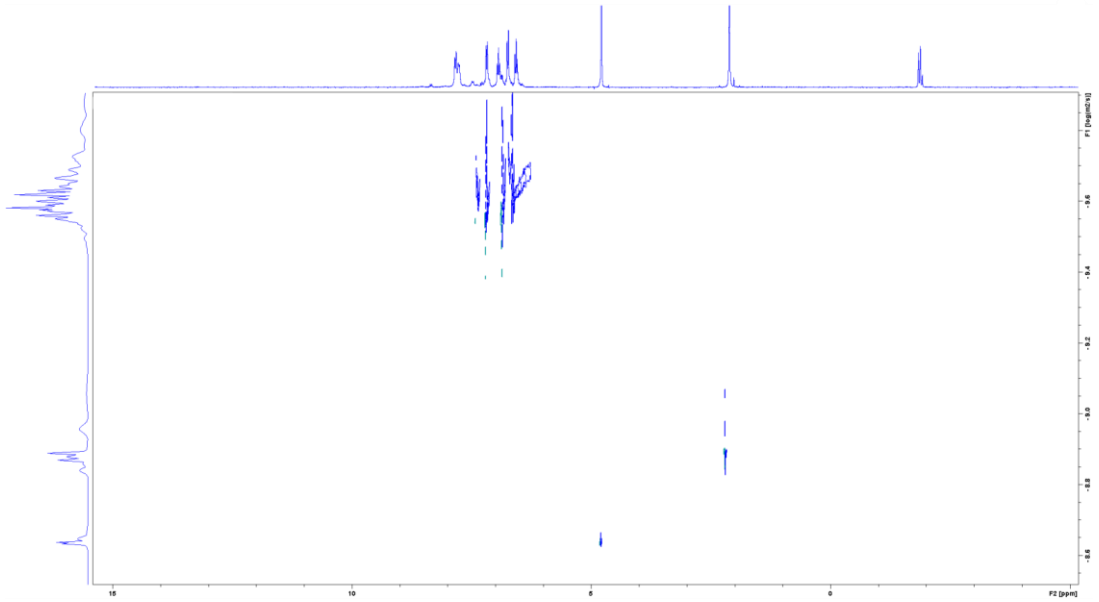

Figure E7. 2D ^{1}H DOSY NMR spectrum of $[Me_3PAu]^+$@cage in D_2O at 298 K.

RhoB-cage complex

Under an atmosphere of N_2, a 2 mL vial was charged with solid RhodamineB (1.19 mg, 2.50 µmol, 1 eq). To this vial, a solution of cage in degassed D_2O (5 mM, 0.6 mL, 3.00 µmol, 1.2 eq) was added, and the resulting mixture was stirred for 30 min at room temperature. The solution was then transferred by syringe to an NMR tube. **^{1}H NMR** (300 MHz, D_2O): δ 7.38 (d, J = 7.2 Hz, 16H), 7.18 (d, J = 8.9 Hz, 16H), 6.84 (d, J = 6.6 Hz, 14H), 6.73 – 6.57 (m, 24H), 3.06 (s, 14H), 0.95 (s, 17H). **2D ^{1}H DOSY NMR** (D_2O, 298 K): $\log_D$ = -9.625. **CSI-HRMS** (negative): m/z (calc) = 1166.8155 (1166.7836) $\{[Ga_4L_6][RhoB]K_2Na_6H_4\}^{3-}$; 1066.9849 (1066.9948) $\{[Ga_4L_6]K_9H_{12}\}^{3-}$; 1035.0047 (1035.0170) $\{[Ga_2L_4]H_4\}^{1-}$; 891.5641 (891.5730) $\{[Ga_4L_6][RhoB]K_3H_4\}^{4-}$; 781.0092 (781.0067) $\{[Ga_4L_6]K_6Na_2H_6\}^{4-}$; 684.5049 (684.4847) $\{[Ga_4L_6][RhoB]Na_6H_4\}^{5-}$; 498.0206 (498.0269) $\{[Ga_2L_2]H_4\}^{2-}$. **UV/Vis** (H_2O, 10 µM): λ_{max}(cage) = 330 nm, A = 1.1013; λ_{max}(RhoB) = 554 nm, A = 0.8552. **Fluorescence** (H_2O, 1 µM, $\lambda_{excitation}$ = 554 nm): λ_{max} = 576 nm, I = 351380.

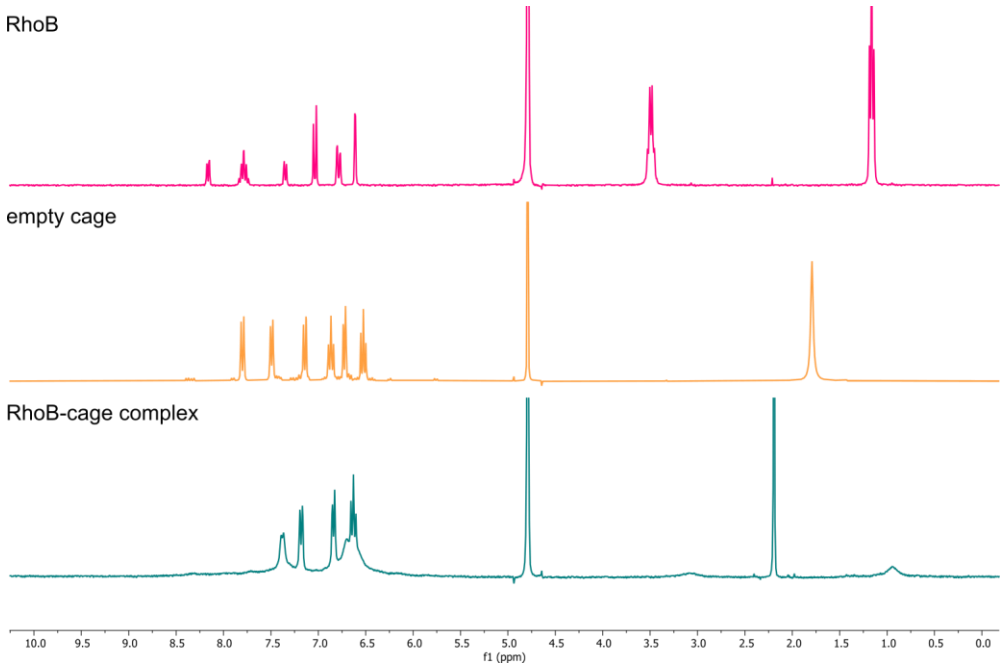

Figure E8. ^{1}H NMR spectra of free RhoB, empty cage, and RhoB-cage complex in D_2O.

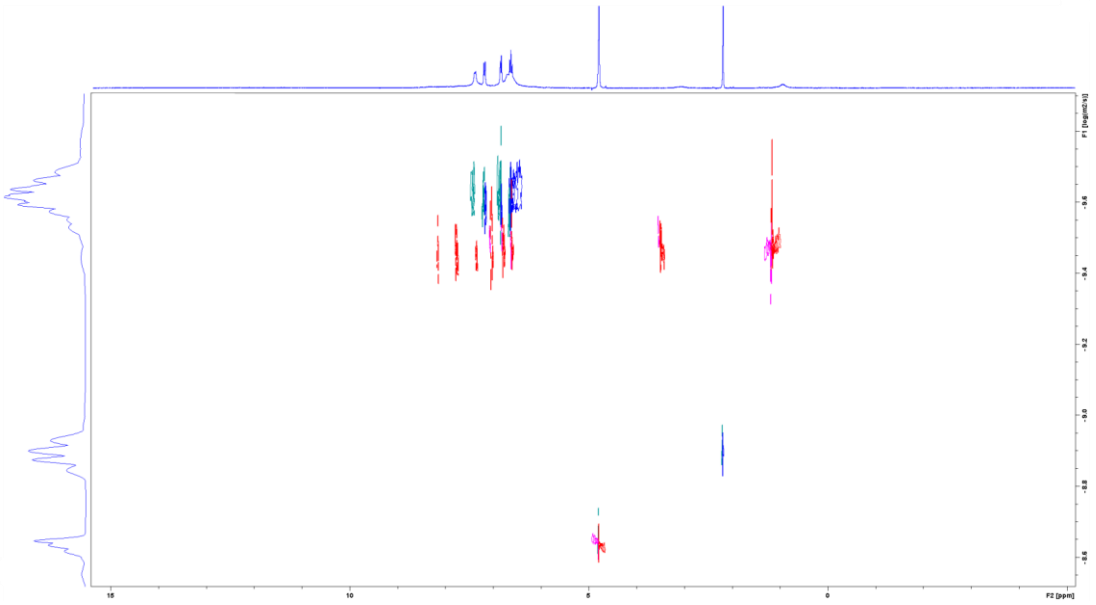

Figure E9. 2D ^{1}H DOSY NMR spectrum of RhoB-cage complex in D_2O at 298 K (blue) and 2D ^{1}H DOSY NMR spectrum of RhoB in D_2O at 298 K (red).

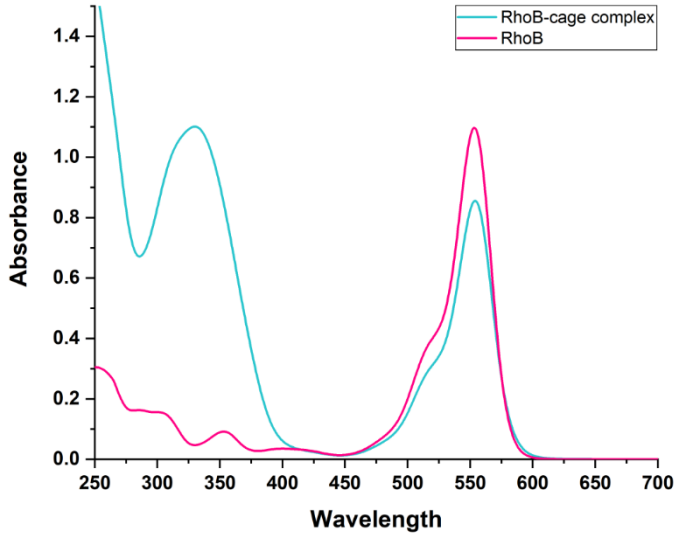

Figure E10. UV/Vis spectra of free RhoB and RhoB-cage complex. Spectra recorded in H_2O at 10 µM.

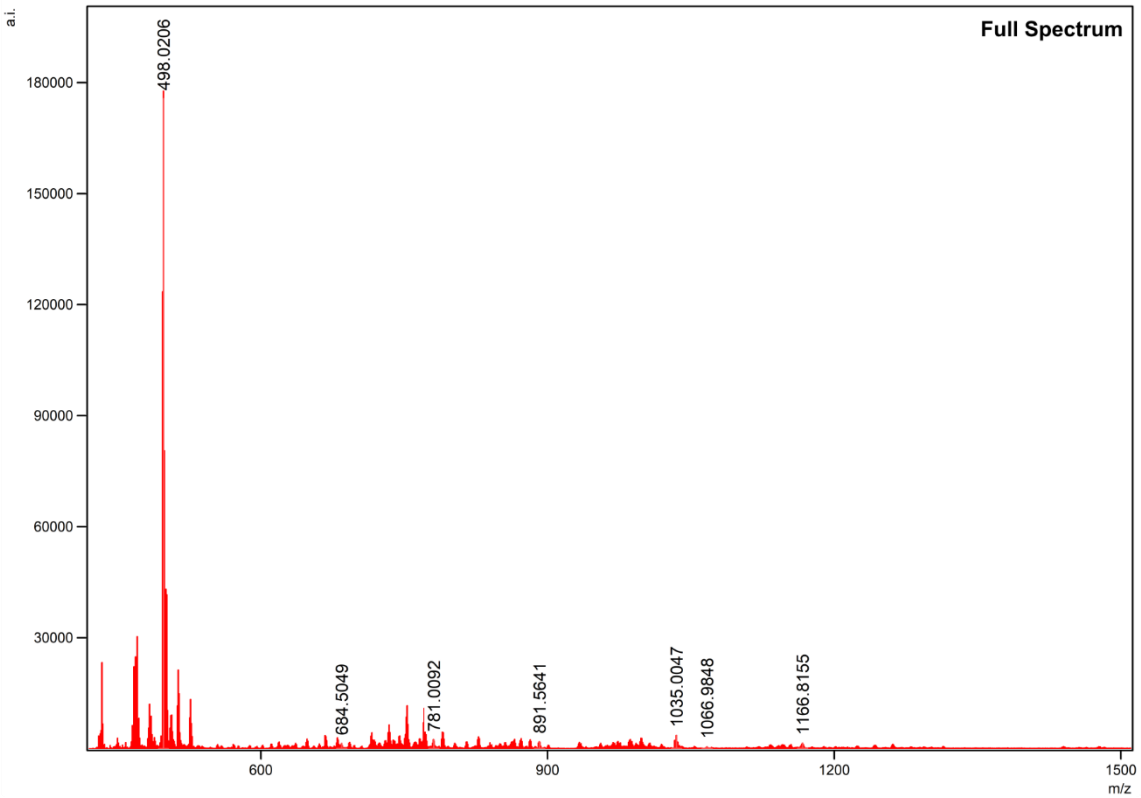

Figure E11. CSI-HRMS spectrum (negative mode) of RhoB-cage complex.

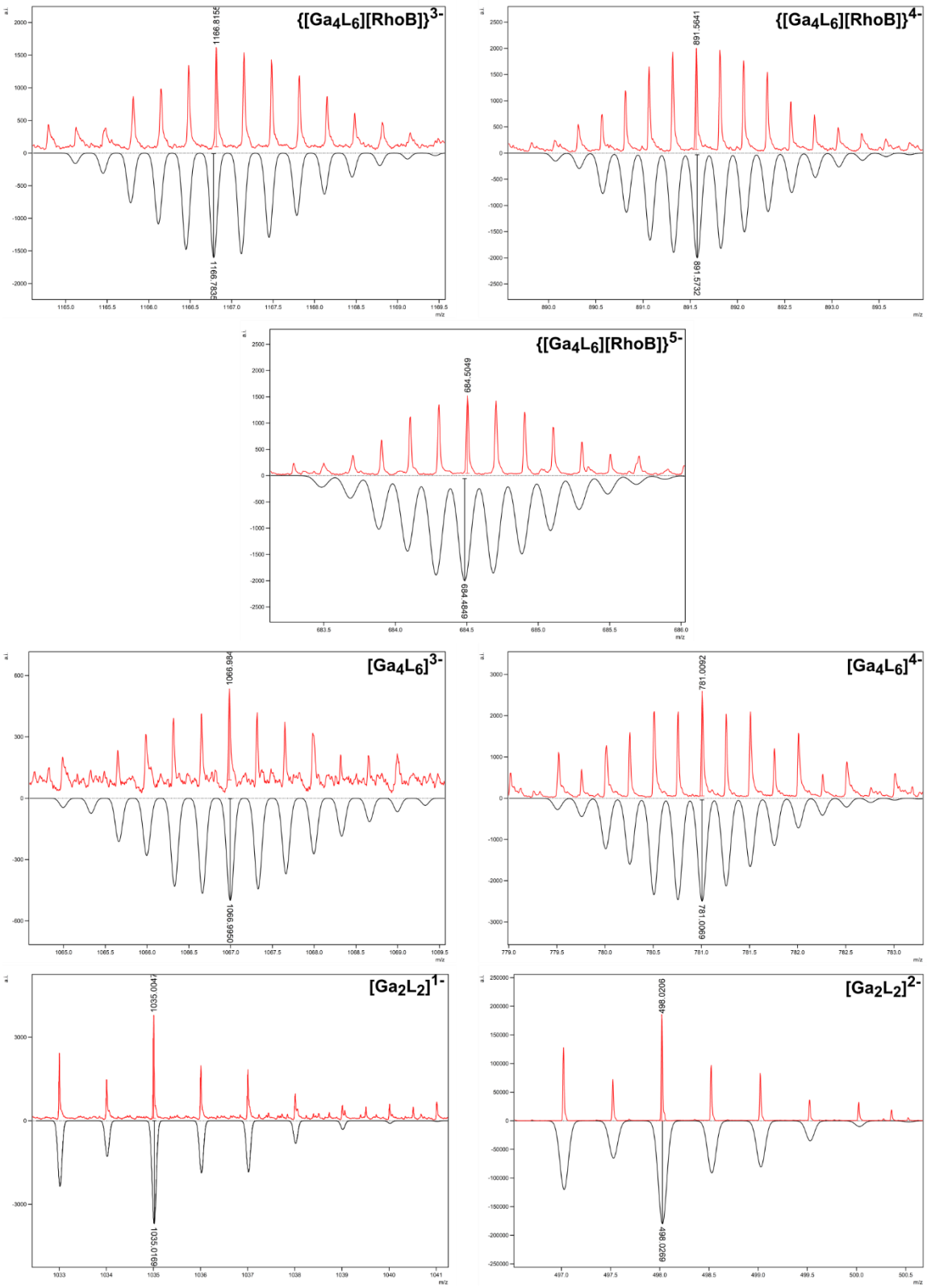

Figure E12. Zooms into CSI-HRMS spectrum of RhoB-cage complex. Measured in red, calculated in black.

CATALYSIS

Large substrate, 3

When 1 eq of a larger substrate, **3**, was stirred with 2.5 mol% of encapsulated cationic gold ($[Me_3PAu]^+$@cage) at room temperature for 16 h, a total conversion of 69% was obtained, with a 1.8:1 ratio of fluorescent product **4a** and its regio-isomer **4b** (Table E2). When 2.5 mol% of free Me_3PAuCl was directly mixed with substrate **3**, only 39% conversion was achieved. This higher conversion for the $[Me_3PAu]^+$@cage complex compared to the free Me_3PAuCl is consistent with previous reports for intramolecular hydroalkoxylation reactions.[32] The catalysis was also carried out in the presence of GSH and excess chlorides, both of which are present in high concentrations in cells. However, for both encapsulated $[Me_3PAu]^+$@cage and free Me_3PAuCl no conversion at all was observed when the catalysis was carried out in the presence of 1 mol% GSH and 50 mM NaCl. It is likely that this lack of protection was due to the large size of the substrate: although the encapsulated $[Me_3PAu]^+$@cage is able to react with the substrate in the absence of biomolecules, we hypothesised that in order to bind to the substrate, the gold centre is partially or fully pulled out of the cage as the substrate is not able to fit through the windows, leaving the gold centre vulnerable to poisoning by GSH and chlorides. Therefore, protection of the gold centre within the cage is not possible for large substrates, and in order to prevent biomolecule poisoning a substrate is needed which is small enough to fit through the windows of the cage and not pull the gold centre out of the protective environment of the cage.

Table E2. Catalysis of large phenyl substrate **3** with free and encapsulated catalyst.

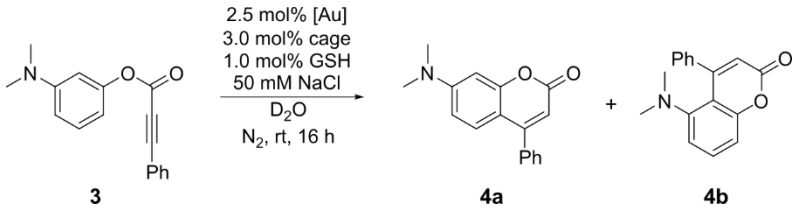

3 **4a** **4b**

Entry	Catalyst	Additive	Conversion (%)	Yield 4a (%)	Yield 4b (%)
1	Me_3PAuCl	None	39	26	13
2	Me_3PAuCl	GSH + NaCl	0	0	0
3	Me_3PAuCl	AgOTf	81	52	29
4	Me_3PAuCl	AgOTf + GSH + NaCl	0	0	0
5	-	AgOTf	0	0	0
6	$[Me_3PAu]^+$@cage	None	69	45	24
7	$[Me_3PAu]^+$@cage	GSH + NaCl	0	0	0

Procedure: Inside a glovebox, Me_3PAuCl, AgOTf, and cage were weighed into schlenks. All further manipulations were carried out under an atmosphere of N_2 on a schlenkline. Stock

solutions of Me_3PAuCl in dry degassed CH_3CN; and AgOTf, cage, and NaCl and GSH in degassed D_2O were prepared. The desired volume of Me_3PAuCl solution (1.4 μmol, 2.5 mol%) was added to a 4 mL vial, and the CH_3CN was then evaporated under vacuum. The desired volume of cage solution (1.67 μmol, 3.0 mol%) was added, and stirred for 30 min at room temperature. Then, the desired volumes of D_2O, then NaCl (15 μmol, 50 mM) and GSH (0.6 μmol, 1 mol%) solution were added. Substrate **3** (13.5 μL, 14 mg, 56 μmol, 1 eq) was then added neat, followed by the desired volume of AgOTf solution (1.4 μmol, 2.5 mol%). The vial was capped, sealed with parafilm, and stirred at room temperature for 16 h. The vial was then removed from the N_2 atmosphere and all further manipulations were carried out under air. 1.0 mL of a 50 mM solution of 1,3,5-trimethoxybenzene in $CDCl_3$ was added, and the vial was shaken. the organic layer was decanted to an NMR tube. The yields of product **4a** and product **4b** were determined by ^{1}H-NMR spectroscopy relative to 1,3,5-trimethoxybenzene as internal standard. Yields given are an average of 2-3 runs.

Stock Solution	Compound/Solvent	Concentration
A	Me_3PAuCl / CH_3CN	11.2 mM
B	Cage / D_2O	11.1 mM
C	AgOTf / D_2O	9.33 mM
D	NaCl + GSH / D_2O	100 mM NaCl; 4 mM GSH

Entry	A (μL)	B (μL)	C (μL)	D (μL)	D_2O (μL)	Total (μL)
1	125	0	0	0	300	300
2	125	0	0	150	150	300
3	125	0	150	0	150	300
4	125	0	150	150	0	300
5	0	0	150	0	150	300
6	0	0	150	150	0	300
7	125	150	0	0	150	300
8	125	150	0	150	0	300

Fluorescence calibration curve of product 2a

Fresh solutions of product **2a** in DMSO were prepared prior to fluorescence measurement. The fluorescence intensity of various concentrations of product **2a** at 433 nm were recorded. The results were processed with Origin 2018 to obtain the calibration equation, which was used to quantify the fluorescence of the catalysis experiments with substrate **1**.

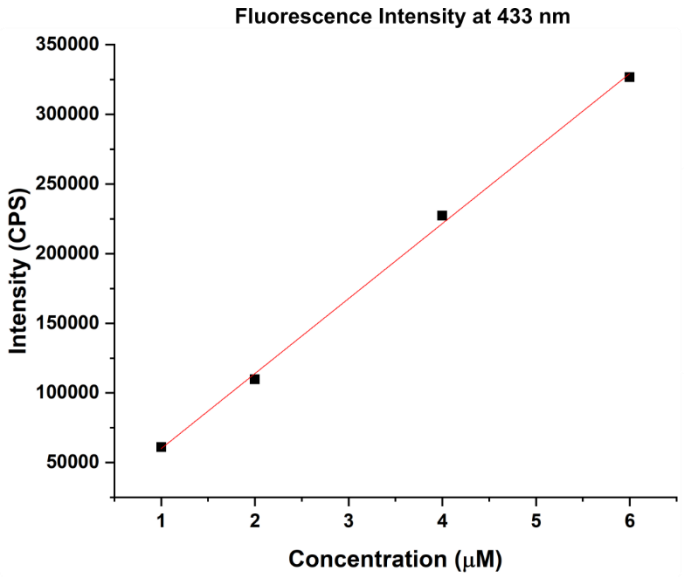

Equation	y = a + b*x
Plot	Intensity
Weight	No Weighting
Intercept	6182.88136 ± 5293.53716
Slope	53843.72881 ± 1402.29225
Residual Sum of Squares	5.80095E7
Pearson's r	0.99932
R-Square (COD)	0.99865
Adj. R-Square	0.99797

Substrate 1 under biological conditions

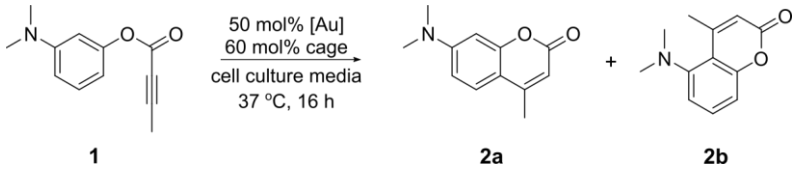

Inside a glovebox, Me_3PAuCl and cage were weighed into schlenks. Under an atmosphere of N_2, stock solutions of Me_3PAuCl in dry degassed CH_3CN (10 mM); and cage degassed H_2O (1.8 mM) were prepared. A stock solution of Me_3PAuCl in DMSO (0.5 mM) was prepared by adding the desired volume of Me_3PAuCl to a vial, evaporating the CH_3CN under vacuum, then diluting with DMSO. A stock solution of Me_3PAuCl and cage in H_2O was prepared by adding the desired volume of Me_3PAuCl to a vial, evaporating the CH_3CN under vacuum, then diluting with the desired volume of cage in H_2O and stirring for 30 min at room temperature. All further manipulations were carried out under air. A stock solution of substrate **1** in DMSO was prepared. The desired volume of Me_3PAuCl solution (15 nmol, 50 mol%) or cage + Me_3PAuCl solution (15 nmol, 50 mol%) was added to the desired cell culture medium in a 4 mL vial, followed by the desired volume of substrate **1** (30 nmol, 1 eq) to give a total volume of 3 mL. The vial was stirred at 37 °C under aerobic conditions for 16 h. This reaction mixture was transferred to a fluorescence cuvette, and the fluorescence spectrum recorded. The yield of **2a** was determined from the fluorescence intensity at 433 nm. Yields given are an average of 2 runs.

Stock Solution	Compound / Solvent	Concentration
A	Me_3PAuCl / DMSO	9.3 mM
B	Me_3PAuCl + Cage / H_2O	9.3 mM Me_3PAuCl; 11.16 mM Cage
C	Substrate **1** / DMSO	93 mM

Entry	A (µL)	B (µL)	C (µL)	Solvent (µL)	Total (µL)
1	30	0	30	2940	3000
2	0	30	30	2940	3000

Substrate 1 with biological additives

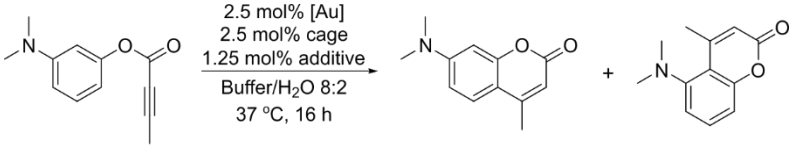

Inside a glovebox, Me_3PAuCl and cage were weighed into schlenks. All further manipulations for stock solution preparation were carried out under an atmosphere of N_2 on a schlenkline. Stock solutions of Me_3PAuCl in dry degassed CH_3CN; and cage, GSH, and His in degassed H_2O; and GSH + His in degassed PBS were prepared. The desired volume of Me_3PAuCl solution (0.465 µmol, 2.5 mol%) was added to a 2 mL vial, and the CH_3CN was then evaporated under vacuum. The desired volume of cage solution (0.558 µmol, 3.0 mol%) was added, and stirred for 30 min at room temperature. Then, the desired volumes of degassed H_2O or degassed PBS, then GSH solution (0.233 µmol, 1.25 mol%) or His solution (0.233 µmol, 1.25 mol%) or GSH + His solution (0.233 µmol, 1.25 mol% GSH; 0.233 µmol, 1.25 mol% His) were added. Substrate **1** (3.72 µL, 3.8 mg, 18.6 µmol, 1 eq) was then added neat. The vial was then removed from the N_2 atmosphere and capped, and stirred at 37 °C under aerobic conditions for 16 h. All further manipulations were carried out under air. A 10 mM solution of the crude reaction mixture was prepared by dilution with DMSO (1.76 mL). A 10 µM solution of the crude reaction mixture was then prepared by diluting the 10 mM solution (3 µL) with DMSO (2997 µL). This 10 µM solution was transferred to a fluorescence cuvette, and the fluorescence spectrum recorded. The yield of **2a** was determined from the fluorescence intensity at 433 nm. Yields given are an average of 3 runs.

Stock Solution	Compound / Solvent	Concentration
A	Me_3PAuCl / CH_3CN	9.3 mM
B	Cage / H_2O	27.9 mM
C	GSH / H_2O	2.9 mM
D	His / H_2O	2.9 mM
E	GSH + His / PBS	2.9 mM GSH; 2.9 mM His

Entry	A (µL)	B (µL)	C (µL)	D (µL)	E (µL)	PBS (µL)	H_2O (µL)	Total (µL)
1	50	0	0	0	0	0	100	100
2	50	0	80	0	0	0	20	100
3	50	0	0	80	0	0	20	100
4	50	0	0	0	80	0	20	100
5	50	0	0	0	0	80	20	100
6	50	20	0	0	0	0	80	100
7	50	20	80	0	0	0	0	100
8	50	20	0	80	0	0	0	100
9	50	20	0	0	80	0	0	100
10	50	20	0	0	0	80	0	100
11	0	20	0	0	0	0	80	100
12	0	20	80	0	0	0	0	100
13	0	20	0	80	0	0	0	100
14	0	20	0	0	80	0	0	100
15	0	20	0	0	0	80	0	100

Substrate 1 with increasing amounts of GSH

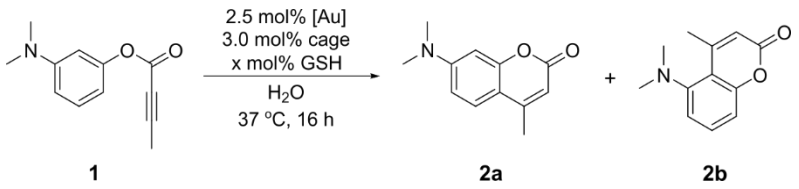

Inside a glovebox, Me_3PAuCl and cage were weighed into schlenks. All further manipulations for stock solution preparation were carried out under an atmosphere of N_2 on a schlenkline. Stock solutions of Me_3PAuCl in dry degassed CH_3CN; and cage and in degassed H_2O were prepared. For reactions without cage, the desired volume of Me_3PAuCl solution (0.465 µmol, 2.5 mol%) was added to a 2 mL vial, and the CH_3CN was then evaporated under vacuum. For reactions with cage present, a stock solution of encapsulated Me_3PAuCl was prepared. The Me_3PAuCl solution (1 eq) was added to a 4 mL vial, then the CH_3CN was evaporated under vacuum. The cage solution (1.2 eq, 11.16 mM) was added, and stirred for 30 min at room temperature. All further manipulations were carried out under aerobic conditions. The desired volume of encapsulated Me_3PAuCl (0.465 µmol, 2.5 mol%) was added to a 2 mL vial. H_2O, then GSH solution, then neat substrate **1** (3.72µL, 3.8 mg, 18.6 µmol, 1 eq) were added. The

vials were capped, and stirred at 37 °C under aerobic conditions for 16 h. A 10 mM solution of the crude reaction mixture was prepared by dilution with DMSO (1.76 mL). A 10 μM solution of the crude reaction mixture was then prepared by diluting the 10 mM solution (3 μL) with DMSO (2997 μL). This 10 μM solution was transferred to a fluorescence cuvette, and the fluorescence spectrum recorded. The yield of **2a** was determined from the fluorescence intensity at 433 nm. Yields given are an average of 3 runs.

Stock Solution	Compound / Solvent	Concentration
A	Me_3PAuCl / CH_3CN	9.3 mM
B	Me_3PAuCl + Cage / H_2O	9.3 mM Me_3PAuCl; 11.16 mM Cage
C	GSH / H_2O	93 mM
D	GSH / H_2O	372 mM

Entry	Eq GSH vs Gold	A (µL)	B (µL)	C (µL)	D (µL)	H_2O (µL)	Total (µL)
1	0.5	50	0	2.5	0	97.5	100
2	0.75	50	0	3.75	0	96.25	100
3	1	50	0	5	0	95	100
4	1.5	50	0	7.5	0	92.5	100
5	2	50	0	10	0	90	100
6	2.5	50	0	12.5	0	87.5	100
7	5	50	0	25	0	75	100
8	7.5	50	0	37.5	0	62.5	100
9	10	50	0	50	0	50	100
10	40	50	0	0	50	50	100
11	0.5	0	50	2.5	0	47.5	100
12	0.75	0	50	3.75	0	46.25	100
13	1	0	50	5	0	45	100
14	1.5	0	50	7.5	0	42.5	100
15	2	0	50	10	0	40	100
16	2.5	0	50	12.5	0	37.5	100
17	5	0	50	25	0	25	100
18	7.5	0	50	37.5	0	12.5	100
19	10	0	50	50	0	0	100
20	40	0	50	0	50	0	100

Cell Culture

A HeLa cell line was cultured and maintained in DMEM medium with 10% FBS. All cells were cultured in an incubator at 37 °C with a 5% CO_2 atmosphere.

MTT Toxicity Assay

HeLa cells were seeded at a density of 1500 cells/well in a 96-well plate and allowed to adhere overnight. Aliquots of substrate **1**, product **2a**, empty cage, $[Me_3PAu]^+$@cage, and Me_3PAuCl were pipetted into the wells to provide final concentrations of 0.1, 1, 10, 50, and 500 µM in PBS and incubated with the cells for 72 h. Measurements were performed for each condition in triplicate. A 10 µL aliquot of a 3-[4,5-dimethyl-2- thiazolyl]-2,5-diphenyl-2H-tetrazolium

bromide (MTT) stock solution (5.0 mg/mL in PBS) was added to each well. After incubation for 2-3 h with MTT, the medium was aspirated, and 200 µL of DMSO was added to dissolve the formazan crystals produced. Cell viability was calculated from the absorbance measured at 570 nm on a fluorescence microplate reader (TECAN).

CONFOCAL MICROSCOPY

HeLa cells were seeded at a density of 10,000 cells/well in an 8-well plate and allowed to adhere overnight. The cells were incubated for 30 min with RhoB or RhoB-cage complex in DMEM + 10% FBS to give a final concentration of 500 nM. The cells were washed 3 times with PBS and then imaged. Confocal imaging was performed using a Leica TCS SP8 confocal laser scanning microscope with the Leica application suite advanced fluorescence software (LASAF, Leica Microsystems B.V., Rijswijk, The Netherlands). The RhoB was excited by a laser at 535 nm and the emission was detected from 600 nm to 700 nm. For each set of experiments, the settings were kept the same.

REFERENCES

[1] J. Rautio, N. A. Meanwell, L. Di, M. J. Hageman, *Nat. Rev. Drug Discov.* **2018**, 17, 559-587.
[2] C. Souza, D. S. Pellosi, A. C. Tedesco, *Expert Rev. Anticancer Ther.* **2019**, 19, 483-502.
[3] M. O. N. van de L'Isle, M. C. Ortega-Liebana, A. Unciti-Broceta, *Curr. Opin. Chem. Biol.* **2021**, 61, 32-42.
[4] R. C. Brewster, E. Klemencic, A. G. Jarvis, *J. Inorg. Biochem.* **2021**, 215, 111317.
[5] M. J. S. A. Silva, P. M. P. Gois, G. Gasser, *ChemBioChem* **2021**, 22, 1740-1742.
[6] Z. Chen, H. Li, Y. Bian, Z. Wang, G. Chen, X. Zhang, Y. Miao, D. Wen, J. Wang, G. Wan, *Nat. Nanotechnol.* **2021**, 16, 933-941.
[7] B. Lozhkin, T. R. Ward, *Bioorg. Med. Chem.* **2021**, 45, 116310.
[8] Z. Li, C. Brouwer, C. He, *Chem. Rev.* **2008**, 108, 3239-3265.
[9] A. S. K. Hashmi, M. Rudolph, *Chem. Soc. Rev.* **2008**, 37, 1766-1775.
[10] Y. Zhang, T. Luo, Z. Yang, *Nat. Prod. Rep.* **2014**, 31, 489-503.
[11] M. Rudolph, A. S. K. Hashmi, *Chem. Soc. Rev.* **2012**, 41, 2448-2462.
[12] M. E. Ourailidou, M. R. H. Zwinderman, F. J. Dekker, *MedChemComm* **2016**, 7, 399-408.
[13] C. Vidal, M. Tomás-Gamasa, P. Destito, F. López, J. L. Mascareñas, *Nat. Commun.* **2018**, 9, 1913.
[14] T.-C. Chang, K. Vong, T. Yamamoto, K. Tanaka, *Angew. Chem.* **2021**, 133, 12554-12562.
[15] Y. Long, B. Cao, X. Xiong, A. S. C. Chan, R. W.-Y. Sun, T. Zou, *Angew. Chem., Int. Ed.* **2021**, 60, 4133-4141.
[16] Q.-Q. Wang, S. Gonell, S. H. A. M. Leenders, M. Dürr, I. Ivanović-Burmazović, J. N. H. Reek, *Nat. Chem.* **2016**, 8, 225-230.
[17] F. Yu, D. Poole III, S. Mathew, N. Yan, J. Hessels, N. Orth, I. Ivanović-Burmazović, J. N. H. Reek, *Angew. Chem., Int. Ed.* **2018**, 57, 11247-11251.
[18] R. Gramage-Doria, J. Hessels, S. H. A. M. Leenders, O. Tröppner, M. Dürr, I. Ivanović-Burmazović, J. N. H. Reek, *Angew. Chem., Int. Ed.* **2014**, 53, 13380-13384.
[19] S. H. A. M. Leenders, M. Dürr, I. Ivanović-Burmazović, J. N. H. Reek, *Adv. Synth. Catal.* **2016**, 358, 1509-1518.
[20] S. Gonell, X. Caumes, N. Orth, I. Ivanović-Burmazović, J. N. H. Reek, *Chem. Sci.* **2019**, 10, 1316-1321.
[21] D. H. Leung, D. Fiedler, R. G. Bergman, K. N. Raymond, *Angew. Chem., Int. Ed.* **2004**, 43, 963-966.
[22] D. H. Leung, R. G. Bergman, K. N. Raymond, *J. Am. Chem. Soc.* **2006**, 128, 9781-9797.
[23] D. H. Leung, R. G. Bergman, K. N. Raymond, *J. Am. Chem. Soc.* **2007**, 129, 2746-2747.
[24] S. S. Nurttila, W. Brenner, J. Mosquera, K. M. van Vliet, J. R. Nitschke, J. N. H. Reek, *Chem.–Eur. J.* **2019**, 25, 609-620.
[25] C. J. Brown, G. M. Miller, M. W. Johnson, R. G. Bergman, K. N. Raymond, *J. Am. Chem. Soc.* **2011**, 133, 11964-11966.
[26] D. M. Kaphan, M. D. Levin, R. G. Bergman, K. N. Raymond, F. D. Toste, *Science* **2015**, 350, 1235.
[27] M. Otte, P. F. Kuijpers, O. Troeppner, I. Ivanović-Burmazović, J. N. H. Reek, B. de Bruin, *Chem.–Eur. J.* **2013**, 19, 10170-10178.
[28] C. Tan, J. Jiao, Z. Li, Y. Liu, X. Han, Y. Cui, *Angew. Chem., Int. Ed.* **2018**, 57, 2085-2090.
[29] J. Jiao, C.Tan, Z. Li, Y. Liu, X. Han, Y. Cui, *J. Am. Chem. Soc.* **2018**, 140, 2251-2259.
[30] A. C. H. Jans, X. Caumes, J. N. H. Reek, *ChemCatChem* **2019**, 11, 287-297.
[31] D. L. Caulder, R. E. Powers, T. N. Parac, K. N. Raymond, *Angew. Chem., Int. Ed.* **1998**, 37, 1840-1843.
[32] Z. J. Wang, C. J. Brown, R. G. Bergman, K. N. Raymond, F. D. Toste, *J. Am. Chem. Soc.* **2011**, 133, 7358-7360.
[33] Z. J. Wang, K. N. Clary, R. G. Bergman, K. N. Raymond, F. D. Toste, *Nature Chem.* **2013**, 5, 100-103.
[34] P. Destito, C. Vidal, F. López, J. L. Mascareñas, *Chem.–Eur. J.* **2021**, 27, 4789-4816.
[35] S.-Y. Jang, D. P. Murale, A. D. Kim, J.-S. Lee, *ChemBioChem* **2019**, 20, 1498-1507.

[36] Y. G. Bai, J. F. Chen, S. C. Zimmerman, *Chem. Soc. Rev.* **2018**, 47, 1811-1821.
[37] J. J. Soldevila-Barreda, N. Metzler-Nolte, *Chem. Rev.* **2019**, 119, 829-869.
[38] V. S. Dave, D. Gupta, M. Yu, P. Nguyen, S. Varghese Gupta, *Drug Dev. Ind. Pharm.* **2017**, 43, 177-189.
[39] H. J. Forman, H. Zhang, A. Rinna, *Mol. Aspects Med.* **2009**, 30, 1-12.
[40] D. P. Nguyen, H. T. H. Nguyen, L. H. Do, *ACS Catal.* **2021**, 11, 5148-5165.
[41] L. van der Koog, T. B. Gandek, A. Nagelkerke, *Adv. Healthcare Mater.* **2022**, 11, 2100639.
[42] F. Campbell, F. L. Bos, S. Sieber, G. Arias-Alpizar, B. E. Koch, J. Huwyler, A. Kros, J. Bussmann, *ACS Nano* **2018**, 12, 2138-2150.
[43] Y. Hayashi, M. Takamiya, P. B. Jensen, I. Ojea-Jiménez, H. Claude, C. Antony, K. Kjaer-Sorensen, C. Grabher, T. Boesen, D. Gilliland. *ACS Nano* **2020**, 14, 1665-1681.
[44] G. Arias-Alpizar, L. Kong, R. C. Vlieg, A. Rabe, P. Papadopoulou, M. S. Meijer, S. Bonnet, S. Vogel, J. van Noort, A. Kros. *Nat. Commun.* **2020**, 11, 3638.
[45] C. M. Hong, M. Morimoto, E. A. Kapustin, N. Alzakhem, R. G. Bergman, K. N. Raymond, F. D. Toste. *J. Am. Chem. Soc.* **2018**, 140, 6591-6595.

Chapter 3

Encapsulation and Reactivity of a Palladium Complex Inside a Supramolecular Cage

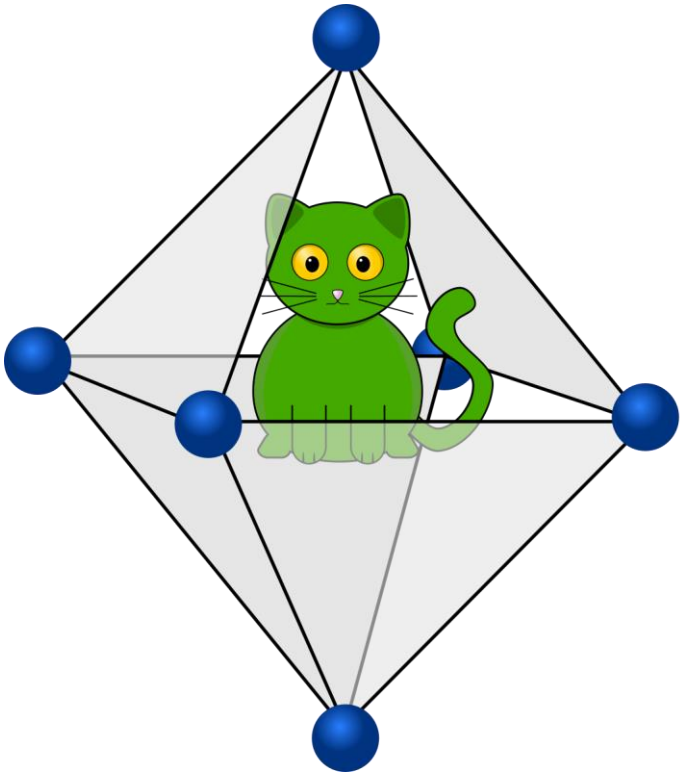

ABSTRACT

Palladium is an extremely versatile catalyst, and can catalyse a wide variety of transformations. Notably, palladium complexes are able to catalyse C–C bond forming reactions under mild conditions. The ability to harness the power of palladium catalysis within living cells would provide the means to carry out a wide range of new to nature reactions. However living cells provide a very harsh environment for palladium complexes, which means that currently palladium catalysis in living cells is limited to heterogeneous systems, or requires the use of stoichiometric quantities of palladium. In this chapter we explore the use of a supramolecular cage as a potential route to protect a palladium catalyst from species present in the biological environment. NMR and UV/Vis spectroscopy studies showed that a water soluble $[Pt_6L_4](NO_3)_{12}$ supramolecular cage (Pt-cage) is stable to biological conditions, even at nanomolar concentrations, and that a palladium complex ($[(Et_3P)_2PdCl_2]$) can be successfully encapsulated within its hydrophobic cavity. Although initial experiments indicated that the Pt-cage itself and perhaps the encapsulated $[(Et_3P)_2PdCl_2]$ could promote the formation of coumarin via an intramolecular hydroarylation reaction, further analysis and confirmation of these results was prevented due to their irreproducibility. Further attempts to probe the catalytic activity of the encapsulated complex were unsuccessful for both a Wacker-Tsuji oxidation reaction and a double silylation of a diketone. Although the catalytic activity of the palladium complex could not be evaluated, we believe that the good stability of the Pt-cage to biological conditions means that encapsulation of metal complexes within its cavity may be a good strategy for further applications of catalysis under biological conditions.

INTRODUCTION

Palladium catalysis provides facile access to a huge range of organic transformations: for example alkylations, arylations, cyclisations, hydrogenations, C–H bond functionalisations, and C–C bond forming reactions.[1] Therefore being able to successfully apply a palladium catalyst inside living cells would open the door to achieve a wide variety of new-to-nature reactions. Indeed, various different homogeneous and heterogeneous palladium systems have already been extensively used as catalysts for deprotection reactions in cells, where allyloxycarbonyl,[2-6] propargyl,[2, 7-11] propgargyloxycarbonyl,[12-14] and allene groups[15] are cleaved to generate an active fluorophore or prodrug. However, while deprotection and intramolecular reactions which require only one substrate molecule are fairly common for transition metal catalysed reactions inside living cells, examples of cross-coupling reactions where two fragments are joined together in a C–C bond-forming reaction are found much less frequently.[16-19] The ability to carry out efficient bioorthogonal cross-coupling reactions would provide a new means to achieve *in situ* drug formation, which could improve targeted and selective drug activation. Currently, only two types of cross-coupling reaction have been demonstrated inside living cells. The Suzuki-Miyaura coupling, which typically couples together aryl halides with aryl boronic acids or esters, has been achieved on cells surfaces and inside cells using heterogeneous palladium nanoparticles, to label proteins and to synthesise a fluorophore and an anticancer drug from non-toxic precursors.[3, 20-23] However, up until now no homogeneous catalyst has been used for a Suzuki-Miyaura coupling reaction in cells. The second cross-coupling reaction which has been attempted in cells is the Sonogashira coupling, a reaction where terminal alkynes are coupled to aryl halides. The good bioorthogonality of alkynes, as they are not found naturally in cells, make the Sonogashira coupling an attractive option for cross-coupling reactions in cells.[24] While this reaction typically requires a Cu(I) co-catalyst, copper-free systems are known.[25] While all examples inside or in the presence of cells do not require copper, this reaction has yet to be carried out catalytically, as large excesses of palladium species are used to achieve the coupling.[26-30] In order to expand the toolbox of cross-coupling reactions inside living cells, a more robust and efficient system needs to be developed in order to carry out such reactions catalytically.

Intracellular conditions are very challenging for palladium complexes. The high concentrations of metal-binding biomolecules, for example glutathione (GSH), can easily lead to poisoning and deactivation of the catalyst.[31] In addition, palladium complexes are known to be easily reduced to nanoparticles under biological conditions.[32] Together this means that a molecular homogeneous palladium catalyst may struggle to remain active under biological conditions. We hypothesised that encapsulation of a palladium catalyst inside a supramolecular metallocage could improve its activity under biological conditions: 1) the cage may provide a physical barrier between the catalyst and the cellular environment, and prevent biomolecular poisons from reaching the catalyst; and 2) isolation of one palladium complex inside each cage may prevent nanoparticle formation, by preventing multiple palladium centres from interacting with one another.

A small palladium complex has been shown by Fujita *et al.* to be encapsulated within a water soluble $[Pd_6L_4](NO_3)_{12}$ metallocage (Pd-cage). The authors demonstrate that the

hydrophobic complex [$(Et_3P)_2PdCl_2$] is able to pass through the windows of this Pd-cage and reside within its apolar cavity. Once inside the cavity of the Pd-cage, the complex was then able to undergo C–H insertion into small terminal alkynes. Interestingly, this C–H bond activation was found to be dependent upon encapsulation of the complex within the Pd-cage, as the free complex was unable to participate in the reaction.[33] However, only stoichiometric reactions were demonstrated for this encapsulated complex. Therefore, before determining whether or not encapsulation of a palladium complex within a supramolecular cage could be a viable strategy for reactions under biological conditions, we first looked to investigate whether or not this palladium complex could react catalytically within the cavity of a supramolecular cage.

RESULTS AND DISCUSSION

STABILITY STUDIES

Although encapsulation of $[(Et_3P)_2PdCl_2]$ has only been reported within the $[Pd_6L_4](NO_3)_{12}$ cage (Pd-cage), we hypothesised that the platinum analogue of this cage, $[Pt_6L_4](NO_3)_{12}$ (Pt-cage) (Figure 1) may be required, as the platinum cage is more stable than its palladium counterpart.[34] The cellular environment contains high concentrations of chlorides (around 5 mM intracellularly and 120 mM extracellularly)[35] and GSH (1–10 mM)[36], both of which may compete with the ligands of the cage and lead to decomposition of the supramolecular structure. Therefore the appropriate supramolecular cage needed to be selected as a host for protecting a catalyst from biological conditions. The stability of the cage towards phosphate buffered saline solution (PBS) and GSH was selected to give an indication of whether or not the cage would be stable in cells. The stability of the Pd-cage to biological conditions was first monitored by ^{1}H NMR spectroscopy (Figure 2a). A 2.5 mM solution of Pd-cage in PBS was stirred at 37 °C in the presence of 3 eq of GSH for 24 h. Immediately upon addition of the Pd-cage to the solution of GSH in PBS, an insoluble yellow precipitate formed. Analysis of the yellow precipitate was not possible due to its insolubility. ^{1}H NMR spectra of the solution were recorded immediately upon addition and after 24 h. Neither spectrum contains peaks in the aromatic region of the spectrum. The ^{1}H NMR spectrum of a solution of Pd-cage in D_2O shows two sets of doublets at 9.05 and 8.55 ppm, which correspond to the pyridine rings of the Pd-cage. It is likely that the chlorides present in the PBS bind to the palladium centres of the Pd-cage, and induce its rapid decomposition. Therefore, the Pd-cage was determined to be an unsuitable supramolecular host for the binding and application of the $[(Et_3P)_2PdCl_2]$ complex under *in vivo* conditions. The platinum analogue of the cage (Pt-cage) was then selected as a candidate for hosting the $[(Et_3P)_2PdCl_2]$ complex (Figure 2b). A 2.5 mM solution of Pt-cage in PBS was stirred at 37 °C in the presence of 3 eq of GSH for 24 h. No precipitation was observed upon addition of the Pt-cage to the solution of GSH in PBS. The ^{1}H NMR spectrum of the solution was recorded immediately upon addition. Two sets of doublets were present at 9.28 and 8.74 ppm, which correspond to the pyridine rings of the Pt-cage. After stirring this solution for 24 h at 37 °C, no precipitation was observed, and the ^{1}H NMR spectrum again revealed two sets of doublets at 9.28 and 8.74 ppm. Since no changes in the ^{1}H NMR spectrum were observed over the course of 24 h, it appears that a 2.5 mM solution of Pt-cage is stable to biological conditions over this time frame.

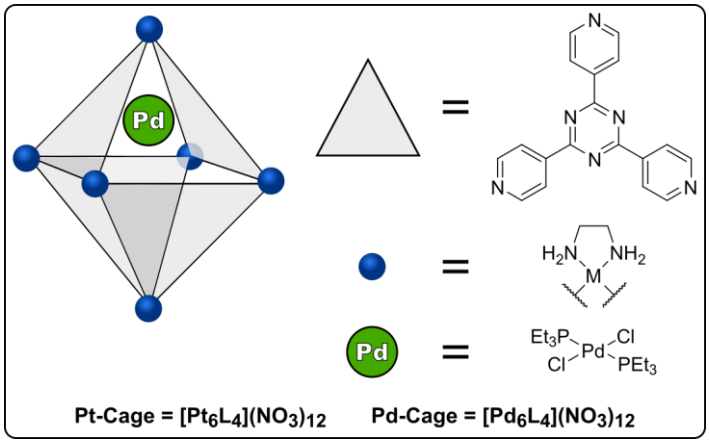

Figure 1. Structures of the $[M_6L_4](NO_3)_{12}$ cage and palladium complex $[(Et_3P)_2PdCl_2]$.

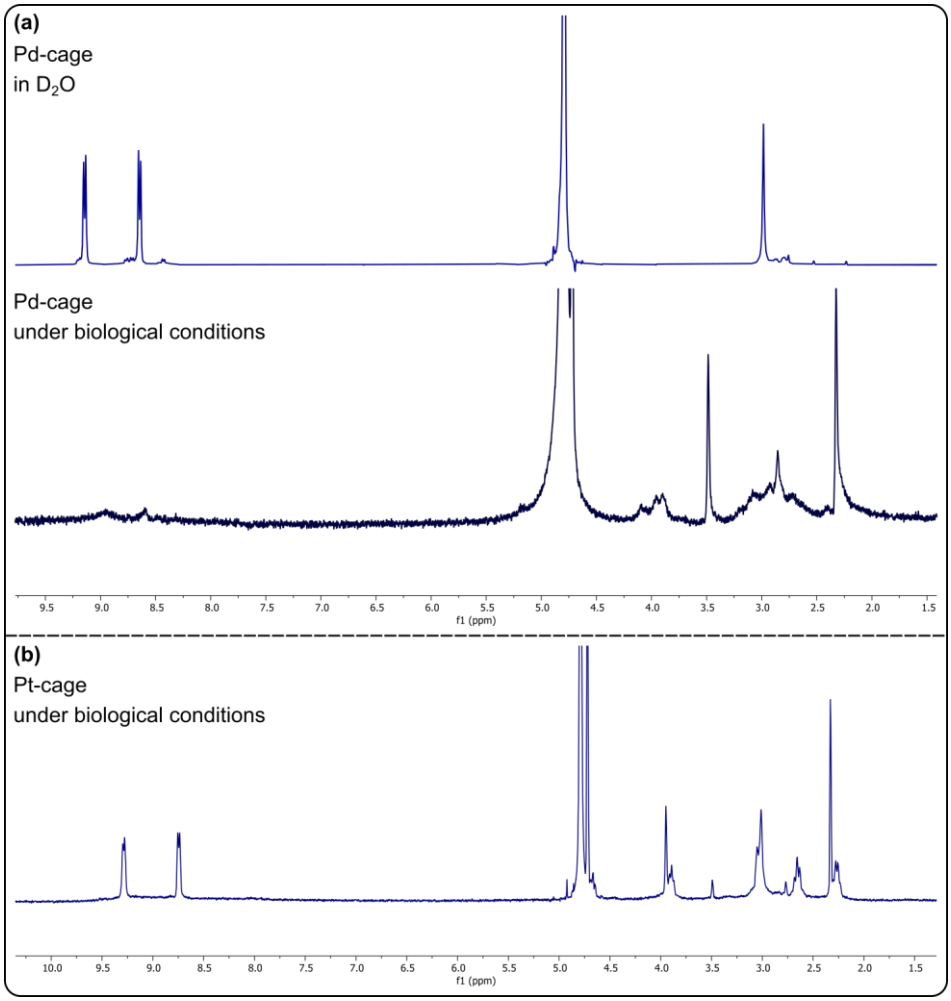

Figure 2. (a) ^{1}H NMR spectra of the Pd-cage in D_2O (above) and the Pd-cage upon immediate addition to PBS in the presence of 3 eq GSH (below). (b) ^{1}H NMR spectrum of the Pt-cage in PBS in the presence of 3 eq GSH after 24 h.

While millimolar concentrations of compounds are typical for catalysis reactions in the lab, much lower concentration in the nanomolar or micromolar range are required in living cells in order to prevent cytotoxicity. Therefore, the stability of the Pt-cage was also investigated at lower concentrations. The stability of a 3 nM solution of the Pt-cage was

monitored by UV/Vis spectroscopy (Figure 3). A solution of 3 nM Pt-cage in PBS in the presence of 2 mM GSH was left at 37 °C for 14 h, with UV/Vis spectra recorded every 20 min. The UV/Vis spectrum of the Pt-cage under these conditions show an absorption band at 214 nm, which corresponds to absorption from the ligands of the Pt-cage. These spectra could not be compared to that of the free ligand, due to its insolubility in water. Almost no change in the spectrum was observed over the course of 14 h. This suggests that a 3 nM solution of the Pt-cage is also stable to biological conditions over this time frame. Together, these NMR spectroscopy and UV/Vis studies show that the Pt-cage is a suitable host for a catalyst under biological conditions, as it does not decompose and remains intact.

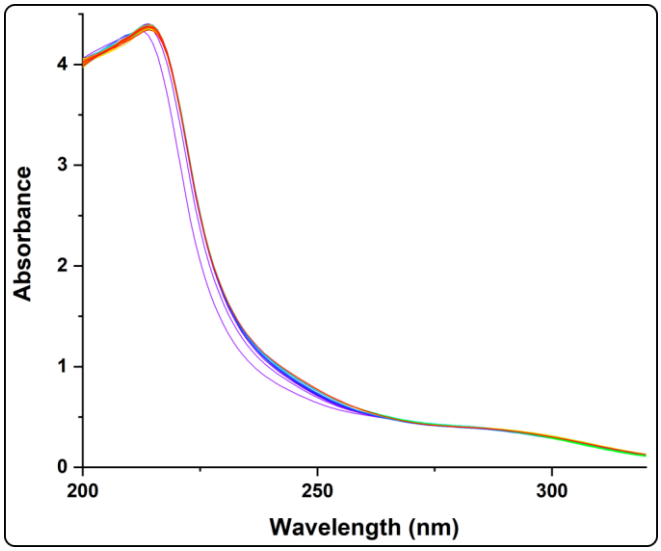

Figure 3. UV/Vis spectra of a 3 nM solution of the Pt-cage in PBS in the presence of 2.5 mM GSH at 37 °C over 14 h.

ENCAPSULATION STUDIES

Encapsulation of $[(Et_3P)_2PdCl_2]$ within the Pt-cage was carried out following a modified literature procedure.[33] An aqueous solution of 1 eq Pt-cage was added to 2 eq of solid $[(Et_3P)_2PdCl_2]$, and the resulting suspension was stirred at room temperature for 5 h. After this time excess solid $[(Et_3P)_2PdCl_2]$ was removed by filtration, and the aqueous solution was measured by NMR spectroscopy (Figure 4a). The ^{1}H NMR spectrum shows two doublets at 8.72 and 9.25 ppm. These doublets correspond to the Pt-cage pyridine rings. No peaks corresponding to the empty Pt-cage were observed, which would appear at 8.63 and 9.15 ppm. The fact that there is only one set of Pt-cage peaks means that only one Pt-cage species is present, and shifting of these peaks downfield with respect to the empty Pt-cage is typical for an encapsulation event. Multiple new broad, ill-defined peaks appeared in the ^{1}H NMR spectrum, at 1.91, 1.13, 0.36, 0.09, -0.37, -0.50, and -0.76 ppm. However, only two peaks are expected for the encapsulated complex, corresponding to the CH_2 and the CH_3 groups on the phosphine ligand. In order to determine if these peaks corresponded to an encapsulated guest or a guest free in solution, ^{1}H NMR diffusion ordered spectroscopy (DOSY) was performed (Figure 4b). The peaks corresponding to the Pt-cage appeared as a band with a $\log_D$ value of -9.69 m^2/s. However only two peaks at 0.37 and -0.50 ppm had the same $\log_D$ value as those of the Pt-cage. The peaks at 1.91 and 1.13 ppm appeared as one band with a $\log_D$ value of -9.44

m^2/s. The remaining peaks at 0.09, -0.37, and -0.76 ppm had $\log_D$ values of -9.63, -9.72, and -9.53 m^2/s respectively, which were similar, although not equal to, the value of that of the Pt-cage. This means that the peaks at 1.91 and 1.13 ppm correspond to an encapsulated guest within the Pt-cage ($[(Et_3P)_2PdCl_2]$@Pt-cage), and the peaks at 1.91 and 1.13 ppm belong to free guest in solution. The peaks of from the phosphine ligands in the $[(Et_3P)_2PdCl_2]$@Pt-cage complex had similar values to those reported for the encapsulated complex within the palladium analogue of the Pt-cage. The peaks which corresponded to free guest could not be compared to $[(Et_3P)_2PdCl_2]$, as this complex is poorly soluble in water. However, there was still some ambiguity as to what species precisely the remaining peaks belonged to, and whether or not it was associated with the Pt-cage. The ^{31}P NMR spectrum (Figure E13) revealed three peaks at 37.07, 18.85, and 17.98 ppm, which confirmed that there are multiple phosphine species present.

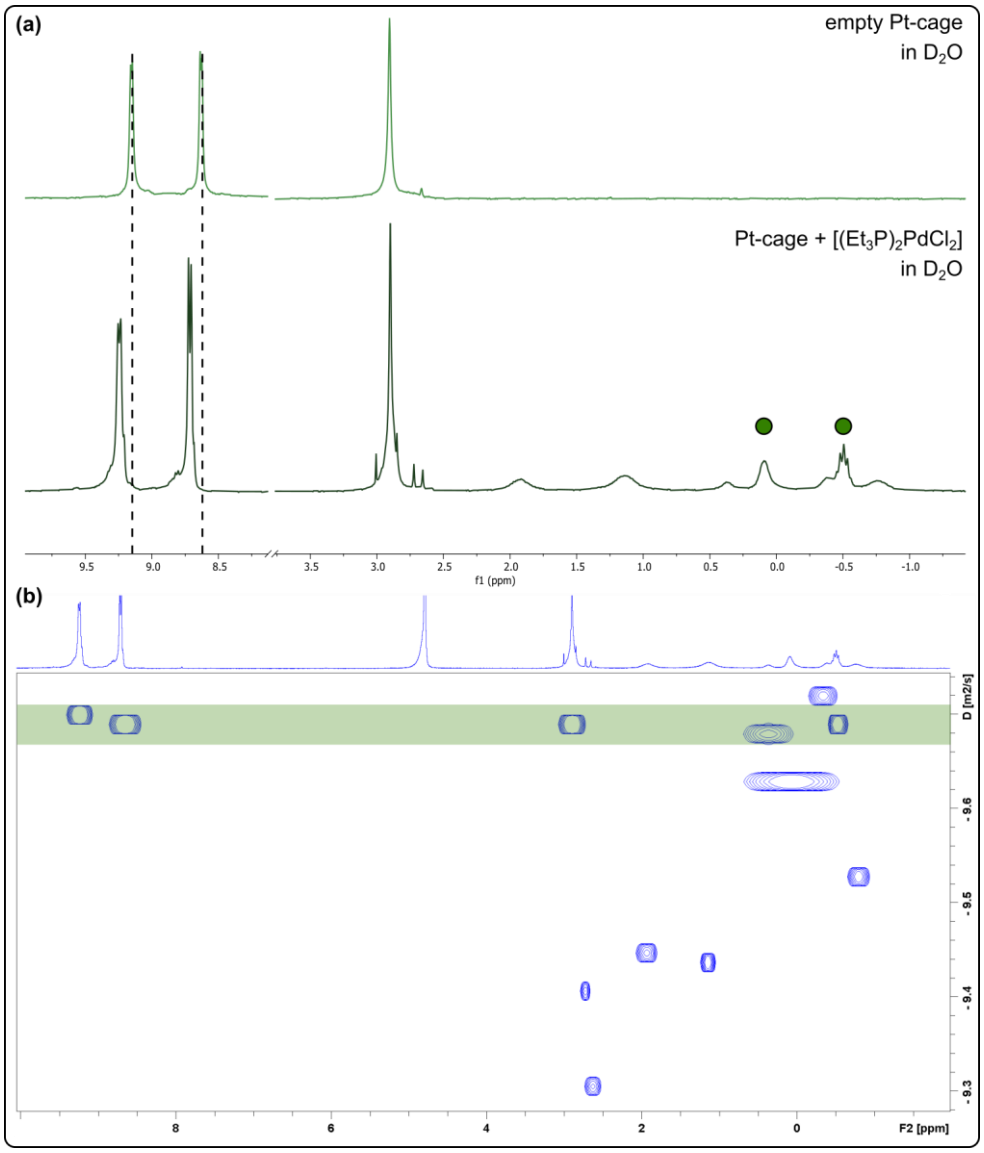

Figure 4. (a) ^1H NMR spectra of the empty Pt-cage and of the Pt-cage after mixing with 2 eq $[(Et_3P)_2PdCl_2]$. Encapsulated guest peaks are indicated with circles. (b) DOSY spectrum of the Pt-cage after mixing with 2 eq $[(Et_3P)_2PdCl_2]$. Peaks with the same $\log_D$ value as the that of the Pt-cage peaks are highlighted in green.

We hypothesised that the other guest peaks could correspond to $[(Et_3P)_2PdX_2]$ species, where either one or both of the chloride ligands were replaced by water ligands. While being soluble in water, the hydrophobic phosphine ligands also render $[(Et_3P)_2PdCl_2]$ soluble in organic solvent, such as chloroform. Therefore, the aqueous solution of $[(Et_3P)_2PdCl_2]$@Pt-cage and free $[(Et_3P)_2PdCl_2]$ was washed with $CDCl_3$, and the two layers were separated. The $CDCl_3$ layer was analysed by NMR spectroscopy (Figure 5a) and field desorption high resolution mass spectrometry (FD-HRMS) (Figure E15). The ^{1}H NMR spectrum reveals a sextet at 2.06 ppm, a nonet at 1.86 ppm, and a multiplet at 1.30–1.13 ppm. In addition, the ^{31}P NMR spectrum shows two peaks, at 33.15 and 17.83 ppm (Figure E13). $[(Et_3P)_2PdCl_2]$ in $CDCl_3$ gives peaks in the ^{1}H NMR spectrum at 1.86 ppm and 1.20 ppm, and peaks in the ^{31}P NMR spectrum at 17.83 ppm. Therefore washing the aqueous solution of $[(Et_3P)_2PdCl_2]$@Pt-cage with $CDCl_3$ results in the extraction of non-encapsulated $[(Et_3P)_2PdCl_2]$ and a second non-encapsulated phosphine-containing complex into the organic layer. The FD-HRMS spectrum shows a peak at 414.0332, which corresponds to $[(Et_3P)_2PdCl_2]$. No other species could be identified in the FD-HRMS spectrum, however it is possible that the second species in the organic layer was a palladium complex where one or both of the chloride ligands was substituted by H_2O, but that this species could not be detected in the mass, possibly due to substitution of the water ligands in the mass spectrometer during the measurement. The water layer was also analysed by ^{1}H NMR spectroscopy (Figure 5b). The Pt-cage peaks at 8.72 and 9.25 ppm remained unchanged. However, several of the upfield peaks had disappeared: two broad peaks at 1.91 and 1.22 ppm, a singlet at 0.91 ppm, and a pentet at -0.47 ppm were present. The ^{31}P NMR spectrum showed only one peak at 17.85 ppm (Figure E13). In addition, the DOSY spectrum again showed that the peaks at 0.91 and -0.47 ppm had the same $\log_D$ value of - 9.69 m^2/s as that of the Pt-cage (Figure E14). However the remaining peaks at 1.91 and 1.22 ppm appeared as one band at -9.12 ppm. This confirms that there is an encapsulated $[(Et_3P)_2PdCl_2]$@Pt-cage complex in solution, alongside a free guest. Further analysis with other NMR spectroscopic techniques and with HRMS did not reveal further insight into the structure of this free guest.

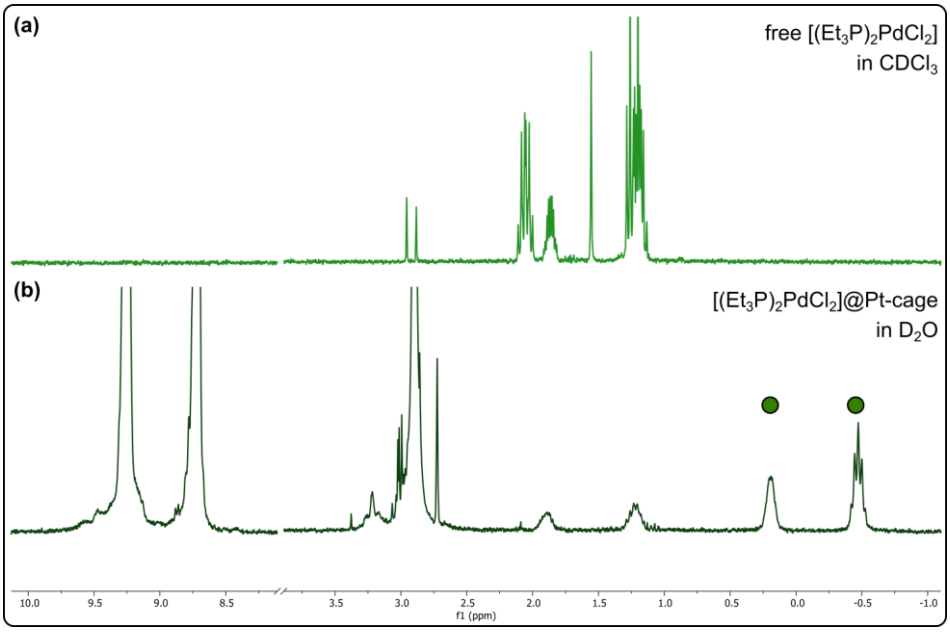

Figure 5. (a) ^{1}H NMR spectrum of the organic layer after washing the aqueous [$(Et_3P)PdCl_2$]@Pt-cage solution with chloroform. (b) ^{1}H NMR spectrum of the aqueous [$(Et_3P)PdCl_2$]@Pt-cage solution with chloroform. Encapsulated guest peaks are indicated with circles.

In an attempt to circumvent the need for washing away free [$(Et_3P)_2PdCl_2$] with $CDCl_3$ to purify the [$(Et_3P)_2PdCl_2$]@Pt-cage complex, the encapsulation was also carried out using 1 eq of [$(Et_3P)_2PdCl_2$]. We hypothesised that since a 1:1 guest complex is formed, by adding only 1 eq of [$(Et_3P)_2PdCl_2$] there would be no excess of free [$(Et_3P)_2PdCl_2$] in solution. Following the same encapsulation procedure as described above, an aqueous solution of 1 eq of Pt-cage was added to 1 eq of solid [$(Et_3P)_2PdCl_2$], and the resulting suspension was stirred at room temperature for 5 h, after which the solution was filtered over syringe filter and measured by NMR spectroscopy. Only two sets of doublets corresponding to the Pt-cage were observed at 9.25 and 8.72 ppm. Peaks corresponding to the empty Pt-cage (8.63 and 9.15 ppm) were not observed. In addition broad peaks were present at 1.92, 1.13, 0.37, 0.09, -0.38, -0.51, and -0.77 ppm. These peaks were identical to those observed when the encapsulation was carried out with 2 eq of [$(Et_3P)_2PdCl_2$] (Figure E12). Therefore even in the presence of only 1 eq of $(Et_3P)_2PdCl_2$ a mixture of both free [$(Et_3P)_2PdCl_2$] and encapsulated [$(Et_3P)_2PdCl_2$]@Pt-cage complex is obtained. The presence of free [$(Et_3P)_2PdCl_2$] upon addition of 1 eq of [$(Et_3P)_2PdCl_2$] to the empty Pt-cage means that empty Pt-cage must also be present in solution; however, the ^{1}H NMR spectrum does not show any peaks corresponding to the empty cage. Therefore variable temperature NMR studies were conducted in order to gain further insight into the system. ^{1}H NMR spectra of the mixture of free [$(Et_3P)_2PdCl_2$] and encapsulated [$(Et_3P)_2PdCl_2$]@Pt-cage complex were recorded at different temperatures (Figure 6). However, the chemical shifts of all the peaks remained constant when the temperature was varied. The observed NMR spectrum of a dynamic system is dependent upon the speed of exchange: if exchange is slow compared to the NMR timescale, separate peaks for both states can be observed; if the exchange is more rapid compared to the NMR timescale, then an average of both states is observed, resulting in one peak corresponding to both states. The fact that two separate sets of peaks are observed for both free and encapsulated [$(Et_3P)_2PdCl_2$] even at

elevated temperatures suggests that exchange is slow compared to the NMR timescale. However, the difference in chemical shift between the two peaks is also important for determining how many peaks are observed: the separation of the peaks (Δν in Hz) determines the limit of exchange rate (k_{lim}) that NMR is able to distinguish between peaks. This relationship is described by the following equation:

$$k_{lim} = \frac{\Delta\nu}{\pi\sqrt{2}}$$

This has the consequence that if the chemical shifts of the two exchanging peaks are too similar (Δν is small), then a single peak will be observed even if exchange is slow.[37] For the peaks belonging to $[(Et_3P)_2PdCl_2]$, the difference in chemical shift between the free peaks (1.91 ppm) and the encapsulated peaks (0.91 ppm) is 300 Hz. This would mean that for the $[(Et_3P)_2PdCl_2]$ peaks, $k_{lim} = 67.5\ s^{-1}$. However, the difference in chemical shift between the Pt-cage peaks of the empty Pt-cage (9.15 ppm) and the $[(Et_3P)_2PdCl_2]$@Pt-cage complex (9.25 ppm) is only 30 Hz. This would mean that for the Pt-cage peaks, $k_{lim} = 6.75\ s^{-1}$. Therefore, if $6.75\ s^{-1} < k_{lim} < 67.5\ s^{-1}$ then two distinct sets of peaks for the free and encapsulated $[(Et_3P)_2PdCl_2]$ complex would be observed, while only one set of Pt-cage peaks would be seen. We therefore propose that upon addition of $[(Et_3P)_2PdCl_2]$ to a solution of empty Pt-cage, a mixture of free $[(Et_3P)_2PdCl_2]$ and encapsulated $[(Et_3P)_2PdCl_2]$@Pt-cage complex is generated, with slow exchange between the two states. Since reducing the number of equivalents of $[(Et_3P)_2PdCl_2]$ yielded the same species as when 2 eq was used, we concluded that indeed the washing step was necessary to obtain a single encapsulated species, and that it was not possible to avoid the presence of excess free $[(Et_3P)_2PdCl_2]$ in solution. Nevertheless, since this free guest species was not associated with the Pt-cage, this solution containing $[(Et_3P)_2PdCl_2]$@Pt-cage complex was used without further purification for experiments investigating the reactivity of the palladium complex inside the Pt-cage.

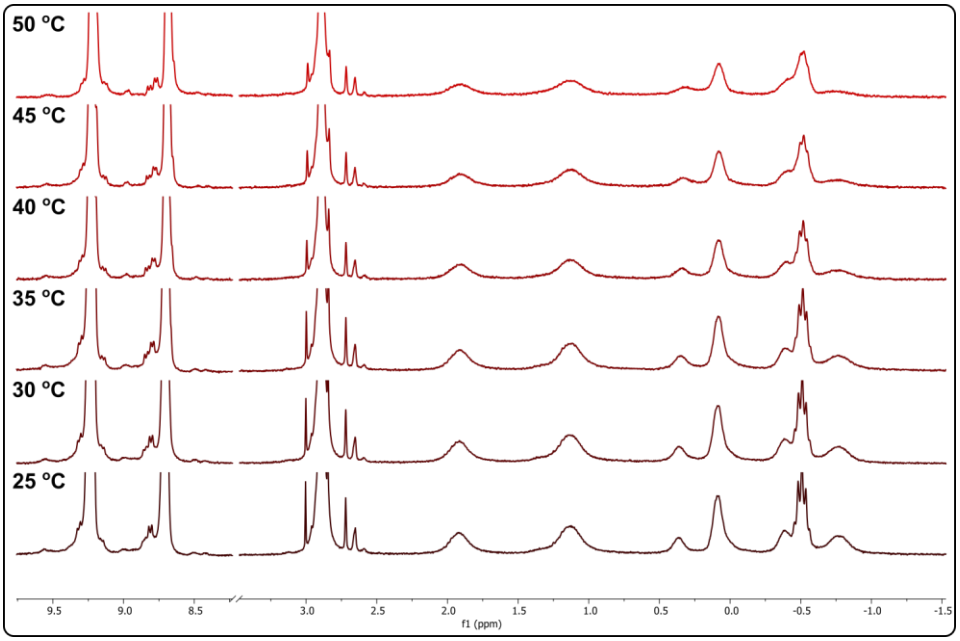

Figure 6. ^{1}H NMR spectra recorded at different temperatures of the mixture of free [$(Et_3P)_2PdCl_2$] and [$(Et_3P)_2PdCl_2$]@Pt-cage complex produced by mixing 1 eq of [$(Et_3P)_2PdCl_2$] with 1 eq of empty Pt-cage.

We next looked to compare the stability of the [$(Et_3P)_2PdCl_2$] complex free in solution in the presence of biological additives to that of the encapsulated complex. The stability of free [$(Et_3P)_2PdCl_2$] and encapsulated [$(Et_3P)_2PdCl_2$]@Pt-cage in the presence of GSH, L-histidine (His), and PBS was monitored by ^{1}H NMR spectroscopy. Due to solubility reasons, the free [$(Et_3P)_2PdCl_2$] complex was dissolved in a 1:1 mixture of THF-d8/PBS in the presence of 1 eq of GSH and 1 eq of His and stirred at 37 °C for 16 h. A ^{1}H NMR spectrum was then recorded, and compared to a ^{1}H NMR spectrum of free [$(Et_3P)_2PdCl_2$] complex in THF-d8/D_2O (Figure 7). The ^{1}H NMR spectrum of free [$(Et_3P)_2PdCl_2$] in THF-d8/D_2O displays two clear peaks: a nonet at 1.82 ppm and a pentet at 1.13 ppm. However, the spectrum of free [$(Et_3P)_2PdCl_2$] in THF-d8/PBS in the presence of GSH and His displays several broad, ill-defined peaks at 2.63, 2.13, and 1.27 ppm. Therefore it appears that the [$(Et_3P)_2PdCl_2$] complex is not stable under these conditions. Next, encapsulated [$(Et_3P)_2PdCl_2$]@Pt-cage was stirred at 37 °C for 16 h in the presence of 1 eq GSH and 1 eq His in a 1:1 mixture of D_2O/PBS, and the ^{1}H NMR spectrum recorded after this time was compared to a ^{1}H NMR spectrum of [$(Et_3P)_2PdCl_2$]@Pt-cage in D_2O (Figure 8). The peaks corresponding to the ethyl groups of encapsulated [$(Et_3P)_2PdCl_2$] appear at 0.19 and -0.47 ppm in D_2O. The solution of [$(Et_3P)_2PdCl_2$]@Pt-cage in D_2O/PBS in the presence of GSH and His was monitored by ^{1}H NMR spectroscopy and DOSY NMR. The ^{1}H NMR spectrum revealed two sets of doublets appeared at 9.19 and 8.65 ppm and a singlet at 2.97 ppm, which correspond to the pyridine rings and the ethylene groups of the Pt-cage respectively, as well as two ill-defined multiplets at -0.51 and -0.82 ppm. All of these peaks appeared as one band in the DOSY spectrum, with a $\log_D$ value of -9.65 m^2/s. This indicates that there is a Pt-cage species present which contains a guest within its cavity. However, many new peaks were also present in the ^{1}H NMR spectrum. A series of ill-defined multiplets appeared at 9.29, 8.78, and -0.26 ppm, all of which had a lower $\log_D$ value in the DOSY spectrum compared to the Pt-cage species. In addition, several new peaks were present between

4.09–1.03 ppm, all of which had high $\log_D$ values in the DOSY spectrum than those of the Pt-cage species. This indicates that these peaks belong to species which are not associated to the Pt-cage. The fact that the ^{1}H NMR spectrum of encapsulated [$(Et_3P)_2PdCl_2$]@Pt-cage under biological conditions is very different from that of [$(Et_3P)_2PdCl_2$]@Pt-cage in D_2O implies that the [$(Et_3P)_2PdCl_2$] complex interacting with the biological additives in some way. Therefore, it appears that [$(Et_3P)_2PdCl_2$] is not stable to biological conditions, whether or not is it free in solution of encapsulated within the Pt-cage. However, it should be noted that these stability studies may not be an accurate representation of the stability of [$(Et_3P)_2PdCl_2$] under catalytic conditions. The decomposition products in both cases could not be identified, so it could not be determined if encapsulation alters the decomposition pathway of the complex. In addition, the reactivity of these decomposition products are also unknown, and it is possible that the palladium complex(es) which are formed in the presence of GSH, His, and PBS are still catalytically active, and that there may still be a difference between the reactivity of the free and encapsulated complex. We therefore looked to investigate the reactivity of both free [$(Et_3P)_2PdCl_2$] and encapsulated [$(Et_3P)_2PdCl_2$]@Pt-cage complex.

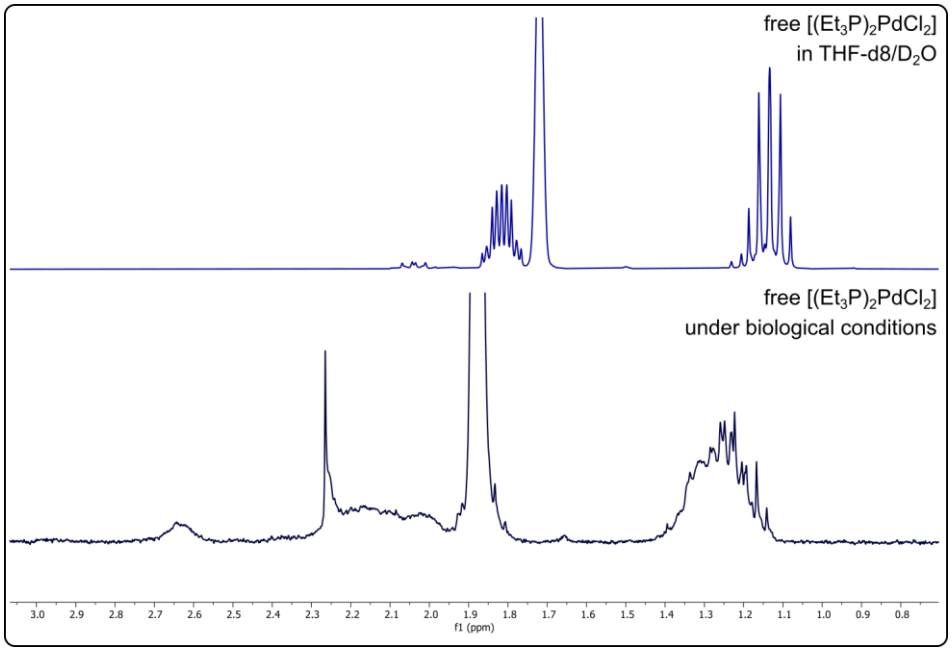

Figure 7. ^{1}H NMR spectra of the free [$(Et_3P)_2PdCl_2$] complex in THF-d8/D_2O (above) and in THF-d8/PBS in the presence of 1 eq of GSH and 1 eq of His after 24 h at 37 °C (below).

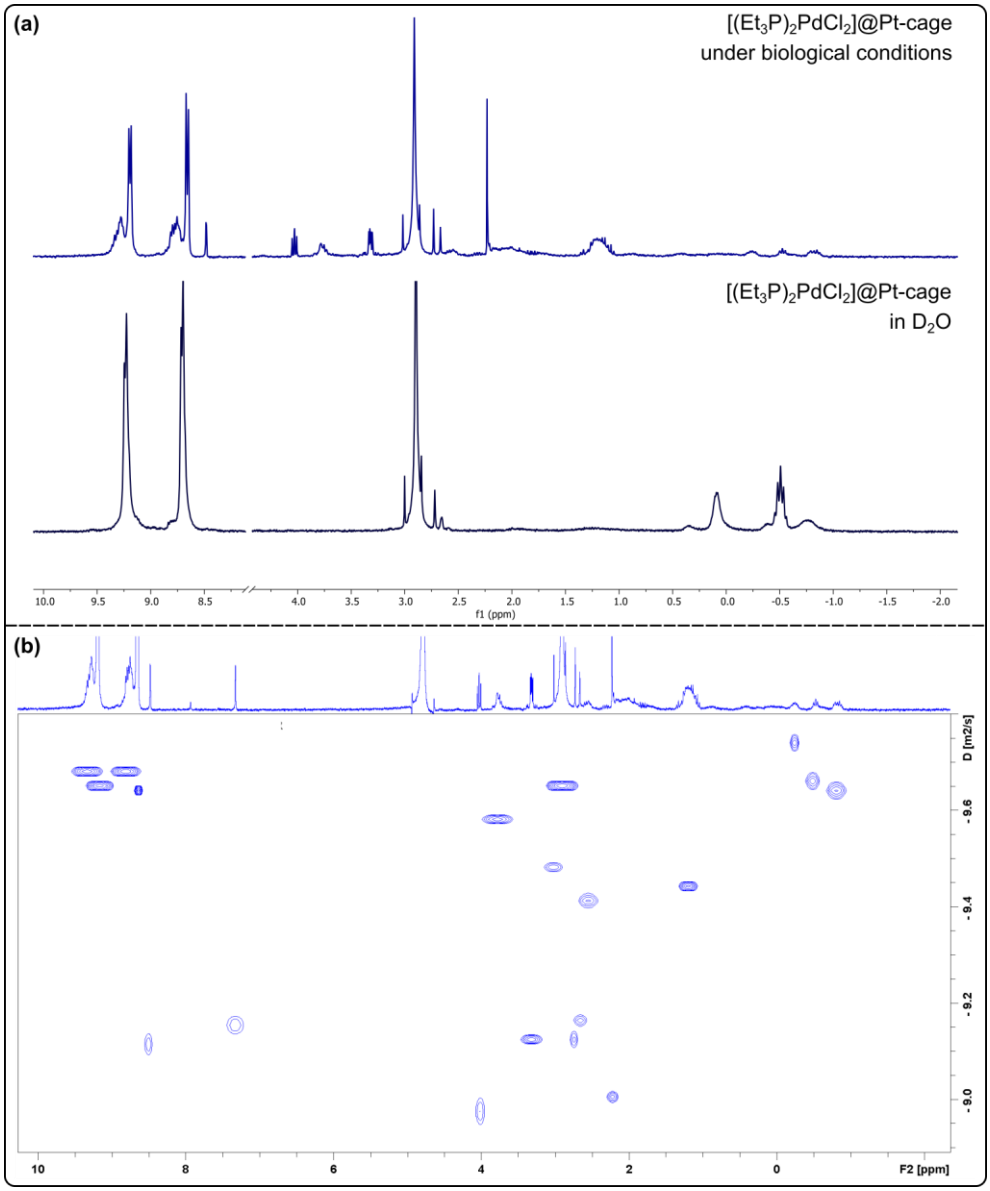

Figure 8. (a) ^{1}H NMR spectra of the encapsulated $[(Et_3P)_2PdCl_2]$@Pt-cage complex in D_2O/PBS in the presence of 1 eq of GSH and 1 eq of His after 24 h at 37 °C (above) and in D_2O (below). (b) DOSY spectrum of encapsulated $[(Et_3P)_2PdCl_2]$@Pt-cage complex in D_2O/PBS in the presence of 1 eq of GSH and 1 eq of His after 24 h at 37 °C.

REACTIVITY

While the final goal would be to achieve cross-coupling reactions by an encapsulated palladium complex, such reactions can be more difficult to achieve than unimolecular reactions, as two substrate molecules are required to come together with the catalyst instead of just one. Therefore, a simple cyclisation reaction was selected for our initial investigations into the activity of the encapsulated complex. Palladium is known to catalyse the Fujiwara-hydroarylation reaction: aryl alkynoates undergo an intramolecular cyclisation in the presence of palladium to generate coumarins.[38-43] This reaction is advantageous for two reasons: 1) the substrate for this reaction requires a terminal alkyne, which encapsulated $[(Et_3P)_2PdCl_2]$ is already known to react with, as well as the fact that terminal alkynes are used for Sonogashira

cross-coupling reactions; and 2) the non-fluorescent substrate cyclises to generate fluorescent coumarin, and this switch-on of fluorescence is a useful tool for monitoring reactions *in vivo*. Therefore, substrate **1** was selected to generate a simple unsubstituted coumarin, product **2**, as a model reaction (Figure 9a). This substrate is fairly small in size and modelling with GFN2-xTB[44] showed that there is ample room for both the palladium complex and substrate **1** within the cavity of the Pt-cage: the palladium complex can reside in one half of the cavity, while the substrate can reside in the other (Figure 9b).

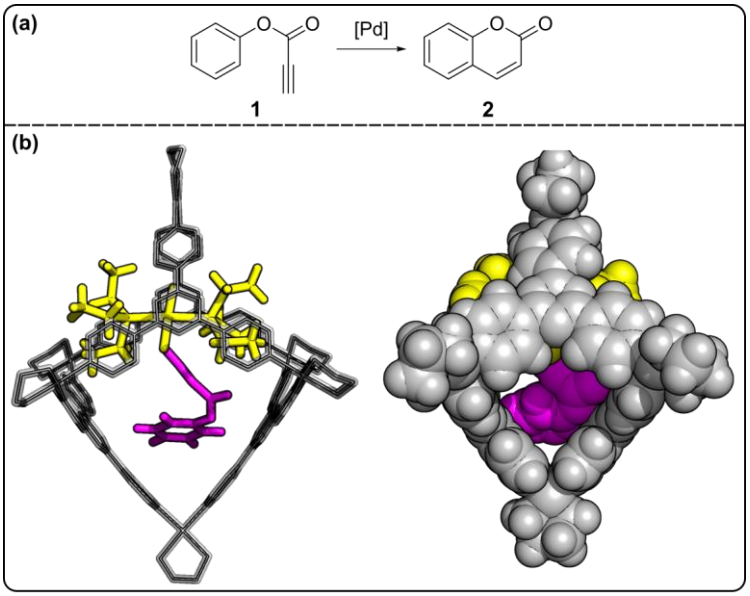

Figure 9. (a) Palladium catalysed intramolecular hydroarylation of substrate **1** to give coumarin product **2**. (b) GFN2-xTB minimised structure of [$(Et_3P)_2PdCl_2$] (yellow) and substrate **1** (purple) inside the Pt-cage (grey).

The reactivity of free [$(Et_3P)_2PdCl_2$] and encapsulated [$(Et_3P)_2PdCl_2$]@Pt-cage complex towards the hydroarylation of substrate **1** was investigated by combining 5 mol% of palladium with 1 eq of substrate **1** in D_2O at 37 °C for 16 h (Table 1). The reactions were monitored by ^1H NMR spectroscopy. When free [$(Et_3P)_2PdCl_2$] was used as catalyst, the ^1H NMR spectrum showed a mixture of substrate **1** and phenol **3**, in a 1:0.26 ratio. When no palladium source was added to the reaction mixture, the ^1H NMR spectrum again showed a mixture of substrate **1** and phenol **3**, in a 1:0.23 ratio. Therefore substrate **1** undergoes partial hydrolysis under the reaction conditions. The peak corresponding to propiolic acid was not observed in the ^1H NMR spectra, likely due to the fact that it appeared below the water peak. As the ratios between substrate **1** and phenol **3** are similar in the presence and absence of free $(Et_3P)_2PdCl_2$, it appears that free $(Et_3P)_2PdCl_2$ does not react with substrate **1**, and that only background hydrolysis occurs. However, when $(Et_3P)_2PdCl_2$@Pt-cage complex was used as catalyst, no peaks corresponding to substrate **1** were observed in the ^1H NMR spectrum. Instead, new peaks at 7.04 and 6.69 ppm appeared alongside peaks corresponding to phenol **3** (Figure 10). Integration of these peaks revealed that they corresponded to a species containing five hydrogens. Although product **2** should contain six hydrogens, the final step of this palladium catalysed intramolecular hydroarylation involves the protodepalladation of the palladium species from the ring-closed compound (Figure 11).[38, 40] For such reaction which

are carried out in water, this proton comes from the surrounding H_2O solvent.[45] However, here, the reaction was carried out in D_2O, which means that instead of being promoted by H^+, the protodepalladation step would be promoted by D^+, which would lead to incorporation of one deuterium atom into product **2**. Analysis of the reaction mixture by electrospray ionisation-HRMS (ESI-HRMS) revealed a peak at 148.0498, which corresponds to a species with molecular formula $C_9H_5D_1O_2$ (Figure E16). Therefore the new peaks in the ^{1}H NMR spectrum belong to monodeuterated product **2**. The ratio of phenol **3** and monodeuterated product **2** in the reaction mixture was 1:3.05. The DOSY spectrum revealed that the peaks corresponding to phenol and to monodeuterated product **2** both appeared as separate bands from that of the Pt-cage, with $\log_D$ values of -9.03 and -9.16 m^2/s respectively. This means that after its synthesis, product **2** has no interaction with the Pt-cage and resides free in solution. In order to confirm that whether or not it was indeed the encapsulated palladium species within the $[(Et_3P)_2PdCl_2]$@Pt-cage complex which was responsible for the generation of product **2**, substrate **1** was reacted with 5 mol% of empty Pt-cage under the same reaction conditions. The ^{1}H NMR spectrum showed a mixture of phenol and monodeuterated product **2**, in a 1:4.15 ratio. Therefore it appears that the Pt-cage itself is able to facilitate the conversion of substrate **1** into product **2**, although from these data it is not clear if the palladium inside the Pt-cage in the $[(Et_3P)_2PdCl_2]$@Pt-cage complex is inactive, or also able to facilitate the reaction.

Table 1. Ratios of substrate **1**, product **2**, and phenol **3** with different catalysts.[a]

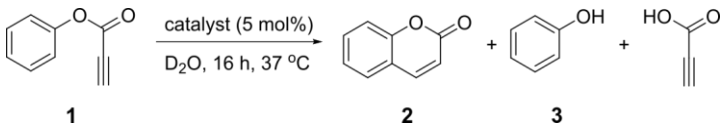

1 **2** **3**

Entry	Catalyst	Ratio 1 : 2 : 3
1	none	1 : 0 : 0.23
2	$[(Et_3P)_2PdCl_2]$	1 : 0 : 0.26
3	$[(Et_3P)_2PdCl_2]$@Pt-cage	0 : 1 : 3.05
4	empty Pt-cage	0 : 1 : 4.15

[a]Conditions: 10 mM substrate **1**, 5 mol% catalyst, D_2O, 37 °C, 16 h. Ratios determined by ^{1}H NMR spectroscopy of the crude reaction mixture.

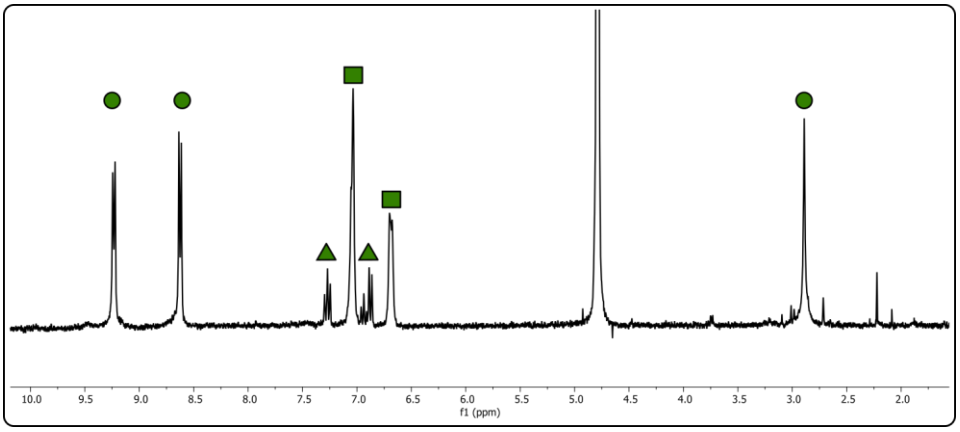

Figure 10. ^{1}H NMR spectrum of the crude reaction mixture of the reaction of substrate **1** in the presence of [$(Et_3P)_2PdCl_2$]@Pt-cage. Pt-Cage peaks are indicated with circles; phenol **3** peaks are indicated with triangles; product **2** peaks are indicated with squares.

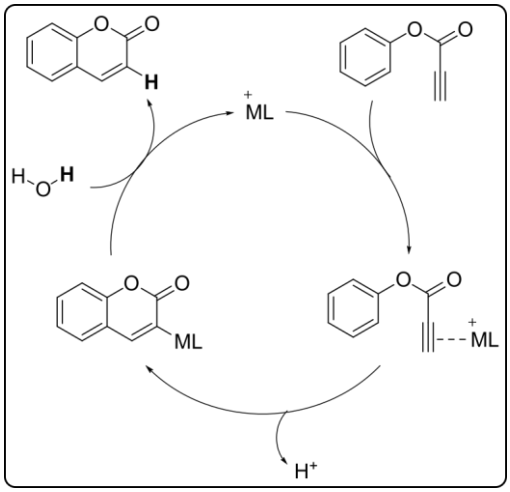

Figure 11. Catalytic cycle for a metal catalysed intramolecular hydroarylation of substrate **1**, where M is Pd or Pt.[40]

In order to accurately quantify the conversions of substrate **1**, the reactions were repeated in triplo under identical reaction conditions as previously. After the reaction was finished, the reaction mixture was extracted into a solution of $CDCl_3$ containing an internal standard, and the ^{1}H NMR spectra measured. However, in every instance where $(Et_3P)_2PdCl_2$@Pt-cage complex and empty Pt-cage where used as catalyst, the ^{1}H NMR spectrum only showed peaks corresponding to substrate **1** and phenol **3**. Therefore unfortunately the results obtained initially appear to not be reproducible, and product **2** could not be formed again. It is not clear as the reason for this irreproducibility, or why product **2** was formed in the initial experiments.

In order to gain insight into whether or not the [$(Et_3P)_2PdCl_2$]@Pt-cage complex is catalytically active at all, its reactivity towards other transformations was briefly investigated. The Wacker-Tsuji oxidation reaction uses a palladium chloride complex to convert an alkene into its corresponding ketone. Water provides the oxygen, and a copper co-catalyst is required to re-oxidise the palladium catalyst using oxygen. In addition, this transformation has been carried out using [$PdCl_2$] in a tandem reaction with an enzyme-catalysed asymmetric reduction

using styrene as substrate to generate an alcohol as the final product, which indicates the potential biocompatibility of the reaction.[46, 47] Therefore the conversion of styrene to acetophenone was selected as a model reaction to investigate the activity of the $[(Et_3P)_2PdCl_2]$@Pt-cage complex towards the Wacker-Tsuji oxidation reaction (Table 2). When 5 mol% of $[PdCl_2]$ was combined with 1 eq CuCl and 1 eq styrene in a 7:1 mixture of CD_3OD/D_2O at 37 °C for 16 h, full conversion to acetophenone was observed by ^{1}H NMR spectroscopy. This result was consistent with that reported in the literature.[47] 5 mol% of $[(Et_3P)_2PdCl_2]$ was also used as catalyst in 7:1 CD_3OD/D_2O, as well as 5 mol% of the $[(Et_3P)_2PdCl_2]$@Pt-cage complex and 5 mol% of the empty Pt-cage in D_2O. In all three cases, after stirring at 37 °C for 16 h only peaks corresponding to styrene were observed in the ^{1}H NMR spectrum. Therefore $[(Et_3P)_2PdCl_2]$ is unable to behave as a catalyst for the Wacker-Tsuji oxidation of styrene, likely because it is too electron rich, and this reaction is unsuitable for providing insight into the catalytic activity of the encapsulated $[(Et_3P)_2PdCl_2]$@Pt-cage complex.

Table 2. Conversion of styrene for Wacker-Tsuji oxidation using different catalysts.[a]

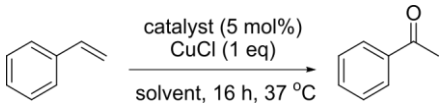

Entry	Catalyst	Solvent	Conversion styrene (%)
1	$[PdCl_2]$	7:1 CD_3OD/D_2O	100
2	$[(Et_3P)_2PdCl_2]$	7:1 CD_3OD/D_2O	0
3	$[(Et_3P)_2PdCl_2]$@Pt-cage	D_2O	0
4	empty Pt-cage	D_2O	0

[a]Conditions: 100 mM styrene, 5 mol% catalyst, 37 °C, 16 h. Conversions determined by ^{1}H NMR spectroscopy after extraction into $CDCl_3$.

Next, $[(Et_3P)_2PdCl_2]$ was explored in the double silylation of α-diketones, as it was reported to be an active catalyst for this reaction.[48] Although the reaction conditions which were used with the catalyst are not biocompatible, as high reaction temperatures were used, this reaction was selected in order to gain insight into the general reactivity of the encapsulated complex. Following the literature procedure, 1 eq benzil was mixed with 1.1 eq hexamethyldisilane in the presence of 5 mol% of $[(Et_3P)_2PdCl_2]$ in toluene-d8, and stirred at 120 °C for 16 h (Table 3). Full conversion to 1,2-diphenyl-1,2-bis(trimethylsiloxy)ethane was observed, which was consistent with the conversion reported in the literature. The same reaction conditions were then applied using D_2O as solvent. Although at room temperature benzil is not soluble in water, at 120 °C everything was dissolved and in solution. In addition, 5 mol% of the $[(Et_3P)_2PdCl_2]$@Pt-cage complex and 5 mol% of empty Pt-cage were also used as catalyst in D_2O. After stirring at 120 °C for 16 h the reaction mixtures were extracted into $CDCl_3$ and monitored by ^{1}H NMR spectroscopy. In all three cases, only peaks corresponding to benzil and hexamethyldisilane were observed. Therefore, using water as solvent inhibits the

$(Et_3P)_2PdCl_2$ catalysed conversion of benzil to 1,2-diphenyl-1,2-bis(trimethylsiloxy)ethane. The palladium catalysed double silylation of α-diketones is also an unsuitable reaction to evaluate the catalytic activity of the $[(Et_3P)_2PdCl_2]$@Pt-cage complex.

Table 3. Conversion of benzil for double silylation reaction using different catalysts.[a]

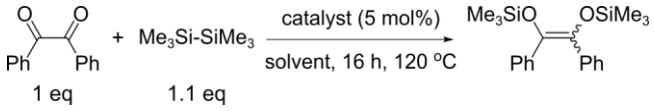

Entry	Catalyst	Solvent	Conversion benzil (%)
1	$[(Et_3P)_2PdCl_2]$	toluene-d8	100
2	$[(Et_3P)_2PdCl_2]$	D_2O	0
3	$[(Et_3P)_2PdCl_2]$@Pt-cage	D_2O	0
4	empty Pt-cage	D_2O	0

[a]Conditions: 10 mM benzil (1 eq), 1.1 eq hexamethyldisilane, 5 mol% catalyst, 120 °C, 16 h. Conversions determined by ^{1}H NMR spectroscopy of crude reaction mixture (entry 1) or after extraction into C_6D_6 (entries 2-4).

CONCLUSION AND OUTLOOK

With the aim of improving the efficiency of palladium catalysis under biological conditions, the reactivity of a palladium complex within a supramolecular host was investigated. While a palladium cage was shown to rapidly decompose in the presence of chlorides and GSH, the platinum analogue of the cage was shown to be stable to these conditions even at very low nanomolar concentrations, confirming its applicability as a stable supramolecular host under biological conditions. The palladium complex $[(Et_3P)_2PdCl_2]$ was then successfully encapsulated within the Pt-cage, although the pure formation of the $[(Et_3P)_2PdCl_2]$@Pt-cage complex was not possible, as free guest remained in solution. Unfortunately, the catalytic activity of this encapsulated complex compared to that of the free complex could not be determined: reproducibility problems led to ambiguity over its reactivity towards the intramolecular hydroarylation of substrate **1**; and the palladium complex was found to be inactive for both the Wacker-Tsuji oxidation of styrene and the double silylation of benzil. Further research should investigate and confirm whether or not the palladium species within the $[(Et_3P)_2PdCl_2]$@Pt-cage complex is catalytically active, and whether or not the Pt-cage improves its activity under biologically relevant conditions.

EXPERIMENTAL

MATERIALS AND METHODS

All commercially available compounds were used as received unless otherwise stated. Styrene was filtered over alumina before use. Pt-Cage[49], Pd-cage,[49] and substrate[50] were synthesised according to literature procedures. Water was degassed by bubbling N_2 for 4 h. PBS was prepared by dissolving PBS tablets in D_2O. All reactions were carried out under aerobic conditions unless otherwise stated. All stock solutions were prepared fresh immediately before catalysis. NMR spectra were performed on a Bruker AV300, AV400, or AV500 spectrometer, with chemical shifts reported in ppm and referenced to solvent residual signal (7.17 ppm for $CDCl_3$, 4.79 ppm for D_2O, 2.08 ppm for toluene-d8, and 7.16 for C_6D_6). 2D ^{1}H DOSY NMR spectra were recorded with a calibrated gradient at 298 K. High resolution mass data were recorded on a HR ToF Bruker Daltonik Gmbh Impact II, an ESI-ToF MS capable of resolution of at least 40000 FWHM, which was coupled to a Bruker cryo-spray unit. Detection was in positive-ion mode and the source voltage was between 4 and 6 kV. The sample was introduced with syringe pump at a flow rate of 18 µL/hr. For electrospray ionisation (ESI), the drying gas (N_2) was held at 180 °C. The machine was calibrated prior to every experiment via direct infusion of a TFA-Na solution, which provided a m/z range of singly charged peaks up to 3500 Da in both ion modes. Software acquisition Compass 2.0 for Otof series. Software processing Compass DataAnalysis 4.0 sri. UV/Vis spectra were recorded on a Hewlett Packard 8453 single beam spectrophotometer in a 1.0 cm path length quartz cuvette with H_2O as background.

STABILITY STUDIES

Cage stability: NMR spectroscopy studies

GSH (1.38 mg, 4.5 µmol, 3 eq) was dissolved in PBS (0.6 mL) in an NMR tube. Pd-cage (5.3 mg, 1.5 µmol, 1 eq) or Pt-cage (4.5 mg, 1.5 µmol, 1 eq) was added to this solution. The NMR tube was left in a water bath at 37 °C for 24 h. ^{1}H NMR spectra were recorded at 37 °C immediately upon addition of Pd-cage or Pt-cage, after 1 h, and after 24 h.

Pt-Cage stability: UV/Vis studies

A 10 mM stock solution of Pt-cage in H_2O (1 µL, 10 nmol) was added to a 2.5 mM solution of GSH in PBS (3 mL, 6 µmol). UV/Vis spectra were recorded at 37 °C every 20 min for 14 h.

$[(Et_3P)_2PdCl_2]$ stability

A stock solution of 5 mM GSH and His in PBS (0.35 mL, 1.75 µmol, 1 eq) was added to a 4 mL vial. A 5 mM solution of either $[(Et_3P)_2PdCl_2]$ in THF-d8 (0.35 mL, 1.75 µmol, 1 eq) or $[(Et_3P)_2PdCl_2]$@Pt-cage (0.35 mL, 1.75 µmol, 1 eq) was then added, and the vial was capped and stirred at 37 °C for 16 h. The reaction mixture was then transferred to an NMR tube, and measured by ^{1}H NMR spectroscopy.

ENCAPSULATIONS

Encapsulations were carried out according to a modified literature procedure.[33] Under an atmosphere of nitrogen, a 5 mM solution of Pt-cage in degassed D_2O (3.5 µmol, 0.7 mL, 1 eq)

was added to a vial containing [$(Et_3P)_2PdCl_2$] (2.90 mg, 7.0 μmol, 2 eq) and the resulting mixture was stirred at room temperature for 5 h. The solution was filtered over syringe filter, then washed with $CDCl_3$ (0.8 mL). **^{1}H NMR** (300 MHz, D_2O): δ 9.24 (d, J = 6.4 Hz), 8.71 (d, J = 6.4 Hz), 3.09 – 2.76 (s), 0.19 (s), -0.47 (p). **DOSY NMR** (D_2O, 298 K): log_D = -9.69. **^{31}P NMR** (300 MHz, D_2O): δ 17.95.

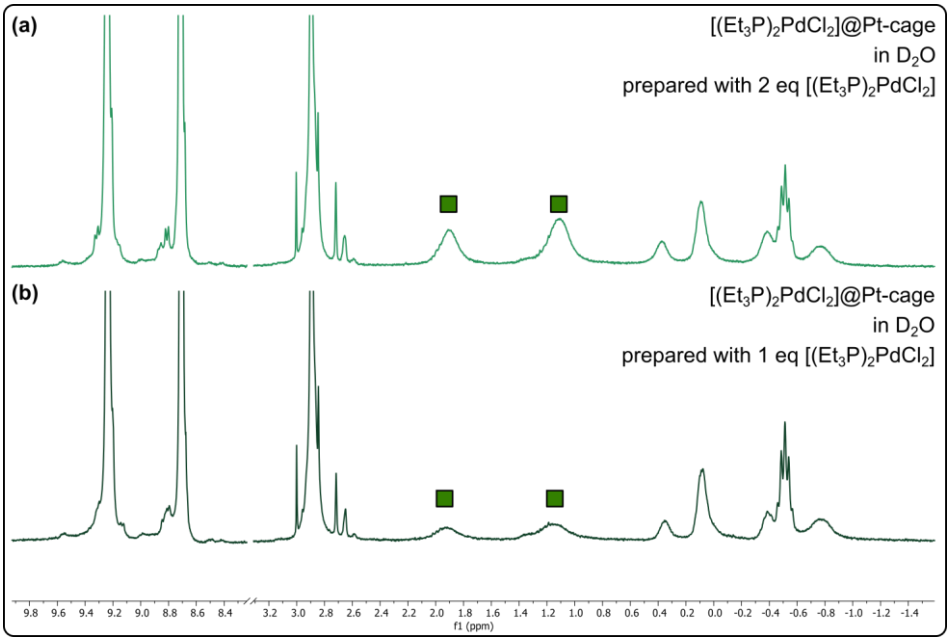

Figure E12. ^{1}H NMR spectra of the mixture of free [$(Et_3P)_2PdCl_2$] and encapsulated [$(Et_3P)_2PdCl_2$]@Pt-cage complex obtained by mixing the 1 eq of empty Pt-cage with (a) 2 eq [$(Et_3P)_2PdCl_2$] and (b) 1 eq [$(Et_3P)_2PdCl_2$].

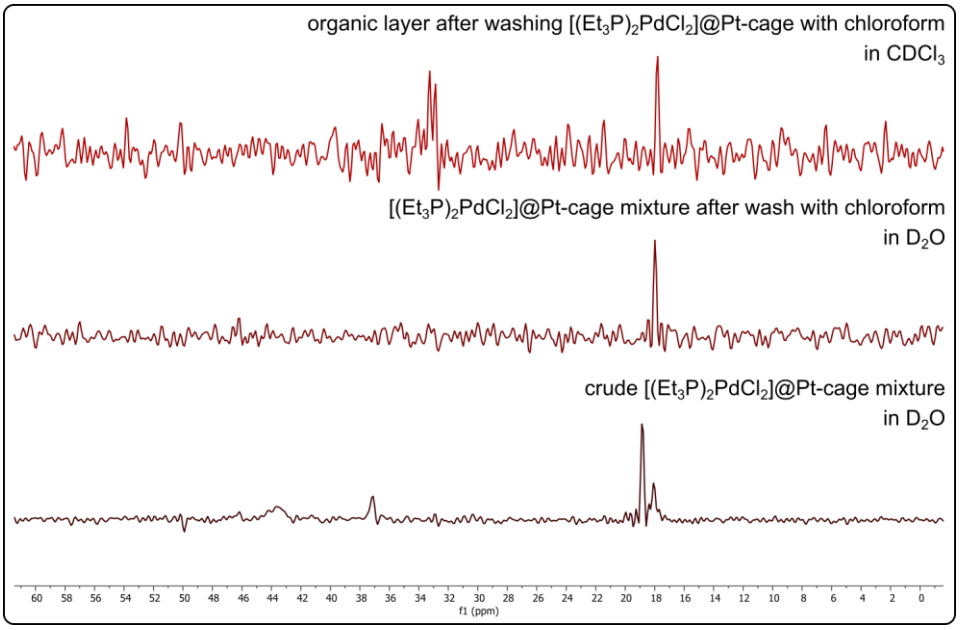

Figure E13. ^{31}P NMR spectra of the [$(Et_3P)_2PdCl_2$]@Pt-cage complex before and after washing with chloroform.

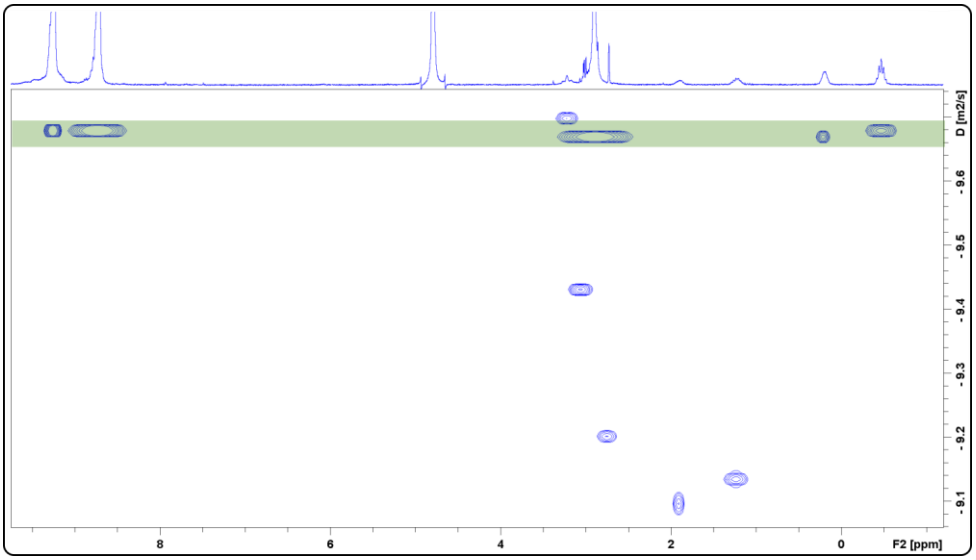

Figure E14. DOSY spectrum of the $[(Et_3P)_2PdCl_2]$@Pt-cage complex after washing with chloroform. Peaks with the same $\log_D$ value as the that of the Pt-cage peaks are highlighted in green.

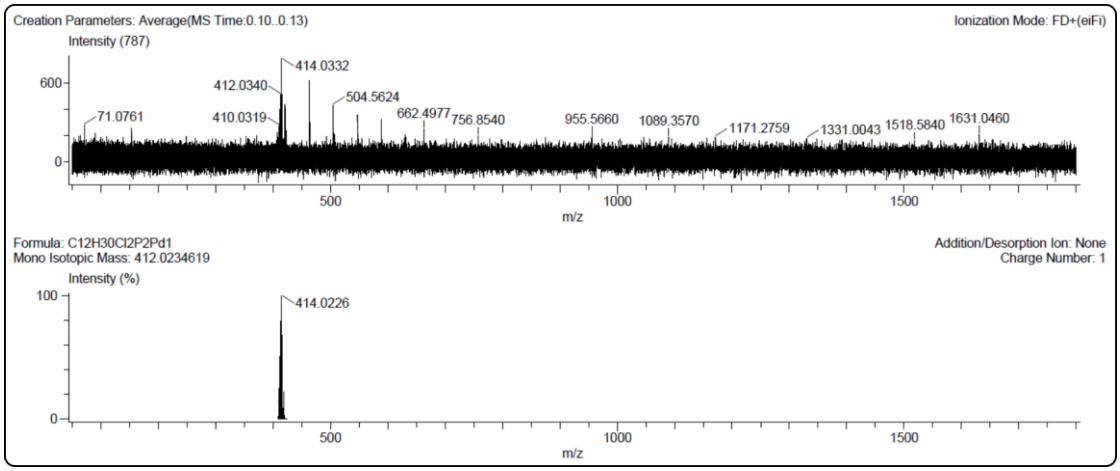

Figure E15. Above: FD-HRMS spectrum of the organic layer after washing the $[(Et_3P)_2PdCl_2]$@Pt-cage complex with chloroform. Below: Calculated spectrum of $[(Et_3P)_2PdCl_2]$.

CATALYSIS: INTRAMOLECULAR HYDROARYLATION OF SUBSTRATE 1

Reaction with $[(Et_3P)_2PdCl_2]$@Pt-cage complex

A 5 mM solution of $[(Et_3P)_2PdCl_2]$@Pt-cage complex in D_2O was prepared as described above. $[(Et_3P)_2PdCl_2]$@Pt-cage complex (70 µL, 0.35 µmol, 5 mol%) was added to a 4 mL vial. D_2O (630 µL) then neat substrate **1** (0.90 µL, 0.93 mg, 7 µmol, 1 eq) were added, and the vial was capped and stirred at 37 °C for 16 h. The reaction mixture was transferred to an NMR tube and measured by ^{1}H NMR spectroscopy.

Spectroscopic data of product **2**:

^{1}H NMR (300 MHz, D_2O): δ 7.10 – 6.99 (m, 3H), 6.74 – 6.64 (m, 2H). **ESI-HRMS** (positive): m/z (calc) = 148.0498 (148.0524) $[M]^+$.

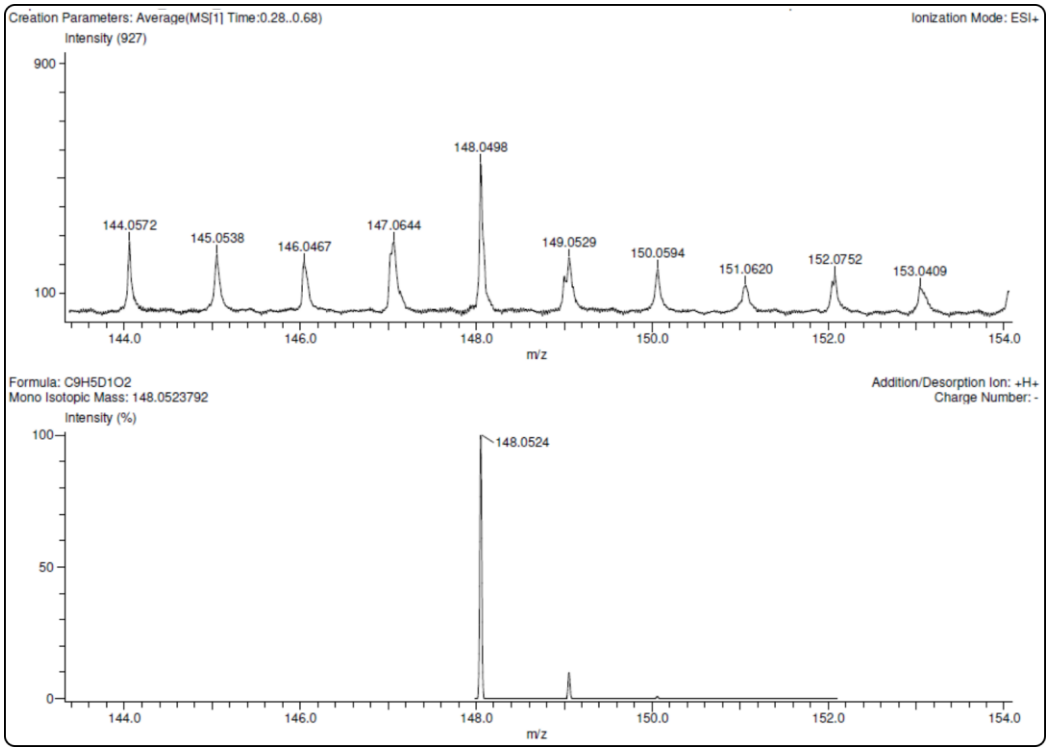

Figure E16. Above: ESI-HRMS of crude reaction mixture of $[(Et_3P)_2PdCl_2]$@Pt-cage with substrate **1**. Below: Calculated spectrum of monodeuterated product **2**.

Reaction with free $[(Et_3P)_2PdCl_2]$

$[(Et_3P)_2PdCl_2]$ (0.14 mg, 0.35 µmol, 5 mol%) was added to a 4 mL vial. D_2O (700 µL) then neat substrate **1** (0.90 µL, 0.93 mg, 7 µmol, 1 eq) were added, and the vial was capped and stirred at 37 °C for 16 h. The reaction mixture was transferred to an NMR tube and measured by ^{1}H NMR spectroscopy.

Reaction with empty Pt-cage

Empty Pt-cage (1.23 mg, 0.35 µmol, 5 mol%) was added to a 4 mL vial. D_2O (700 µL) then neat substrate **1** (0.90 µL, 0.93 mg, 7 µmol, 1 eq) were added, and the vial was capped and stirred at 37 °C for 16 h. The reaction mixture was transferred to an NMR tube and measured by ^{1}H NMR spectroscopy.

Reaction with in absence of catalyst

D_2O (700 µL) then neat substrate **1** (0.90 µL, 0.93 mg, 7 µmol, 1 eq) were added to a 4 mL vial, and the vial was capped and stirred at 37 °C for 16 h. The reaction mixture was transferred to an NMR tube and measured by ^{1}H NMR spectroscopy.

Catalysis: Wacker-Tsuji oxidation of styrene

A 5 mM solution of $[(Et_3P)_2PdCl_2]$@Pt-cage complex in D_2O was prepared as described above. CuCl (1.98 mg, 20 µmol, 1 eq) was weighed into a 4 mL vial. Catalyst (1 µmol, 5 mol%), then CD_3OD and D_2O (final total volume of 0.2 mL), then neat styrene (2 µL, 20 µmol, 1 eq) was added. The vial was capped and stirred at 120 °C for 16 h. 1 mL $CDCl_3$ was added to the

reaction mixture, and the vial was shaken. The organic layer was decanted to an NMR tube and measured by ^{1}H NMR spectroscopy.

Entry	Catalyst	Solvent
1	$[PdCl_2]$	7:1 CD_3OD / D_2O
2	$[(Et_3P)_2PdCl_2]$	7:1 CD_3OD / D_2O
3	$[(Et_3P)_2PdCl_2]$@Pt-cage	D_2O
4	empty Pt-cage	D_2O

CATALYSIS: DOUBLE SILYLATION OF BENZIL

A 5 mM solution of $[(Et_3P)_2PdCl_2]$@Pt-cage complex in D_2O was prepared as described above, and a 100 mM stock solution of benzil in CD_3OD was prepared. Catalyst (0.35 µmol, 5 mol%) was added to a pressure tube, followed by solvent (final total volume of 0.7 mL), benzil (70 µL, 7 µmol, 1 eq), and neat hexamethyldisilane (1.58 µL, 1.13 mg, 7.7 µmol, 1.1 eq). The pressure tube was then sealed and stirred at 120 °C for 16 h. For reactions in toluene-d8, the crude reaction mixture was transferred to an NMR tube and measured with ^{1}H NMR spectroscopy. For reaction in D_2O, 0.8 mL C_6D_6 was added the reaction mixture and the tube was shaken. The organic layer was decanted to an NMR tube and measured by ^{1}H NMR spectroscopy.

Entry	Catalyst	Solvent
1	$[(Et_3P)_2PdCl_2]$	toluene-d8
2	$[(Et_3P)_2PdCl_2]$	D_2O
3	$[(Et_3P)_2PdCl_2]$@Pt-cage	D_2O
4	empty Pt-cage	D_2O

REFERENCES

[1] N. Della Ca', *Catalysts* **2021**, 11, 588.

[2] M. Martínez-Calvo, J. R. Couceiro, P. Destito, J. Rodríguez, J. Mosquera, J. L. Mascareñas, *ACS Catal.* **2018**, 8, 6055-6061.

[3] R. M. Yusop, A. Unciti-Broceta, E. M. V. Johansson, R. M. Sánchez-Martín, M. Bradley, *Nat. Chem.* **2011**, 3, 239-243.

[4] A. Unciti-Broceta, E. M. V. Johansson, R. M. Yusop, R. M. Sánchez-Martín, M. Bradley, *Nat. Protoc.* **2012**, 7, 1207-1218.

[5] M. A. Miller, B. Askevold, H. Mikula, R. H. Kohler, D. Pirovich, R.Weissleder, *Nat. Commun.* **2017**, 8, 15906.

[6] M. A. Miller, H. Mikula, G. Luthria, R. Li, S. Kronister, M. Prytyskach, R. H. Kohler, T. Mitchison, R. Weissleder, *ACS Nano* **2018**, 12, 12814-12826.

[7] M. Santra, S.-K. Ko, I. Shin, K. H. Ahn, *Chem. Commun.* **2010**, 46, 3964-3966.

[8] G. Y. Tonga, Y. Jeong, B. Duncan, T. Mizuhara, R. Mout, R. Das, S. T. Kim, Y.-C. Yeh, B. Yan, S. Hou, V. M. Rotello, *Nat. Chem.* **2015**, 7, 597-603.

[9] T. Lv, J. Wu, F. Kang, T. Wang, B. Wan, J.-J. Lu, Y. Zhang, Z. Huang, *Org. Lett.* **2018**, 20, 2164-2167.

[10] J. T. Weiss, J. C. Dawson, K. G. Macleod, W. Rybski, C. Fraser, C. Torres-Sánchez, E. E. Patton, M. Bradley, N. O. Carragher, A. Unciti-Broceta, *Nat. Commun.* **2014**, 5, 3277.

[11] M. Sancho-Albero, B. Rubio-Ruiz, A. M. Pérez-López, V. Sebastián, P. Martín-Duque, M. Arruebo, J. Santamaría, A. Unciti-Broceta, *Nat. Catal.* **2019**, 2, 864-872.

[12] J. Li, J. Yu, J. Zhao, J. Wang, S. Zheng, S. Lin, L. Chen, M. Yang, S. Jia, X. Zhang, P. R. Chen, *Nat. Chem.* **2014**, 6, 352-361.

[13] J. Wang, B. Cheng, J. Li, Z. Zhang, W. Hong, X. Chen, P. R. Chen, *Angew. Chem. Int. Ed.* **2015**, 54, 5364-5368.

[14] Y. Liu, S. Pujals, P. J. M. Stals, T. Paulöhrl, S. I. Presolski, E. W. Meijer, L. Albertazzi, A. R. A. Palmans, *J. Am. Chem. Soc.* **2018**, 140, 3423-3433.

[15] J. Wang, S. Zheng, Y. Liu, Z. Zhang, Z. Lin, J. Li, G. Zhang, X. Wang, J. Li, P. R. Chen, *J. Am. Chem. Soc.* **2016**, 138, 15118-15121.

[16] A. H. Ngo, S. Bose, L. H. Do, *Chem.–Eur. J.* **2018**, 24, 10584-10594.

[17] R. C. Brewster, E. Klemencic, A. G. Jarvis, *J. Inorg. Biochem.* **2021**, 215, 111317.

[18] Y. G. Bai, J. F. Chen, S. C. Zimmerman, *Chem. Soc. Rev.* **2018**, 47, 1811-1821.

[19] M. Martínez-Calvo, J. L. Mascareñas, *Coord. Chem. Rev.* **2018**, 359, 57-79.

[20] C. D. Spicer, T. Triemer, B. G. Davis, *J. Am. Chem. Soc.* **2012**, 134, 800-803.

[21] C. D. Spicer, B. G. Davis, *Chem. Commun.* **2013**, 49, 2747-2749.

[22] F. M. Wang, Y. Zhang, Z. Du, J. S. Ren, X. G. Qu, *Nat. Commun.* **2018**, 9, 8.

[23] J. Clavadetscher, E. Indrigo, S. V. Chankeshwara, A. Lilienkampf, M. Bradley, *Angew. Chem. Int. Ed.* **2017**, 56, 6864-6868.

[24] M. E. Ourailidou, M. R. H. Zwinderman, F. J. Dekker, *MedChemComm* **2016**, 7, 399-408.

[25] R. Chinchilla, C. Nájera, *Chem. Soc. Rev.* **2011**, 40, 5084-5121.

[26] G. Cheng, R. K. V. Lim, C. P. Ramil, Q. Lin, *Chem. Commun.* **2014**, 50, 11679-11682.

[27] N. Li, R. K. V. Lim, S. Edwardraja, Q. Lin, *J. Am. Chem. Soc.* **2011**, 133, 15316-15319.

[28] R. K. V. Lim, N. Li, C. P. Ramil, Q. Lin, *ACS Chem. Biol.* **2014**, 9, 2139-2148.

[29] N. Li, C. P. Ramil, R. K. V. Lim, Q. Lin, *ACS Chem. Biol.* **2015**, 10, 379-384.

[30] J. Li, S. Lin, J. Wang, S. Jia, M.Yang, Z. Hao, X. Zhang, P. R. Chen, *J. Am. Chem. Soc.* **2013**, 135, 7330-7338.

[31] Y. M. Wilson, M. Dürrenberger, E. S. Nogueira, T. R. Ward, *J. Am. Chem. Soc.* **2014**, 136, 8928-8932.
[32] P. Destito, C. Vidal, F. López, J. L. Mascareñas, *Chem.–Eur. J.* **2021**, 27, 4789-4816.
[33] Y. Kohyama, T. Murase, M. Fujita, *J. Am. Chem. Soc.* **2014**, 136, 2966-2969.
[34] F. Ibukuro, T. Kusukawa, M. Fujita, *J. Am. Chem. Soc.* **1998**, 120, 8561-8562.
[35] A. V. Melkikh, M. I. Sutormina, *J. Theor. Biol.* **2008**, 252, 247-254.
[36] H. J. Forman, H. Zhang, A. Rinna, *Mol. Aspects Med.* **2009**, 30, 1-12.
[37] D. A. Poole, S. Mathew, J. N. H. Reek, *J. Am. Chem. Soc.* **2021**, 143, 16419-16427.
[38] C. Jia, D. Piao, T. Kitamura, Y. Fujiwara, *J. Org. Chem.* **2000**, 65, 7516-7522.
[39] S. Kumar, R. K. Saunthwal, M. Mujahid, T. Aggarwal, A. K. Verma, *J. Org. Chem.* **2016**, 81, 9912-9923.
[40] T. Kitamura, K. Otsubo, *J. Org. Chem.* **2012**, 77, 2978-2982.
[41] N. Chernyak, V. Gevorgyan, *J. Am. Chem. Soc.* **2008**, 130, 5636-5637.
[42] K. Szwaczko, *Inorganics* **2022**, 10, 23.
[43] A. Carral-Menoyo, N. Sotomayor, E. Lete, *Catal. Sci. Technol.* **2020**, 10, 5345-5361.
[44] C. Bannwarth, S. Ehlert, S. Grimme, *J. Chem. Theory Comput.* **2019**, 15, 1652-1671.
[45] M. L. O'Duill, K. M. Engle, *Synthesis* **2018**, 50, 4699-4714.
[46] H. Sato, W. Hummel, H. Gröger, *Angew. Chem. Int. Ed.* **2015**, 54, 4488-4492.
[47] I. Schnapperelle, W. Hummel, H. Gröger, *Chem.–Eur. J.* **2012**, 18, 1073-1076.
[48] H. Yamashita, N. P. Reddy, M. Tanaka, *Chem. Lett.* **1993**, 22, 315-318.
[49] S. H. A. M. Leenders, R. Becker, T. Kumpulainen, B. de Bruin, T. Sawada, T. Kato, M. Fujita, J. N. H. Reek, *Chem.–Eur. J.* **2016**, 22, 15468-15474.
[50] A. Jolit, C. F. Dickinson, K. Kitamura, P. M. Walleser, G. P. A. Yap, M. A. Tius, *Eur. J. Org. Chem.* **2017**, 6067-6076.

Chapter 4

Aqueous Olefin Metathesis Facilitated by a Supramolecular Cage

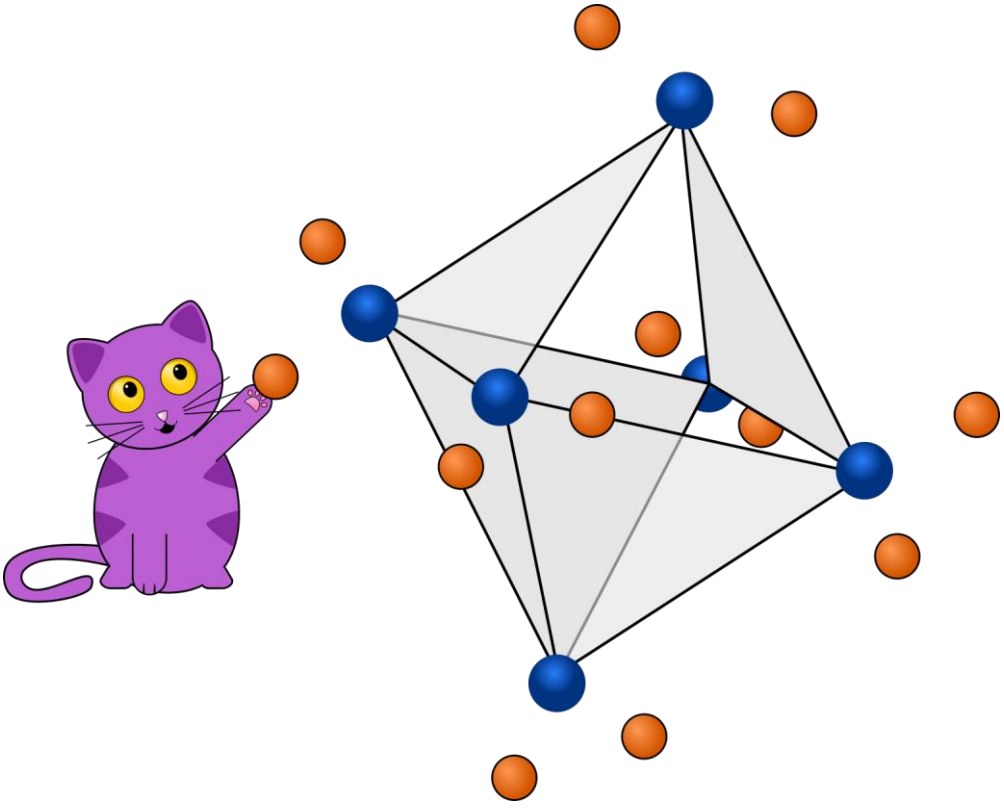

ABSTRACT

Olefin metathesis is a potentially useful reaction to carry out inside living cells; however, catalyst poisoning by cellular components renders this challenging. This chapter explores the encapsulation of an olefin metathesis catalyst inside a supramolecular cage as a strategy to protect the catalyst from the cellular environment under aqueous conditions. NMR spectroscopy studies reveal that encapsulation of standard apolar metathesis catalysts within the cavity of the cage is not possible. However the yield of a ring-closing metathesis of a diallyl substrate carried out with AquaMet as the water soluble catalyst in the aqueous phase was greatly improved by the presence of the cage. Detailed NMR spectroscopy, GFN2-xTB, and UV/Vis spectroscopy studies show that the catalyst does not bind or interact with the cage in any way. Interestingly, the counterions of the cage seem to influence the reaction. Indeed catalytic experiments in the presence of KNO_3 show that it is the nitrate counterions of the cage which improves the yield and the rate of the reaction. We anticipate that these improved reaction kinetics may provide a means to also improve aqueous olefin metathesis under biologically relevant conditions.

INTRODUCTION

Ruthenium catalysed olefin metathesis is an extraordinarily useful transformation in organic synthesis,[1-4] providing access to a wide range of products, including ring structures and heterocycles,[5-7] functionalised olefins,[8] and polymers.[9] The versatility of this transformation has led to its application in a variety of areas, for example the total synthesis of bioactive organic compounds,[10-12] and in the production of pharmaceuticals.[13-16] Importantly, olefin metathesis only requires mild reaction conditions, with many examples running at, or close to, room temperature,[17-21] as well as tolerating the presence of both of water and oxygen.[22-28] Therefore it is not surprising that the pursuit of applying the metathesis reaction *in vivo*, for example for *in situ* drug formation or biomolecule labelling, is of current interest.[29-32] Indeed the applicability of this transformation in biological settings has recently been demonstrated with olefin metathesis-mediated labelling of proteins by incorporation of unnatural alkene-containing amino acids into the desired protein.[30, 33-36]

Applying any catalytic reaction inside living cells is not straight-forward, as the large quantities of intracellular salts, reducing agents, and thiols, as well as the presence of many other biomolecules, typically results in low reaction yields and turnover numbers. As a result, the catalyst is typically applied in close to stoichiometric amounts.[29, 37-41] Despite these challenges, olefin metathesis has been successfully carried out inside living cells. The two reported examples making use of artificial metalloenzymes to protect the catalyst from the poisoning environment of the cell. Ward and co-workers recently presented olefin metathesis in *E. coli* bacteria by docking a Hoveyda-Grubbs derived catalyst inside streptavidin. Here, catalyst poisoning was avoided by targeting the periplasm of the bacteria, where there are much lower levels of the metal-binding (and reducing) agent glutathione compared to the interior of the cell.[42] A similar catalyst was also shown to be protected from thiol poisoning by docking it within the hydrophobic pocket of serum albumin, allowing for the generation of a cytotoxic compound within the cytoplasm of cancer cells.[43]

While artificial metalloenzymes provide a route to provide protection against biomolecule binding, there are many other inhibiting components within a cellular environment to which the catalysts are vulnerable. Aqueous olefin metathesis has received a lot of attention over the last decade,[44] because many biologically relevant compounds are water soluble,[45] and because water is a more environmentally friendly alternative to the typical chlorinated or aromatic solvents which are traditionally used for metathesis.[46-49] However, the activity of metathesis catalysts at low catalyst loadings is highly sensitive to the presence of water. Not only is the rate of catalyst initiation lowered,[50, 51] but the chlorides readily dissociate from the ruthenium centre.[52] Coordination of hydroxide ions generates Ru-$(OH)_n$ species, which are completely inactive in metathesis and rapidly decompose via the loss of the carbene ligand.[53-56] Even very low quantities of water can result in a significant loss of activity.[57, 58] In addition, basic biomolecules may pose a threat to the base-sensitive metallocyclobutane intermediate formed during the catalytic cycle.[56, 59, 60] Finally, metathesis catalysts are also susceptible to bimolecular decomposition pathways.[61-64]

There have been several strategies employed to overcome these problems, by improving the stability of the catalyst. The rate of decomposition can be reduced by addition of Brønsted acids to remove hydroxide ions from solution,[51] or by addition of chloride salts to prevent the chloride displacement.[54, 65, 66] It has also been shown that cationic metathesis catalysts can be protected by encapsulating the complex inside a supramolecular host. Encapsulating the catalyst within the cavity of a supramolecular cage separates the catalyst from the surrounding solvent and also prevents catalyst degradation by bimolecular pathways.[67] However, this approach has so far been limited to organic solvent, due to the solubility of the supramolecular capsule which was used. We therefore looked to design a system whereby an olefin metathesis catalyst would be protected from biomolecule poisoning and from the aqueous environment by encapsulation within the hydrophobic cavity of a water soluble supramolecular cage. To this purpose, we selected the octahedral $[Pt_6L_4](NO_3)_{12}$ metallocage as additive for a ring-closing metathesis (RCM) reaction (Figure 1). Next to being water soluble, this cage is also known to encapsulate apolar organic compounds and metal complexes as guests.[68-71] The platinum analogue of this cage was selected because of its greater kinetic stability and robustness compared to its palladium counterpart.[72]

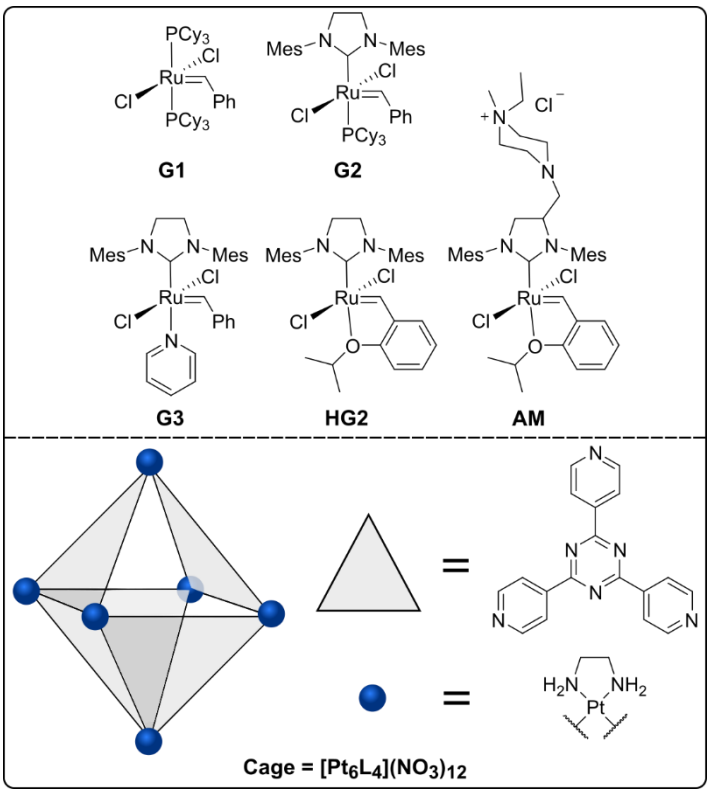

Figure 1. Structures of metathesis catalysts and the cage used in this study.

RESULTS AND DISCUSSION

ENCAPSULATION STUDIES

$[Pt_6L_4](NO_3)_{12}$ cages (and palladium analogues) are known to encapsulate neutral and anionic guests, whereas the binding of cationic guests is disfavoured due to charge repulsion with the cationic platinum centres.[73] Therefore a variety of hydrophobic metathesis catalysts were selected for encapsulation: Grubbs 1st generation, **G1**, and Grubbs 2nd generation, **G2**, catalysts; the Grubbs 3rd generation "fast-initiating" catalyst, **G3**; and the Hoveyda-Grubbs 2nd generation catalyst, **HG2**. These are commonly used metathesis catalysts, and offer a range of polarities and size. Encapsulation studies were carried out by vigorously stirring a solution of 1 eq of the cage in D_2O with a solution of 3 eq of catalyst in CD_2Cl_2 at room temperature for 2 h. The binding of hydrophobic guests within a water soluble host can be analysed by NMR spectroscopy in D_2O, as solubilisation of the guest within the cavity of the cage results in the appearance of guest peaks in the ^1H NMR spectrum, which are not visible in the control experiments in the absence of host as the free guest is insoluble in water. For both organic soluble phosphine-containing catalysts, **G1** (Figure 2) and **G2** (Figure 3), new broad peaks in the region between 1.5 and -0.7 ppm appeared in the ^1H NMR spectrum upon mixing with the cage solution. These peaks correspond to the cyclohexyl protons of the phosphine group, which were observed along with those of the cage in the water layer. Comparison to the free complex measured in CD_2Cl_2 showed that these new peaks are shifted upfield, which is typical for guest binding. In the experiment in which **G1** was used as guest, a new set of doublets appeared corresponding to the cage pyridine rings appeared at 9.25 and 8.72 ppm. The doublets belonging to the empty cage, at 9.17 and 8.65 ppm, were still present. However when **G2** was used as guest, only one set of doublets was present at 9.22 and 8.69 ppm. ^1H NMR diffusion ordered spectroscopy (DOSY) was used to probe whether or not these guest molecules were in the cage. The DOSY spectrum revealed a broad band with a $\log_D$ value of -9.56 m^2/s for the peaks between 1.5 and -0.7 ppm belonging to the PCy_3 group. This band appeared at a lower $\log_D$ value as that of the cage peaks, -9.77 m^2/s. This indicates that the PCy_3 ligand and the cage are two separate species in solution. Analysis of the PCy_3 guest was further probed by ^{31}P NMR spectroscopy. A single peak at 51.55 ppm was observed in the ^{31}P NMR spectrum, which was also shifted with respect to the signal of the free complex, at 29.04 ppm (in CD_2Cl_2). This single peak is within the range which is typical for oxidised phosphorus compounds. Therefore there is no binding in the cage when either **G1** or **G2** is mixed with the cage, but instead the PCy_3 ligand becomes oxidised to $O{=}PCy_3$ and enters the water layer, but does not go inside the cavity of the cage.

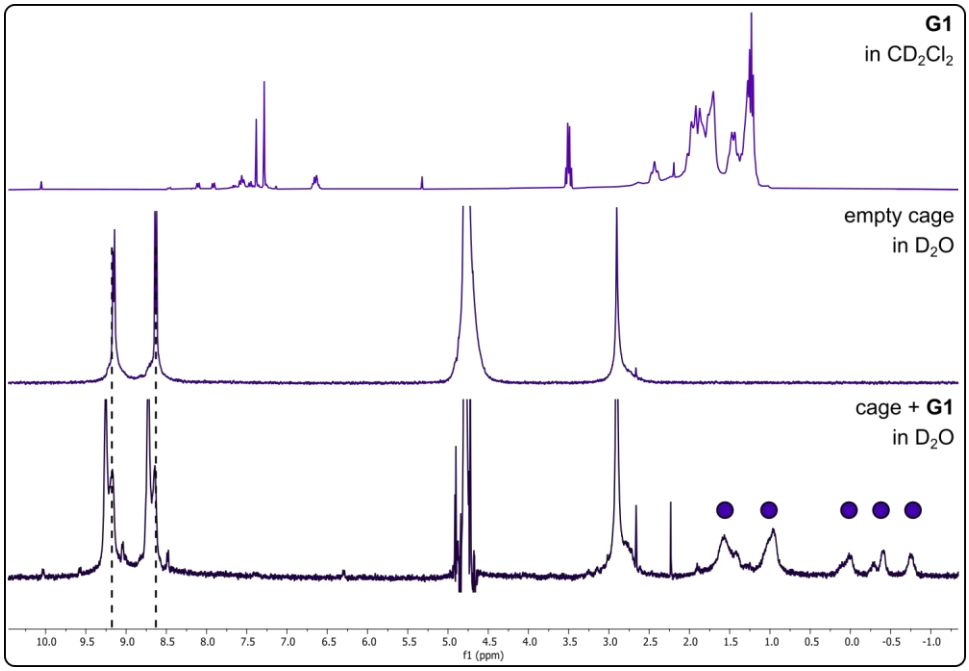

Figure 2. ^{1}H NMR spectra of free **G1**, the empty cage, and after mixing 1 eq of cage with 3 eq **G1** (cage + **G1**). The new upfield guest peaks are indicated with circles.

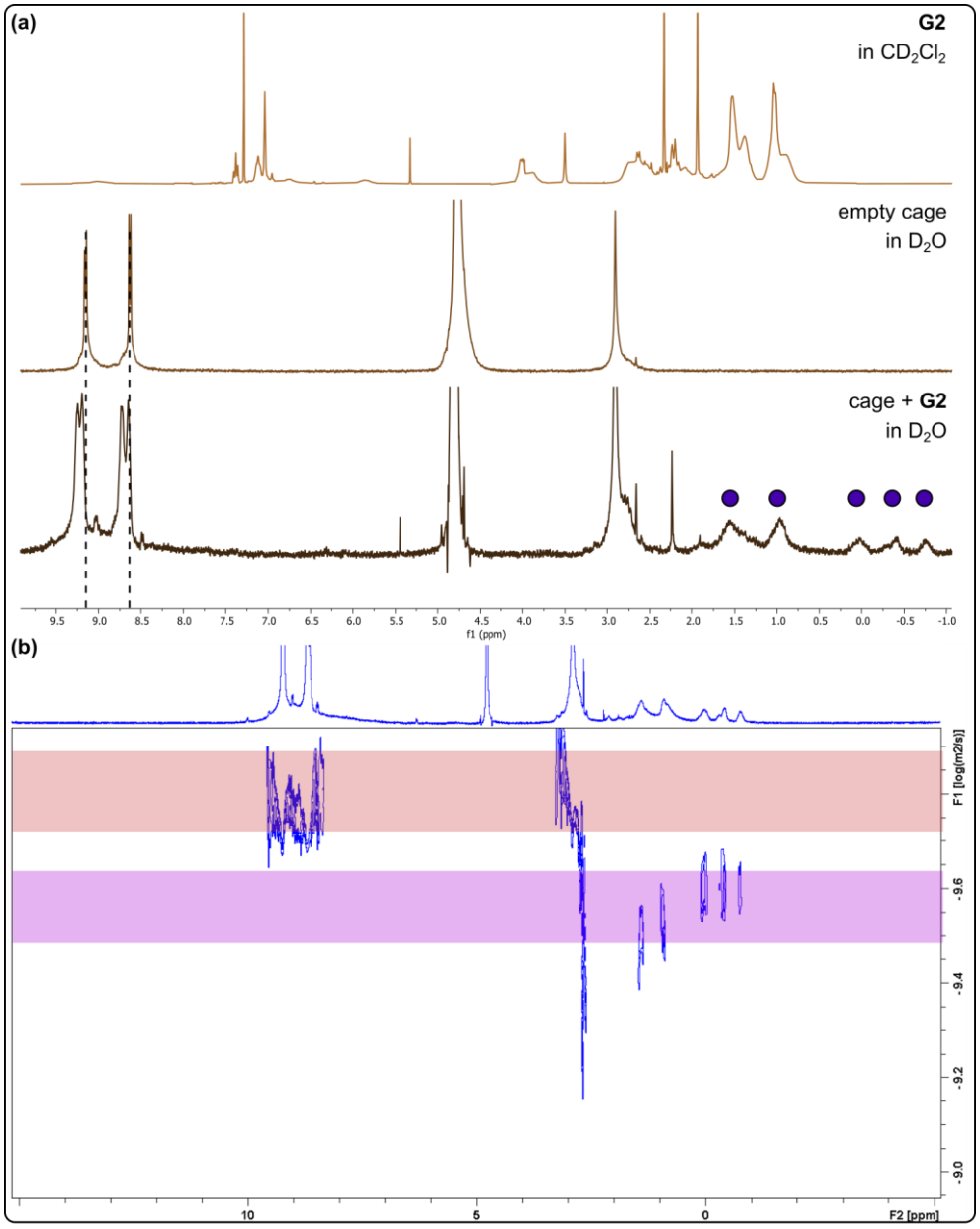

Figure 3. (a) ^{1}H NMR spectra of free **G2**, empty cage, and after mixing 1 eq of cage with 3 eq **G2** (cage + **G2**). The new upfield guest peaks are indicated with circles. (b) DOSY spectrum of cage + **G2**. The band corresponding to the cage is highlighted in red. The band corresponding to the oxidised PCy_3 is highlighted in purple.

The two phosphine-free catalysts (**G3** and **HG2**) were also mixed with the cage using the same procedure as for **G1** and **G2**. When the pyridine-containing catalyst **G3** was mixed with the cage new peaks appeared in the ^{1}H NMR spectrum of the D_2O layer between 7.30 and 10.10 ppm. The signals of the cage in the ^{1}H NMR spectrum were only very slightly shifted, from 9.15 and 8.63 ppm to 9.19 and 8.64 ppm. In addition, the new peaks appeared as a broad band in the DOSY spectrum with a $\log_D$ value of -8.77 m^2/s, which is significantly lower than the $\log_D$ value of the cage signals (-9.77 m^2/s) (Figure 4). This indicates that the cage and the species corresponding to the new peaks in the ^{1}H NMR spectrum are two separate species, and that a guest@cage complex has not been formed. Most likely the new peaks come from pyridine ligand, which had dissociated from the complex and entered the water layer. Finally,

when **HG2** was mixed with the cage only peaks of the empty cage were observed in the ^{1}H NMR spectrum after mixing the solutions of cage and catalyst. This means that no binding event occurred. These experiments show that none of these apolar metathesis catalysts bind in the $[Pt_6L_4](NO_3)_{12}$ cage. So far, it was not possible to facilitate aqueous olefin metathesis with these standard catalysts using the water soluble cage.

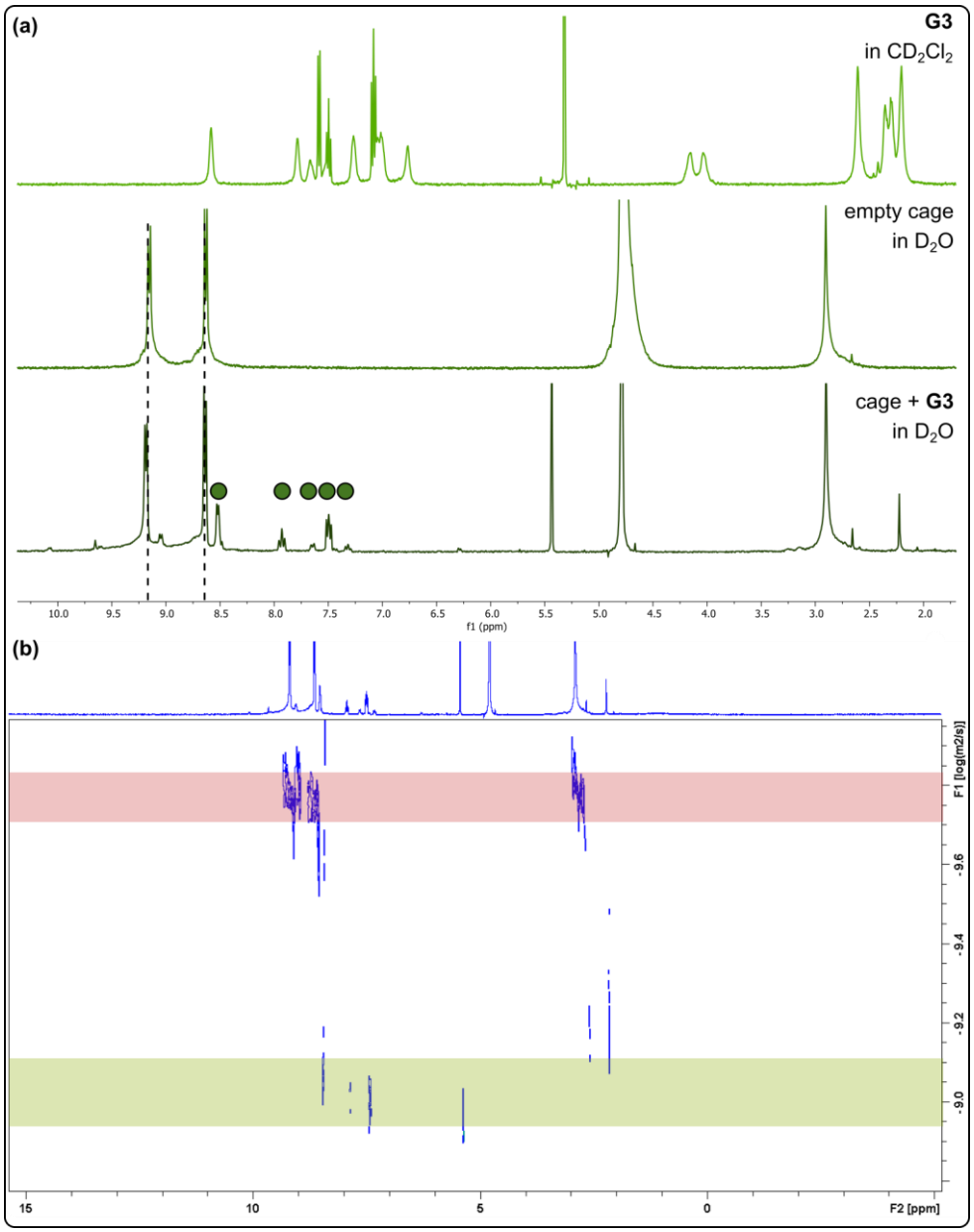

Figure 4. (a) ^{1}H NMR spectra of free **G3**, empty cage, and after mixing 1 eq of cage with 3 eq **G3** (cage + **G3**). The new upfield guest peaks are indicated with circles. (b) DOSY spectrum of cage + **G3**. The band corresponding to the cage is highlighted in red. The band corresponding to the new guest peaks is highlighted in green.

CATALYSIS WITH AQUAMET

Next, we went on to investigate the effect of the cage on a water soluble analogue of the **HG2** catalyst, AquaMet (AM). We initially hypothesised that charge repulsion between the cationic ammonium group on the NHC ligand of the catalyst and the cationic platinum centres

may reduce the affinity of the catalyst for the cage; however partial encapsulation of the complex, with the apolar ruthenium centre residing in the hydrophobic cavity and the cationic ammonium group remaining outside by perforating the large windows of the cage, should be possible. Modelling with GFN2-xTB[74] indicated that there would be enough space within the cavity of the cage for such an interaction to occur (Figure 5). In addition, the water solubility of the free complex means that the catalyst and cage can be just mixed in water, without the need for a biphasic pre-encapsulation step. The size of **HG2** and **G3** is comparable to the size of AM, however NMR spectroscopy studies (see section *Encapsulation Studies*) showed that no encapsulation of these complexes occurred. The biphasic encapsulation may have prevented encapsulation, as perhaps the complexes were too well solubilised in the organic layer to enter the water layer and interact with the cage. It is also possible that the complexes (partially) decomposed during the encapsulation process. Therefore we envisioned that by-passing this pre-encapsulation step would increase the likelihood of AM going in the cage, whereas the analogous apolar complexes which were not soluble in water did not. In order to validate this hypothesis, the metathesis activity of AM in the both the absence and presence of cage was investigated. Encapsulated complexes often exhibit different activity compared to the free unbound analogue in solution, and therefore a difference in yield could indicate that the cage is interacting with the catalyst in some way. To this end, the ring-closing metathesis of *N*,*N*-diallyltosyl amine, **1**, was selected as a model reaction (Table 1). When 2.5 mol% of AM was combined with substrate **1** in water at 37 °C for 2 h, an 18% yield of ring-closed product **2** was achieved. This low yield is likely due to rapid decomposition of the catalyst in water. However, when AM was mixed with 1 eq of cage before addition of substrate, a drastic improvement in yield was observed, whereby a 69% yield of **2** was observed. The presence of the cage during catalysis had a clear, positive influence on the yield of **2**. Next we investigated the origin of this effect and if this was due to encapsulation of the complex.

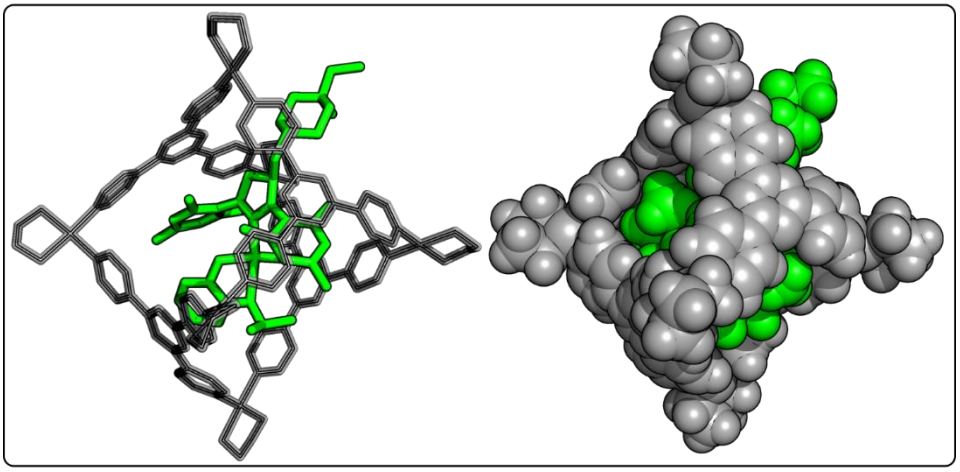

Figure 5. GFN2-xTB minimised structure of AM inside the cage.

Table 1. Yield of RCM of substrate **1** in the presence and absence of cage.[a]

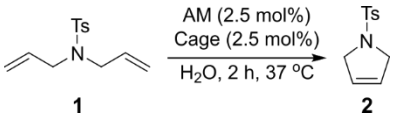

1 2

Entry	Additive	Yield (%)
1	None	18
2	Cage	69

[a]Conditions: 50 mM substrate **1**, 2.5 mol% AM, 2.5 mol% cage, H_2O, 37 °C, 2 h. Yield determined by ^1H NMR spectroscopy relative to 1,3,5-trimethoxybenzene as internal standard.

AquaMet Binding Studies

The binding of the complex and the cage could not be probed by DOSY due to the instability of AM in water, as rapid decomposition is observed as soon as it is dissolved in water. However, UV/Vis spectroscopy could be used to investigate the interaction. It has previously been reported that AM exhibits improved stability in solution when encapsulated within a resorcin[4]arene capsule, where decomposition is less rapid compared to a catalyst free in solution.[67] Therefore the decomposition of the free complex was compared to that of the complex in the presence of cage. Decomposition can be monitored by UV/Vis spectroscopy, as the complex has a MLCT band at 375 nm. The decomposition of the complex is accompanied by a decrease in absorbance at this wavelength.[54] UV/Vis spectra of AM in solution were recorded over the course of 1 h at 37 °C, and a decomposition profile was generated by plotting the decrease in absorption at 375 nm over time (Figure 6). The plot obtained for AM in the presence of cage was not substantially different from that of free AM. This independence upon the presence of cage shows that the ruthenium centre is not protected by the cavity of the cage, perhaps because it resides free in solution. The AM complex itself is a pre-catalyst, which upon activation in the presence of substrate liberates the isopropoxybenzylidene moiety (ligand) from the ruthenium centre (Scheme 1). This simple unsubstituted isopropoxybenzylidene ligand has been demonstrated to operate under the boomerang mechanism, whereby the ligand can re-bind to the ruthenium centre, regenerating the stable pre-catalyst species.[75-78] We therefore hypothesised that while the cage does not bind the ruthenium complex, it may instead bind this ligand during catalysis, thereby improving the activity and thus the yield by preventing recombination of the ligand with the ruthenium centre and increasing the amount of active species in solution.

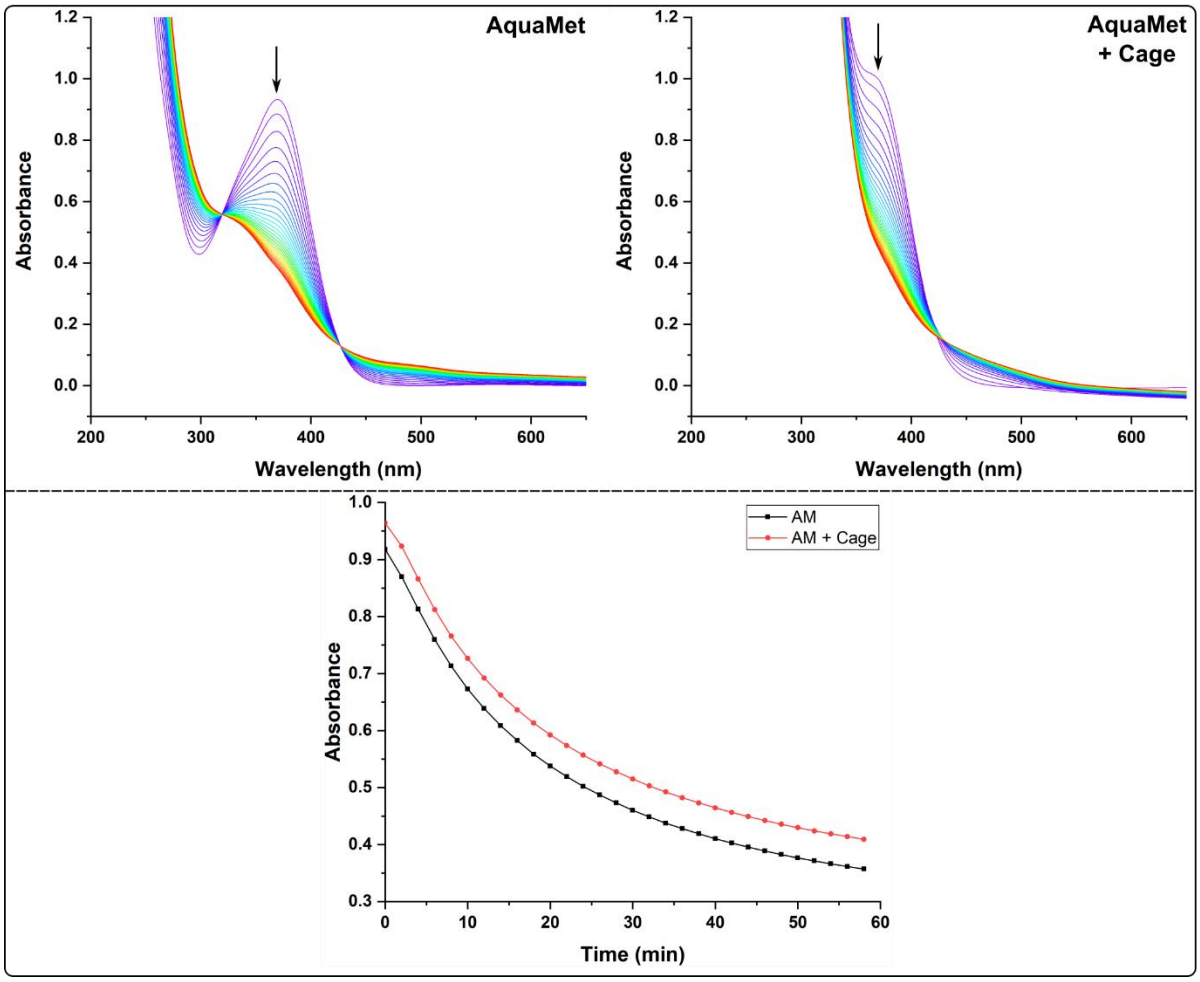

Figure 6. Above: UV/Vis spectra over 1 h of AM in solution at 37 °C in the presence and absence of cage, Below: The change in absorption over time at 375 nm.

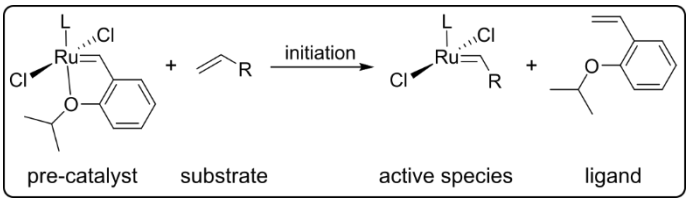

Scheme 1. Initiation of Hoveyda-Grubbs catalysts.

LIGAND BINDING STUDIES

We set out to establish if the ligand could bind within the cavity of the cage. As the relatively hydrophobic ligand is only poorly soluble in water, we anticipated that solubilisation within the apolar cavity would be a driving force for its encapsulation. Its small size also allows multiple ligands being bound within one cage. Modelling with GFN2-xTB supports that there is ample room inside the cavity for up to three ligands to bind (Figure 7). Binding studies were carried out by ^{1}H and DOSY NMR spectroscopy using 1 eq of cage in the presence of 20 eq of ligand (Figure 8). The broad peaks of the poorly soluble free ligand sharpened in the presence of cage. In addition, the doublet belonging to the cage shifted from 9.16 ppm to 9.28 ppm. New up-field peaks appeared at 3.53 ppm and at 0.25 ppm, which are attributed to the isopropyl

group on the ligand that is bound in the cage. Clearly, exchange of the free ligand and that bound in the cage is slow on the NMR time scale, as they appear in the NMR spectrum as a different set of peaks. The peaks belonging to the free ligand appeared as a broad band in the DOSY spectrum with a diffusion constant of -9.33 m^2/s. However, the new up-field peak at 0.25 ppm appeared within the same band as that of the new shifted cage peaks, with a diffusion constant of -9.80 m^2/s, indicating that this peak corresponds to ligand which is bound to the cage. As there are no peaks in the ^1H NMR spectrum which correspond to the empty cage, it appears that at this stoichiometry the cage is fully saturated with ligand. Unfortunately, a binding constant could not be determined for the formation of this host-guest complex, as the insolubility of the ligand in water prevented an accurate titration from being carried out. However, integration of the isopropyl group at 0.25 ppm relative to an internal standard indicated that two ligands are bound inside the cage. Together these data show that the ligand is indeed encapsulated inside the cage.

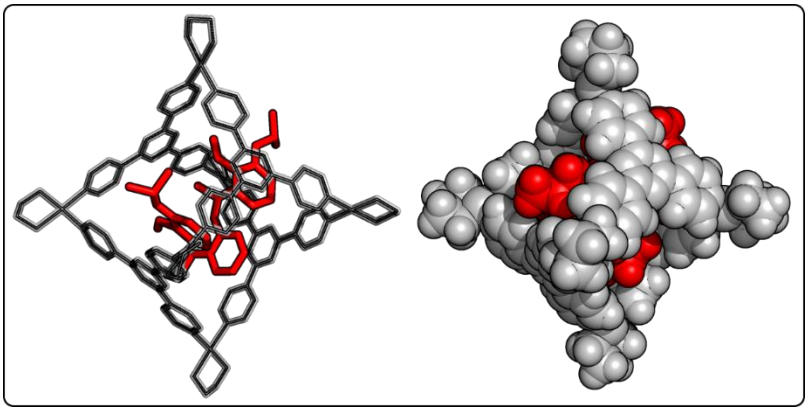

Figure 7. GFN2-xTB minimised structure of three ligands encapsulated within the cage.

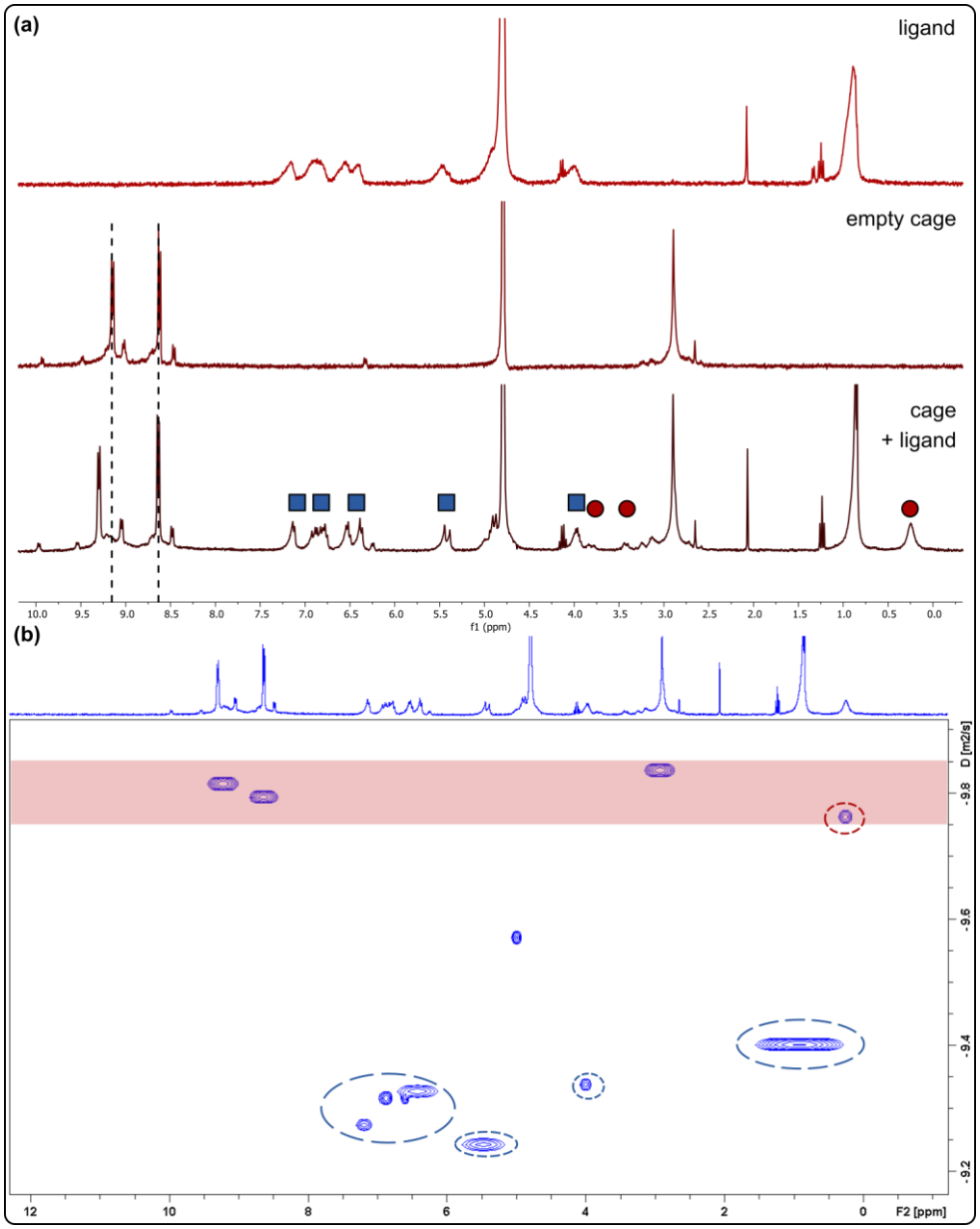

Figure 8. (a) ^{1}H NMR spectra of free ligand, empty cage, and after mixing 1 eq of cage with 20 eq ligand (cage + ligand). The new upfield guest peaks are indicated with circles, while peaks belonging to the non-encapsulated free ligand are indicated with squares. (b) DOSY spectrum of cage + ligand. The band corresponding to the cage is highlighted in red. The peaks corresponding to the new guest peaks are circled in red, while the peaks from the free ligand are circled in blue.

In order to establish whether ligand binding could be responsible for the improved yield in the presence of the cage, the kinetics of the reaction were investigated. If indeed encapsulation of the ligand during catalysis was preventing the boomerang mechanism from occurring, and therefore increasing the amount of active species in solution, then a difference in rate for the reaction with cage should be observed compared to the reaction without. The kinetics of the reaction were probed by following the amount of ethene produced using a bubble counter (Figure 9, black and red lines).[79-80] Since one equivalent of ethene is produced for every equivalent of product **2** formed, the number and size of bubbles can be used to determine the amount of ethene produced, which can then be equated to the amount of product formed.

This could be confirmed by extraction of the reaction mixture into toluene at the end of the reaction and quantifying product formation by ^{1}H NMR spectroscopy relative to 1,3,5-trimethoxybenzene that was used as internal standard. When following the reaction in the bubble counter using AM as the catalyst a modest final yield of 12% was obtained, with the maximum TOF reaching 252 μmol ethene mol cat^{-1} min^{-1} at 13 min.[1] When the reaction was carried out in the presence of the cage, a final yield of 45% was achieved with a maximum TOF of 3852 μmol ethene mol cat^{-1} min^{-1} at 7 min. In both cases, the final yield was attained after around 1 h at which point the catalyst was determined to be fully deactivated, as the addition of fresh substrate after this time did not result in an increase in yield. Importantly, when the cage was present, around 75% of the final yield was achieved already within 10 min, whereas without cage at the same point only around 15% of the final yield was obtained. Therefore, the yield improvement is caused by the cage increasing the rate of the catalysis, and the cage does not appear to influence the lifetime of the catalyst.

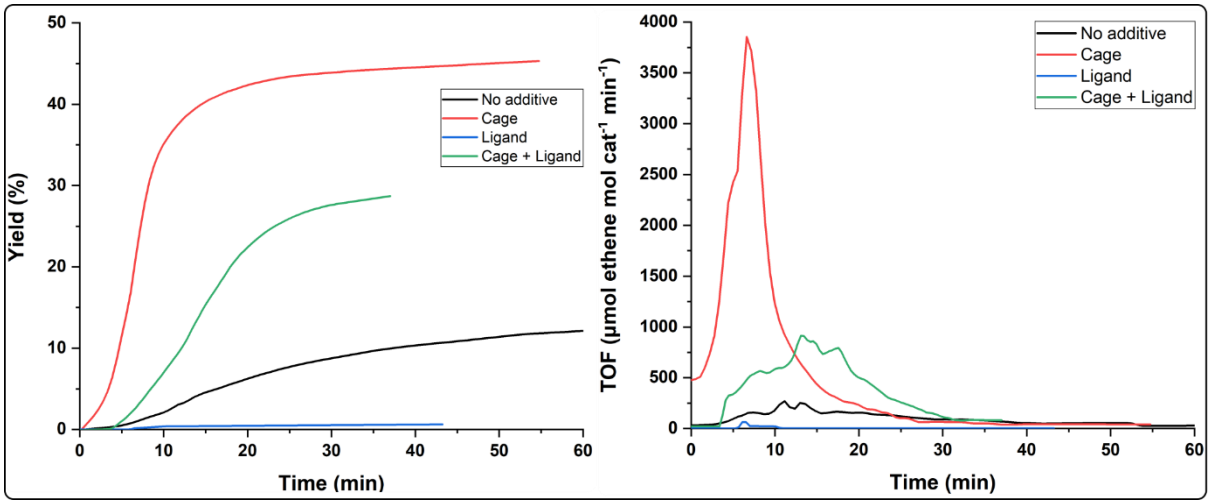

Figure 9. Reaction profiles for RCM of substrate **1** with AM (black line) in the presence of cage (red line), 50 mol% ligand (blue line), and cage and 50 mol% ligand (green line) generated by monitoring the amount of ethene produced over time.

CATALYSIS WITH FILLED CAVITY

We next studied if the observed rate enhancement in the presence of cage was due to the binding of the ligand in the cavity of the cage. Therefore catalysis was carried out with an excess of ligand in order to pre-saturate the cavity with ligand before addition of the catalyst. Under these conditions the same rate and yield should be obtained independently of whether or not the cage is present. (Figure 10). When free AM was mixed with 50 mol% of ligand (20 eq with respect to the AM) before addition of substrate **1**, a slight reduction in activity was observed, with a 14% yield of **2**. However, when 50 mol% of ligand was first mixed with the cage before addition of AM and substrate **1**, product **2** was obtained with a 42% yield. Although this yield was lower compared to the reaction without excess ligand, it was still an improvement

[1] The lower yield obtained when the reaction was carried out in the bubble counter compared to the previous reactions was attributed to the 11 x larger scale, which was required to meet the detection limit of ethene production by the machine.

compared to the reaction without cage. Kinetic data were obtained under these conditions for comparison to the other experiments. Following these reactions with the bubble counter (Figure 9, green and blue lines) revealed that in the presence of excess ligand, for the reaction with cage a final yield of 29% was achieved with a maximum TOF of 911 μmol ethene mol cat^{1} min^{-1} at 13 min. Although in both cases the excess of ligand reduces the rate of the catalyst, presumably by favouring recombination to form the pre-catalyst, the cage still improves the activity of the AM even when its cavity is saturated with ligand, indicating that encapsulation of the ligand was not actually responsible for the rate increase. In order to probe this further, the cage was again pre-saturated before catalysis, with a guest which does not inhibit catalysis. Hydroxyadamantane (Ad-OH) was selected for this purpose, as it known that 4 Ad-OH molecules bind strongly inside the cage.[81] When AM was added to this pre-mixed 4Ad-OH@cage complex, a final yield of 77% of **2** was obtained. The improved yield of **2** in the presence of cage was completely unaffected by filling the cavity. Therefore, binding events at the inside of the cage cannot be responsible for the improved reactivity that was observed due to the presence of the cage. As for every equivalent of cage also 12 eq of nitrate counterions are added, we suspected that these anions may cause the positive effects on the catalysis. Indeed, when AM was mixed with 12 eq of KNO_3, an 76% yield of **2** was observed. Most likely, an interaction between the nitrate counterions of the cage and the AM results in a new nitrate complex which is much more active in the RCM of **1** than the AM alone.

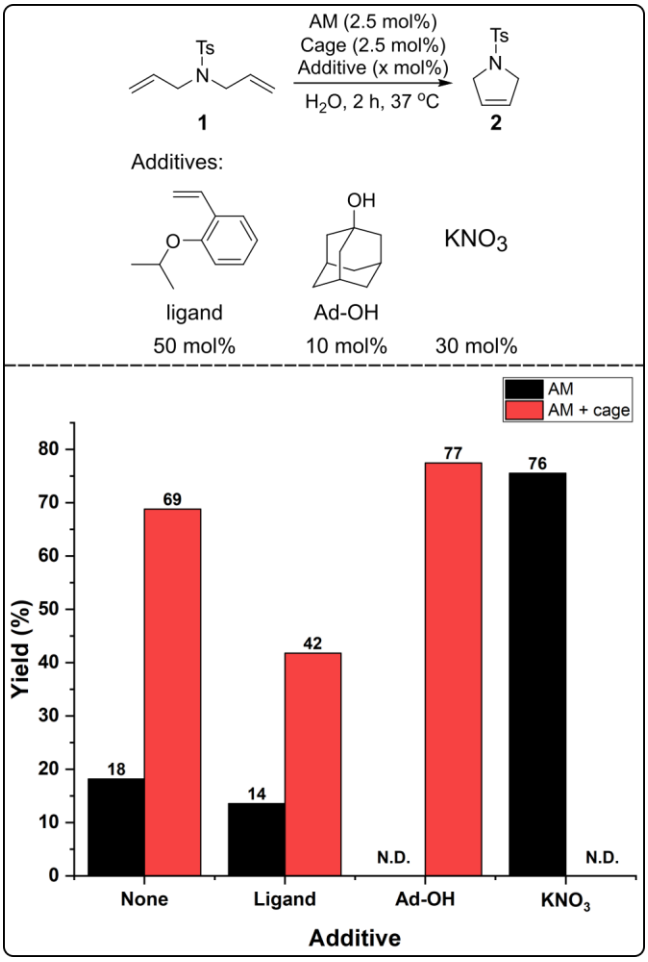

Figure 10. Yields for the RCM of substrate **1** in the presence of various additives. For reactions with ligand and Ad-OH in the presence of cage, the cage was pre-saturated with guest before addition of AM and **1**.

CONCLUSION AND OUTLOOK

In conclusion, we aimed for the binding of metathesis catalysts in water soluble cages for the purpose of potential application in living cells. Initial experiments using apolar catalysts that are soluble in organic solvents, show that these are not encapsulated within the cavity of a $[Pt_6L_4](NO_3)_{12}$ cage. The presence of the cage during the ring-closing metathesis of substrate **1** with AM as water soluble catalyst results in an almost four-fold increase in yield for the ring-closed product **2**. Detailed experiments show that this is due to a dramatic increase in the rate of the reaction. Despite the cage being able to bind the ligand which is released from the pre-catalyst, this binding event was not responsible for improving the reactivity of the AM. Instead, experiments in the presence of cages with a filled cavity showed that the increase in yield is not a result of the cavity. Instead, the presence of nitrate counterions, introduced by the cationic cages, make the AM catalyst more active. Although the total lifetime of the catalyst is the same as in the absence of nitrate, the improved reaction kinetics bestowed upon the AM by the nitrate means that productive catalysis can occur faster than water-induced decomposition. Therefore, the cage itself would not able to protect the catalyst from biological conditions; neither by providing a physical barrier from biomolecules nor by improving stability in water to prevent decomposition. However, the activity of AM under aqueous conditions can be dramatically improved upon the addition of nitrate. The origin of this nitrate effect, and its application under biological conditions, will be discussed in the next chapter.

EXPERIMENTAL

MATERIALS AND METHODS

All commercially available compounds were used as received. **G3**,[82] cage,[68] substrate **1**,[83] and ligand[84] were synthesised according to literature procedures. Milli-Q Ultrapure grade water was used for all reactions. All reactions were carried out under aerobic conditions unless otherwise stated. All catalysis results are an average of three experiments. All stock solutions were prepared fresh immediately before catalysis. NMR spectra were performed on a Bruker AV300, AV400, or AV500 spectrometer, with chemical shifts reported in ppm and referenced to solvent residual signal (2.50 ppm for toluene-d8, 4.79 ppm for D_2O). 2D ^1H DOSY NMR spectra were recorded with a calibrated gradient at 298 K. UV/Vis spectra were recorded on a Hewlett Packard 8453 single beam spectrophotometer in a 1.0 cm path length quartz cuvette with H_2O as background. Bubble counting data was processed according to reported procedure.[80]

CATALYSIS

Stock solutions of cage (12.6 mM) and AM (12.6 mM) in H_2O were prepared. The desired volume of H_2O (total volume of 250 µL), cage solution (25 µL, 0.31 µmol, 2.5 mol%), and neat ligand (1.1 µL, 1.01 mg, 6.25 µmol, 50 mol%) were mixed in a 4 mL vial. AM solution (25 µL, 0.31 µmol, 2.5 mol%) then neat substrate **1** (2.8 µL, 3.0 mg, 12.5 µmol, 1 eq) were added, and the vial was capped and stirred at 37 °C for 2 h. 0.8 mL of a 10 mM solution of 1,3,5-trimethoxybenzene in toluene-d8 was added, and the vial was shaken. The organic layer was decanted to an NMR tube and measured. The yields of the product were determined by ^1H NMR spectroscopy relative to 1,3,5-trimethoxybenzene as internal standard.

KINETIC MEASUREMENTS WITH THE BUBBLE COUNTER

Cage (24 mg, 6.88 µmol, 2.5 mol%) was added to a 10 mL vial and dissolved in H_2O (5 mL) which was placed in the bubble counter (see ref [79] for bubble counter set-up). The vial was then pre-heated to 37 °C while purging the vial with N_2. After stabilisation of the temperature, neat ligand was injected through the septum in the reactor head. Then, a 13.76 mM solution of AM in H_2O (6.88 µmol, 0.5 mL, 2.5 mol%) was added via capillary, then neat substrate (63 µL, 69 mg, 275 µmol, 1 eq) was added via septum. The reaction mixture was stirred at 37 °C until no further bubbles were produced. 1 mL of a 0.25 M solution of 1,3,5-trimethoxybenzene in toluene-d8 was added, and the vial was shaken. The organic layer was decanted to an NMR tube and measured. The yield of the product was determined by ^1H NMR spectroscopy relative to 1,3,5-trimethoxybenzene as internal standard.

AQUAMET DECOMPOSITION

Spectra of a 100 µM solution of AquaMet (3 mL) with and without cage (1 eq) in H_2O were recorded at 37 °C every 2 min for 1 h.

CATALYST ENCAPSULATIONS

Under an atmosphere of N_2, to a 2.5 mM solution of cage in D_2O was added 3 eq of catalyst as a 15 mM solution in DCM. The mixture was stirred vigorously for 2 h at room temperature.

The DCM was then removed *in vacuo* by bubbling N_2 through the solution, and the resultant precipitate was removed by filtration over a syringe filter. Yield of encapsulation was determined by ^{1}H NMR spectroscopy by the ratio of empty cage peaks to new cage peaks.

REFERENCES

[1] R. H. Grubbs, S. Chang, *Tetrahedron* **1998**, 54, 4413-4450.
[2] T. M. Trnka, R. H. Grubbs, *Acc. Chem. Res* **2001**, 34, 18-29.
[3] M. R. Becker, R. B. Watson, C. S. Schindler, *Chem. Soc. Rev.* **2018**, 47, 7867-7881.
[4] A. H. Hoveyda, A. R. Zhugralin, *Nature* **2007**, 450, 243-251.
[5] A. Deiters, S. F. Martin, *Chem. Rev.* **2004**, 104, 2199-2238.
[6] I. Nakamura, Y. Yamamoto, *Chem. Rev.* **2004**, 104, 2127-2198.
[7] S. Kotha, M. Meshram, Y. Dommaraju, *Chem. Rec.* **2018**, 18, 1613-1632.
[8] R. H. Grubbs, *Tetrahedron* **2004**, 60, 7117-7140.
[9] M. L. Gringolts, Y. I. Denisova, E. S. Finkelshtein, Y. V. Kudryavtsev, *Beilstein J. Org. Chem.* **2019**, 15, 218-235.
[10] A. Fürstner, *Chem. Commun.* **2011**, 47, 6505-6511.
[11] K. C. Nicolaou, P. G. Bulger, D. Sarlah, *Angew. Chem. Int. Ed.* **2005**, 44, 4490-4527.
[12] H. C. M. a. S. B. William, *Curr. Top. Med. Chem.* **2005**, 5, 1521-1540.
[13] M. Tyagi, F. Begnini, V. Poongavanam, B. C. Doak, J. Kihlberg, *Chem.–Eur. J.* **2020**, 26, 49-88.
[14] A. C. Flick, C. A. Leverett, H. X. Ding, E. McInturff, S. J. Fink, C. J. Helal, C. J. O'Donnell, *J. Med. Chem.* **2019**, 62, 7340-7382.
[15] M. Yu, S. Lou, F. Gonzalez-Bobes, *Org. Process Res. Dev.* **2018**, 22, 918-946.
[16] C. S. Higman, J. A. M. Lummiss, D. E. Fogg, *Angew. Chem. Int. Ed.* **2016**, 55, 3552-3565.
[17] D. O. Ponkratov, A. S. Shaplov, Y. S. Vygodskii, *Polym. Sci. Ser. C* **2019**, 61, 2-16.
[18] D. Burtscher, K. Grela, *Angew. Chem. Int. Ed.* **2009**, 48, 442-454.
[19] J. Tomasek, J. Schatz, *Green Chem.* **2013**, 15, 2317-2338.
[20] P. A. Thomas, B. B. Marvey, *Molecules* **2016**, 21, 16.
[21] N. Rios-Lombardia, J. Garcia-Alvarez, J. Gonzalez-Sabin, *Catalysts* **2018**, 8, 28.
[22] L. Piola, F. Nahra, S. P. Nolan, *Beilstein J. Org. Chem.* **2015**, 11, 2038-2056.
[23] S. J. Ton, D. E. Fogg, *ACS Catal.* **2019**, 9, 11329-11334.
[24] J. Tomasek, M. Seßler, H. Gröger, J. Schatz, *Molecules* **2015**, 20, 19130-19141.
[25] B. M. Novak, R. H. Grubbs, *J. Am. Chem. Soc.* **1988**, 110, 7542-7543.
[26] S. J. Connon, M. Rivard, M. Zaja, S. Blechert, *Adv. Synth. Catal.* **2003**, 345, 572-575.
[27] A. Michrowska, Ł. Gułajski, Z. Kaczmarska, K. Mennecke, A. Kirschning, K. A. Grela, *Green Chem.* **2006**, 8, 685-688.
[28] K. Skowerski, G. Szczepaniak, C. Wierzbicka, Ł. Gułajski, M. Bieniek, K. Grela, *Catal. Sci. Technol.* **2012**, 2, 2424-2427.
[29] A. H. Ngo, S. Bose, L. H. Do, *Chem.–Eur. J.* **2018**, 24, 10584-10594.
[30] M. S. Messina, H. D. Maynard, *Mater. Chem. Front.* **2020**, 4, 1040-1051.
[31] T. Matsuo, *Catalysts* **2021**, 11, 359.
[32] A. Boto, C. C. González, D. Hernández, I. Romero-Estudillo, C. J. Saavedra, *Org. Chem. Front.* **2021**, 8, 6720-6759.
[33] Y. A. Lin, J. M. Chalker, B. G. Davis, *ChemBioChem* **2009**, 10, 959-969.
[34] Y. A. Lin, O. Boutureira, L. Lercher, B. Bhushan, R. S. Paton, B. G. Davis, *J. Am. Chem. Soc.* **2013**, 135, 12156-12159.
[35] J. M. Chalker, Y. A. Lin, O. Boutureira, B. G. Davis, *Chem. Commun.* **2009**, 3714-3716.
[36] A. Brik, *Adv. Synth. Catal.* **2008**, 350, 1661-1675.
[37] Y. G. Bai, J. F. Chen, S. C. Zimmerman, *Chem. Soc. Rev.* **2018**, 47, 1811-1821.
[38] S. Alonso-de Castro, A. Terenzi, J. Gurruchaga-Pereda, L. Salassa, *Chem.–Eur. J.* **2019**, 25, 6651-6660.

[39] S.-Y. Jang, D. P. Murale, A. D. Kim, J.-S. Lee, *ChemBioChem* **2019**, 20, 1498-1507.
[40] M. Martínez-Calvo, J. L. Mascareñas, *Coord. Chem. Rev.* **2018**, 359, 57-79.
[41] J. J. Soldevila-Barreda, N. Metzler-Nolte, *Chem. Rev.* **2019**, 119, 829-869.
[42] M. Jeschek, R. Reuter, T. Heinisch, C. Trindler, J. Klehr, S. Panke, T. R. Ward, *Nature* **2016**, 537, 661.
[43] S. Eda, I. Nasibullin, K. Vong, N. Kudo, M. Yoshida, A. Kurbangalieva, K. Tanaka, *Nat. Catal.* **2019**, 2, 780-792.
[44] V. Sabatino, T. R. Ward, *Beilstein J. Org. Chem.* **2019**, 15, 445-468.
[45] T. Brendgen, T. Fahlbusch, M. Frank, D. T. Schühle, M. Seßler, J. Schatz, *Adv. Synth. Catal.* **2009**, 351, 303-307.
[46] L. Laville, C. Charnay, F. Lamaty, J. Martinez, E. Colacino, *Chem.–Eur. J.* **2012**, 18, 760-764.
[47] J. B. Binder, J. J. Blank, R. T. Raines, *Organic Letters* **9**, 4885-4888 (2007).
[48] K. Skowerski, J. Białecki, A. Tracz, T. K. Olszewski, *Green Chem.* **2014**, 16, 1125-1130.
[49] Ł. Gułajski, A. Tracz, K. Urbaniak, S. J. Czarnocki, M. Bieniek, T. K. Olszewski, *Beilstein J. Org. Chem.* **2019**, 15, 160-166.
[50] J. C. Foster, S. Varlas, L. D. Blackman, L. A. Arkinstall, R. K. O'Reilly, *Angew. Chem. Int. Ed.* **2018**, 57, 10672-10676.
[51] D. M. Lynn, B. Mohr, R. H. Grubbs, *J. Am. Chem. Soc.* **1998**, 120, 1627-1628.
[52] M. Kim, M.-S. Eum, M. Y. Jin, K.-W. Jun, C. W. Lee, K. A. Kuen, C. H. Kim, C. S. Chin, *J. Organomet. Chem.* **2004**, 689, 3535-3540.
[53] A. Y. Goudreault, D. M. Walden, D. L. Nascimento, A. G. Botti, S. N. Steinmann, C. Michel, D. E. Fogg, *ACS Catal.* **2020**, 10, 3838-3843.
[54] J. C. Foster, M. C. Grocott, L. A. Arkinstall, S. Varlas, M. J. Redding, S. M. Grayson, R. K. O'Reilly, *J. Am. Chem. Soc.* **2020**, 142, 13878-13885.
[55] B. Bhushan, Y. Y. A. Lin, M. Bak, A. Phanumartwiwath, N. Yang, M. K. Bilyard, T. Tanaka, K. L. Hudson, L. Lercher, M. Stegmann, *J. Am. Chem. Soc.* **2018**, 140, 14599-14603.
[56] W. L. McClennan, S. A. Rufh, J. A. M. Lummiss, D. E. Fogg, *J. Am. Chem. Soc.* **2016**, 138, 14668-14677.
[57] A. G. Santos, G. A. Bailey, E. N. dos Santos, D. E. Fogg, *ACS Catal.* **2017**, 7, 3181-3189.
[58] C. O. Blanco, J. Sims, D. L. Nascimento, A. Y. Goudreault, S. N. Steinmann, C. Michel, D. E. Fogg, *ACS Catal.* **2021**, 11, 893-899.
[59] B. J. Ireland, B. T. Dobigny, D. E. Fogg, *ACS Catal.* **2015**, 5, 4690-4698.
[60] D. L. Nascimento, I. Reim, M. Foscato, V. R. Jensen, D. E. Fogg, *ACS Catal.* **2020**, 10, 11623-11633.
[61] D. L. Nascimento, M. Foscato, G. Occhipinti, V. R. Jensen, D. E. Fogg, *J. Am. Chem. Soc.* **2021**, 143, 11072-11079.
[62] V. Thiel, K.-J. Wannowius, C. Wolff, C. M. Thiele, H. Plenio, *Chem.–Eur. J.* **2013**, 19, 16403-16414.
[63] G. A. Bailey, M. Foscato, C. S. Higman, C. S. Day, V. R. Jensen, D. E. Fogg, *J. Am. Chem. Soc.* **2018**, 140, 6931-6944.
[64] D. L. Nascimento, D. E. Fogg, *J. Am. Chem. Soc.* **2019**, 141, 19236-19240.
[65] T. Matsuo, T. Yoshida, A. Fujii, K. Kawahara, S. Hirota, *Organometallics* **2013**, 32, 5313-5319.
[66] D. C. Church, L. Takiguchi, J. K. Pokorski, *Polym. Chem.* **2020**, 11, 4492-4499.
[67] L. J. Jongkind, M. Rahimi, D. Poole Iii, S. J. Ton, D. E. Fogg, J. N. H. Reek, *ChemCatChem* **2020**, 12, 4019-4023.
[68] S. H. A. M. Leenders, R. Becker, T. Kumpulainen, B. de Bruin, T. Sawada, T. Kato, M. Fujita, J. N. H. Reek, *Chem.–Eur. J.* **2016**, 22, 15468-15474.

[69] M. Yoshizawa, J. K. Klosterman, M. Fujita, *Angew. Chem. Int. Ed.* **2009**, 48, 3418-3438.
[70] T. Murase, M. Fujita, *Chem. Rec.* 2010, 10, 342-347.
[71] S. Horiuchi, T. Murase, M. Fujita, *J. Am. Chem. Soc.* **2011**, 133, 12445-12447.
[72] F. Ibukuro, T. Kusukawa, M. Fujita, *J. Am. Chem. Soc.* **1998**, 120, 8561-8562.
[73] H. Takezawa, R. Tabuchi, H. Sunohara, M. Fujita, *J. Am. Chem. Soc.* **2020**, 142, 17919-17922.
[74] C. Bannwarth, S. Ehlert, S. Grimme, *J. Chem. Theory Comput.* **2019**, 15, 1652-1671.
[75] J. M. Bates, J. A. M. Lummiss, G. A. Bailey, D. E. Fogg, *ACS Catal.* **2014**, 4, 2387-2394.
[76] M. Bieniek, A. Michrowska, D. L. Usanov, K. Grela, *Chem.–Eur. J.* **2008**, 14, 806-818.
[77] S. B. Garber, J. S. Kingsbury, B. L. Gray, A. H. Hoveyda, *J. Am. Chem. Soc.* **2000**, 122, 8168-8179.
[78] J. S. Kingsbury, J. P. A. Harrity, P. J. Bonitatebus, A. H. Hoveyda, *J. Am. Chem. Soc.* **1999**, 121, 791-799.
[79] T. K. Slot, N. R. Shiju, G. Rothenberg, *Angew. Chem. Int. Ed.* **2019**, 58, 17273-17276.
[80] T. K. Slot, N. Riley, N. R. Shiju, J. W. Medlin, G. Rothenberg, *Chem. Sci.* **2020**, 11, 11024-11029.
[81] T. Kusukawa, M. Fujita, *J. Am. Chem. Soc.* **2002**, 124, 13576-13582.
[82] J. A. Love, J. P. Morgan, T. M. Trnka, R. H. Grubbs, *Angew. Chem. Int. Ed.* **2002**, 41, 4035-4037.
[83] K. Vehlow, S. Maechling, S. Blechert, *Organometallics* **2006**, 25, 25-28.
[84] T. S. Ahmed, J. M. Grandner, B. L. H. Taylor, M. B. Herbert, K. N. Houk, R. H. Grubbs, *Organometallics* **2018**, 37, 2212-2216.

Chapter 5

Kinetic Protection of a Water Soluble Olefin Metathesis Catalyst for Potential Use Under Biological Conditions

ABSTRACT

Olefin metathesis catalysts are vulnerable to many different decomposition pathways under biologically relevant conditions. In the previous chapter we showed that the water soluble metathesis catalyst AquaMet cannot be protected from these decomposition pathways by protection in a supramolecular cage. In this chapter we show that kinetic protection of AquaMet from biological conditions can be achieved by generating a new nitrate-containing catalyst. Analysis by mass spectrometry and kinetic studies monitored by UV/Vis spectroscopy and bubble counting data show that replacing the chloride ligands of the AquaMet with nitrate ligand generates a new nitrate catalyst which both initiates faster and performs catalysis at a much faster rate than AquaMet. Catalytic studies into the ring closing metathesis of a diallyl substrate show that the nitrate catalyst is able to generate higher yields of the ring-closed product compared to AquaMet, both in water and under biological conditions. This is explained by the relative rate of the catalysis reaction compared to the rates of the decomposition pathways. This new strategy of kinetic protection of a transition metal catalyst may have future applications for other catalytic reactions applied in vivo.

INTRODUCTION

Olefin metathesis provides access to a wide variety polymers,[1] small molecules,[2] and cyclic compounds.[3-5] Accomplishing efficient olefin metathesis *in vivo* is of great interest for applications in prodrug activation, *in situ* drug synthesis, and biomolecule labelling.[6-9] Indeed, the value of this transformation has already been demonstrated in the field of protein labelling,[7, 10-13] and for the synthesis of small coumarin-based compounds inside cancer cells.[14, 15] However, the cellular environment poses a substantial threat to the activity of metathesis catalysts, as catalyst decomposition can readily occur through several deactivation pathways. Cells contain large quantities of metal-binding biomolecules, such as glutathione (GSH), a thiol found in 2–10 mM concentrations in cells,[16] and L-histidine (His), an imidazole-containing amino acid, which can readily deactivate metal catalysts by strong binding to the metal centre, resulting in low catalytic activity.[6, 17-21] However, this is not the only deactivation pathway which can inhibit metathesis catalysts. The cytoplasm of cells is an aqueous environment, and, particularly at low catalyst loadings, ruthenium based olefin metathesis catalysts are highly sensitive to the presence of even low quantities of water.[22, 23] The rate of catalyst initiation is lowered,[24, 25] and the chlorides readily dissociate from the ruthenium centre,[26] followed by coordination of hydroxide ions to generate Ru-$(OH)_n$ species, which are completely inactive in metathesis and rapidly decompose via loss of the carbene ligand.[27-30] Moreover, during the catalytic cycle a base-sensitive metallocyclobutane intermediate is formed. Therefore the presence of basic biomolecules may result in deprotonation of this cyclic intermediate, resulting in decomposition of the intermediate and subsequent formation of a species which is not active in metathesis.[30-32] Finally, metathesis catalysts are also susceptible to bimolecular decomposition pathways involving dimerization of the ruthenium centres.[33-36]

Several strategies have been employed to overcome these deactivation reactions. In the two reported examples of *in vivo* olefin metathesis, biomolecule poisoning is prevented by incorporating the catalyst inside the cavity of an artificial metalloenzyme. In addition, the rate of catalyst decomposition in water can be reduced by addition of Brønsted acids to remove hydroxide ions from solution,[25] or by addition of chloride salts to prevent the chloride displacement.[28, 37, 38] It has also been shown that cationic metathesis catalysts can be protected against bimolecular decomposition pathways in organic solvent by encapsulating the complex inside a supramolecular host.[39] In Chapter 3 we attempted catalyst encapsulation in a water soluble supramolecular cage, but it was demonstrated that encapsulation in $[Pt_6L_4](NO_3)_{12}$ type cages does not occur and the cage itself does not influence the reaction. Instead, initial experiments show that the presence of the nitrate counterions of the cage greatly improved the reactivity of AquaMet (**AM**) in water, as a much faster reaction rate was observed in the presence of nitrate salt compared to without. Although nitrate-containing catalysts have previously been reported to afford good reactivity in organic solvents,[40-42] often for Z-selective metathesis,[43-46] to the best of our knowledge there have been no reports of the use of nitrate to improve the reactivity of ruthenium complexes in aqueous olefin metathesis. We hypothesised that we could use the fast reaction kinetics to our advantage for application under biological conditions: if the presence of nitrate increases the rate of catalysis such that it

becomes faster than the rates of the decomposition reactions, then the reactivity of **AM** could be improved simply by the presence of a nitrate salt as additive. We therefore investigated if the metathesis activity of **AM** under biological conditions could be improved by using nitrate to bestow kinetic protection upon the catalyst.

RESULTS AND DISCUSSION

FORMATION OF THE NITRATE CATALYST

The ring closing metathesis of substrate **1** was selected as a model reaction to investigate the effects of nitrate upon the metathesis activity of **AM** (Figure 1). Previous experiments had shown that **AM** generated only an 18% yield of ring closed product **2** in water, but that this yield was drastically improved to 76% by the presence of 12 eq of KNO_3 with respect to **AM**. We hypothesised that the origin of the improved activity in the presence of KNO_3 was due to binding of nitrate to the ruthenium centre, perhaps by displacing one or both of the chlorides from the **AM**, thereby generating a new nitrate catalyst, **NO_3-AM**. An aqueous solution of **AM** was mixed with an aqueous solution containing an excess of KNO_3 and analysed by electrospray ionisation high resolution mass spectrometry (ESI-HRMS). Two monocationic ruthenium species containing nitrate were observed (Figure E11 and Figure E12): a peak at 794.3120 which corresponds to the **AM** complex with one of the chlorides replaced by a nitrate, $[(IMes)(iPrOstyrene)RuCl(NO_3)]^+$; and a peak at 821.3313 which corresponds to the **AM** complex with no chlorides and two nitrates present, $[(IMes)(iPrOstyrene)Ru(NO_3)_2]^+$. This shows that when **NO_3-AM** is generated from **AM** and KNO_3 a mixture of nitrate-containing species are formed. For the $[(IMes)(iPrOstyrene)RuCl(NO_3)]^+$ species, only one of the chlorides has been replaced by a nitrate ligand, with the other still bound to the ruthenium. For the $[(IMes)(iPrOstyrene)Ru(NO_3)_2]^+$ species, both of the chlorides have been replaced by two nitrate ligands. There are several possibilities as to the exact structures of the complexes. It has been shown for nitrate-containing complexes soluble in organic solvents that the nitrate can be bound to the ruthenium centre in either a monodentate[40, 42] or bidentate[41, 43-46] fashion, as depicted in Figure 1. It is likely that in both cases the nitrate would be present as a monodentate ligand, as this would result in less steric crowding around the ruthenium centre, although a bidentate nitrate ligand could also be possible. These possible structures are illustrated in Figure 1. Rapid decomposition of the complex in aqueous solution upon the addition of KNO_3 to **AM** was observed, resulting in the formation of insoluble brown precipitates which could not be analysed by NMR spectroscopy. Therefore it was not possible to isolate the **NO_3-AM** complex in order to determine the exact structure of the catalyst.

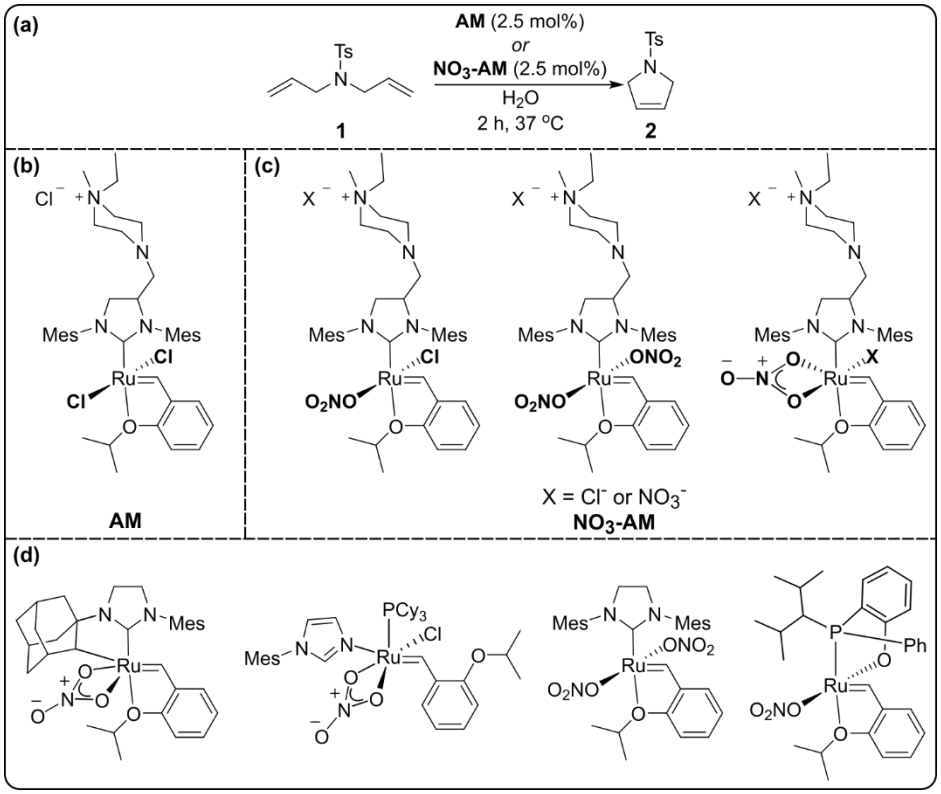

Figure 1. (a) Ring closing metathesis of substrate **1** by **AM** or **NO_3-AM**. (b) Structure of **AM**. (c) Possible structures of **NO_3-AM**. (d) Structures of nitrate-containing metathesis catalysts which are soluble in organic solvents in the literature (refs 40–46).

As the **NO_3-AM** catalyst cannot be isolated, it needs to be generated *in situ* by mixing KNO_3 with **AM** just before the start of the catalysis. Therefore we investigated the optimum amount of nitrate to add in order to obtain the greatest improvement in yield of product **2** (Figure 2). To this end the ring closing metathesis of substrate **1** was carried out in the presence of 2–160 eq of KNO_3 with respect to **AM** in water. The addition of 24 eq of KNO_3 gave a total yield of 83% of product **2**. Increasing the equivalents of nitrate salt beyond this value did not substantially increase the yield beyond this value. Therefore, all further studies were carried out with 24 eq of nitrate.

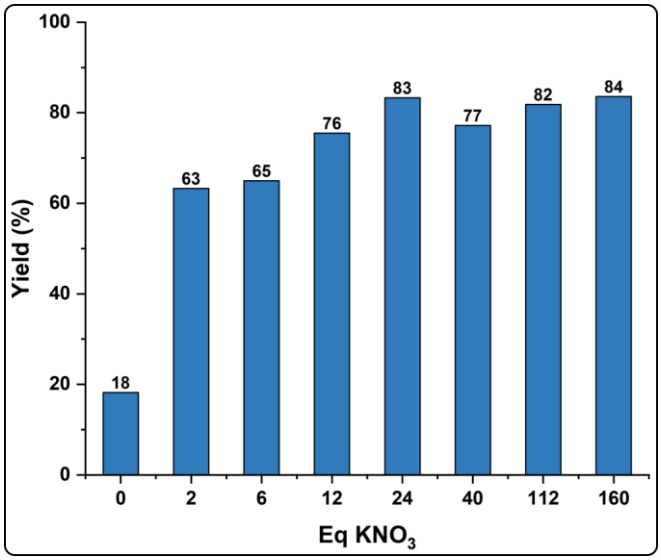

Figure 2. Yield of ring closed product **2** with increasing equivalents of KNO_3 with respect to **AM**. Conditions: 2.5 mol% **AM**, KNO_3 (x equivalents with respect to **AM**), 50 mM substrate **1**, H_2O, 37 °C, 2 h. Yields determined by ^1H NMR spectroscopy relative to 1,3,5-trimethoxybenzene as internal standard.

KINETIC STUDIES

We hypothesised that there are several possibilities as to the origin of the superior rate and yields achieved by the **NO_3-AM** catalyst compared to **AM**. It is known that **AM** is highly vulnerable to various decomposition pathways in the presence of water, so therefore it is possible that the nitrate complex formed is simply more stable than its chloride analogue. This would make the **NO_3-AM** catalyst less susceptible to decomposition and therefore it would result in a higher concentration of active catalyst in solution. What is also important to consider is that **NO_3-AM** and **AM** are pre-catalysts: in both cases the isopropoxystyrene ligand must first be replaced by a substrate molecule to enter the catalytic cycle. The rate of this initiation step is dependent on the dissociation of the ether moiety from the ruthenium centre, a step which is known to be dependent on the structure of the catalyst. Therefore another possible reason for the better reactivity is that **NO_3-AM** is able to initiate faster. Faster initiation would mean that the active species is generated more quickly during the reaction, meaning that more catalytic cycles can take place before the complex is decomposed by the aqueous environment compared to a slower initiating catalyst over the same time frame. Alternatively, **NO_3-AM** may simply be a more active catalyst than its chloride counterpart, which effectively means that it produces more product if the decomposition rates are the same.

In order to gain insight into the comparative stability of **NO_3-AM** and **AM**, the fate of the pre-catalysts was monitored by UV/Vis spectroscopy over time (Figure 3). The decomposition of metathesis catalysts can be monitored by following the decrease in absorption of the MLCT band in the visible region;[28] for **AM** this band is found at 370 nm. When left in solution for 1 h at 37 °C, a steady decrease in the intensity of this peak is observed, from an absorbance of 0.93 down to 0.38, which was accompanied by two sharp isosbestic points at 319 and 427 nm. When **NO_3-AM** was subjected to the same conditions, the MLCT band in the first spectrum recorded was shifted compared to **AM**, with absorption at 376 nm.

However, in the second spectrum measured 2 min later, and in all subsequent spectra, this peak was shifted to 370 nm, the same wavelength observed as for **AM**, and again a similar decrease in absorption at this wavelength from 0.85 to 0.31 was accompanied with the appearance of sharp isosbestic points at 319 and 427 nm. Therefore it appears that **NO_3-AM** is readily decomposed in the presence of water to give the same decomposition product as **AM**. This indicates that the stability of the catalyst towards decomposition is largely unaffected by the nature of the anionic ligand, as both the nitrate and chloride complexes resulted in similar decomposition rate profiles.

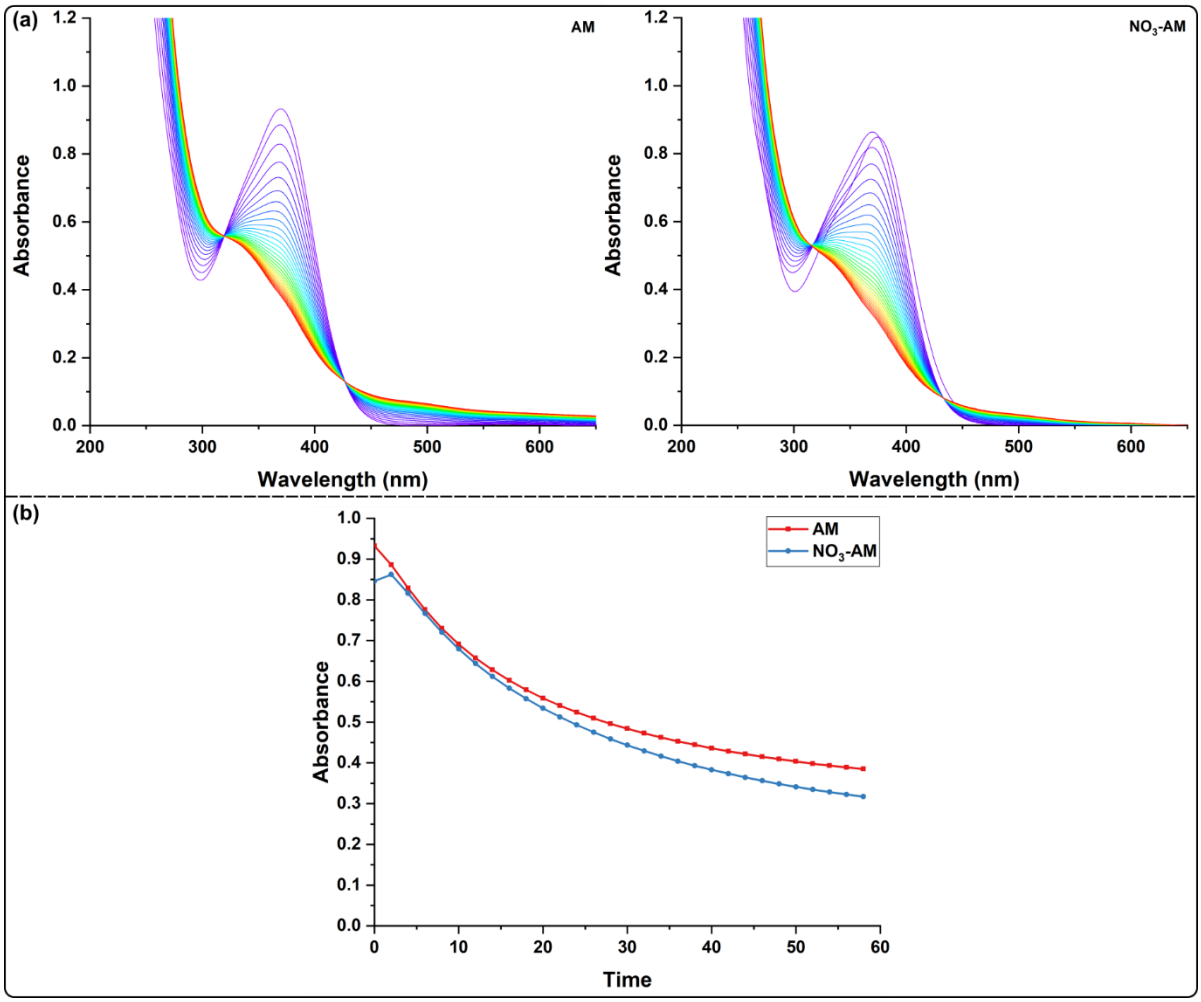

Figure 3. (a) UV/Vis spectra of **AM** and **NO_3-AM** pre-catalysts in H_2O at 37 °C over 1 h. (b) Change in absorbance at 370 nm for **AM** and **NO_3-AM** in H_2O at 37 °C over 1 h.

Having established that the pre-catalysts exhibit similar stabilities, the behaviour of the active species under catalytic conditions was then investigated. Insight into the active species can be obtained by UV/Vis spectroscopy, as the decrease in absorption of the MLCT band also corresponds to initiation of the pre-catalyst, as well to decomposition.[47] The catalysts were mixed with substrate **1** in water stirred at 37 °C, with samples measured every 5 min (Figure 4). The decrease in absorption of the MLCT band at 372 nm for **NO_3-AM** was much steeper than for **AM**: the absorption for **NO_3-AM** decreased from 1.18 to 0.35 after a total reaction time of 1 h; however the absorption for **AM** only decreased from 1.21 to 0.51. Since both the

AM and **NO_3-AM** pre-catalysts displayed similar decomposition profiles, the larger decrease in the MLCT band for **NO_3-AM** under catalytic conditions suggests that the initiation rate of the nitrate complex is higher than that of **AM**. To confirm this hypothesis, the rate of product formation was determined by following the amount of ethene produced using a bubble counter.[48-49] As described previously in chapter 3, the amount of ethene produced can be equated to the amount of product formed. The kinetic profiles of the ring closing metathesis of substrate **1** by both **AM** and **NO_3-AM** were determined in water (Figure 5). In the bubble counter, **AM** in water was able to generate **2** in a 12% yield. A short incubation time of around 3 min was observed, before a maximum turnover frequency (TOF) of 252 μmol ethene mol cat^{-1} min^{-1} at 13 min was obtained. In contrast, **NO_3-AM** generated product **2** almost immediately from the start of the reaction. A 31% final yield of **2** was obtained, with a much higher TOF of 3121 μmol ethene mol cat^{-1} min^{-1} achieved after only 1.5 min. In both cases, the final yield was obtained after 1 h, at which point the catalyst was fully deactivated. This was confirmed as the addition of fresh substrate after 1 h did not lead to more product formation. The lack of incubation time for **NO_3-AM** again points to the catalyst being faster at initiating than **AM**, which is in line with the UV/Vis experiments. The kinetic profile was also determined for an experiment where the KNO_3 was added to the reaction 10 minutes after the reaction was started. The TOF increased almost immediately from 213 to 3519 μmol ethene mol cat^{-1} min^{-1} upon addition of an aqueous solution of KNO_3, giving a final yield of 47% of product **2** after a total reaction time of 1.5 h. The fact that this rapid improvement in TOF is also observed when KNO_3 is added even after the **AM** pre-catalyst has already initiated implies that formation of **NO_3-AM** not only improves the initiation of the catalyst in comparison to **AM**, but also drastically improves the catalytic activity of the active species.

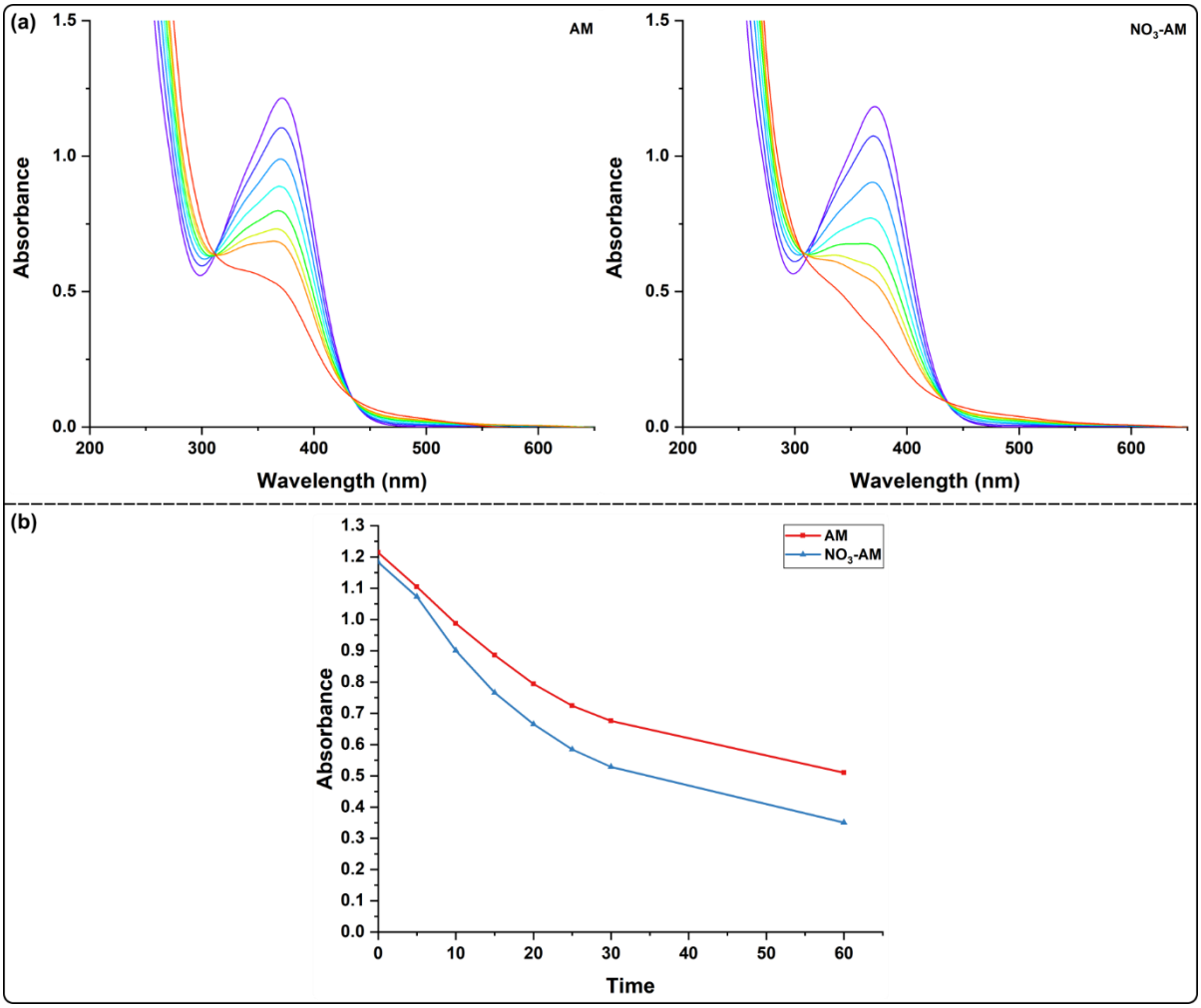

Figure 4. (a) UV/Vis spectra of 2.5 mol% **AM** and 2.5 mol% **NO_3-AM** during ring closing metathesis of substrate **1** in H_2O at 37 °C over 1 h. (b) Change in absorbance at 370 nm for 2.5 mol% **AM** and 2.5 mol% **NO_3-AM** during ring closing metathesis of substrate **1** in H_2O at 37 °C over 1 h.

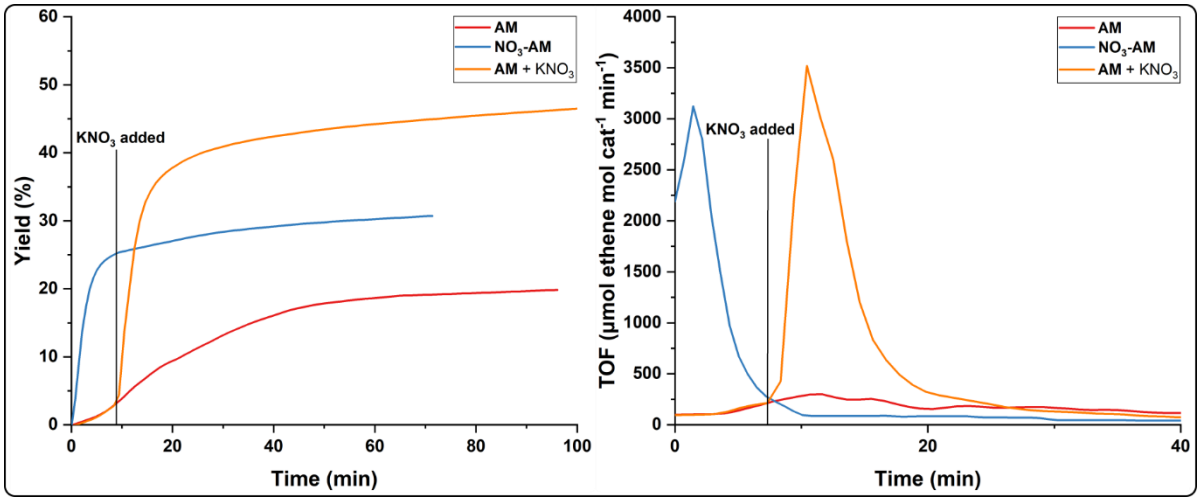

Figure 5. Yield and TOF of ring closing metathesis of substrate **1** in the bubble counter in H_2O. Red line: **AM** was used as the catalyst. Blue line: **NO_3-AM** was used as the catalyst by pre-mixing 24 eq KNO_3 with **AM** before addition of substrate **1**. Orange line: **AM** was used as the catalyst, and KNO_3 was added approximately 10 min after the start of the reaction. Conditions: 50 mM substrate **1**, 2.5 mol% **AM** or **NO_3-AM**, 60 mol% KNO_3, H_2O, 37 °C.

Catalysis Under Biological Conditions

We next explored whether this improvement in initiation and catalytic activity could be translated to better performance under biological conditions. Therefore catalysis was carried out in the presence of metal binding biomolecules. Standard reactions were performed in the presence of a) 1 eq GSH b) 1 eq His with respect to the catalyst, and c) in PBS buffer. Both the effect on the performance of **AM** and **NO_3-AM** was probed by using substrate **1** (Figure 6). When **NO_3-AM** was used as catalyst in the presence of GSH and His yields of 78% and 67% were obtained respectively. These additives did not substantially decrease the yield compared to the reaction in water (83%). When **AM** was used as a catalyst a 24% yield was observed in the presence of GSH and a 27% yield in the presence of His. Interestingly, the presence of these additives resulted in an increased yield compared to the reaction in water without additives (18%). Performing the reaction in PBS buffer resulted in a 59% yield when **NO_3-AM** was catalyst and an 11% yield when **AM** was catalyst. Therefore PBS buffer had a clear inhibiting affect upon catalysis, regardless of the catalyst used. Since PBS buffer contains a high concentration of chlorides (140 mM), it is expected that chloride competes with the nitrate for binding to the ruthenium centre, and therefore the reduced yield for **NO_3-AM** may be due to the fact that generation of the more active nitrate species is less favoured and that a larger proportion of the catalyst remains as its bis-chloride **AM** form than in it does in water. Although the concentration of intracellular chlorides is rather low (around 5 mM), the concentration of extracellular chlorides is around 120 mM, so replacement of the nitrate ligands for chlorides may be a problem during incubation of the catalyst with cells.[50] Phosphates are also present in PBS buffer, and these may also induce catalysis inhibition.

Next we investigated the performance of the catalysts in the presence of the biological additives combined, as they are in cells. **AM** was only able to generate product **2** in a 5% yield in the presence of the mixture of GSH, His and PBS. In contrast, **NO_3-AM** in the presence of

these inhibitory additives was still able to generate product **2** in a 42% yield. The catalytic efficiency of both **AM** and **NO_3-AM** is greatly reduced under these conditions compared to their reactivity in water. However, the yield obtained when **NO_3-AM** was catalyst is a huge improvement in yield not only compared to **AM** in the presence of biological additives, but also compared to **AM** in water. Therefore, the fast reaction kinetics achieved by **NO_3-AM** allows the catalyst to not only overcome decomposition by water, but also decomposition by biomolecule poisoning.

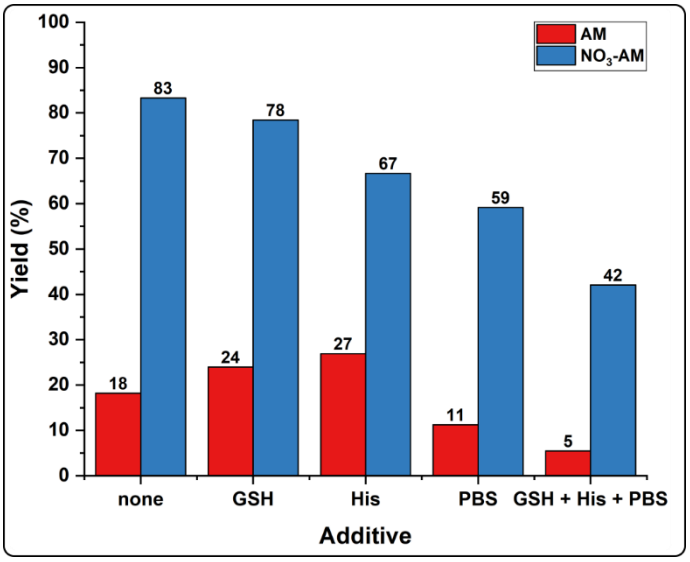

Figure 6. Yield of ring closed product **2** by **AM** (red) or **NO_3-AM** (60% KNO_3, blue) in water (no additive) or in the presence of biological additives. Conditions: 2.5 mol% **AM** or **NO_3-AM** (60 mol% KNO_3), 50 mM substrate **1**, 2.5 mol% GSH, 2.5 mol% His, H_2O or PBS, 37 °C, 2 h. Yields determined by ^{1}H NMR spectroscopy relative to 1,3,5-trimethoxybenzene as internal standard.

Next, kinetic studies were carried out in the presence of biological additives in order to confirm that the reason for improved yield in the presence of KNO_3 under biological conditions is also due to enhancement of the reaction rate. The stability of the pre-catalysts in the presence of the biological additives was monitored by UV/Vis spectroscopy. Spectra were recorded over 1 h of aqueous solutions of **AM** and **NO_3-AM** at 37 °C in PBS in the presence of 1 eq of GSH and 1 eq of His with respect to the catalyst (Figure 7). In both cases, in the first spectrum recorded the absorbance of the MLCT bands at 375 and 370 nm respectively had already decreased to around 0.2, and thereafter steadily increased in absorption to around 0.3. As was observed for the pre-catalysts in water, the resultant spectra observed were the same for both **AM** and **NO_3-AM**. It is likely that the rapid initial disappearance of the MLCT band was due to immediate biomolecule binding, as the soft ruthenium centre is likely to bind strongly to the soft sulfur atom of GSH. Therefore the stability of the pre-catalysts was confirmed to not be dependent upon the presence of nitrate in the presence of biological additives, as was the case for the pre-catalysts in water. The behaviour of the complexes under catalytic conditions was then observed in order to determine whether or not catalyst initiation also followed the same trend under biological conditions as in water. The catalysts were mixed with substrate **1** in PBS in the presence of 1 eq GSH and 1 eq His with respect to catalyst and stirred at 37 °C, with samples measured every 5 min by UV/Vis spectroscopy (Figure 8). While for **AM** the

absorption at 370 nm decreased from 0.59 to 0.47, the absorption for **NO_3-AM** decreased from 0.62 to 0.43. Interestingly, the decrease in absorption for both catalysts followed the same profile for the first 25 min, after which **NO_3-AM** decreased more steeply than **AM**. The fact that the decomposition rate profiles are the same for both catalysts during this initial timeframe of the reaction, indicates that under biological conditions there may not be a large difference between the catalysts in the rate of initiation. Catalysis was therefore carried out in the bubble counter to gain better insight into the difference in activity of the active catalysts (Figure 9). Both catalysts were again mixed with 1 eq GSH and 1 eq His with respect to catalyst in a PBS/H_2O mixture in the presence of substrate **1** at 37 °C. When **AM** was used as a catalyst, after 2 h no bubbles were detected. At this time the reaction mixture was extracted into touene-d8 and measured by ^{1}H NMR spectroscopy. Only peaks corresponding to substrate **1** were observed in the ^{1}H NMR spectrum, indicating that the presence of biological additives completely prevented the formation of **2**. In contrast, when **NO_3-AM** was catalyst product 2 was generated in a 12% yield in the presence of biological additives, with a maximum TOF of 797 μmol ethene mol cat^{-1} min^{-1} within the first minute of the reaction. This immediate spike in TOF implies that **NO_3-AM** is indeed still able to initiate faster under biologically relevant conditions than **AM** in water. The kinetic profile was again determined when KNO_3 was added 10 minutes after the start of the reaction under biological conditions. The TOF immediately increased from 62 to 726 μmol ethene mol cat^{-1} min^{-1} upon addition of KNO_3 and a final yield of 20% of product **2** was obtained after a total reaction time of 1.5 h. The delayed addition of KNO_3 resulted in a rapid increase in activity of the catalyst. Therefore it appears that under biological conditions the presence of nitrate increases the rate of ring closing metathesis of substrate **1** with **AM** by increasing the activity of the catalyst, and likely also improves the rate of initiation.

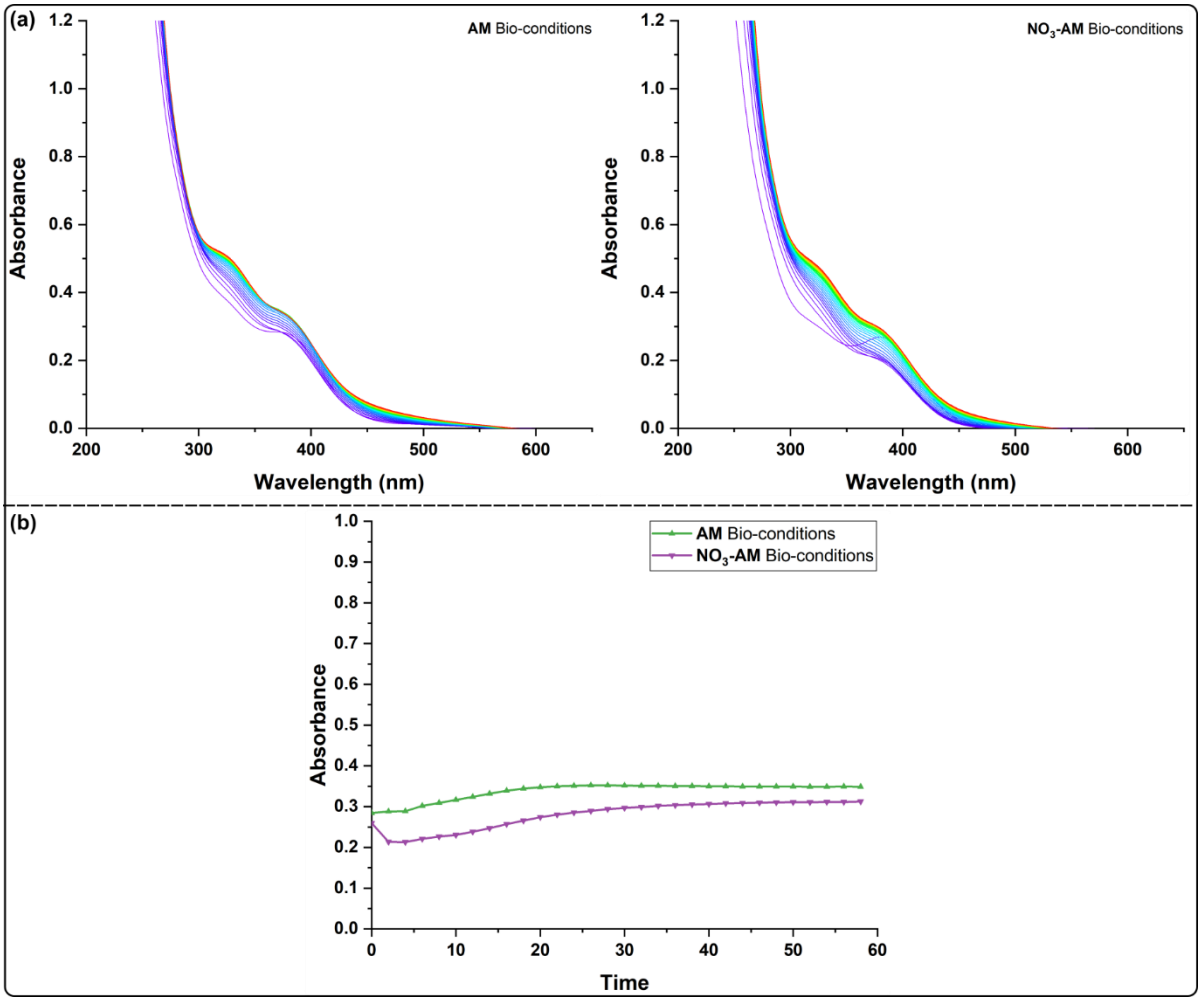

Figure 7. (a) UV/Vis spectra of **AM** and **NO_3-AM** pre-catalysts in PBS in the presence of 1 eq GSH and 1 eq His at 37 °C over 1 h. (b) Change in absorbance at 370 nm for **AM** and **NO_3-AM** in PBS in the presence of 1 eq GSH and 1 eq His at 37 °C over 1 h.

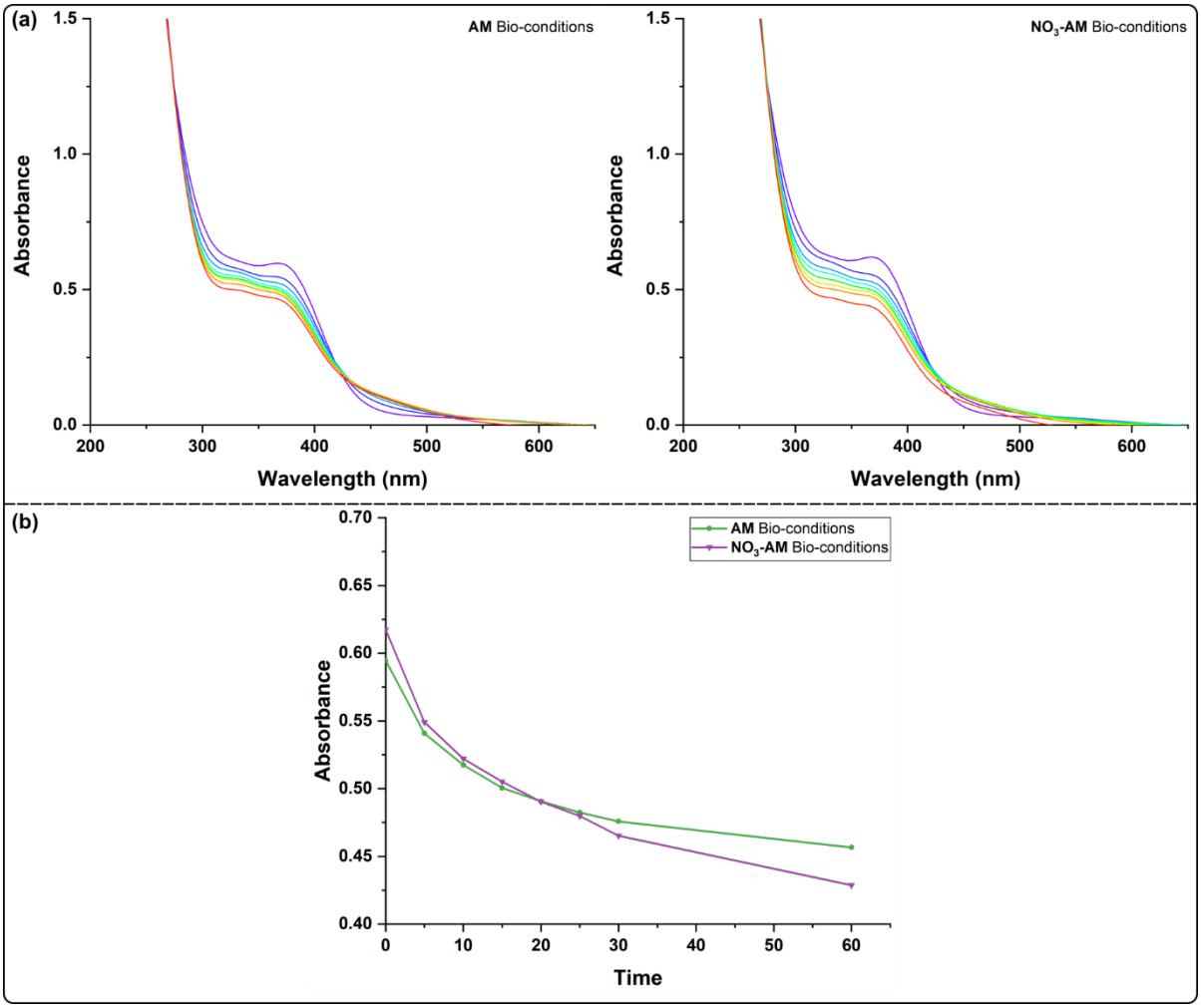

Figure 8. (a) UV/Vis spectra of 2.5 mol% **AM** and 2.5 mol% **NO_3-AM** during ring closing metathesis of substrate **1** in PBS/H_2O in the presence of 2.5 mol% GSH and 2.5 mol% His at 37 °C over 1 h. (b) Change in absorbance at 370 nm for 2.5 mol% **AM** and 2.5 mol% **NO_3-AM** during ring closing metathesis of substrate **1** in PBS/H_2O in the presence of 2.5 mol% GSH and 2.5 mol% His at 37 °C over 1 h.

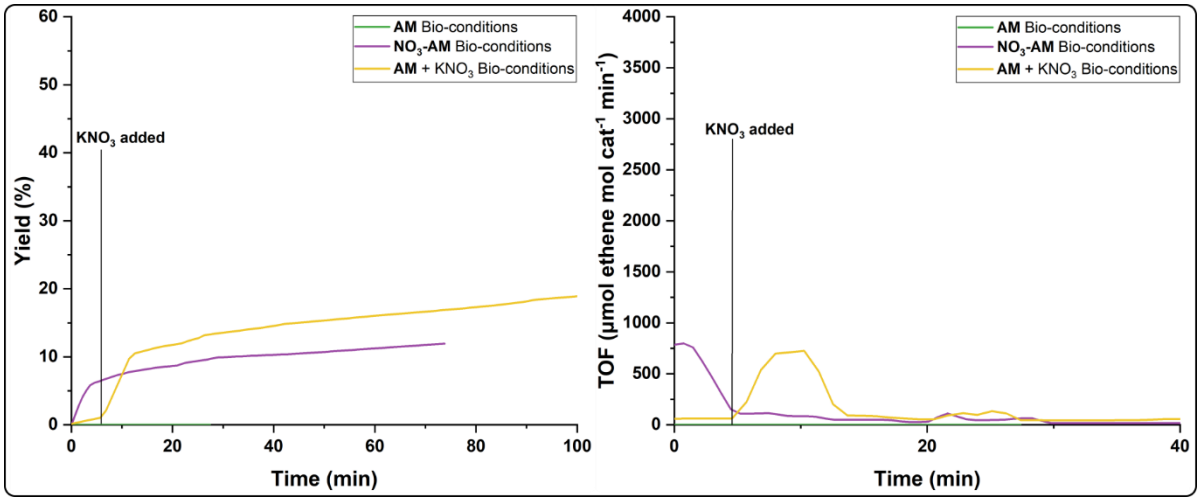

Figure 9. Yield and TOF of ring closing metathesis of substrate **1** in the bubble counter in the presence of a mixture of biological additives. Green line: **AM** was used as the catalyst. Purple line: **NO_3-AM** was used as the catalyst by pre-mixing 24 eq KNO_3 with **AM** before addition of the biological additives and substrate **1**. Yellow line: **AM** was used as the catalyst, and KNO_3 was added approximately 10 min after the start of the reaction. Conditions: 50 mM substrate **1**, 2.5 mol% **AM** or **NO_3-AM**, 60 mol% KNO_3, 2.5 mol% GSH, 2.5 mol% His, PBS/H_2O, 37 °C.

CONCLUSION AND OUTLOOK

The water soluble **AM** metathesis catalyst is exceedingly vulnerable to various decomposition pathways under aqueous conditions. Primarily, water itself results in rapid decomposition of the complex through replacement of the chloride ligand to generate catalytically inactive hydroxide species, and the presence of a mixture of biological additives renders the catalyst almost completely inactive. However, the addition of nitrate to **AM** results in a dramatic improvement upon its catalytic activity towards the ring closing metathesis of substrate **1**, as the ring-closed product **2** is generated in an 83% yield in water, and in a 42% yield even in the presence of a mixture of biological additives. This improved activity of the resultant **NO_3-AM** complex is due to the much faster reaction kinetics: product formation is faster than decomposition or poisoning, allowing the catalyst to convert the substrate in substantial amounts before the catalyst is inactivated, and in this way the catalyst is protected from biologically relevant conditions. This kinetic protection of the catalyst is therefore a facile and useful route to protecting an aqueous olefin metathesis catalyst under biological conditions, and future work should investigate whether or not this method of protection is also feasible inside of living cells.

EXPERIMENTAL

MATERIALS AND METHODS

All commercially available compounds were used as received. Substrate **1** was synthesised according to a literature procedure.[51] Milli-Q Ultrapure grade water was used for all reactions. All reactions were carried out under aerobic conditions. PBS buffer was prepared by dissolving PBS tablets in Milli-Q water. All catalysis results are an average of three experiments. All stock solutions were prepared fresh immediately before catalysis. NMR spectra were performed on a Bruker AV300, AV400, or AV500 spectrometer, with chemical shifts reported in ppm and referenced to solvent residual signal (2.50 ppm for toluene-d8, 4.79 ppm for D_2O). High resolution mass data were recorded on a HR ToF Bruker Daltonik Gmbh Impact II, an ESI-ToF MS capable of resolution of at least 40000 FWHM, which was coupled to a Bruker cryo-spray unit. Detection was in positive-ion mode and the source voltage was between 4 and 6 kV. The sample was introduced with syringe pump at a flow rate of 18 µL/hr. For electrospray ionisation (ESI), the drying gas (N_2) was held at 180 °C. The machine was calibrated prior to every experiment via direct infusion of a TFA-Na solution, which provided a m/z range of singly charged peaks up to 3500 Da in both ion modes. Software acquisition Compass 2.0 for Otof series. Software processing Compass DataAnalysis 4.0 sri. UV/Vis spectra were recorded on a Hewlett Packard 8453 single beam spectrophotometer in a 1.0 cm path length quartz cuvette with H_2O as background. Bubble counting data was processed according to reported procedure.[49]

CATALYSIS

General procedure

Stock solutions of KNO_3, **AM**, GSH, and His in H_2O were prepared. The desired volume of H_2O or KNO_3 (18 µmol, 60 mol%) was mixed together with **AM** (0.75 µmol, 2.5 mol%). Then, the desired bioadditive (0.75 µmol, 2.5 mol%) was added, followed by neat substrate **1** (6.8 µL, 7.5 mg, 30 µmol, 1 eq). The vial was capped and stirred at 37 °C for 2 h. 0.8 mL of a 40 mM solution of 1,3,5-trimethoxybenzene in toluene-d8 was added, and the vial was shaken. The organic layer was decanted to an NMR tube and measured. The yields of the product were determined by ^{1}H NMR spectroscopy relative to 1,3,5-trimethoxybenzene as internal standard.

Stock Solution	Compound / Solvent	Concentration
A	KNO_3 / H_2O	180 mM
B	**AM** / H_2O	7.5 mM
C	GSH / H_2O	7.5 mM
D	His / H_2O	7.5 mM
E	GSH + His / PBS	7.5 mM GSH; 7.5 mM His

Entry	A (µL)	B (µL)	C (µL)	D (µL)	E (µL)	PBS (µL)	H_2O (µL)	Total (µL)
1	0	100	0	0	0	0	500	600
2	0	100	400	0	0	0	100	600
3	0	100	0	400	0	0	100	600
4	0	100	0	0	400	0	100	600
5	0	100	0	0	0	400	100	600
6	100	100	0	0	0	0	400	600
7	100	100	400	0	0	0	0	600
8	100	100	0	400	0	0	0	600
9	100	100	0	0	400	0	0	600
10	100	100	0	0	0	400	0	600

Order of addition

The effect of the order of addition of the reaction components was investigated. 2.5 mol% **AM** was mixed with 2.5 mol% GSH and 2.5 mol% His in PBS, and 30 mol% KNO_3 (12 eq with respect to **AM**), before addition of 1 eq of substrate **1**, and the yield of product **2** was determined after 2 h at 37 °C. For **AM** alone, the yield of **2** decreased to just 5% in the presence of the biological additives. However, in the presence of 30 mol% KNO_3 the yield of **2** was still higher than that of **AM** alone in water. Interestingly, the order of addition of the nitrate had an influence upon the yield. When the **AM** was mixed first with the biological additives before addition of KNO_3, a final yield of 24% was obtained. However, when the **AM** and KNO_3 were pre-mixed before addition of the biological additives, the yield was improved to 28%. It is likely that the inhibition of catalysis in the presence of biological additives is due to their strong binding to the metal centre, which would deactivate the catalyst by blocking substrate coordination and subsequent product formation. The nitrate may then be unable to displace the biological additives from the ruthenium centre. However, if the **AM** and nitrate are pre-mixed before addition of the additives, this may increase the quantity of active ruthenium-nitrate

species generated, and it is this higher quantity of catalyst in solution which results in higher yields compared to adding the nitrate after the biological additives.

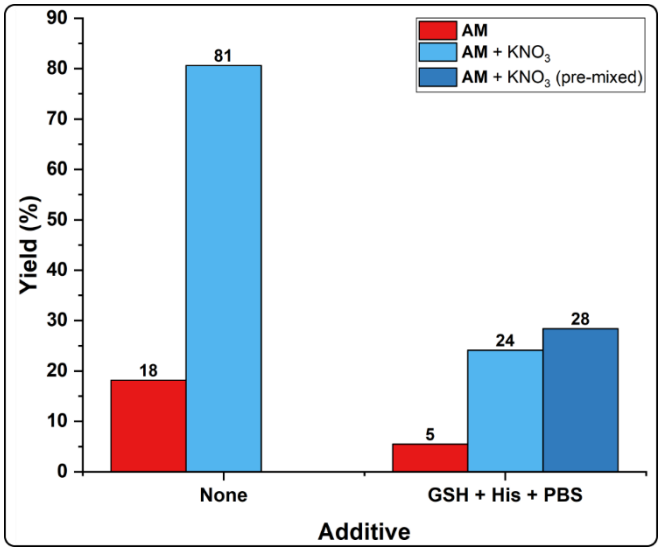

Figure E10. Yield of ring closing metathesis of substrate **1** in water and under biological conditions with **AM** in the presence KNO_3, where nitrate was added either after addition of biological additives (**AM** + KNO_3) or before addition of biological additives (**AM** + KNO_3 pre-mixed). Conditions: 2.5 mol% **AM** or **NO_3-AM** (30 mol% KNO_3), 50 mM substrate **1**, 2.5 mol% GSH, 2.5 mol% His, H_2O or PBS, 37 °C, 2 h. Yields determined by ^{1}H NMR spectroscopy relative to 1,3,5-trimethoxybenzene as internal standard.

KINETIC MEASUREMENTS WITH THE BUBBLE COUNTER

Stock solutions of **AM** and KNO_3 in H_2O and GSH and His in PBS were prepared. H_2O (4.0 mL) in a 10 mL vial was placed in the bubble counter (see ref (*48*) for bubble counter set-up). The vial was then pre-heated to 37 °C while purging the vial with N_2. Purging with N_2 is required for the functioning of the bubble counter. After stabilisation of the temperature, **AM** (6.88 µmol, 2.5 mol%) then KNO_3 (165 µmol, 60 mol%) then bio-additives (6.88 µmol, 2.5 mol%) then neat substrate **1** (62.6 µL, 69.1 mg, 275 µmol, 1 eq) were added via cannula in the reactor head. For reactions in the absence of KNO_3 or bio-additives, an equal volume of H_2O was added instead. The reaction mixture was stirred at 37 °C until no further bubbles were produced. 1 mL of a 275 mM solution of 1,3,5-trimethoxybenzene in toluene-d8 was added, and the vial was shaken. The organic layer was decanted to an NMR tube and measured. The yield of the product was determined by ^{1}H NMR spectroscopy relative to 1,3,5-trimethoxybenzene as internal standard.

Stock Solution	Compound / Solvent	Concentration
A	KNO_3 / H_2O	330 mM
B	**AM** / H_2O	13.8 mM
C	GSH + His / PBS	13.8 mM GSH; 13.8 mM His

Entry	A (mL)	B (mL)	C (mL)	H_2O (mL)	Total (mL)
1	0	0.5	0	5.0	5.5
2	0	0.5	0.5	4.5	5.5
3	0.5	0.5	0	4.5	5.5
4	0.5	0.5	0.5	4.0	5.5

AquaMet Pre-Catalyst Decomposition

Spectra of a 100 μM solution of **AM** (0.3 μmol, 3 mL, 1 eq) in the H_2O or PBS with the desired additives were recorded at 37 °C every 2 min for 1 h.

Entry	Additives	Solvent
1	none	H_2O
2	KNO_3 (1.2 mM)	H_2O
3	GSH (100 μM) + His (100 μM)	PBS
4	KNO_3 (1.2 mM) + GSH (100 μM) + His (100 μM)	PBS

AquaMet Decomposition Under Catalytic Conditions

Stock solutions of KNO_3 in H_2O and GSH and His in PBS were prepared. **AM** (1.61 mg, 2.0 μmol, 2.5 mol%) was weighed into a 20 mL vial and dissolved in H_2O. KNO_3 (48.0 μmol, 60 mol%) then bio-additives (2.0 μmol, 2.5 mol%) then neat substrate **1** (18.2 μL, 20.1 mg, 80 μmol, 1 eq) were added, and the mixture was stirred at 37 °C. For reactions in the absence of KNO_3 or bio-additives, an equal volume of H_2O was added instead. After the desired amount of time, 1 mL of the reaction mixture was diluted with 1 mL of H_2O in a cuvette and the UV/Vis spectrum was recorded. Samples were measured before addition of substrate, and at 5, 10, 15, 20, 25, 30, and 60 min.

Stock Solution	Compound / Solvent	Concentration
A	KNO_3 / H_2O	120 mM
B	GSH + His / PBS	1.25 mM GSH; 1.25 mM His

Entry	A (mL)	B (mL)	H_2O (mL)	Total (mL)
1	0	0	10.0	10.0
2	0	1.6	8.4	10.0
3	0.4	0	9.6	10.0
4	0.4	1.6	8.0	10.0

NO_3-AM Mass Spectrometry Measurements

An aqueous solution of **AM** (2.5 mM, 0.1 mL, 1 eq) was mixed with an aqueous solution of KNO_3 (60 mM, 0.1 mL, 24 eq) and measured with ESI-HRMS.

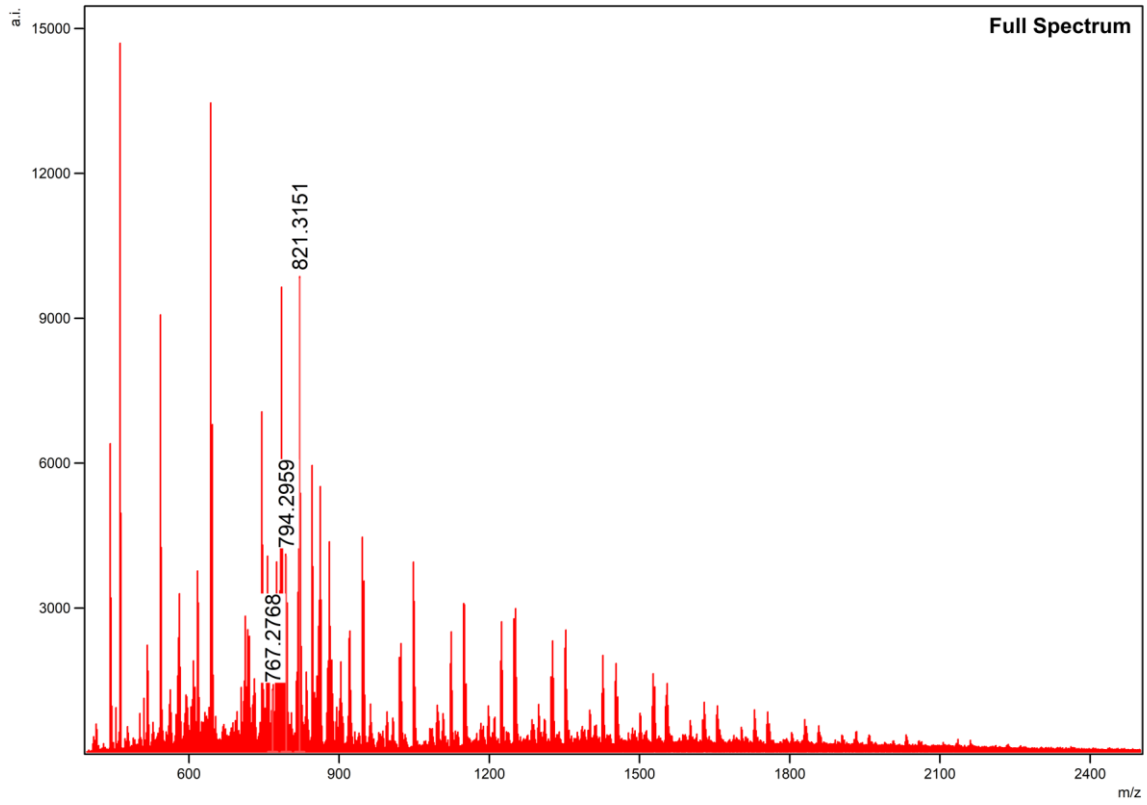

Figure E11. ESI-HRMS spectrum (positive mode) of **AM** + 24 eq KNO_3.

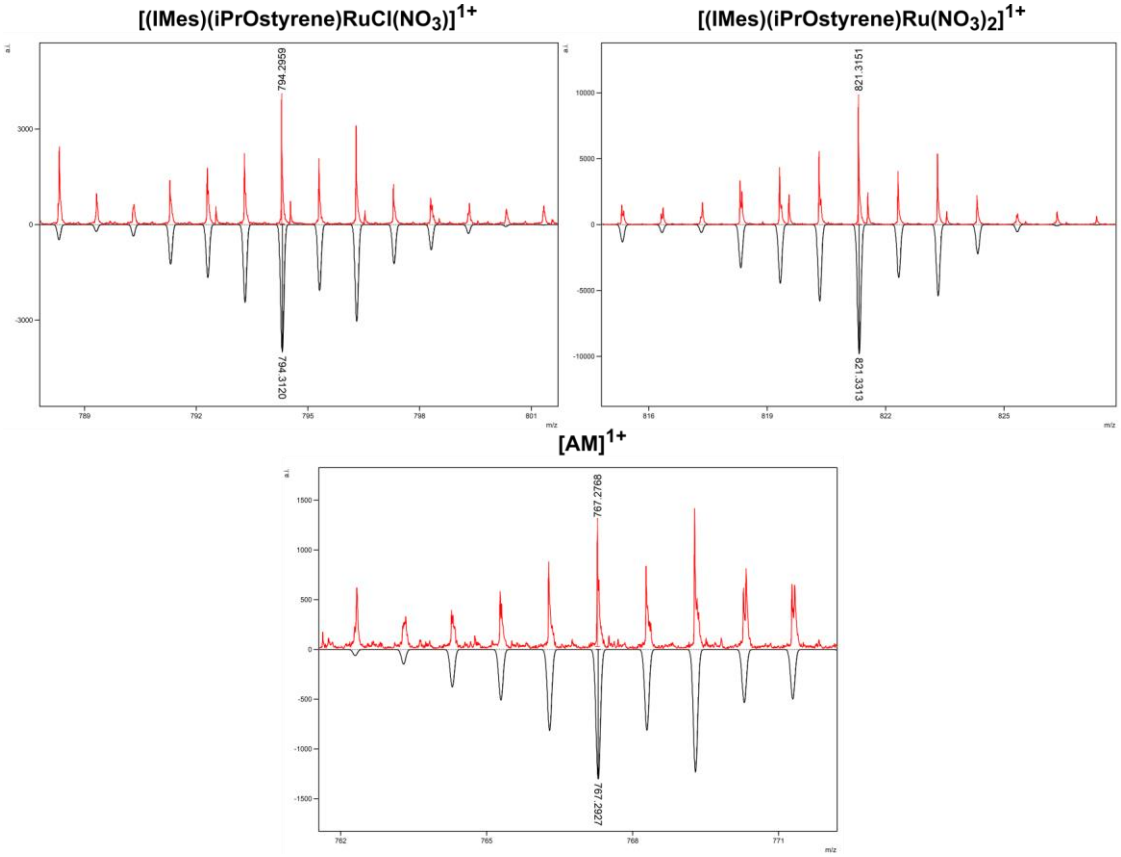

Figure E12. Zooms into ESI-HRMS spectrum of **AM** + 24 eq KNO_3. Measured in red, calculated in black.

REFERENCES

[1] M. L. Gringolts, Y. I. Denisova, E. S. Finkelshtein, Y. V. Kudryavtsev, *Beilstein J. Org. Chem.* **2019**, 15, 218-235.

[2] R. H. Grubbs, *Tetrahedron* **2004**, 60, 7117-7140.

[3] A. Deiters, S. F. Martin, *Chem. Rev.* **2004**, 104, 2199-2238.

[4] I. Nakamura, Y. Yamamoto, *Chem. Rev.* **2004**, 104, 2127-2198.

[5] S. Kotha, M. Meshram, Y. Dommaraju, *Chem. Rec.* **2018**, 18, 1613-1632.

[6] A. H. Ngo, S. Bose, L. H. Do, *Chem.–Eur. J.* **2018**, 24, 10584-10594.

[7] M. S. Messina, H. D. Maynard, *Mater. Chem. Front.* **2020**, 4, 1040-1051.

[8] T. Matsuo, *Catalysts* **2021**, 11, 359.

[9] A. Boto, C. C. González, D. Hernández, I. Romero-Estudillo, C. J. Saavedra, *Org. Chem. Front.* **2021**, 8, 6720-6759.

[10] Y. A. Lin, J. M. Chalker, B. G. Davis, *ChemBioChem* **2009**, 10, 959-969.

[11] Y. A. Lin, O. Boutureira, L. Lercher, B. Bhushan, R. S. Paton, B. G. Davis, *J. Am. Chem. Soc.* **2013**, 135, 12156-12159.

[12] J. M. Chalker, Y. A. Lin, O. Boutureira, B. G. Davis, *Chem. Commun.* **2009**, 3714-3716.

[13] A. Brik, *Adv. Synth. Catal.* **2008**, 350, 1661-1675.

[14] M. Jeschek, R. Reuter, T. Heinisch, C. Trindler, J. Klehr, S. Panke, T. R. Ward, *Nature* **2016**, 537, 661.

[15] S. Eda, I. Nasibullin, K. Vong, N. Kudo, M. Yoshida, A. Kurbangalieva, K. Tanaka, *Nat. Catal.* **2019**, 2, 780-792.

[16] H. J. Forman, H. Zhang, A. Rinna, *Mol. Aspects Med.* **2009**, 30, 1-12.

[17] Y. G. Bai, J. F. Chen, S. C. Zimmerman, *Chem. Soc. Rev.* **2018**, 47, 1811-1821.

[18] S. Alonso-de Castro, A. Terenzi, J. Gurruchaga-Pereda, L. Salassa, *Chem.–Eur. J.* **2019**, 25, 6651-6660.

[19] S.-Y. Jang, D. P. Murale, A. D. Kim, J.-S. Lee, *ChemBioChem* **2019**, 20, 1498-1507.

[20] M. Martínez-Calvo, J. L. Mascareñas, *Coord. Chem. Rev.* **2018**, 359, 57-79.

[21] J. J. Soldevila-Barreda, N. Metzler-Nolte, *Chem. Rev.* **2019**, 119, 829-869.

[22] A. G. Santos, G. A. Bailey, E. N. dos Santos, D. E. Fogg, *ACS Catal.* **2017**, 7, 3181-3189.

[23] C. O. Blanco, J. Sims, D. L. Nascimento, A. Y. Goudreault, S. N. Steinmann, C. Michel, D. E. Fogg, *ACS Catal.* **2021**, 11, 893-899.

[24] J. C. Foster, S. Varlas, L. D. Blackman, L. A. Arkinstall, R. K. O'Reilly, *Angew. Chem. Int. Ed.* **2018**, 57, 10672-10676.

[25] D. M. Lynn, B. Mohr, R. H. Grubbs, *J. Am. Chem. Soc.* **1998**, 120, 1627-1628.

[26] M. Kim, M.-S. Eum, M. Y. Jin, K.-W. Jun, C. W. Lee, K. A. Kuen, C. H. Kim, C. S. Chin, *J. Organomet. Chem.* **2004**, 689, 3535-3540.

[27] A. Y. Goudreault, D. M. Walden, D. L. Nascimento, A. G. Botti, S. N. Steinmann, C. Michel, D. E. Fogg, *ACS Catal.* **2020**, 10, 3838-3843.

[28] J. C. Foster, M. C. Grocott, L. A. Arkinstall, S. Varlas, M. J. Redding, S. M. Grayson, R. K. O'Reilly, *J. Am. Chem. Soc.* **2020**, 142, 13878-13885.

[29] B. Bhushan, Y. A. Lin, M.Bak, A. Phanumartwiwath, N. Yang, M. K. Bilyard, T. Tanaka, K. L. Hudson, L. Lercher, M. Stegmann, S. Mohammed, B. G. Davis, *J. Am. Chem. Soc.* **2018**, 140, 14599-14603.

[30] W. L. McClennan, S. A. Rufh, J. A. M. Lummiss, D. E. Fogg, *J. Am. Chem. Soc.* **2016**, 138, 14668-14677.

[31] B. J. Ireland, B. T. Dobigny, D. E. Fogg, *ACS Catal.* **2015**, 5, 4690-4698.

[32] D. L. Nascimento, I. Reim, M. Foscato, V. R. Jensen, D. E. Fogg, *ACS Catal*. **2020**, 10, 11623-11633.
[33] D. L. Nascimento, M. Foscato, G. Occhipinti, V. R. Jensen, D. E. Fogg, *J. Am. Chem. Soc.* **2021**, 143, 11072-11079.
[34] V. Thiel, K.-J. Wannowius, C. Wolff, C. M. Thiele, H. Plenio, *Chem.–Eur. J.* **2013**, 19, 16403-16414.
[35] G. A. Bailey, M. Foscato, C. S. Higman, C. S. Day, V. R. Jensen, D. E. Fogg, *J. Am. Chem. Soc*. **2018**, 140, 6931-6944.
[36] D. L. Nascimento, D. E. Fogg, *J. Am. Chem. Soc.* **2019**, 141, 19236-19240.
[37] T. Matsuo, T. Yoshida, A. Fujii, K. Kawahara, S. Hirota, *Organometallics* **2013**, 32, 5313-5319.
[38] D. C. Church, L. Takiguchi, J. K. Pokorski, *Polym. Chem.* **2020**, 11, 4492-4499.
[39] L. J. Jongkind, M. Rahimi, D. Poole III, S. J. Ton, D. E. Fogg, J. N. H. Reek, *ChemCatChem* **2020**, 12, 4019-4023.
[40] M. R. Buchmeiser, I. Ahmad, V. Gurram, P. S. Kumar, *Macromolecules* **2011**, 44, 4098-4106.
[41] M. Malinowska, M. Kozlowska, A. Hryniewicka, J. W. Morzycki, , *J. Organomet. Chem.* **2019**, 896, 154-161.
[42] M. Jović, S. Torker, P. Chen, *Organometallics* **2011**, 30, 3971-3980.
[43] B. K. Keitz, K. Endo, P. R. Patel, M. B. Herbert, R. H. Grubbs, *J. Am. Chem. Soc.* **2012**, 134, 693-699.
[44] Y. Dang, Z.-X. Wang, X. Wang, *Organometallics* **2012**, 31, 8654-8657.
[45] M. A. Pribisko, T. S. Ahmed, R. H. Grubbs, *Polyhedron* **2014**, 84, 144-149.
[46] S. L. Mangold, D. J. O'Leary, R. H. Grubbs, *J. Am. Chem. Soc.* **2014**, 136, 12469-12478.
[47] N. Peschek, K.-J. Wannowius, H. Plenio, *ACS Catal.* **2019**, 9, 951-959.
[48] T. K. Slot, N. R. Shiju, G. Rothenberg, *Angew. Chem. Int. Ed.* **2019**, 58, 17273-17276.
[49] T. K. Slot, N. Riley, N. R. Shiju, J. W. Medlin, G. Rothenberg, *Chem. Sci.* **2020**, 11, 11024-11029.
[50] A. V. Melkikh, M. I. Sutormina, *J. Theor. Biol.* **2008**, 252, 247-254.
[51] K. Vehlow, S. Maechling, S. Blechert, *Organometallics* **2006**, 25, 25-28.

Summary

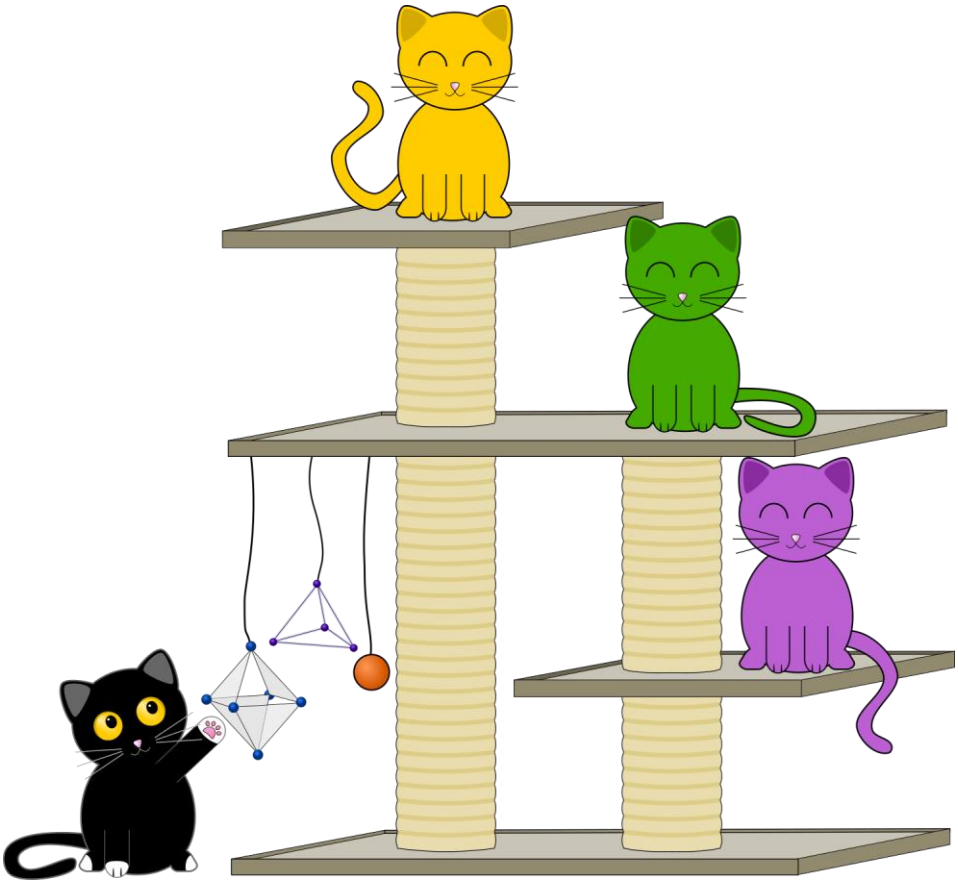

Transition metal catalysis is an invaluable tool to access a vast range of transformations which are otherwise difficult to achieve. While it is integral to synthetic chemistry in the lab, its power to control reactivity within living cells has only recently been discovered. Although nature has evolved enzymes which are able to carry out reactions extremely efficiently, their high levels of selectivity come at the cost of a limited substrate scope, and a limited range of transformations. Therefore transition metal catalysts are becoming an increasing popular method to accomplish new-to-nature reactions within living cells. Having access to a wide scope of efficient transition metal catalysed bioorthogonal reactions provides the opportunity to further develop new methods for biomolecular labelling and imaging, and new mechanisms for prodrug activation. This has the potential to further advance our understanding of biological systems and reduce unwanted side effects during drug treatments by improving the specificity and targeting with controlled metal-mediated activation. However, the environment of the cell is very different to the conditions which are typically required for transition metal catalysts to function, meaning that achieving *in vivo* transition metal catalysis is not a straightforward task.

In **Chapter 1** we explore the progress made in the field of *in vivo* transition metal catalysis over the last 20 years. A large range of catalytic systems have been applied in cells, covering a range of reactions and catalysts. The field is dominated by relatively simple deprotection reactions, where a small terminal group is cleaved to generate an active fluorophore or drug, but more complicated reactions involving bond-forming transformations and even cross-couplings have also been demonstrated. One common theme among all of these examples is poisoning of the catalyst by the biological components – high concentrations of metal-binding molecules in cells, in particular thiols, results in often irreversible binding of biomolecules to the metal centre, which deactivates the catalyst. This means that low yields and low catalytic efficiencies are found throughout the field. New strategies need to be developed in order to protect the metal catalysts from poisoning and improve their activity in cells and we propose that encapsulation of the catalyst within a supramolecular cage can fulfil this need. There are several examples of supramolecular cages which impart size selectivity upon the encapsulated catalyst, where small substrates can enter the cage and react with the catalyst, but large substrates are blocked by the windows of the cage. In addition, in many cases encapsulation improves the reactivity of the catalyst, with higher yields or selectivities being achieved as a result of pre-organising the substrate and catalyst, increasing the local concentration of the catalyst, and stabilising reactive catalytic intermediates. We therefore envision that by encapsulating the metal catalyst within a supramolecular cage, the catalyst may be protected from poisoning by blocking large biomolecules from reaching the metal centre, and in addition the overall performance of the catalyst may be improved due to confinement effects.

This hypothesis was validated in **Chapter 2**, were the effect of encapsulation on a gold catalyst under biological conditions was investigated. A small gold complex, Me_3PAuCl, which catalyses an intramolecular hydroarylation reaction to form a fluorescent dye, was encapsulated within a small anionic supramolecular cage, which has previously been demonstrated to undergo size selective reactions. It was demonstrated that the encapsulated gold complex was able to produce the dye in higher yields than the free complex under aqueous aerobic conditions and in the presence of various biological additives (Figure 1). The

cytotoxicity of the reaction components was determined, and it was found that the substrate for the reaction was highly cytotoxic. This means that low concentrations (1 μM) of substrate would be required to carry out the reaction inside living cells; however, catalysis carried out at this concentration in cell culture media was completely inhibited. In addition, cell permeability studies using confocal microscopy revealed that the cage itself was unable to cross the cell membrane. Although this catalytic system was unsuitable for application in living cells, the protective effect of the supramolecular cage was indeed demonstrated for reactions carried out *ex vivo*. Therefore encapsulation of a catalyst represents a viable strategy for improving catalysis under biological conditions.

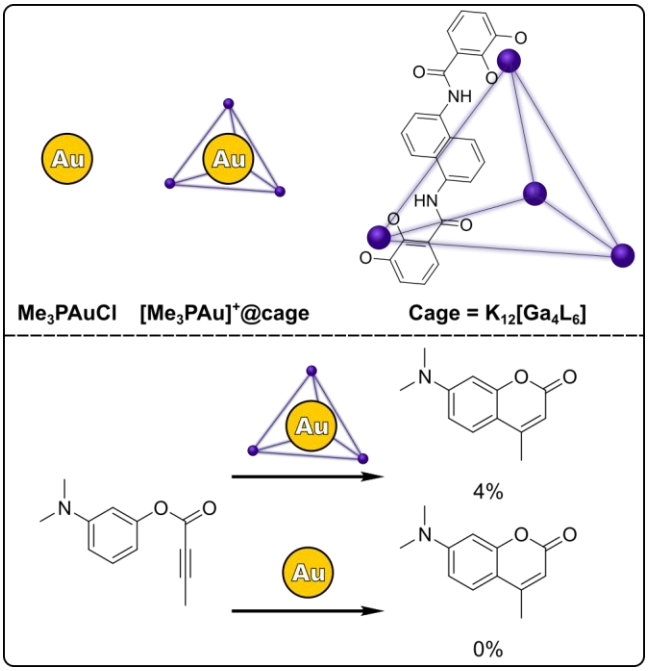

Figure 1. Above: Structures of the gold complex and the cage used in Chapter 2. Below: Yields of the gold catalysed intramolecular hydroarylation using free and encapsulated gold under biological conditions.

In **Chapter 3** we expanded this strategy to a palladium complex. Here a cationic supramolecular cage was selected, as cationic or neutral species are known to be more cell permeable than anionic species. Although palladium-based cages are unstable to biological conditions, we demonstrated that a platinum-based cage is stable to biological conditions, even at nanomolar concentrations. A small palladium complex, $[(Et_3P)_2PdCl_2]$, was successfully encapsulated within the cavity of this cage; however, purification of the complex was not possible, and a mixture of free palladium and encapsulated palladium was obtained. The reactivity of this encapsulated palladium complex was then investigated. We first looked at its reactivity towards the formation of a fluorescent dye via an intramolecular hydroarylation. Although the free palladium complex was completely inactive, initial experiments indicated that the encapsulated palladium complex and/or the cage itself were able to generate the dye. However, a lack of reproducibility meant that these results could not be confirmed. Further attempts to evaluate the reactivity of the encapsulated palladium complex were carried out using the Wacker-Tsuji oxidation of styrene and the double silylation of benzil as model

systems (Figure 2). However, in all cases no reactivity was observed and it was not possible to determine if the encapsulated palladium complex is catalytically active.

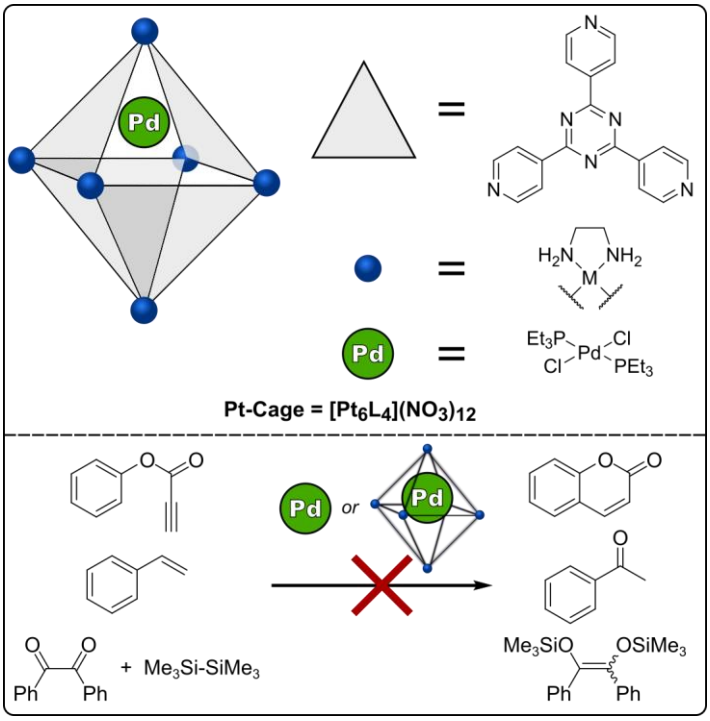

Figure 2. Above: Structures of the palladium complex and platinum cage used in Chapter 2. Below: Intramolecular hydroarylation, Wacker-Tsuji oxidation, and double silylation reactions attempted for the palladium complex.

We then set out to investigate if this same platinum cage could act as a protective host for a ruthenium olefin metathesis catalyst in **Chapter 4**. Encapsulation of standard apolar metathesis catalysts within this cage was not possible. However, the presence of the cage greatly improved the catalytic activity of a water soluble metathesis catalyst, AquaMet, compared to reactions carried out in the absence of cage. The presence of the cage greatly increased the rate of the reaction, which resulted in higher final yields of the product. Interestingly, it was found that the cause of this improvement was not due to any encapsulation effect, as NMR spectroscopy, GFN2-xTB, and UV/Vis spectroscopy studies revealed that there was no interaction between the catalyst and the cage. Instead, it was found that it was the nitrate counterions of the cage which were responsible for the improvement in activity, and that activity of the metathesis catalyst could be greatly improved by the presence of KNO_3 (Figure 3).

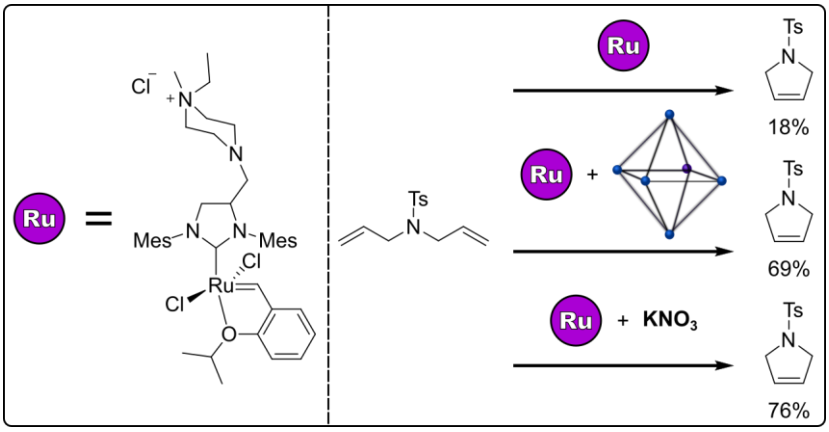

Figure 3. Left: Structure of AquaMet. Right: Yields of ruthenium catalysed ring closing metathesis with AquaMet, AquaMet in the presence of cage, and AquaMet in the presence of nitrate.

In **Chapter 5** we report out investigations on how to use these improved reaction kinetics in the presence of nitrate to improve the efficiency of olefin metathesis under biological conditions. Mass spectrometry studies show that the nitrate anions substitute the chloride ligand of the AquaMet to generate a new nitrate-AquaMet complex. It is this new nitrate complex which then exhibits faster initiation and faster catalysis than the standard chloride complex. These improved kinetics were also observed in the presence of biological additives (Figure 4). This means that the addition of nitrate to AquaMet provides kinetic protection for the metathesis reaction: the nitrate-complex was sufficiently fast that it was able to generate the product in good yields before becoming poisoned and deactivated by the biological additives; in contrast, the slower chloride-complex was poisoned before it was able to undergo catalysis.

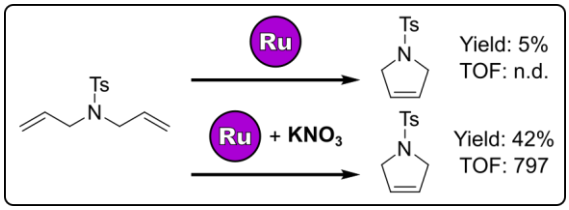

Figure 4. Yields and turnover frequencies (given in μmol ethene mol cat^{-1} min^{-1}) for ring closing metathesis in the presence of biological additives with AquaMet or AquaMet in the presence of nitrate.

In this thesis, we showed that new strategies are needed in the field of *in vivo* transition metal catalysis in order to overcome catalyst poisoning and improve catalytic activity. We have developed two new strategies for this purpose: physical protection, and kinetic protection. A supramolecular host can provide a physical barrier against biomolecules, and in this way poisoning can be reduced. However, the choice of host and the design of the catalytic system is highly important. First, the cage itself needs to be cell permeable in order to be able to deliver the catalyst to the inside of the cell. Secondly, a balance needs to be struck with respect to the size of the cage: very small windows will mean that the catalyst is well protected as this will make it difficult for biomolecules to enter the cage; however, this will also mean that the substrate scope will be limited to only very small molecules. For instances where a larger substrate is desired, a compromise needs to be made where larger windows allow for the larger

substrate, but this also allow smaller biomolecules to reach the catalyst, leading to limited protection only. Alternatively, kinetic protection can be used. Although catalyst poisoning is not prevented and will still occur, if a sufficiently fast reaction is selected then productive catalysis can take place before catalyst deactivation, and sufficient yield of the desired product can still be obtained. We applied these strategies to only three catalysts; however, we believe that these strategies show a lot of potential and in the future could also be expanded to other catalysts and other reactions.

Samenvatting

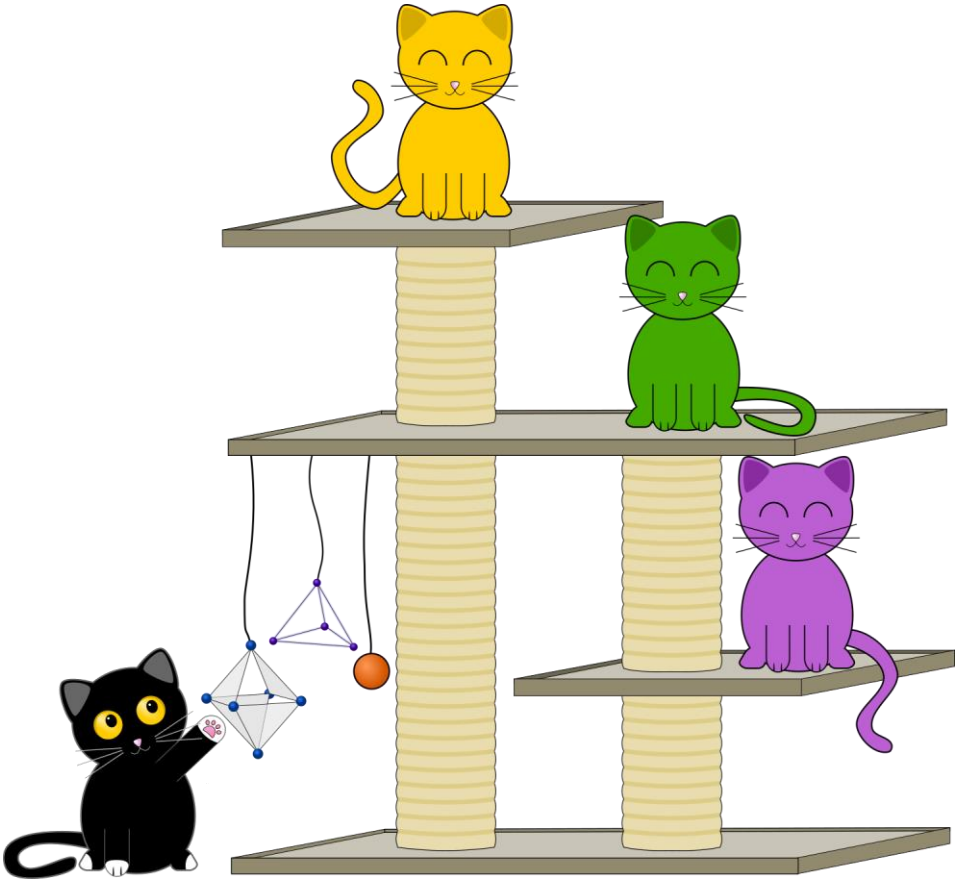

Overgangsmetaalkatalyse is van onschatbare waarde voor een zeer grote hoeveelheid chemische transformaties die anders zeer moeilijk zouden zijn. Binnen de synthetisch organische chemie in het lab is het bijna onmisbaar, maar de kracht van de overgangsmetaalkatalyse om chemische transfomaties binnen een levende cel te kunnen sturen is nog maar recentelijk ontdekt. Alhoewel er in de natuur veel verschillende enzymen zijn die chemische reacties zeer efficient en selectief uit kunnen voeren, zijn deze enzymen vaak zeer beperkt met betrekking tot substraten en verschillende chemische transformaties. Om deze reden word steeds vaker overgangsmetaalkatalyse ingezet om 'new-to-nature' reacties uit te kunnen voeren binnen een levende cel. Een breed bereik aan efficiente bioorthogonale overgangsmetaal gekatalyseerde reacties bied mogelijkheden voor de verdere ontwikkeling van nieuwe biomoleculaire labelling en imaging, alsmede voor nieuwe mechanismes voor de activatie van prodrugs. Deze kennis van biologische systemen zou vervolgens kunnen gebruikt kunnen worden om ongewenste zijreacties tijdens behandelingen met medicijnen te kunnen voorkomen door verbetering van de specificiteit aan de hand van reacties waarbij activatie word gestuurd door een overgangsmetaal. Echter verschild de omgeving binnen een levende cel aanzienlijk van de condities die typisch gebruikt worden voor overgangsmetaalkatalyse waardoor het bewerkstelligen van in vivo overgansmetaalkatalyse zeker geen makkelijke taak is.

In **Hoofdstuk 1** word gekeken naar de ontwikkelingen binnen de *in vivo* overgangsmetaalkatalyse gedurende de afgelopen 20 jaar. Een grote hoeveelheid verschillende katalytische systemen zijn getest in combinatie met cellen om verschillende chemische transformaties uit te voeren. Het veld word vooral gedomineerd door relatief simpele ontschermingsreacties waarbij een kleine eindgroep word verwijderd om zo een actief fluorfoor of geneesmiddel te genereren. Enkele meer complexe reacties waarbij nieuwe bindingen gevormd worden of zelfs cross-coupling reacties, zijn ook al aangetoond. Een terugkomend thema bij deze reacties is katalysatorvergiftiging aan de hand van de biologische componenten aanwezig in de celomgeving: hoge concentraties aan metaalbindende moleculen, voornamelijk thiolen, binden vaak irreversibel aan het overgangsmetaal wat leid to deactivatie van de katalysator. Hierdoor worden er binnen dit veld voornamelijk lage opbrengsten en lage katalytische efficientie gemeld. Om katalysatorvergiftiging tegen te gaan zijn nieuwe strategieën nodig waarbij het overgangsmetaal word beschermd tegen vergiftiging en zo de katalytische werking binnen een cel verbeterd kan worden. Hiervoor stellen wij voor de katalysator in een supramoleculaire kooi te plaatsen. Er zijn een aantal verschilende literatuur voorbeelden van inkapseling in een supramolecaire kooi waarbij er sprake is van selectiviteit op grootte. Hierbij kunnen kleine substraten wel bij de katalysator in de kooi, maar worden grootte substraten geblokkeerd door de ramen van de kooi. Verder zijn er veel voorbeelden waarbij inkapseling van de katalysator leid to verbetering van de reactiviteit, met hogere opbrengsten en selectiviteit, als gevolg van verhoogde lokale concentraties van de katalysator, pre-orientatie van het substraat., en stabilisatie van reactieve katalytische intermediairen. Aan de hand hiervan stellen wij het mogelijk dat inkapseling van een overgangsmetaalkatalysator in een supramoleculaire kooi zou kunnen leiden tot bescherming van de katalysator tegen vergiftiging door de van grote biomoleculen toegang tot de metaalkern te blokkeren alsmede

dat de katalytische werking nog verder verbeterd zou kunnen worden door de andere hierbovengenoemde inkapselingseffecten.

Deze hypothese werd in **Hoofdstuk 2** onderzocht, waarbij er werd gekeken naar de effecten van het inkapselen van een goud katalysator op de katalytische werking onder biologische condities. Een klein goud complex, Me_3PAuCl, waarvan bekend is dat het werkt als katalysator voor een intramoleculaire hydroarylatie waarbij een fluorescente kleurstof wordt gevromd, werd ingebracht in een kleine anionische supramoleculaire kooi die eerder gebruik was voor selectiviteit op grootte binnen katalytische reacties. Er is aangetoond dat onder aerobische condities in water en toevoeging van verschillende biologische additieven, het gebruik van het ingekapselde goud complex leidde to een veel hogere opbrengst van het fluorescente product dan wanneer het vrije goud complex gebruikt werd (Figuur 1). De cytotoxiciteit van de reactieve componenten werd ook bepaald waarbij bleek dat het substraat zeer cytotoxisch is. Dit betekent dat slechts lage concentraties (1 μM) substraat gebruikt kunnen worden binnen een levende cel. Echter wezen proeven met deze lage concentraties binnen een cel cultuur medium uit dat er onder deze omstandigheden geen katalyse plaatsvind. Cel permeabiliteits onderzoek waarbij gebruikt werd gemaakt van confocal microscopie bleek dat het niet mogelijk is voor de kooi om de cellen binnen te dringen. Alhoewel deze katalyse dus ongeschikt is gebleken voor gebruik binnen levende cellen, heeft het wel de beschermende werking van het inbrengen van een katalysator in een supramoleculaire kooi aangetoond voor *en vivo* reacties. Dit laat dus zien dat inkapseling van een katalysator wel een bruikbare strategie is voor het verbeteren van katalyse onder biologische condities.

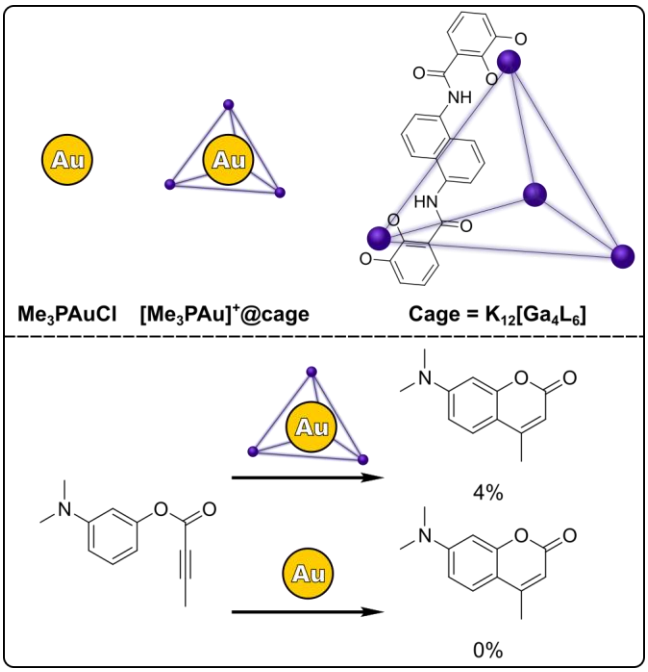

Figuur 1. Boven: Structure van de in hoofdstuk 2 gebruikte goud complex en supramoleculaire kooi. Onder: Opbrengsten van de goud gekatalyseerde intramolculaire hydroarylatie onder biuologische condities gebruikmakend van vrij en ingekapseld goud complex.

In **Hoofdstuk 3** is de strategie verder uitgebreid naar een palladium complex. Hierbij werd er gekozen voor een kationische supramoleculaire kooi omdat het van kationische en

neutrale complexen bekend is dat deze beter cellen kunnen binnen dringen. Alhoewel op palladium gebasserde kooien instabiel zijn onder biologische condities, hebben wij aangetoond dat analoge platina kooienwel stabiel zijn onder deze condities, zelfs in nanomolaire concentraties. Een klein palladium complex, [$(Et_3P)_2PdCl_2$], is succesvol ingebracht in de platina kooi, echter was volledige opzuivering vervolgens niet mogelijk en werd er alleen een mengsel van vrij en ingekapselde complexen verkregen. De reactiviteit van dit mengsel is vervolgens onderzocht. Ten eerste werd onderzocht of het mengsel actief was als katalysator voor de intramoleculaire hydroarylatie en dus zou leidde tot productie van de bijbehorden fluorescente kleurstof. Echter, door een gebrek een reporduceerbaarheid konden deze resultaten niet verder gebruikt worden. Voor verder onderzoek naar de reactivitiet van het ingekapelde palladium complex werden de Wacker-Tsuji oxidatie van styrene en de dubbele allylatie van benzil gebruikt als model systemen (Figuur 2). Echter werd in alle gevallen geen katalyse waargenomen en was het dus niet mogelijk om te bpelaen of het ingekapselde complex katalytisch actief is.

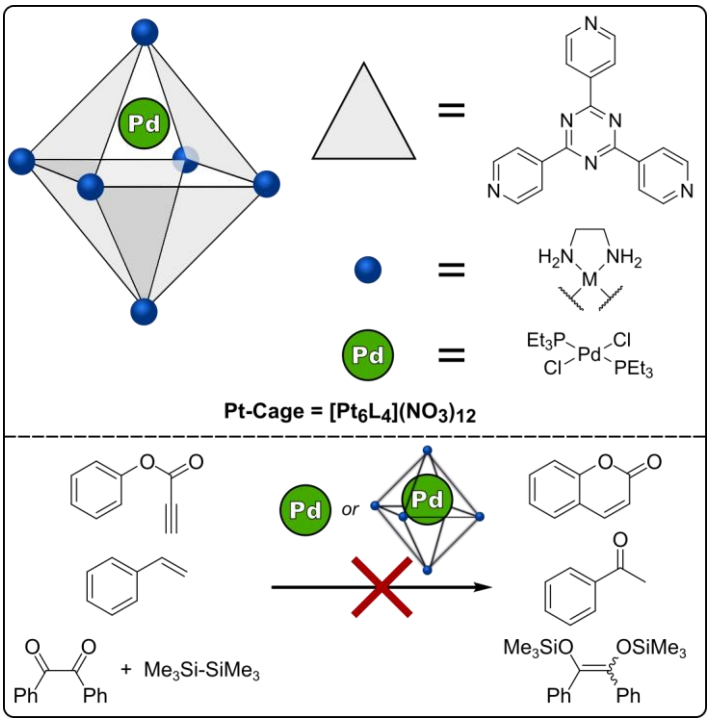

Figuur 2. Boven: Structuren van het palladium complex en de platina kooi die gebruikt zijn in hoofdstuk 3. Onder: Intramoleculaire arylatie, Wacker-Tsuji oxidatie, en dubble allylatie reacties die zijn geprobeerd met het palladium complex.

Vervolgens zijn wij in **Hoofdtstuk 4** gaan onderzoeken of dezelfde platina kooi gebruikt zou kunnen worden voor het beschermen van een ruthenium olefine metathese katalysator. Inkapselen van de standaard apolaire metathese katalysatoren binnen de geladen kooi bleek niet mogelijk. Echter leidde de aanwezigheid van de kooi wel tot een grote verbetering van de katalytische activiteit van een in water oplosbare metathese katalysator, AquaMet. Invergelijking met analoge reacties uitgevoerd zonder kooi. De aanwezigheid van de kooi leidde tot een aanzienlijk snellere reactie waarbij een grotere opbrengst werd behaald. Interessant genoeg bleek dat deze verbetering niet het resultaat is van inkapseling van de

katalysator, aangezien NMR spectroscopie, GFN2-xTB, en UV/Vis spectroscopie aantoonde dat er geen interactie is tussen de katalysator en de kooi. In plaats daarvan bleek dat het de aanwezigheid van de nitraat tegenionen van de kooi is dat zorgt voor de grote toename in activiteit, en dat de activiteit van de metathese katalysator aanzienlijk verbeterd kan worden door aanwezigheid van kalium nitraat KNO_3 (Figuur 3).

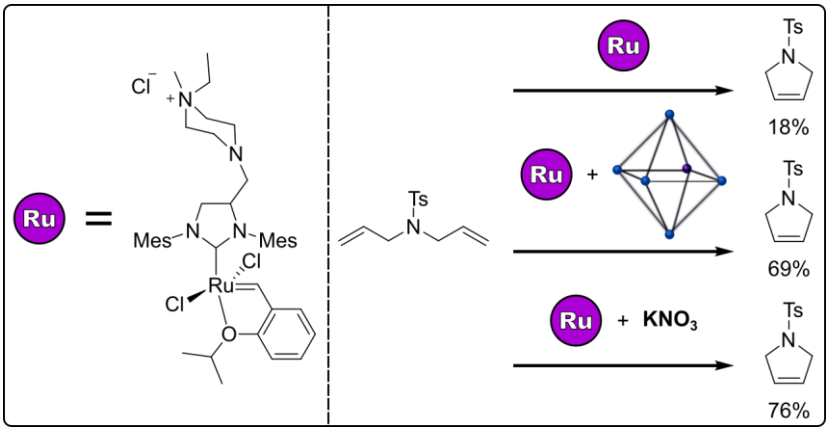

Figuur 3. Links: Structuur van AquaMet. Rechts: Opbrengsten van ruthenium gekatalyseerde ring sluitende metathese met AquaMet, AuqaMet in aanwezigheid van de kooi, en AquaMet in aanwezigheid van nitraat.

In **Hoofdstuk 5** kijken wij verder naar de resultaten in aanwezigheid van nitraat om zo te onderzoeken hoe wij deze verbeterde reactie kinetiek kunnen gebruiken voor reacties onder biologische condities. Uit massa spectrometrisch onderzoek bleek dat de nitraat anionen de chloor ionen van het AquaMet vervangen om zo het analoge nitraat complex te vormen. Dit nieuwe nitraat complex is een veel effectievere katalysator dan het standaard chloride complex. De verbeterde reactie kinetiek werd ook waargenomen in de aanwezigheid van verschillende biologisch additieven (Figuur 4). Dit betekent dat toevoeging van nitraat aan AquaMet zorgt voor kinetische bescherming van de metathese reaction: reactie met het nitraat complex is dusdanig snel dat het veel substraat kan omzetten naar product voordat het vergiftigd en dan gedeactiveert word door de biologische additieven, in tegenstelling to het chloride complex.

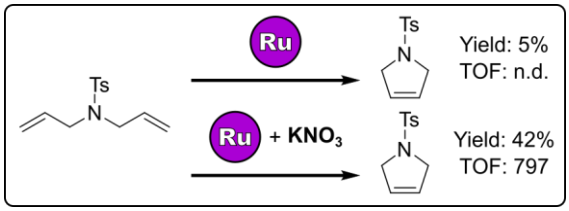

Figuur 4. Opbrengsten en omzet frequenties (gegeven in µmol ethene mol cat^{-1} min^{-1}) voor de ring sluitings metathese in de aanwezigheid van biologische additieven met AquaMet of AquaMet in aanwezigheid van nitraat.

In deze thesis hebben we laten zijn dat er nieuwe strategieën nodig zijn binnen de *in vivo* overgangsmetaalkatalyse om vergiftiging van de katalysator te voorkomen en zo katalytische activiteit te verbetern. Hiervoor hebben wij twee nieuwe strategieën ontwikkeld: fysieke bescherming, en kinetische bescherming. Een supramoleculaire kooi can gebruikt worden om een fysieke barriere om de katalysator te creeëren en zo deze te beschermen tegen

vergiftiging. Echter is de keuze van katalysator en het ontwerp van het katalytische systeem zeer belangrijk. Ten tweede moet de juiste balans gevonden worden betreffende de afmetingen van de kooi: hele kleine ramen zorgen voor optimale afscherming tegen biomoleculen, maar maken interacties met substraten ook moeilijker en beperken zo de hoeveelheid substraten die gebruikt kunnen worden. Ingevallen waar een grote substraat wenselijk is moet er een compromis gesloten worden waarbij er grotere ramen worden gebruikt zodat het substraat de kooi binnen kan maar waardoor ook kleinere biomoleculen toegang krijgen wat dus leid to beperkte bescherming van de katalysator. Als alternatief kan ook kinetische bescherming gebruikt worden. Alhoewel in dit geval katalysator vergiftiging nogsteeds plaatsvind, zal een reactie de snel genoeg verloopt nogsteeds productief zijn omdat de katalyse plaatsvind voordat de katalysator word gedeactiveerd waardoor het gewenste product nogsteeds verkegen kan worden. Alhoewel wij deze strategieën hebben toegepast op slecths drie verschillende katalysatorn, zijn wij ervan overtuigd dat deze strategieë potentie tonen om in de toekomst verder toegepast to worden bij andere katalytisatoren en katalystische reacties.

List of Publications

Publications related to this thesis:

In Vivo Transition Metal Catalysis: Progress, Challenges, and Novel Supramolecular Solutions
Catriona C. James,[1, 2, 4] Bas de Bruin,[1, 4, 8] Joost N. H. Reek.[1, 4, 8]
Manuscript in preparation.

Protection of a Gold Catalyst by a Supramolecular Cage for Application in Living Cells
Catriona C. James,[1, 2, 4] Dinghao Wu,[5] Eduard O. Bobylev,[6] Alexander Kros,[1, 4, 8] Bas de Bruin,[1, 4, 8] Joost N. H. Reek.[1, 4, 8]
Manuscript in preparation.

Kinetic Protection of a Water Soluble Olefin Metathesis Catalyst for Potential Use Under Biological Conditions
Catriona C. James,[1-4] Pieter C. M. Laan,[7] Bas de Bruin,[1, 4, 8] Joost N. H. Reek.[1, 4, 8]
Manuscript in preparation.

[1] Conceptual ideas
[2] Experimental work
[3] Computational work
[4] Preparation of manuscript
[5] Cell experiments
[6] CSI-MS measurements
[7] Processing and interpretation of kinetic data
[8] Project supervision

Publications outside of this thesis:

Ruthenium-based PACT compounds based on an N,S non-toxic ligand: a delicate balance between photoactivation and thermal stability
Jordi-Amat Cuello-Garibo, Catriona C. James, Maxime A. Siegler, Sylvestre Bonnet, *Chem. Sq.* **2017**, 1, 2.

Selective Preparation of a Heteroleptic Cyclometallated Ruthenium Complex Capable of Undergoing Photosubstitution of a Bidentate Ligand
Jordi-Amat Cuello-Garibo, Catriona C. James, Maxime A. Siegler, Samantha L. Hopkins, Sylvestre Bonnet, *Chem. Eur. J.* **2019**, 25, 1260-1268.

Acknowledgements

Four and half years and some 800 experiments later and finally, somehow, I have this book. Accomplishing this PhD has been the hardest thing I have ever done, and I still can't quite believe that it's finished. Of course, this PhD doesn't just belong to me, as it would not have been possible without a lot of help and support, and I would like to thank these people in the coming pages.

Firstly, I would like to thank my supervisors, **Joost** and **Bas**. I want to thank you for giving me so much freedom while working on this project. When I started I didn't quite imagine how challenging this would be, but when I was struggling with failing projects you allowed me to instead explore new ideas and concepts. Allowing me to explore my own ideas has given me the opportunity to grow, and I have learned so much from these past years, both scientifically and personally. I would also like to thank you for always having suggestions and advice to find the next step when I was stuck on a project, and I am really proud of the work that we have accomplished together.

Next, I would like to thank all of my committee members. Prof. Dr. **Jan** van Maarseveen thank you for always being a friendly face around the E building. Your positive attitude and endless excitement about science have always made it a pleasure to talk with you. Dr. **Sonja** Pullen, although we were only able to work together a short time, I am so glad that you joined HomKat. It has truly been a pleasure to get to know you and have such a friendly, happy person within the lab. Thank you Dr. **Francesco** Mutti for agreeing to be on my committee and taking the time to read my thesis. Dr. **Chris** Slootweg I would like to thank you for being on my committee, I have really enjoyed getting to know you these last years. Thank you Prof. Dr. **Alexander** Kros for a truly inspiring collaboration. I really learned a lot from working together with you and your group, and I would like to thank you for all your help and input with the gold project. Finally, Prof. Dr. **Sylvestre** Bonnet thank you for agreeing to be on my committee. I really enjoyed my time working with you during my masters, and I would like to thank you for the guidance and support you gave during that time which inspired me to do this PhD.

My wonderful paranymph **Eline**, I am so grateful that we could go on our PhD journeys together! You've been there every step of the way from beginning to end and I can't imagine how I could've done it without you. Every single failed experiment or struggling project you were always there, and would always drop what you're doing to listen and give advice. Even on the bad days when I felt like I would never finish, I could motivate myself to come in because I knew you would be there for (very) long tea breaks and walks around the science park. Thank you for bringing so much laughter and fun to my time in the E building.

Eddy, where would I have been these last years without you! You really know everything there is to know about cages, and you were always there to give advice, suggestions, and help with mass. I had so much fun working, conferencing, and partying with you! Who knew Groningen has such a wild night life. And, most importantly, thanks for being the best karaoke partner I could ever ask for.

Thank you to all the staff working at HomKat! **Jarl** and **Tiddo** it was a lot of fun working with you in the E building, and thank you for lots of nice discussions and input during minimeetings. **Andreas** thanks for all the NMR help, you are always ready for a borrel. Thank you **Ed** for all

the mass measurements! Thank you to **Fatna**, **Taasje**, and **Erik** for keeping HomKat running smoothly. **Simon**, thank you for being one of the most helpful and knowledgeable people I have ever met! You always give useful advice about chemistry, the PhD, and life in general, and I'm so grateful. You are the life and soul of the party, and I'm going to miss working with you!

Thank you to my in vivo amigos! **Eva** I was so glad when you joined the in vivo team, and we could have some nice discussions/complaining about the in vivo struggles! You have some really cool projects, and I wish you lots of success with them! **Jianghua** good luck with the rest of your PhD! **Dinghao**, thank you so much for all of your help with the cell experiments! I really learned so much from working with you. I am very grateful for all your help and enthusiasm on this project. I had so much fun working with you, you are such a friendly and helpful person, I always enjoyed coming through to Leiden to work with you! Best of luck with the rest of your PhD!

Thanks to everyone who made E1.34 a great place to work! **Xander** we had lots of fun times! Thanks for all your help and advice in the lab. **Roel** we may never see eye to eye on Scooter, but it was still a lot of fun working together in the lab these past years (except for the explosions maybe!). **Marianne** I'm so happy that we were lab neighbours! You were so kind and helpful when I first joined HomKat, thank you for making me feel so welcome in E1.34! **Johan** it's been such a pleasure working with you. You always give new perspectives when I ask for advice, and you bring so much fun to the borrels! **Minghui** you are truly the queen of columns! It's been so nice to work and teach with you. **Jasslie** it was great to have you in the lab, even though we were not together for very long! **Demi** it was nice to have such a friendly face in our lab! **Xavier** thanks for all the fun times in the lab and at the borrels. And thank you to the rest of the E1.34 lab members, **Brian**, **Dirk**, and **Niklas** for making our lab such a fun place to work. And of course thank you to everyone who made our office so gezellig! **Joeri** thank you so much for always motivating me when I was complaining in the office! **David** thanks for all the NMR and cage advice, and for all the fun (and sometimes pessimistic) conversations. **Tom** it was a lot of fun teaching with you, and sharing some of the more "interesting" reports we received! And thanks to **Esther**, **Fengshao**, **Bo**, and **Shang** for the nice working atmosphere.

And, of course, thank you to all my HomKat colleagues for making the E building such a great place to work. **Pieter** the bubble maestro, thank you so much for all your help with my metathesis adventures! I really appreciate all the effort you put in to build my bubble counting set up and to process all the data. You are such a positive and helpful person, even when the bubble counter was not behaving you always motivated me to keep going! **Nicole** van Leeuwen, it's been so much fun hanging out with you, whether it's spending days quenching the toluene still or playing board games! **Didjay** I'm so glad you were here with me these last four years. Thank you for introducing me to Etmo and getting me addicted to the gym – zumba with you was really the highlight of my week! **Marie**, you are such a kind and fun person and I always loved talking and going to the gym even with you, even though I think we will forever disagree on BBB versus spinning. **Wojciech** it's always great to talk with you, and you made teaching the practicum a lot of fun. **Tessel** your projects were always super cool and I learned a lot from all your presentations! **Tijmen** it's always been nice to chat with you, and good luck

with your fellowship. **Lotte** thanks for always bringing a cheerful attitude to our minimeetings! **Felix** thanks for all the fun times at the borrel. **Rens** it was nice to talk about bubbles with you and have you on the in vivo team! Thank you to all of my cage colleagues **Lukas** Jongkind, **Shaotao**, **Bin**, **Raoel**, **Arnout**, **Anne**, and **Valentinos** for sharing your invaluable cage wisdom with me. **Sandra** thank you for all your advice and help when I first joined the group. **Lukas** Wolzak it was nice to launch our careers together. **Tania**, we both joined HomKat at the same time and started hydroformylation projects, and I really enjoyed our time together! And finally thank you **Kaj**, **Klaas**, **Pim**, **Sander**, **Zohar**, and **Daniel** for the gezellig HomKat atmosphere!

My time in the E building would not have been the same without SOC! My Bert Haanstrabuddies **Marissa** and **Gaston** thanks for all the fun times at the E building and on IJburg! You're both such kind, fun people and it's always a pleasure to see you. **Nicole** Oudhof thank you for always being so positive and happy person, I always feel motivated and energised after talking with you! **Andy** and **Becky** I'm so glad I got to know you! Thanks for bringing so much fun to Amsterdam! And of course thank you to **Matthew**, **Simone**, **Vivi**, **Steven**, **Bas** de Jong, **Nick**, and all the many SOC students for always letting me crash the SOC borrels! Thanks for all the fun times!

It would not have been possible to get through these last four and half years without the help of my friends. **Bas**, **Pim**, **Brendan**, **Jobber**, **Kit**, **Vera**, **Boris**, and **Roy** thank you all for many many fun times! Thanks for listening when I complained about my research, and for getting me through the hard times with board games and beer!

Flip, this book would not have been possible without you. You taught me so much, not only about chemistry and lab techniques, but also to have confidence in my scientific ideas. I am deeply thankful for all the help and support you gave me, all the way from the very beginning of my PhD, and of course for all the fun times. Thank you to my favourite home-office colleague, **Noodle**, for bringing so much love and happiness to my life, and of course for doing your best to distract me from working at home.

I never would've got here without my girls **Sam**, **Kerris**, **Rosie**, **Mairi,** and **Shannon**. I can't believe we're still putting up with each other after all these years! Thank you for getting me to the Netherlands in the first place (crying in the middle of Princes Street seems like a lifetime ago), and for always being a phone call away when I needed to talk, and of course for keeping me sane during the lockdown! I love all of you weirdos, and you all deserve unlimited Barny Rubble points.

Finally, thank you to **Mum** and **Dad**. Thank you for all the love and support you have given me my whole life, which got me here. Thank you for always being there for me, for helping me when things were tough, and for celebrating my accomplishments with me. I am so lucky to have you, and I love you so much.